LABORATORY AND FIELD STUDIES OF COLLOID MOBILIZATION IN A SOUTHEASTERN COASTAL PLAIN AQUIFER

by

Christopher H. Swartz

M.S., Geological Sciences, Ohio State University, 1993
B.S., Geological Sciences, Ohio State University, 1990

Submitted to the Department of Civil and Environmental Engineering
In Partial Fulfillment of the Requirements for the Degree of

Doctor of Philosophy
in Civil and Environmental Engineering

at the

MASSACHUSETTS INSTITUTE OF TECHNOLOGY
February, 1998

Signature of
Author_____
Department of Civil and Environmental Engineering
January 15, 1997

Certified by_____
Philip M. Gschwend
Professor of Civil and Environmental Engineering
Thesis Supervisor

Accepted by_____
Joseph M. Sussman
Chairman, Departmental Committee on Graduate Studies

Laboratory and Field Studies of Colloid Mobilization in a Southeastern Coastal Plain Aquifer

by
Christopher H. Swartz

Submitted to the Department of Civil and Environmental Engineering
January 15, 1998 in Partial Fulfillment
of the Requirements for the Degree of
Doctor of Philosophy in Civil and Environmental Engineering

Abstract

The mechanisms which control release of clay-size aquifer solids from a Southeastern Coastal Plain deposit as colloids to groundwater were investigated in laboratory packed-column studies and *in situ*. The approximately 100,000 yr old deposit, an iron oxyhydroxide- and kaolinite-rich quartz sand, is located at the Baruch Forest Sciences Institute, Georgetown, SC. Radionuclide and heavy metal wastes from the Savannah River Nuclear Processing Facility have contaminated another Southeastern Coastal Plain aquifer in geographic proximity to the Georgetown aquifer. Colloid-facilitated transport of these wastes is suspected in this contaminated aquifer, thus warranting study of colloid mobilization mechanisms in the regional deposits.

To aid us in developing a conceptual model of how interstitial clay-size fines were bound in this deposit, we used analytical and transmission electron microscopy (AEM-TEM) to observe the nanometer-scale associations among phases in prepared thin sections of the sediment. We also used wet-chemical selective extraction techniques to aid us in interpreting the AEM-TEM observations. Amorphous iron oxyhydroxides were found to be distributed among, and intimately associated with, clay mineral booklets (predominantly kaolinite) and were thought to serve as an electrostatic or bonding intermediary among the kaolinite booklets.

We tested our binding-mechanism model by subjecting sediment-packed columns to various chemically perturbing solutions. The response of the sediment to these solutions indicated that mobilization of colloids compositionally representative of the entire bulk matrix appeared to occur only when reductive or ligand-promoted dissolution of the iron oxyhydroxides was initiated *and* sufficient repulsive interactions were generated among matrix constituents. We hypothesized that bonds among the amorphous iron oxyhydroxides and kaolinite rendered electrostatic perturbations (e.g., phosphate containing solutions) ineffective in inducing mobilization of the kaolinite. Such electrostatic perturbations only mobilized an iron-rich subfraction of the matrix (suspected to be goethite).

Use of a single well injection-withdrawal method to investigate colloid mobilization in the Georgetown aquifer allowed us to test our bond-breaking hypothesis *in situ*. The trends observed in the data from these injection-withdrawal experiments corresponded well to those observed in the column experiments. In addition, competitive adsorption behavior observed in the field experiments aided in explaining why an anionic surfactant, sodium dodecyl sulfate, could not induce preferential mobilization of the iron-rich subfraction of the matrix. Electrophoretic mobility measurements of model goethite colloids suspended in appropriately concentrated solutions of the surfactant had indicated that this adsorbate would generate sufficient electrostatic repulsion in the sediment to mobilize goethite.

Thesis Supervisor: Philip M. Gschwend
Title: Professor of Civil and Environmental Engineering

Acknowledgments

Much of the data presented in this thesis could not have been obtained without the help of others. I am indebted to Mike Frongillo, Anthony Garrett-Reed, and David Bell of the electron microscopy facility at the Center for Materials Science, MIT, for providing instruction on use of the Jeol 200CX and HB603 VG-STEM. Their expert help made possible the images appearing in Chapter 2. Pat Reilly of the electron microscopy facility in the Department of Biology at MIT patiently shared with me the ultramicrotomy techniques needed to slice a chunk of sediment into wonderously thin (50 nm!) sections. Stacy Kirsch of Electron Microscopy Sciences, Warrenton, PA, gave advice on diamond blade purchases (a sizeable enough investment to warrent a worried gulp before placing the order) and provided us with initial thin sections of the Georgetown sediment.

Without the help of Tom Williams, a professor of Forest Sciences at Clemson University stationed at the Baruch Institute, none of the field work would have been possible. Above and beyond the call of duty, Tom worked to insure that I had everything I needed for the field experiments, including myriad cans of bug spray. He also provided crucial information regarding the best local "low country" cuisine in the Georgetown area. Louwanda Jolley and Jim Morris, at the Baruch Institute as well, also helped me in carrying out the field experiments. Louwanda Jolley also performed ion chromatography analysis of a groundwater sample. This data appears in Chapter 2.

April Ulery, a former post doc in the Gschwend lab, and former Gschwend lab student Britt Holmén indoctrinated me with the secrets of sediment analysis, not to mention the required chants necessary to appease the soil science gods and ensure a successful sediment extraction.

I owe a long list of thank you's to John Macfarlane, Gschwend lab research chemist, for guidance in all matters dealing with lab instrumentation and computers, for enduring insect assaults, wild boars, and the "icemen" during field work in South Carolina, and at times, for bankrolling my lunch at the trucks.

I would like to thank lab- and cubicle-mate Allison McKay for the many fruitful discussions we've shared over the years, and for sharing her Word Perfect and Endnote prowess as we suffered together the "thesis deadline blues". I must also thank past and present Gschwend lab-ites Rachel Adams, Örjan Gustaffson, Carol Johnson, Chris Long, Kris McNeil, Tom Ravens, Barbara Southworth, and Lukas Wick for many lab and group meeting discussions which helpted to bring this research into focus, and for making the lab a fun place to work in.

My thesis committee members Harry Hemond, Lynn Gelhar, and Tina Voelker provided valuable insights, without which this work would not be whole. Finally, I owe much to my advisor Phil Gschwend. I have benefited enormously from his keen insight over the years, and his infectious desire to understand "how things work" will remain an invaluable inspiration for all my future endeavors.

Table of Contents

List of Tables

List of Figures

Chapter 4:

Chapter 5:

Chapter 1:

Introduction

1.1 Motivation

It has become increasingly apparent that elucidating the mechanisms which bind clay-size fines within sediment matrices is an important factor in understanding subsurface transport of inorganic and organic contaminants. Clay-size fines comprise the inorganic and organic phases which coat primary grains (e.g., quartz, calcite) and fill the interstitial pores among these grains. These clay-size solids, e.g., iron, aluminum, and manganese sesquioxides and clay minerals, are preferential sites for adsorption of heavy metals (Suarez and Langmuir, 1976; Costen et al., 1995). The clay-size fraction also harbors the bulk of the organic matter present in many sediments, as an inverse correlation between sediment grain size and fraction organic matter has been demonstrated (Barber et al., 1992; Fontes et al., 1992; Holmén and Gschwend, 1997). This correlation would implicate the coatings and interstitial matrix in the sorption of hydrophobic organic contaminants (HOC's) as well (Kaplan et al., 1993; Holmén and Gschwend, 1997). Thus, mobilization of clay-size fines, which can harbor heavy metals and HOC's, as colloids to groundwater could facilitate transport of these contaminants in the subsurface. Prediction of subsurface contaminant migration would then be made more difficult than if only traditional retarded advection-dispersion were acting (McCarthy and Zachara, 1989; Ryan and Elimelech, 1996; Roy and Dzombak, 1997). Indeed, colloid facilitated transport has been implicated in several studies of toxic metal (Puls and Powell, 1992; Gounaris et al., 1993; Newman et al., 1993; Kaplan et al., 1995), radionuclide (Short et al., 1988; Penrose et al., 1990; Kaplan et al., 1994), and HOC (Gounaris et al., 1993) migration.

Mineral coatings and matrices are also an important element in the aggregative structure of sediments (Rao et al., 1976; Nkedi-Kizza et al., 1982). Dead-end pore throats and microporous, tortuous paths created by the coating/matrix structure are thought to contribute significantly to physical nonequilibrium transfer of solutes from pores in which advective "mobile" transport occurs to those "immobile" pores in which diffusion-limited

transport dominates (Rao et al., 1979; Nkedi-Kizza et al., 1983; Wu and Gschwend, 1988; Brusseau et al., 1991). Thus, alteration of the microporous structure of sediments via mobilization of the coatings/matrices could have a significant effect on the transport properties of the aquifer. Given these considerations, knowledge of the mechanisms which bind coating and matrix constituents is relevant in the much broader context of understanding and predicting subsurface transport processes.

1.2 Background

A host of diagenetic processes, acting on the primary minerals present in geologic deposits, create the clay-size phases residing typically among quartz framework grains (Boggs, 1987). Weathering products and transported elemental material commonly precipitate as sesquioxides of iron, aluminum, manganese, and silicon, carbonates, and alumino-silicate minerals (e.g., clay minerals such as kaolinite and vermiculite) (Hendershot and Lavkulich, 1983; Sposito, 1984). X-ray amorphous and crystalline phases often occur together in intimate association in many sediments (Jefferson et al., 1975; Bigham et al., 1978; Wang et al., 1993).

The chemical and physical mechanisms which maintain these intimate associations are the focus of mobilization studies. The prediction of the response of a sediment to chemical or physical perturbations, manifest as release of clay-size fines as colloids to groundwater, is the goal of these studies. The driving force for this research is the potential for colloid-facilitated transport of contaminants and alteration of sediment transport properties, as discussed above. A few investigations have focused on the identifying the role that physical phenomena like pore fluid velocity play in colloid mobilization (McDowell-Boyer, 1992; Kaplan et al., 1993). Most research efforts, though, have concentrated on understanding the response of sediments to chemical perturbations. The effect of elevated pH (Kia et al., 1987; Ryan and Gschwend, 1994; Roy and Dzombak, 1996) and acidic pH (Seaman et al., 1995), changes in ionic strength of pore fluids (Khilar and Fogler, 1984; McDowell-Boyer, 1992; Ryan and

Gschwend, 1994; Roy and Dzombak, 1996), and presence of surface potential altering adsorbates (Ryan and Gschwend, 1994; Kaplan et al., 1995; Seaman et al., 1995) have all been studied in packed column systems containing synthetic and natural components.

All of these chemical perturbations are realistic in the context of naturally occurring and anthropogenically generated geochemical processes, and all have been implicated in colloid mobilization. For example, acidic pH is a common result of discharge of heavy metal waste drainage to subsurface waters and is thought to have induced mobilization of colloids at a nuclear processing facility site (Kaplan et al., 1994; Kaplan et al., 1995). The "water sensitivity" of deposits, i.e., observed reductions in permeability concomitant with changes in ionic strength and elevated pH of the pore fluids, has been documented in the context of petroleum extraction (Khilar and Fogler, 1984; Cerda, 1987; Kia et al., 1987) and in subsurface environments where freshwater-seawater interfaces exist (Goldenberg and Margaritz, 1983). These permeability reductions have been attributed to mobilization and redistribution of sediment fines in response to these chemical perturbations. Dissolved organic matter, naturally present in most groundwaters, can alter the surface charge characteristics of aquifer solids through adsorption, resulting in mobilization of colloids (Ryan and Gschwend, 1992; Kaplan et al., 1993; Ryan and Gschwend, 1994). Dissolved organic matter and simple organic acids originating from landfill leachate (Gounaris et al., 1993) and other anthropogenic activities can have the same effect. Surface potential altering adsorbates can also be introduced into aquifers via remediation strategies such as those designed to enhance solubility of organic contaminants (Clarke et al., 1992; West and Harwell, 1992) or create retardation barriers to curb spreading of the same (Wagner et al., 1994; Hayworth and Burris, 1997) through injection of ionic surfactants. These adsorbates may induce colloid mobilization as well. Injection of anionic surfactants has lead to significant permeability reductions in some sediments (Nash et al., 1987; Renshaw et al., 1997). With such effects demonstrated, it is not hard to imagine the ability of adsorbates present in landfill leachate or heavy metal waste discharges to induce mobilization of colloids which facilitate the transport

of co-contaminants. These mobilization events can concomitantly alter the advective-diffusive properties of the aquifer as a result of fines redistribution.

1.3 Objectives of Research

Even as research focusing on colloid mobilization has appeared increasingly in the literature, Seaman et al., (1995) noted that few studies have analyzed the phenomena using relatively undisturbed natural sediments. Many early studies used only synthetic porous media (Cerda, 1987; Cerda, 1988; McDowell-Boyer, 1992). More recently, Ryan and Gschwend (1994) studied mobilization in a shallow, coastal plain aquifer sand, but they oven-dried and sieved the sediment before studying its colloid release behavior in packed columns.

The diversity in diagenetic processes acting on different deposits and the varying time periods over which these processes act require that systematic studies of colloid mobilization be conducted on a variety of natural sediments in order to broaden our understanding of the range of mechanisms which may bind aquifer fines. To this end, we chose to conduct such studies with field-moist sediment samples obtained from a shallow, Southeastern coastal plain deposit located on the grounds of the Baruch Forest Sciences Institute, Georgetown, SC (**Figure 1.1**). The deposit, an iron oxide coated beach sand, is in geographic proximity to the Barnwell formation (Aiken plateau region near Savannah River, S.C.) (**Figure 1.1**). Samples from the Barnwell formation have been used to study possible mechanisms facilitating the transport of radionuclides and heavy metals from the nearby Savannah River nuclear processing facility (Seaman et al., 1995). The Georgetown deposit, a relatively young deposit diagenetically, is a more shallow (approximately 3 m depth) aquifer than the Barnwell Formation (approximately 20 m). Contaminants introduced by recharge from ground surface (e.g., heavy metals from tailings piles) pass first through the more shallow, subsurface environment. Thus, our study hopes to augment the understanding of colloid generation mechanisms which might occur in such an environment.

The goal of this study was to understand the mechanisms binding clay-size fines in the

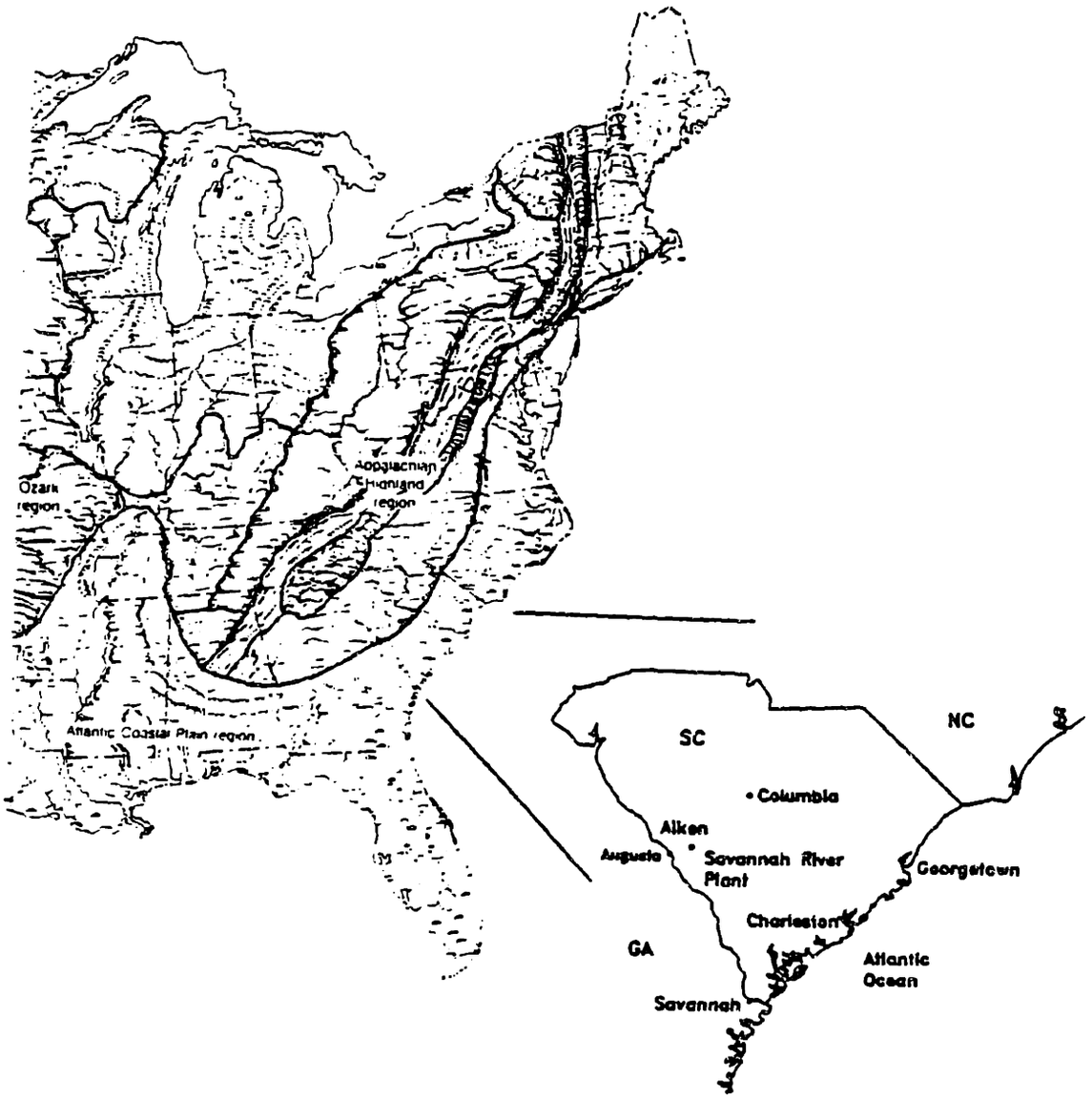

Figure 1.1: Map delineating the Atlantic Coastal Plain deposits of the United States and the location of the field site at the Baruch Forest Sciences Institute (Georgetown, SC) and its proximity to the Savannah River nuclear processing facility. Both sites are located within the Southeastern Coastal Plain physiographic province. The map of the physiographic provinces was taken from Press and Sevier (1978).

Georgetown aquifer. We began with a detailed investigation of how the sediment matrix was constructed, using electron microscopy to observe phase associations in the matrix. We surmised that knowledge of these associations would give us clues as to what mechanisms bound matrix constituents, allowing predictions to be made about which chemical perturbations would induce colloid mobilization in the aquifer. With that knowledge, we could then progress to studying the response of the sediment to chemical perturbations in controlled laboratory systems. Such studies would allow us to "test" binding mechanism hypotheses developed from the electron microscopic observations. Finally, these hypotheses were tested *in situ* to verify the robustness of the laboratory findings.

Observation of matrix constituent juxtapositions. We anticipated that observation of mineral juxtapositions in the Georgetown sediment via high resolution transmission and analytical electron microscopy techniques (HRTEM-AEM) would provide us with clues as to the constituents which have a key role in binding the matrix fines (Chapter 2). Only a few studies have attempted to observe the nanometer-scale mineral juxtapositions among matrix constituents in sediments using electron microscopy (Bennett et al., 1981; Santos et al., 1989; Banfield et al., 1991; Lee et al., 1991). Difficulties involved in preparing samples for microscopy, while maintaining the undisturbed, original structure of the sample, have been the greatest hinderance in applying high resolution electron microscopy to such analyses (DeVitre et al., 1989; Perret et al., 1991).

Using a relatively recently developed, hydrophilic, low viscosity embedding resin which more easily penetrates micropores (Bachhuber and Frösch, 1983; Perret et al., 1991), we were able to obtain uniform thin sections of the Georgetown interstitial matrix amenable to high resolution imaging. Spatial juxtapositions among matrix constituents, identified using electron diffraction and elemental composition derived from energy dispersive x-ray analysis, were noted in the HRTEM-AEM analysis, as were the crystalline nature.

In conjunction with the HRTEM-AEM analysis, selective extraction techniques were employed on the different size-fractions of sieved samples of the Georgetown sediment to

determine the amounts of free iron oxyhydroxides, and amorphous silica present. These constituents were thought to play key roles based on the HRTEM-AEM observations. These measurements allowed us to make inferences about the relative abundances of phases observed in the HRTEM-AEM analysis, and to refine our model of the mechanisms potentially binding the Georgetown matrix fines.

Analysis of sediment response to chemically perturbing solutions. We systematically tested our HRTEM-AEM derived model of binding mechanisms using columns packed with moist Georgetown sediment which were subjected to different solutions devised to discriminate potential electrostatic mechanisms from chemical and mechanical binding mechanisms (Chapter 3). Solution chemistries which (1) altered electric double layer thickness, (2) altered the surface potential of variably-charged matrix constituents without concomitant dissolution of phases or bond-breaking between phases, or (3) altered surface potential of variably-charged constituents while concomitantly dissolving phases (iron oxyhydroxide constituents were targeted in this respect) and possibly breaking bonds among constituents were tested to differentiate which mechanisms predominate in the Georgetown sediment. The elemental compositions of the dissolved and colloidal phases eluting from the columns were used, in conjunction with the response of the sediment to the perturbing solutions, to deduce the key mechanisms binding the fines.

In situ mobilization of colloids. To determine the response of the Georgetown sediment to chemical perturbations *in situ*, a single-well injection/withdrawal methodology was developed and employed (Chapter 4). To our knowledge, no published accounts of *in situ* colloid mobilization exist at present, although Kaplan et al. (1993) did employ large scale lysimeters (3m x 3m x 1.5 m dimensions) to study the effect of dissolved organic carbon and flow rate on colloid generation in the Blanton sand (Savannah River site, Aiken, S.C.). We believed it was important to augment and verify the laboratory mobilization data with "ground truth" derived data. The methodology developed provides a means to efficiently and conveniently test aquifer response to various chemically perturbing solutions *in situ*.

The methodology developed to study colloid mobilization *in situ* also appears to a valuable tool to study competitive adsorption phenomena. Data obtained from these field experiments suggested that competitive adsorption phenomena were controlling the ability of certain adsorbates to induce colloid mobilization in the aquifer (Chapter 5). Such data aided in explaining discrepancies observed between the mobilization behavior exhibited by the sediment in response to certain adsorbates and behaviors that would be predicted based on interpretation of electrophoretic mobility studies involving those adsorbates in model colloid systems.

1.4 References

Bachhuber K. and Frösch D. (1983) Melamine resins, a new class of water-soluble embedding media for electron microscopy. *J. Microsc.* **130**, 1-9.

Banfield J. F., Jones B. F., and Veblen D. R. (1991) An AEM-TEM study of weathering and diagenesis, Abert Lake, Oregon: Diagenetic modification of the sedimentary assemblage. *Geochim. Cosmochim. Acta* **55**, 2795-2810.

Barber L. B., Thurman E. M., and Runnells D. D. (1992) Geochemical heterogeneity in a sand and gravel aquifer: Effect of sediment mineralogy and particle size on the sorption of chlorobenzenes. *J. Contam. Hydrol.* **9**, 35-54.

Bennett R. H., Bryant W. R., and Keller G. H. (1981) Clay fabric of selected submarine sediments: Fundamental properties and models. *J. Sed. Pet.* **51**, 217-232.

Bigham J. M., Golden D. C., Buol S. W., Weed S. B., and Bowen L. H. (1978) Iron oxide mineralogy of well-drained utisols and oxisols: II. Influence on color, surface area, and phospate retention. *Soil Sci. Soc. Am. J.* **42**, 825-830.

Boggs S. (1987) *Principles of Sedimentology and Stratigraphy*. Merrill Publishing Company.

Brusseau M. L., Jessup R. E., and Rao P. S. C. (1991) Nonequilibium sorption of organic chemicals: Elucidation of rate-limiting processes. *Environ. Sci. Technol.* **25**, 134-142.

Cerda C. (1988) Mobilization of quartz fines in porous media. *Clays Clay Min.* **36**, 491-497.

Cerda C. M. (1987) Mobilization of kaolinite fines in porous media. *Coll. Surf.* **27**, 219-241.

Clarke A. N., R. D. Mutch J., Wilson D. J., and Oma K. H. (1992) Design and implementation of pilot scale surfactant washing/flushing technologies including surfactant reuse. *Wat. Sci. Tech.* **26**, 127-135.

Costen J. A., Fuller C. C., and Davis J. A. (1995) Pb^{2+} and Zn^{2+} adsorption by a natural aluminum and iron-bearing surface coating on an aquifer sand. *Geochim. Cosmochim. Acta* **59**, 3535-3547.

DeVitre R. R., Belzille N., Leppard G. G., and Tessier A. (1989) Diagenetic manganese and iron oxyhydroxide particles collected from a Canadian lake: Morphology and chemical composition. In *Heavy metals in the Environment* (ed. J. P. Vernet) 217-220. Elsevier.

Fontes M. R., Weed S. B., and Bowen L. H. (1992) Association of microcrystalline goethite and humic acid in some oxisols from Brazil. *Soil Sci. Soc. Am. J.* **56**, 982-990.

Goldenberg L. C. and Margaritz M. (1983) Experimental investigation on irreversible changes of hydraulic conductivity on the seawater-freshwater interface in coastal aquifers. *Water Resourc. Res.* **19**, 77-85.

Gounaris V., Anderson P. R., and Holsen T. M. (1993) Characteristics and environmental significance of colloids in landfill leachate. *Environ. Sci. Technol.* **27**, 1381-1387.

Hayworth J. S. and Burris D. R. (1997) Nonionic surfactant-enhanced solubilization and recovery of organic contaminants from within cationic surfactant-enhanced sorbent zones. 1. Experiments. *Environ. Sci. Technol.* **31**, 1277-1283.

Hendershot W. H. and Lavkulich L. M. (1983) Effect of sesquioxide coatings on surface charge of standard mineral and soil samples. *Soil Sci. Soc. Am. J.* **57**, 1252-1260.

Holmén B. A. and Gschwend P. M. (1997) Estimating sorption rates of hydrophobic organic compounds in iron oxide- and aluminosilicate clay-coated aquifer sands. *Environ. Sci. Technol.* **31**, 105-113.

Jefferson D. A., Tricker M. J., and Winterbottom A. P. (1975) Electron-microscopic and Mössbauer spectroscopic studies of iron-stained kaolinite minerals. *Clays Clay Min.* **23**, 355-360.

Kaplan D. I., Bertsch P. M., and Adriano D. C. (1995) Facilitated transport of contaminant metals through an acidified aquifer. *Groundwater* **33**, 708-717.

Kaplan D. I., Bertsch P. M., Adriano D. C., and Miller W. P. (1993) Soil-borne mobile colloids as influenced by water flow and organic carbon. *Environ. Sci. Technol.* **27**, 1193-1200.

Kaplan D. I., Bertsch P. M., Adriano D. C., and Orlandini K. A. (1994) Actinide association with groundwater colloids in a coastal plain aquifer. *Radiochimica Acta* **66/67**, 189-195.

Khilar K. C. and Fogler H. S. (1984) The existence of a critical salt concentration for particle release. *J. Colloid Int. Sci.* **101**, 214-224.

Kia S. F., Fogler H. S., and Reed M. G. (1987) Effect of pH on colloidally induced fines migration. *J. Colloid Int. Sci.* **118**, 158-168.

Lee S. Y., Hyder L. K., and Alley P. D. (1991) Microstructural and mineralogical characterization of selected shales in support of nuclear waste repository studies. In *Microstructure of Fine-grained Sediments* (ed. R. H. Bennett, W. R. Bryant, and M. H. Hulbert) 61-72. Springer-Verlag.

McCarthy J. F. and Zachara J. M. (1989) Subsurface transport of contaminants. *Environ. Sci. Technol.* **23**, 496-502.

McDowell-Boyer L. M. (1992) Chemical mobilization of micron sized particles in saturated porous media under steady flow conditions. *Environ. Sci. Technol.* **26**, 586-593.

Nash J., Traver R. P., and Downey D. C. (1987) Surfactant Enhanced In Situ Soil Washing. U.S. Air Force Engineering and Services Center.

Newman M. E., Elzerman A. W., and Looney B. B. (1993) Facilitated transport of selected metals in aquifer material packed columns. *J. Contam. Hydrol.* **14**, 233-246.

Nkedi-Kizza P., Biggar J. W., vanGenuchten M. T., Wierenga P. J., Selim H. M., Davidson J. M., and Kilcrease D. P. (1983) Modeling tritium and chloride 36 transport through an aggregated oxisol. *Water Resourc. Res.* **19**, 691-700.

Nkedi-Kizza P., Rao P. S. C., Jessup R. E., and Davidson J. M. (1982) Ion exchange and diffusive mass transfer during miscible displacement through an aggregated oxisol. *Soil Sci. Soc. Am. J.* **46**, 471-476.

Penrose W. R., Polzer W. L., Essington E. H., Nelson D. M., and Orlandini K. A. (1990) Mobility of plutonium and americium through a shallow aquifer in a semiarid region. *Environ. Sci. Technol.* **24**, 228-234.

Perret D., Leppard G. G., Muller M., Belzile N., DeVitre R., and Buffle J. (1991) Electron microscopy of aquatic colloids: Non-perturbing preparation of specimens in the field. *Water Res.* **25**, 1333-1343.

Puls R. W. and Powell R. M. (1992) Transport of inorganic colloids through natural aquifer material: Implications for contaminant transport. *Environ. Sci. Technol.* **26**, 614-621.

Rao P. S. C., Davidson J. M., Jessup R. E., and Selim H. M. (1979) Evaluation of conceptual models for describing nonequilibrium adsorption-desorption of pesticides during steady-flow in soils. *Soil Sci. Soc. Am. J.* **43**, 22-28.

Rao P. S. C., Green R. E., Ahuja L. R., and Davidson J. M. (1976) Evaluation of a capillary bundle model for describing solute dispersion in aggregated soils. *Soil Sci. Soc. Am. J.* **40**, 815-820.

Renshaw C. E., Zynda G. D., and Fountain J. C. (1997) Permeability reductions induced by sorption of surfactant. *Water Resourc. Res.* **33**, 371-378.

Roy S. B. and Dzombak D. (1996) Colloid release and transport processes in natural and model porous media. *Coll. Surf.* **107**, 245-.

Roy S. B. and Dzombak D. A. (1997) Chemical factors influencing colloid-facilitated transport of contaminants in porous media. *Environ. Sci. Technol.* **31**, 656-664.

Ryan J. N. and Elimelech M. (1996) Colloid mobilization and transport in groundwater. *Coll. Surf. A.* **107**, 1-56.

Ryan J. N. and Gschwend P. M. (1992) Effect of iron diagenesis on the transport of colloidal clay in an unconfined sand aquifer. *Geochim. Cosmochim. Acta* **56**, 1507-1521.

Ryan J. N. and Gschwend P. M. (1994) Effect of solution chemistry on clay colloid release from an iron oxide-coated aquifer sand. *Environ. Sci. Technol.* **28**, 1717-1726.

Santos M. C. D., Mermut A. R., and Ribeiro M. R. (1989) Submicroscopy of clay microaggregates in an oxisol from Pernambuco, Brazil. *Soil Sci. Soc. Am. J.* **53**, 1895-1901.

Seaman J. C., Bertsch P. M., and Miller W. P. (1995) Chemical controls on colloid generation and transport in a sandy aquifer. *Environ. Sci. Technol.* **29**, 1808-1815.

F. Press and R. Sevier (1978) *Earth*. W. H. Freeman and Co.

Short S. A., Lowson R. T., and Ellis J. (1988) $^{234}U/^{238}U$ and $^{230}Th/^{234}U$ activity ratios in the colloidal phases of aquifers in lateritic weathered zones. *Geochim. Cosmochim. Acta* **52**, 2555-2563.

Sposito G. (1984) *The Surface Chemistry of Soils*. Oxford University Press.

Suarez D. L. and Langmuir D. (1976) Heavy metal relationships in a Pennsylvania soil. *Geochim. Cosmochim. Acta* **40**, 589-598.

Wagner J., Chen H., Brownawell B. J., and Westall J. C. (1994) Use of cationic surfactants to modify soil surfaces to promote sorption and retard migration of hydrophobic organic compounds. *Environ. Sci. Technol.* **28**, 231-237.

Wang H. D., White G. N., Turner F. T., and Dixon J. B. (1993) Ferrihydrite, lepidocrocite, and goethite in coatings from east Texas vertic soils. *Soil Sci. Soc. Am. J.* **57**, 1381-1386.

West C. C. and Harwell J. H. (1992) Surfactants and subsurface remediation. *Environ. Sci. Technol.* **26**, 2324-2330.

Wu S.-C. and Gschwend P. M. (1988) Numerical modeling of sorption kinetics of organic compounds to soil and sediment particles. *Water Resourc. Res.* **24**, 1373-1383.

Chapter 2:

An AEM-TEM Study of Nanometer-Scale Mineral Associations in an Aquifer Sand: Implications for Colloid Mobilization*

*This chapter is an augmented version of C. H. Swartz, A. L. Ulery, and P. M Gschwend (1997) An AEM-TEM study of nanometer-scale mineral associations in an aquifer sand: Implications for colloid mobilization. *Geochimica et Cosmochimica Acta* **61**, pp. 707-718.

2.1 Introduction

The existence of mobile colloidal phases in groundwaters has become increasingly recognized (Gschwend and Reynolds, 1987; Short et al., 1988; Degueldre et al., 1989; Backhus et al., 1993). It has been suggested that, in some instances, colloidal material may play an important role in the facilitated subsurface transport of contaminants (McCarthy and Zachara, 1989; McDowell-Boyer, 1992). For example, colloids have been implicated in the transport of radionuclides (Buddemeier and Hunt, 1988; Penrose et al., 1990) and heavy metals (Newman et al., 1993; Kaplan et al., 1995).

Concomitantly, greater attention has been given to the fine-grained inorganic material which often coats and fills interstitial voids between primary grains (e.g., quartz) in aquifer sediments. It has become evident that these matrices of clay-size mineral particles can serve as reservoirs for colloidal phases released to groundwaters (Ryan and Gschwend, 1990; Kaplan et al., 1993). The origin of this material is commonly ascribed to transport and deposition of clay-size material or to authigenic formation (Hendershot and Lavkulich, 1983; Sposito, 1984). The weathering products and transported material are often reprecipitated as amorphous or crystalline iron, manganese, and aluminum sesquioxide coatings (Schwertmann and Taylor, 1989; Wang et al., 1993), and phyllosilicate minerals such as kaolinite are commonly intimately associated with these sesquioxides (Ryan and Gschwend, 1992; Malengreau et al., 1994). Elucidation of the mechanisms which induce release of these inorganic colloids from immobile sediment matrices to moving groundwater appears necessary to predict accurately subsurface contaminant transport.

Based on recent investigations, mineral particles in coatings and matrix appear to be mobilized upon subjecting a sediment to chemical perturbations in pore fluid chemistry (Cerda, 1987; McDowell-Boyer, 1992; Ryan and Gschwend, 1994; Seaman et al., 1995). These perturbations include changes in pH, E_H, ionic strength, and cation chemistry. It has been hypothesized that, in many instances, coatings and matrix material are bound in sediment

by electrostatic forces existing between mineral surfaces of fixed (e.g., kaolinite faces) and variable charge (e g., kaolinite edges, free oxyhydroxides of iron and aluminum) (Ryan and Gschwend, 1994; Seaman et al., 1995). However, the necessity of dissolution of cementitious phases has been implicated in colloid release also (Gschwend et al., 1990; Ryan and Gschwend, 1990; Ronen et al., 1992).

Transmission electron microscopy (TEM) and analytical electron microscopy (AEM) techniques have been used to investigate the actual physical/spatial associations between clay-size phases in sediment matrices. Bennett et al. (1981) used TEM to determine whether clay fabrics correlated with physico-chemical forces thought to drive the arrangement of particles in marine sediment microstructures. Likewise, TEM has been used to study the nature and orientation of clay particles and location of organic matter in an aggregated, tropical, weathered soil (Santos et al., 1989).

We utilized AEM-TEM and high resolution TEM (HRTEM) to investigate the chemical composition and intimate associations among inorganic phases in samples of a representative aquifer sediment and in colloid samples mobilized from the sediment matrix to gain insight into its inorganic colloid release behavior. In particular, we focused on characterizing the distribution and crystalline nature of the free oxyhydroxides of iron in the interstitial matrix because these iron phases have been hypothesized to be major binding agents of aquifer fines (Ryan and Gschwend, 1990; Ryan and Gschwend, 1992). In addition, we sought to determine if other free oxyhydroxide components, such as amorphous siliceous phases, were present. Our objective was to use the data obtained to determine which phase(s) might play a dominant role in holding the interstitial fines together.

2.2 Methodology

2.2.1 Sediment Characterization

Sediments used in this investigation were collected from a site on the grounds of the Baruch Forest Sciences Institute, Georgetown, S.C. This site has been used in the past to study dissolved organic carbon (DOC) mobility and iron redox chemistry in the shallow, unconfined aquifer that is present there (Liang et al., 1993; McCarthy et al., 1993). This aquifer is part of the Southeastern Coastal Plain aquifer system and is approximately 3 m thick. The aquifer is composed of an iron oxide-coated, fine beach sand deposit of marine origin, approximately 100,000 years old, and is underlain by a 1 m thick clay layer (Williams and McCarthy, 1991). The water table is typically 1 m below the surface at the site.

Sediment was obtained from the C horizon at a depth of 2.0 to 2.4 m during collection of a 5 cm diameter continuous core by hollow stem auger at the site in June, 1993. Drilling fluids were not used during the coring procedure, which utilized a split spoon sampler. The sample was placed in a sealed, plastic bag, and refrigerated for later analysis. The coring took place in an oxidized zone of the aquifer, approximately fifty meters hydraulically upgradient of the study site of Liang et al. (1993).

Size Fractionation. Samples of the sediment were size fractionated for use in characterizing the mineralogy, total iron, free oxyhydroxides of iron and aluminum, and opaline silica present in each fraction. The <1000 μm fraction was separated into five fractions by wet sieving: 1000-500, 500-250, 250-125, 125-63, and <63 μm. Sieving was carried out using polyethylene sieves and artificial groundwater chemically mimicking that found at the site (30 μM Mg; 150 μM Na; 10 μM K; 30 μM Ca; 30 μM SO_4; 190 μM Cl; 30 μM HCO_3; pH=5.2). All solutions used in investigating the physical and chemical properties of the sediment were prepared with Milli-Q purified water (Millipore) and reagent grade chemicals. A <2 μm fraction was obtained by the pipet method from sedimentation of a sample of the <63 μm fraction (Gee and Bauder, 1986).

Heavy mineral separation. Heavy minerals were separated from the size fractions by

density using bromoform. Five to ten grams of each of the fractions were placed in a separatory funnel with 50 ml of bromoform. Material with density greater than 2.89 g/cm^3 was allowed to settle, collected on filter paper, washed with acetone to remove the bromoform, and allowed to air dry.

Mineral characterization. X-ray diffraction (XRD) was used to identify mineral phases in the <2 μm and heavy mineral fractions. Suspensions of the <2 μm fraction were centrifuged at 3400 g for 15 min to create a paste which was applied to glass slides. The heavy mineral fractions were crushed to a powder and applied to glass slides with double sided tape. Samples were CuKα irradiated using a Rigaku RU300 diffractometer operating under the following conditions: 50 kV, 200 mA, 0.5° divergence slit, 0.3 mm receiving slit. The diffraction patterns were obtained in the range 5° to 80° 2θ at a scan speed of 5°/min. Vermiculite was identified after collapse of the 1.4 nm d-spacing upon K-saturation at room temperature. Kaolinite and gibbsite were quantified by thermal gravimetric analysis using a DuPont 9900 Thermal Analyzer (Willington, DE). Kaolinite No. KGa-1 (Ward's Inc., Rochester, NY) was used as a standard for kaolin loss between 450 and 550°C. Gibbsite loss near 300°C was compared to standard gibbsite No. C-730. Samples were heated from room temperature to 1000°C at a rate of 20°C per minute under nitrogen.

Selective extractions. Analyses of total iron in each of the size fractions were performed by digesting 0.1 g samples of each fraction in a teflon beaker with a solution consisting of 0.5 mL aqua regia and 3 mL HF (Thompson and Walsh, 1989). The suspensions were evaporated to dryness over a 12 h period, and residue was redissolved in 4 mL concentrated ultrapure HCl and diluted to 30 mL with water.

Free oxyhydroxides of iron, and associated aluminum, were determined using the method of Ryan and Gschwend (1991). Thirty mL of a 0.05 M Ti(III)-0.05 M citrate-0.05 M EDTA solution at pH 7.0 and 3.33 mL of 1 M HCO_3 were added to 0.1 g of each size fraction in 50 mL centrifuge tubes and shaken for 2 h with a wrist action shaker. The suspensions were centrifuged at 3400 g and a small amount (5 mL) of supernatant was

carefully pipetted off for dilution and analysis. Several samples of the supernatant were also filtered with 0.02 μm syringe filters (Whatman Anotop) prior to dilution for comparison with unfiltered samples. All analyses for iron and aluminum were performed using a Perkin Elmer model 4100ZL graphite furnace atomic absorption spectrometer. Standards were prepared with certified atomic absorption standards (Fisher Scientific).

Amorphous free oxyhydroxides of iron and aluminum were determined using the ammonium oxalate method (Schwertmann, 1964; Jackson et al., 1986). A 1 L solution, containing 567 mL of 0.2 M ammonium oxalate and 433 mL of 0.2 M oxalic acid, was brought to pH 3.0 with NaOH. Twenty five mL of this solution were added to 0.1 g of each size fraction in 50 mL centrifuge tubes. The tubes were immediately wrapped in aluminum foil to exclude light and were shaken for 2 h. The suspensions were centrifuged and approximately 5 mL samples were pipetted off for dilution and analysis.

Amorphous opaline silica was extracted with Tiron (4,5-dihydroxy-1,3-benzene disulfonic acid) using the method of Kodama and Ross (1991). One hundred twenty mL of a 0.09 M solution of Tiron, with 0.05 M Na_2CO_3 and 0.08 M NaOH added to buffer pH at 10.5, were added to 0.1 g of the <63 μm fraction. The samples were heated in a water bath at 80°C for 1 h. Subsamples were passed through 0.03 μm polycarbonate membranes (Nucleopore) and diluted for analysis by graphite furnace A.A. Peerless clay (South Carolina kaolin) (R. T. Vanderbilt Co., N.J.) was used as a standard to ensure that kaolinite was not being dissolved with the method.

Column Experiments to Mobilize Colloids. Column experiments, similar in design and function to those performed by Ryan and Gschwend (1994), were conducted to mobilize inorganic colloids from the Georgetown sediment (see section 3.2.2 in Chapter 3). Approximately 5 g of sediment were flushed with distilled water elevated to pH 9.0 with the addition of NaOH. Turbidity was monitored in line with a turbidimeter (Ratio X/R, Hach). Aqueous samples of the effluent were collected for later AEM-TEM analysis.

2.2.2 Electron Microscopy

Sample preparation. Because the focus of this study was to observe undisturbed associations between the submicrometer grains in the sediment matrix, care was taken to maintain the natural state of the sediment in the preparation of samples for transmission electron microscopy. To circumvent the need to desiccate our samples prior to embedding and to insure more adequate penetration of the embedding resin, an innovative embedding medium, Nanoplast® (Polysciences, Inc.), was used. Because Nanoplast® is a water-soluble resin, there is no need to dry out the sample beforehand (Frösch and Westphal, 1989). Indeed, even aqueous samples have been directly embedded in the resin to view such phenomena as colloidal associations in lakewater samples (Perret et al., 1991; Leppard, 1993). The polymerization stage does involve a heating/desiccation step, but sample alteration due to dehydration and shrinkage is thought to be minimal due to the production of water during the polymerization process (Bachhuber and Frösch, 1983).

The resin was prepared using 1.0 g Nanoplast® and 0.0035 g hardener. This recipe was found to alleviate brittleness and fracturing without sacrificing strength. Two hundred μL of the resin was added by syringe to a compartment in a special mold (BEEM, Polysciences, Inc.), and approximately 0.01 g of moist Georgetown sediment was taken from storage and placed in the resin. For colloidal samples released from the sediment, 50 μL of aqueous sample collected from column studies were immediately mixed with 150 μL of resin in the mold. The molds were then placed in a desiccator and the desiccator was placed in an oven set at 40°C for 48 h. Afterward, the molds were taken out of the desiccator and placed in the oven again, this time at 60°C for 48 h.

Ultramicrotomy was performed on trimmed faces of the samples using a DuPont Sorvar MT5000 Ultramicrotome at a speed of 0.5 mm/sec and a 45° diamond knife (Diatome). Fifty to 70 nm thick sections (thickness indicated by grey to silver color of thin sections in reflected light) were collected on 3 mm copper grids coated with formvar. Some of the grids were coated with a 0.10 nm thick carbon coating to prevent charging when under

the electron beam.

Microscopy. Microtomed sections were examined using three electron microscopes. A JEOL 200CX, operating at 200 kV, was used for initial examination of all sections. The JEOL has a 0.24 nm point-to-point resolution and a coefficient of spherical aberration (C_s) of 1.2 mm. A Topcon 002B high resolution microscope (HRTEM) (200 kV, 0.18 nm point-to-point resolution, C_s= 0.4 mm) was used to obtain lattice fringe images of crystalline areas and to investigate crystalline/amorphous material associations in the sediment. Lattice spacings were calculated from lattice fringe counts measured directly from the high resolution electron micrographs with a Peak Anastigmat® micrograph viewer with a magnification of four times. Amorphous areas were recorded by focusing and stigmating the HRTEM on an area and quickly translating to a new area of specimen and obtaining micrographs within one minute or less to minimize radiation induced artifact. A VG HB603 scanning transmission electron microscope (STEM) (VG Microscopes, East Grinstead, UK), equipped with a energy dispersive x-ray (EDX) spectrometer (Link Analytical), was used to obtain elemental maps of selected areas in the sediment. The STEM was operated at 250 kV and has a 0.30 nm point-to-point resolution and a C_s = 4.5 mm. The beam width in the scanning mode is approximately 5.0 nm. Maps containing spatial distributions (as intensity per pixel) of selected elements (Si, Al, Fe) in the sections were obtained at a discretization of 128 by 128 pixels. The intensity data obtained from the EDX probe is directly proportional to the number of atoms of a particular element in the volume (probe area multiplied by the section thickness) analyzed. The EDX probe is operated with a 1 nm diameter. However, beam broadening caused by the thin section thickness expands the probe to a 2 to 4 nm diameter for a 50 nm thick sample (Garrett-Reed, 1995). Thus, the spatial resolution limit of a pixel in an EDX map is approximately 3 nm by 3 nm. In an image optically magnified to 50,000 times (1 cm= 200 nm), the elemental information contained in one pixel is gathered from an area of approximately 12 nm by 12 nm in the sample. For an image optically magnified to 200,000 times (1 cm= 50 nm), the information contained in each pixel is obtained from an area of

approximately 3 nm by 3 nm. Finally, a Cambridge Stereoscan 240 scanning electron microscope (SEM) equipped with an EDX spectrometer (Link Analytical) was used to study bulk sediment samples under low magnification. These samples were embedded in Spurrs® epoxy resin and sectioned with a diamond saw (Holmén, 1994).

Image analysis software (Aldus Photostyler 2.0) was used to colorize and superimpose elemental map files obtained from the VG STEM in order to elucidate spatial relationships among elements. Each element map was assigned a particular hue: green for Si; red for Al; and blue for Fe. Superposition of maps produces new colors if spatial comapping occurs among the elements. For example, yellow pixels will be produced if Si (green) and Al (red) comap, purple appears if Fe (blue) and Al comap, and white pixels occur if all three elements comap. Another software package (Image Pro Plus) was used to extract intensity data from specific areas of the element maps or along traverses across maps. The extracted data was used to calculate elemental mole ratios in the selected pixels using the appropriate Cliff-Lorimer (K) factors. These factors were experimentally determined with standards by the National Institute of Standards and Technology (Gaithersburg, MD). Error introduced by not correcting for the particular history of the spectrometer attached to the HB603 is expected to be $\leq$ 5% (Bell, 1996).

2.3 Results and Discussion

2.3.1 Sediment Characterization

The sediment is composed predominantly of medium to fine sand (**Table 2.1**). The <63 μm fraction is 12% by weight of the sediment, and the clay-size (<2 μm) material makes up approximately 2.5% by weight of the sediment. The <63 μm fraction has a low organic carbon content, typically only 0.6% by weight (Holmén and Gschwend, 1997).

The mineralogy of the sediment is dominated by quartz, with minor amounts of feldspar and mica in the sand- and silt-size fractions. Ilmenite ($FeTiO_3$) and rutile (TiO_2) are the chief heavy minerals present. These heavy minerals are present mostly in the fine sand-

Table 2.1. Distribution of grain size fractions, heavy minerals, and Fe and Al associated with free oxyhydroxide phases

Size Fraction (μm)	wt. %	Heavy Min. wt. %	Total Fe (μmol/g)[a]	TICEB Fe (μmol/g)[b]	AOD Fe (μmol/g)[c]	TICEB Al (μmol/g)[b]
Bulk		na[e]	180 (15)[d]	180 (7)	18 (1)	40 (28)
>1000	5	na	na	13 (9)	<1	<1
1000-500	18	na	8.8 (1.8)	9 (2)	<1	<1
500-250	26	<0.1	9.3 (0.8)	11 (8)	<1	<1
250-125	38	0.3	9.3 (0.3)	14 (4)	1.4 (1)	<1
125-63	1	6	440 (17)	99 (36)	12 (2)	18 (10)
<63	12	2	1360 (95)	1250 (166)	64 (2)	320 (30)

[a]Determined by digestion with HF-HCl-HNO_3 (Thompson and Walsh, 1989)
[b]Determined by Ti-Citrate-EDTA-HCO_3 method (TiCEB) (Ryan and Gschwend, 1991)
[c]Determined by ammonium oxalate method (AOD) (Jackson, et al., 1986)
[d]One standard deviation, based on 3 replicates, enclosed in parentheses
[e]not analyzed

to silt-size fractions (**Table 2.1**). Finely divided iron oxyhydroxides and clay minerals fill the interstitial voids between sand-size grains. Readily detected minerals include goethite (α-FeOOH), kaolinite, gibbsite ($Al(OH)_3$), quartz, and vermiculite in the <2 μm fraction (**Figure 2.1**). Minor components such as lepidocrocite may also be present, as suggested by the small peak at 14° 2θ (6.3 Å d spacing) (**Figure 2.1**). Kaolinite is the largest component of the clay-size (<2 μm) fraction (40 to 45% by weight), typical for sediments in the Southeastern Coastal Plain (Dixon, 1989). Gibbsite constitutes approximately 4% to 8% of the <2 μm fraction. The measured Al concentrations ($9.3 \times 10^{-8} \pm 4.6 \times 10^{-8}$ M) in groundwater at the site were indistinguishable from expectations assuming gibbsite dissolution equilibrium (7.9×10^{-8} M), calculated using a solubility constant (K_s) equal to $10^{-33.5}$ and a pH of 5.2 (Morel and Hering, 1993).

Most of the Fe in all of the size fractions comprises Fe incorporated in free iron oxyhydroxides, the largest amount being in the <63 μm fraction (**Table 2.1**). The small amounts of Ti(III)-extractable Fe in the larger size fractions probably represent iron oxyhydroxide coatings which were not entirely removed from the quartz grains during wet sieving. The total Ti(III)-extractable Fe (1250 μmol g^{-1}, **Table 2.1**), minus the amount of ammonium oxalate-extractable Fe (64 μmol g^{-1}, or 5% of Ti(III)-extractable Fe, **Table 2.1**), equals the amount of Fe incorporated in crystalline free iron oxyhydroxides (1190 μmol g^{-1}). To calculate the weight percent crystalline free iron oxyhydroxides in the <63 μm fraction, the chemical formula FeOOH (representing goethite and lepidocrocite) was used. On this basis, crystalline iron oxyhydroxides make up approximately 10% by weight of the <63 μm fraction of the Georgetown sediment.

The values for Ti(III)-extractable Fe and total Fe in the <63 μm fraction were nearly the same (**Table 2.1**), although the slightly larger amount of total Fe could have included some structural Fe released from heavy minerals (e.g., ilmenite) and Fe-substituted kaolinite. Heavy mineral content was highest in the 125-63 μm fraction, coinciding with a total Fe content that was over four times more than the Ti(III)-extractable Fe (**Table 2.1**).

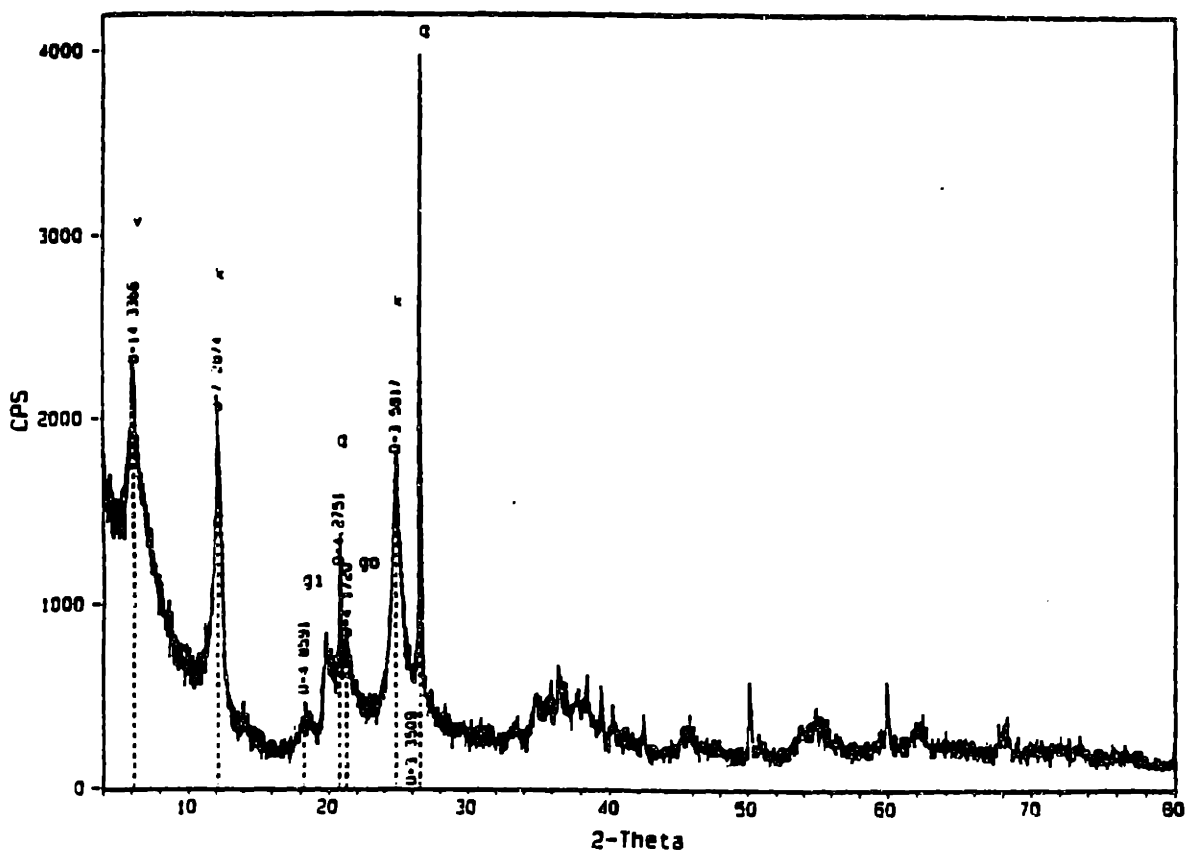

Figure 2.1: XRD pattern of the <2 μm size fraction of the Georgetown sediment. v=vermiculite, k=kaolinite, gi=gibbsite, go=goethite, q=quartz.

Total Al was measured only in the <63 μm fraction (4380±100 μmol g^{-1}, data not shown in **Table 2.1**). Ti(III)-extractable Al was small in each of the fractions except for the <63 μm fraction (320 μmol g^{-1}, **Table 2.1**). Ammonium oxalate-extractable Al was detected only in the <63 μm fraction (46±2 μmol g^{-1}, data not shown in **Table 2.1**). Data presented below (see section *Iron Character and Distribution*) indicate that most of the Ti(III)-extractable Al was associated with the goethite.

The data in **Table 2.2** provides some measure of the vertical heterogeneity present in the sediment profile. These data were obtained from analysis of an intact core collected at the same time the discrete sample we utilized in the AEM-TEM analysis was collected. Size fractionation, Ti (III)-extractable Fe, ammonium oxalate-extractable Fe, and mineralogy of the <2 μm size fraction were determined for selected horizon increments (Ulery, unpublished data).

2.3.2 Electron Microscopy

General Morphology. Silt- and clay-size mineral materials filled the voids between the sand-size quartz grains in the Georgetown sediment (**Figure 2.2**). The roughly 200 μm diameter quartz grains were separated by spaces filled with mineral particles too small to be resolved at the magnification used in **Figure 2.2**. Fragments of quartz, tens of micrometers in diameter, were incorporated in the interstitial matrix as well. It is the nanometer-scale associations among these phases that we investigated using AEM-TEM. SEM-EDX analysis of the matrix indicated the presence of abundant Si, Al, and Fe, as expected for a kaolinite- and goethite-rich matrix.

Clay Mineral Arrangement. Clay minerals (kaolinite, vermiculite) present in the Georgetown sediment made up a large portion by weight of the <2 μm fraction. In the Georgetown matrix, stacked assemblages, or "books", of face-associated kaolinite particles, tens of nanometers thick and up to 100 to 200 nm long, were prevalent (**Figure 2.3**, point a). These books were assembled in domains up to several micrometers wide and several micrometers long, extending through the matrix in a chain-like manner. This type of clay particle arrangement has been observed in other "undisturbed" sediments (Collins and McGown, 1974; Bennett et al., 1981).

Table 2.2: Selected properties of some horizons of the Georgetown, SC soil and sediment[1]

Horizon	Depth (cm)	Sand (% w/w of total)	Silt	Clay	TICEB Fe[2] (mg g^{-1})	AOD Fe[3] (mg g^{-1})	Mineralogy[4]
A	0-11	92.6	6.2	1.2	1.2	0.4	K, HIV, Q
E2	18-31	88.8	8.1	3.1	1.3	ND[5]	ND
Blt	31-50	77.3	8.8	13.9	6.7	1.1	K, HIV, Gb, Gt
BC	148-163	88.0	3.9	6.1	8.5	ND	K, V, Gb, Gt
C2	263-274	94.4	2.4	3.2	13.9	1.3	K, V, M, Gb, Gt, L
C8	319-328	96.9	1.4	1.7	1.6	0.4	K, V, M, Gb, Gt

[1]taken from Ulery, unpublished data.
[2]Ti(III)-citrate-EDTA-bicarbonate method of Ryan and Gschwend (1991)
[3]ammonium oxalate method (Jackson et al., 1986)
[4]determined by x-ray diffraction of the <2 μm size fraction, K= kaolinite, HIV= hydroxy interlayer vermiculite, Q= quartz, Gb= gibbsite, Gt= goethite, V= vermiculite, M= mica, L= lepidocrocite
[5]ND= not determined

Figure 2.2: SEM backscatter image of the mineral material filling the interstitial matrix (marked M) between approximately 200 μm diameter quartz grains and smaller quartz fragments (marked Q). The scale bar represents 100 μm.

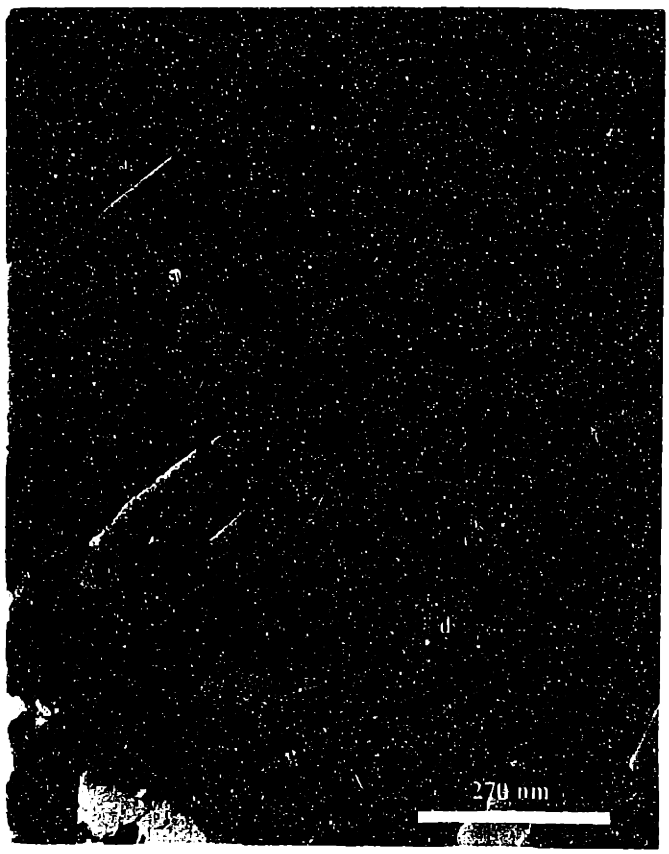

Figure 2.3: TEM image of clay associations in the Georgetown matrix. Points marked as the following: (a) kaolinite book with face-face contacts, (b) void possibly created by ultramicrotome tearing, (c) edge-face contact with boundary marked by arrows, (d) books oriented with faces at right angles or obliquely to the image plane, (e) suspected naturally occurring void space. The scale bar represents 270 nm.

Edge-face contacts represented boundaries where domains of clay books were rotated at right angles or obliquely to the domains observed "on edge" (**Figure 2.3**, point c and marked with arrows). It was difficult to discern individual particles in these domains due to the low contrast these areas exhibited (**Figure 2.3**, point d). Possibly, intergrowth among particles could contribute to difficulty in identification of book boundaries (Collins and McGown, 1974). Voids, 50 nm or less in diameter, appeared within these domains and were suspected to be undisturbed pore spaces representative of the matrix (**Figure 2.3**, point e). The separations between some books in our samples (see **Figure 2.3**, point b) may have been due to tearing that occurred as a result of the microtoming process (Smart and Tovey, 1981).

Iron Character and Distribution-Crystalline Iron. Iron-rich zones in thin sections of the Georgetown matrix were easily observed in the TEM due to the stronger contrast and morphological differences they exhibited versus the clays around them. These iron-rich aggregates were typically subcircular in profile and approximately 500 nm in diameter, as can be seen in the Si, Al, and Fe composite STEM-EDX map of two representative aggregates (**Figures 2.4a,b**). Higher magnification revealed that these iron-rich zones were composed of spheroidal subunits approximately 5 to 10 nm in diameter, and analysis of electron diffraction patterns taken from these areas confirmed the presence of polycrystalline goethite. In addition, lattice fringe images with spacings 4.2 Å apart, representing the [110] lattice plane spacing of goethite (4.17 Å spacing), were recorded in these aggregates (**Figure 2.5**, subhorizontally oriented set of fringes). The subvertically oriented set of lattice fringes, spaced 3.6 Å apart, probably represents the [120] lattice spacing of goethite (3.38 Å) observed off of its zone axis or perhaps the [002] lattice spacing of kaolinite (3.57 Å) underlying the goethite (**Figure 2.5**). However, an electron diffraction pattern was not recorded for this particular area of the specimen to determine which mineral was represented by the 3.6 Å spaced lattice fringes. All of the goethite aggregates observed in the matrix were relatively isolated and were separated by hundreds of nanometers from each other so that only approximately 10 aggregates were found per 100 μm^2 of matrix.

Figure 2.4 appears on the next page

Figure 2.4: STEM-EDX Si, Al and Fe composite map of two representative goethite aggregates (next page). Green pixels indicate presence of Si; red, Al; and blue, Fe. Yellow pixels indicate comapping of Si and Al and represent the clay minerals. Purple pixels indicate association of Al with the goethite. The red particle is probably gibbsite ($Al(OH)_3$). The scale bar represents 400 nm. Each pixel represents approximately 12 x 12 nm of sample area.

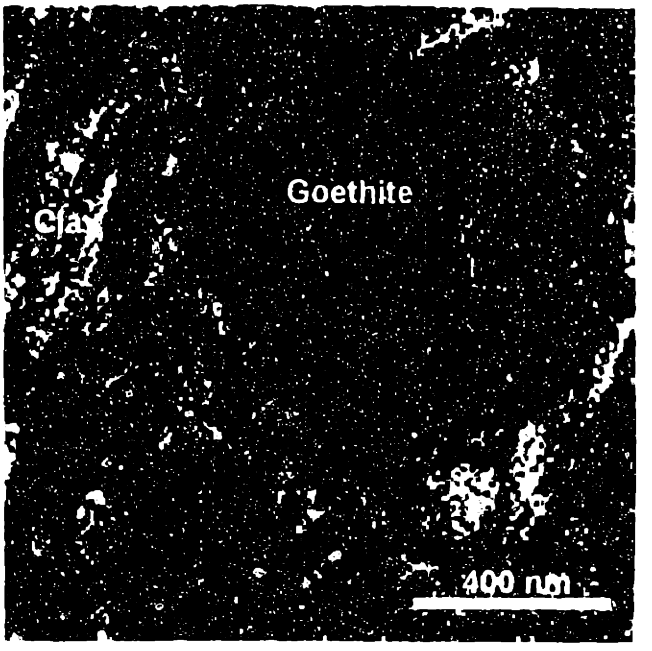
Goethite
400 nm

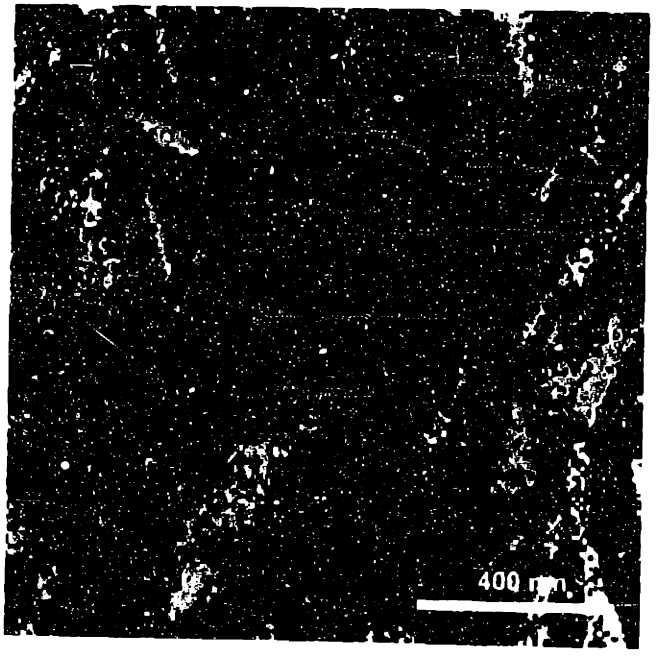
400 nm

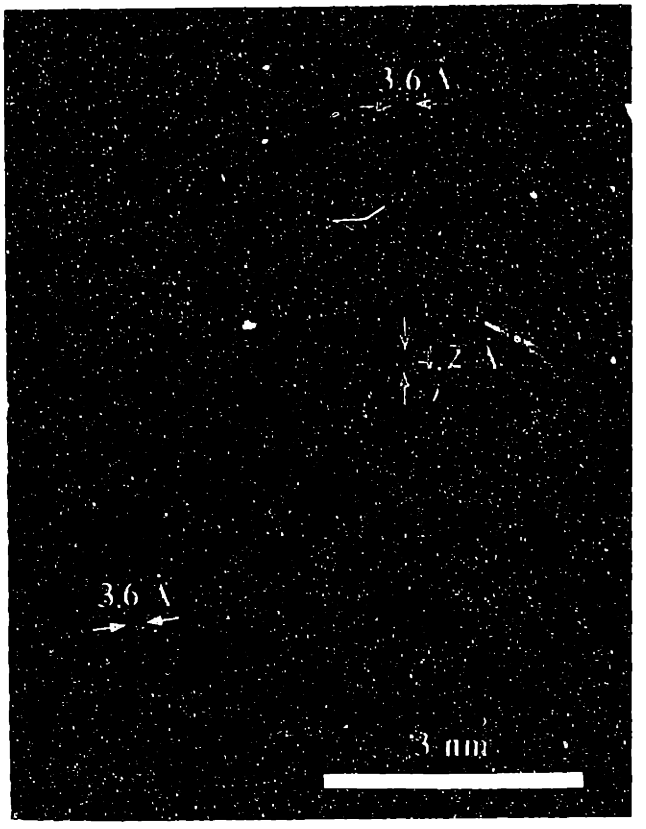

Figure 2.5: HRTEM lattice fringe image of goethite. The subhorizontally oriented fringes have spacings 4.2 Å apart and indicate the [110] lattice planes of goethite. The subvertically oriented fringes spaced 3.6 Å apart possibly represent the [120] lattice spacing of goethite (3.38 Å) or the [002] lattice planes of kaolinite (3.57 Å), which underlies the goethite. The scale bar represents 3 nm. Magnification is 6,500,000x.

A significant amount of Al was found to be associated with the goethite aggregates (**Figure 2.4**). The mole fraction of Al/Fe, calculated using Al and Fe intensity data within the boundaries of the goethite aggregates, was found to be 0.24±0.08 (n= 5 aggregates). The Al/Fe mole ratio determined by STEM-EDX corresponds well to that calculated (0.23 Al/Fe) using the amount of Ti(III)-extractable Al for the <63 fraction (320 μmole g^{-1}, **Table 2.1**) minus the ammonium oxalate-extractable Al (46 μmole g^{-1}). The calculations assume the total Ti(III)-extractable Al, less the oxalate- extractable Al, is associated with the Fe (1190 μmole g^{-1}) in goethite.

Iron Character and Distribution-Amorphous Iron. In addition to the iron signal representing the goethite aggregates, we also detected a population of Fe dispersed relatively homogeneously throughout the clay-dominated matrix (**Figure 2.6**). This population of iron consisted predominantly of particles on the order of, or less than, the pixel size (12 nm) in **Figure 2.6** (examples marked a). Higher magnification STEM-EDX Si, Al, and Fe composite maps indicated that much of this Fe was directly associated with the surfaces of individual clay particles (**Figure 2.7**), perhaps as gel-like coatings. It appeared that the Fe (**Figure 2.7**, blue to purple, marked Fe) was present as approximately a 10 nm thick medium positioned between the faces of two clay books (**Figure 2.7**, yellow, marked K). Some larger, more discrete particles, or aggregates of particles, tens of nanometers in diameter, were also represented by the dispersed Fe signal (**Figure 2.6**, examples marked b).

We believe this dispersed Fe signal represents much of the ammonium oxalate-extractable Fe (64 μmol g^{-1}) in the <63 μm fraction. This Fe may be present as amorphous iron oxyhydroxides, Fe ions, and/or Fe polymers on the clay mineral surfaces. The Al/Fe mole ratio for portions of this dispersed Fe phase was found to be 0.44± 0.14 (n= 10 particles) using Al and Fe intensity data from the centers of particles large enough to observe discernable boundaries (i.e., particles such as those marked b in **Figure 2.6**). This ratio is lower than the Al/Fe mole ratio (0.72) calculated using the ammonium oxalate-extractable Al (46 μmole g^{-1}) and Fe (64 μmol g^{-1}) data for the <63 μm fraction, possibly due to the bias of

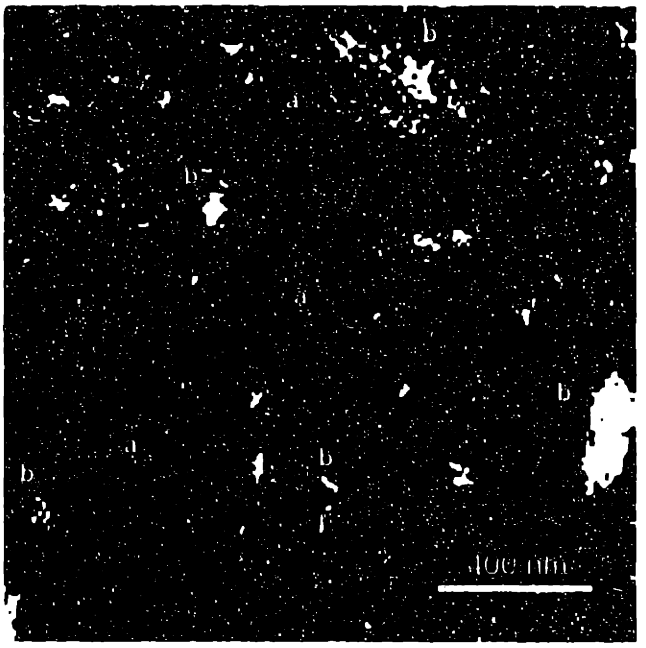

Figure 2.6: STEM-EDX map of iron distributed among the clay particles. The fainter population of pixels (marked a) represent amorphous iron oxyhydroxides, adsorbed Fe, and possibly structural Fe in the clays at the scale of approximately 12 nm or less (the sample area represented by each pixel), whereas the particles marked "b" likely represent larger particles of amorphous iron oxyhydroxide tens of nanometers in diameter. The scale bar represents 400 nm.

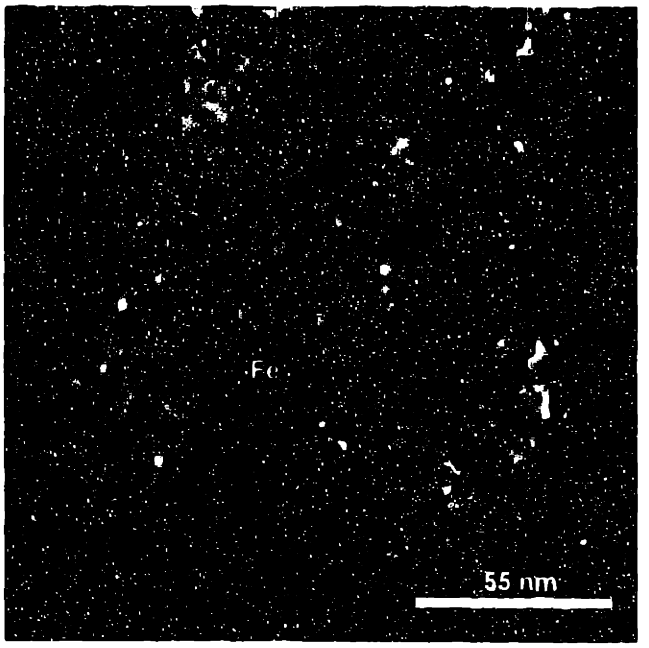

Figure 2.7: STEM-EDX Si, Al and Fe composite map of the associations between the dispersed, amorphous iron oxyhydroxide phase (marked Fe) and kaolinite particles (marked K). The 10 nm thick iron phase (blue) lies between two clay books (yellow). The scale bar represents 55 nm. Each pixel represents approximately 3 x 3 nm of sample area.

sampling only the larger particles. However, this ratio is much higher than the Al/Fe mole ratio calculated for the crystalline oxyhydroxides (0.23, see section on crystalline iron above), and supports our interpretation that the homogeneously dispersed Fe signal mostly represents the ammonium oxalate-extractable Fe phases.

A portion of the homogeneously dispersed Fe signal could represent structural Fe incorporated in kaolinite and vermiculite as well. Structural Fe incorporated in kaolinite from South Carolina sediments has been found to be approximately 1.0% by weight (Jefferson et al., 1975). As the percent by weight of kaolinite in the Georgetown <2 μm size fraction is at least 40%, the amount of structural Fe present in the matrix therefore could be approximately 0.4% by weight. Such structural Fe would probably be represented by discrete Fe signals 3 nm or less in dimension and would be indistinguishable from simple adsorbed Fe or discrete Fe polymers in the STEM-EDX maps.

Evidence for an Amorphous, Siliceous Phase. Observation of sample sections under HRTEM revealed areas among the clay domains which appeared amorphous in nature (**Figure 2.8**). Lattice fringes, spaced 2.5 Å apart, appear in the central portion of the image (**Figure 2.8**) and likely correspond to the [200] (2.50 Å) or the [130] (2.54 Å) lattice plane spacing of kaolinite. A phase lacking periodicity surrounds these fringes and appears to cover more underlying crystalline material. These amorphous areas were too large and continuous to be attributed to the dispersed amorphous Fe phase. They lacked the contrast of the Fe-rich phase as well.

STEM-EDX evidence suggested that a siliceous phase was responsible for these amorphous areas, as an excess of Si was observed in parts of the matrix (**Figure 2.9a**). Of the 128 data points from this representative traverse across a distance of approximately 1.5 μm in the matrix, 25% indicated essentially infinite Si/Al ratios (points along the y axis of **Figure 2.9a**). Spatially, these Si-enriched areas corresponded to dimensions several tens of nanometers wide in the mapped traverses. Other points fell along a line representing a 1:1 Si/Al ratio and indicate the presence of kaolinite (**Figure 2.9a**). The points which fell on the

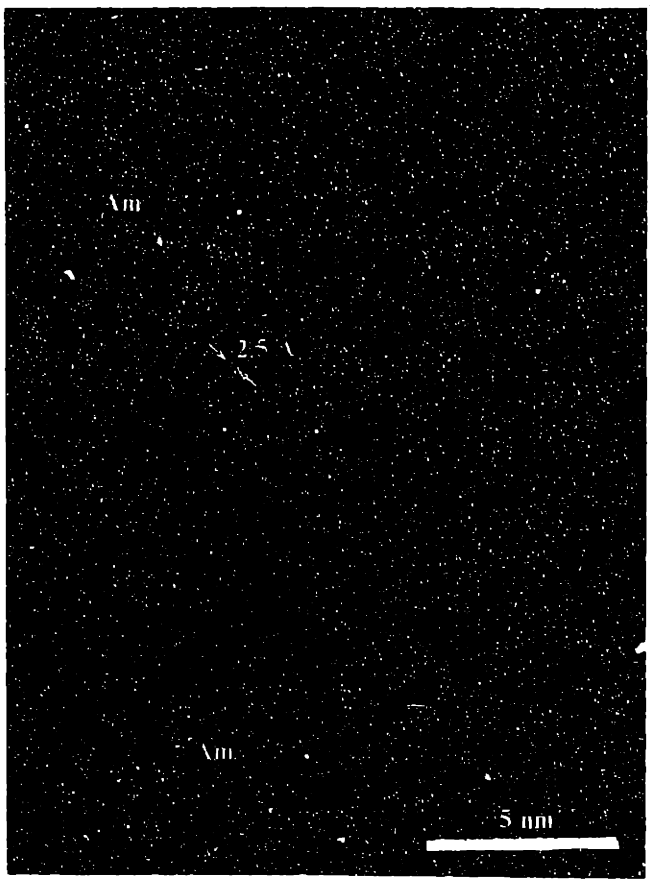

Figure 2.8: HRTEM image of a crystalline phase associated with an amorphous phase. Lattice fringes spaced 2.5 Å apart possibly represent the [200] (2.50 Å) or the [130] (2.54 Å) lattice plane spacing of kaolinite. The fringes are surrounded or partially coated by an amorphous phase (marked Am). The scale bar represents 5 nm. Magnification is 4,970,000x.

x axis represented Si-lacking phases and probably corresponded to the dispersed, amorphous Fe/Al-rich phase or gibbsite particles. The points representing voids (intensity values of zero for both Si and Al) were not plotted. The Si-rich areas represented in the traverse in **Figure 2.9a** could be observed in the STEM-EDX Al, Fe, and Si composite map from which the traverse was taken (**Figure 2.10**). Note the abundance of green pixels in **Figure 2.10**. These pixels represent a Si-rich phase that does not comap with either Al or Fe (**Figure 2.10**).

When data from traverses across other areas of matrix were plotted, Si/Al ratios fluctuating closely about the expected value of 1:1 for kaolinite were observed (**Figure 2.9b**). The average Si/Al ratio was 1.2 ± 0.5 for this 1.5 μm traverse. The few points representing Si/Al ratios of 2:1 to 3:1 possibly indicated interspersed vermiculite, as Si/Al ratios in the range of 1.5:1 to 5.6:1 are commonly observed in relatively unweathered vermiculite (Douglas, 1989). Vermiculite was identified by XRD in this sediment (**Figure 2.1**).

Confusion with quartz can not explain the infinite Si/Al ratios observed, as quartz grains observed in sections were microscopically obvious at approximately 1 to 2 μm and were too large to contribute to the ubiquitous Si that mapped with dimensions on the order of tens of nanometers in these areas. Possible silica contamination due to grinding of quartz grains during ultramicrotoming was ruled out, as EDX analysis of the Nanoplast® near the boundaries of the matrix revealed very little background Si.

A hydrous alumino-silicate exhibiting no long range order would also produce an electron amorphous "coating" if associated with the kaolinite and vermiculite in the matrix. Allophanic phases, however, are considered extractable by ammonium oxalate (Wada, 1989). Only 46 μmols g^{-1} Al (0.1 % by weight) were extracted from the <63 μm fraction, and this amount of Al appeared, for the most part, to be associated with the amorphous free Fe phase.

We suggest that the phase represented by the infinite Si/Al ratios is a form of opaline silica, probably of biogenic origin. Biogenic opal has no long range order and is a common constituent in forested soils, as it is a product of plant processes (Wilding and Drees, 1973; Wilding et al., 1979; Drees et al., 1989). Because the Georgetown sediment samples were

Figure 2.9 appears on the next page

Figure 2.9: Variation in Si and Al in two different traverses across matrix. (a) (next page) Si is plotted versus Al for the first traverse of 1.5 μm. Three different populations of points are present. Points falling along the y axis indicate a siliceous phase with essentially infinite Si/Al ratios. Points falling along the dashed line representing a 1:1 Si/Al ratio indicate kaolinite. Points along the x axis indicate Si-lacking phases, probably the dispersed, amorphous Fe-Al phase, or gibbsite. (b) (next page) Si/Al ratio is plotted against the x coordinate for the second 1.5 μm traverse. The majority of points oscillate around a mean Si/Al ratio of 1.2±0.5, and indicate kaolinite particles. Si/Al ratios of 2:1 to 3:1 possibly represent vermiculite. For each plot, each data point represents intensity data taken from an area of approximately 12 x 12 nm in the samples.

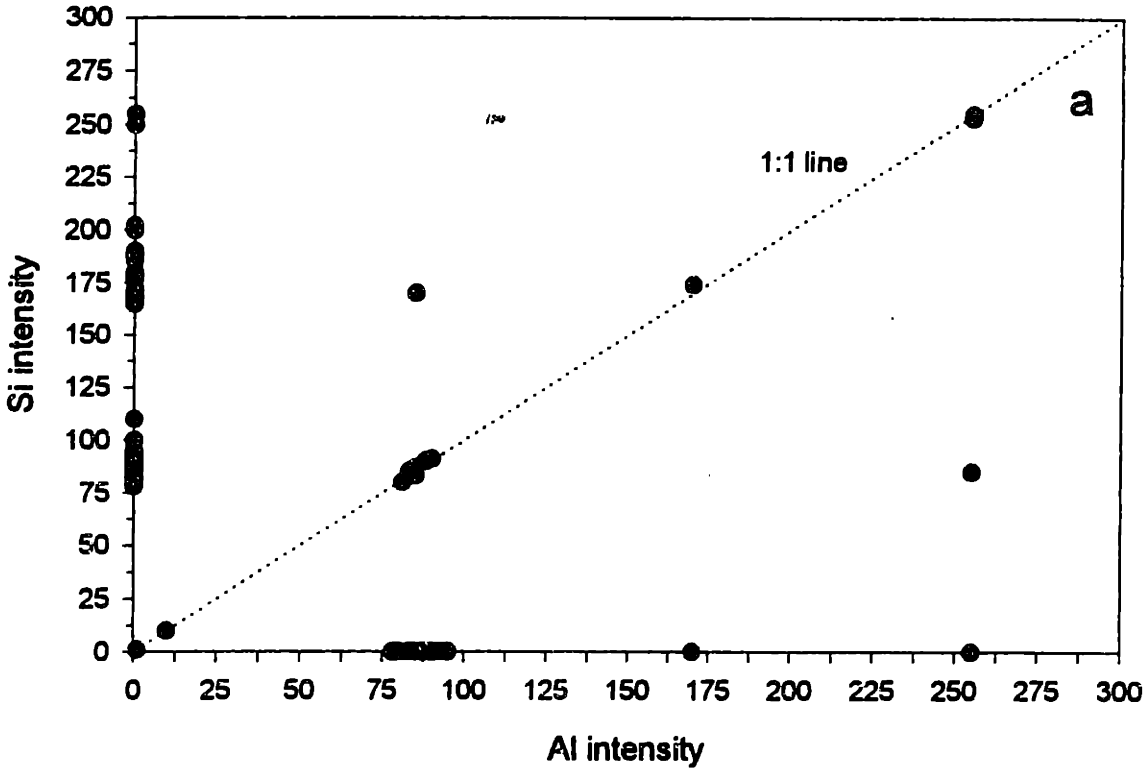
a
1:1 line
Si intensity
Al intensity
0
25
50
75
100
125
150
175
200
225
250
275
300

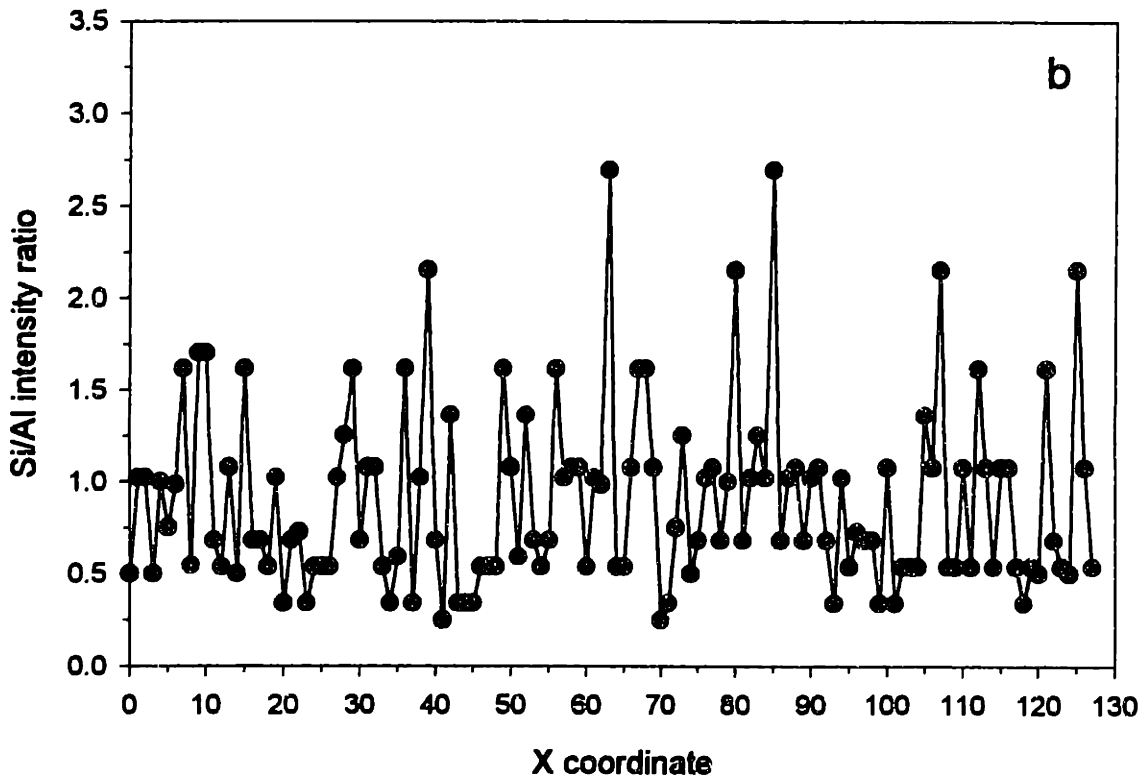
b
Si/Al intensity ratio
X coordinate
0.0
0.5
1.0
1.5
2.0
2.5
3.0
3.5
0
10
20
30
40
50
60
70
80
90
100
110
120
130

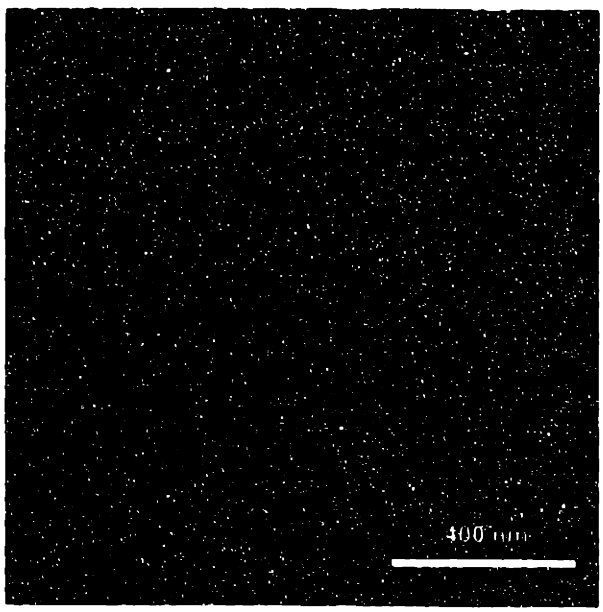

Figure 2.10: STEM-EDX Fe, Al, and Si composite map of the area in which the traverse in **Figure 2.9a** was taken. Note the abundance of green pixels, indicating the presence of a Si-rich phase which does not comap with Al or Fe. The scale bar represents 400 nm.

recovered from the C horizon of a heavily forested soil, it is reasonable to conclude that an opaline silica phase is responsible, at least in part, for the amorphous character of portions of the matrix observed under HRTEM. Siliceous, cementitious coatings on and between clay particles have been observed previously in sediment and shale samples using AEM-TEM (Banfield et al., 1991; Lee et al., 1991). Tiron extraction of the <63 μm fraction revealed 1.2 ± 0.6 x 10^{-3} moles Si g^{-1} (based on three replicates), indicating that opaline silica constituted approximately 10% by weight of this size fraction. This calculation assumed the opal contained 18% by weight water (Kodama and Ross, 1991). In addition, groundwater composition data support the conclusion that this Si phase is opal, as dissolved Si concentrations were found to be 14±2 ppm for samples from three different wells screened near the depth at which the sediment sample was collected. The solubility of opal can range from 0.5 to 10 ppm, depending on the amount of adsorbed iron and aluminum (Wilding et al., 1979; Bartoli and Wilding, 1980).

2.3.3 Implications for Colloid Mobilization

From the associations observed among the clay minerals, the iron oxyhydroxide phases, and the siliceous phase in the STEM-EDX and TEM/HRTEM images, some general hypotheses of the binding forces acting in the Georgetown matrix can be constructed. Electrostatic interactions can help to explain the edge-face associations observed among the clay "books" (**Figure 2.3**). The interparticle associations among kaolinite books could be controlled by the differences in surface charge between the edges, which have a variable charge dependent on pH, and the faces, which have a constant negative charge (vanOlphen, 1977; Newman and Hayes, 1990). Because the pH_{pzc} of kaolinite edges occurs around a pH of 7.0 (Herrington et al., 1992), the faces and edges of kaolinite plates can possess opposite charge. In theory, electrostatic considerations would dictate a "card house" structure in which individual clay plates are associated face-to-edge to limit electrostatic repulsion (vanOlphen, 1977). In the Georgetown sediment, these edge-face associations were observed among the aggregates of clay platelets, or books (**Figure 2.3**). High electrolyte concentration diminishes

double layer repulsive forces among clay platelets so that attractive van der Waals forces can allow the similarly charged surfaces of the clays to assemble in the domains of face-associated books observed in the Georgetown sediment (**Figure 2.3**) (Collins and McGown, 1974; Yariv and Cross, 1979). Because the Georgetown sediment was deposited in a marine beach environment, it is likely that saline or brackish pore fluids promoted this arrangement as the clays were emplaced after the beach sand was deposited and fines were winnowed out. Most kaolinite in the southeastern Coastal plain sediments is thought to be inherited, or emplaced by infiltration after primary deposition of the beach sand (Dixon, 1989).

Aggregation of the clay books could be promoted by the presence of a net positively charged phase which serves as an electrostatic intermediary and diminishes repulsive forces among the faces of juxtaposed clay booklets. It is also possible that the intermediary phase could promote aggregation among the clay books through the creation of bonds between itself and the surface functional groups of the clay books. In either case, the distribution of this phase among the clay books would be an important factor in its ability to act as a binding agent and hold the fines together.

The TEM and STEM-EDX data presented above indicate that the goethite phase is manifested in the Georgetown sediment as discrete, isolated aggregates (**Figure 2.4**). This distribution pattern, observed in the clay fractions of some tropical soils as well (Greenland et al., 1968; Jones et al., 1982; Schwertmann and Kampf, 1985), would render goethite ineffective as an electrostatic or cementitious binding agent in the Georgetown sediment even though it is approximately 10% by weight of the <63 μm size fraction and makes up 95% of total Ti(III)-extractable Fe. Rather, it appears that the dispersed, amorphous iron oxyhydroxide phase (**Figure 2.6**), which represents only 5% of total Ti(III)-extractable Fe, serves as an intermediary among the clay books (**Figure 2.7**). Although the dispersed Fe phase is only 0.4% by weight of the matrix material, minor amounts (0.1% to 1% by weight) of iron polycation phases have been shown to promote effectively aggregation among fine-grained clay particles (Oades, 1984). Indeed, Deshpande et al. (1968), found that removal of

the majority of the free iron oxides thought to occur as discrete particles in a variety of soils had little effect on the aggregative properties of the soils. In addition, Fe phases of low crystallinity have been shown to be more effective at aggregating soil fines than crystalline phases such as goethite and hematite (Schahabi and Schwertmann, 1970). The reason for the greater effectiveness of the Fe phases of lower crystallinity probably lies in their larger, more reactive surface areas, which can differ in surface area from goethite by as much as ten times (Schindler and Stumm, 1987; Schwertmann and Taylor, 1989).

The iron which precipitated as the goethite and amorphous iron oxyhydroxides may have originated from dissolution of iron-containing heavy minerals present in the grains deposited primarily. Ilmenite ($FeO \cdot TiO_2$) was observed in x-ray diffraction patterns of the heavy mineral fraction of the Georgetown sediment. Ryan and Gschwend (1992) believed that release and redistribution of Fe from the heavy minerals present in the Cohansey sand could account for much of the Fe deposited in oxidized layers of that sediment. The relatively high Al/Fe mole ratio of the amorphous iron oxyhydroxide phases (0.72) may indicate that the Fe and Al which constitutes these amorphous phases may have a different source than the goethite aggregates, which had an Al/Fe mole ratio of 0.23. The Fe and Al making up these amorphous phases may have been transported from surface soils by complexation with plant exudates, much like the Si thought to makeup the amorphous siliceous phase. Because Al is considered to be strongly bound by plant exudates like oxalic acid, a higher Al/Fe mole ratio may be expected in such sources (Sjörberg and Öhman, 1985).

Thus, the free iron oxyhydroxide phase associations observed in the Georgetown sediment may not be typical of a variety of sediments comparable in mineralogy and weathering history. The importance of correctly assigning the function of intermediary predominantly to that of the amorphous iron phase, rather than to a crystalline phase such as goethite, lies in consideration of the differing pH_{pzc}'s, solubilities, and site densities of the two phases. By assuming goethite to be the active intermediary, one would incorrectly estimate the amount of surface-active solute needed to reverse surface charge or the amount of free iron

oxyhydroxide needed to be dissolved in order to induce mobilization of mineral colloids.

The AEM-TEM data suggest that at least two types of mechanisms serve to bind the Georgetown matrix (**Figure 2.11**). The homogeneously dispersed, amorphous Fe phase might operate as an intermediary among the clay books, as discussed above. This amorphous Fe phase might reduce repulsive electrostatic interactions among the clay books by serving as an net positively charged intermediary (**Figure 2.11a**). The positioning of the amorphous iron phase between the faces of the kaolinite books in **Figure 2.7** supports the interpretation that at least some of the amorphous Fe-clay book associations are electrostatic in origin. It is also possible that bonds exist between the amorphous iron phase and the faces of the clay books. The AEM-TEM data, however, can not be used to differentiate between these types of binding mechanisms.

The presence of an amorphous siliceous phase in the Georgetown matrix suggests another possible mechanism necessary for colloid release. The opaline silica might mechanically bind the clay aggregates in a web-like cage (**Figure 2.11b**). It is also possible that opaline silica possesses bond linkages with the clay books in a manner similar to that suggested for the amorphous Fe phase. Finally, the opaline phase might be electrostatically associated with the clay minerals, especially the clay edges, and the iron oxyhydroxides. In this respect, the opal would be just another participant in the overall electrostatic balance holding the matrix material intact.

If these components have a significant role in holding the Georgetown matrix together, evidence of their roles may be observable in opal-clay particle associations in the colloids released from the sediment (**Figure 2.12**). The most obvious feature in this STEM-EDX map of colloids mobilized from the Georgetown sediment at pH 8.4 is the abundance of green pixels, indicating a large amount of siliceous material in this sample of column effluent. Much of this siliceous material occurred in large (tens of nanometers) clumps or aggregates (**Figure 2.12a**). In TEM, much of this siliceous material appeared crust-like or web-like in nature, suggesting possibly that this material encrusted or mechanically bound clay particle

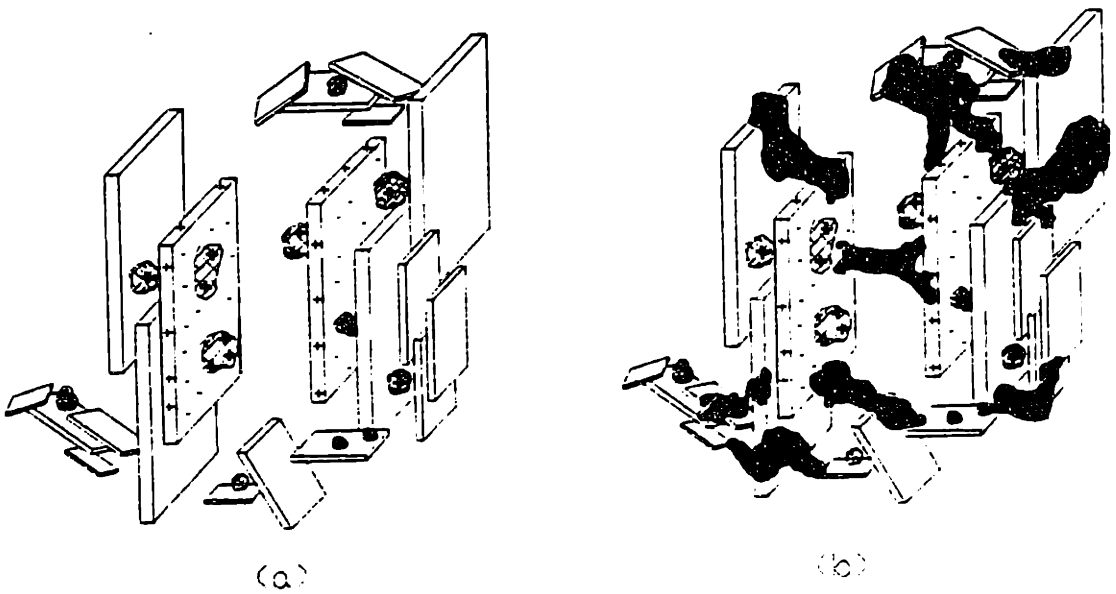

Figure 2.11: Schematic diagram of the nanometer-scale associations among mineral particles in the Georgetown matrix. (a) an amorphous iron oxyhydroxide phase (hatched) could act as an electrostatic or bonding intermediary between kaolinite books. Positive charge (dispersed Fe phase and the edges of kaolinite books) and negative charge (faces of kaolinite books) are partially represented. (b) Opaline silica (solid) could act as a cemetitious phase, incorporating micrometer-scale aggregates of associated clay and iron oxyhydroxide particles in a web-like encasement. Partial dissolution may be required to release the clay and iron oxyhydroxide particles within.

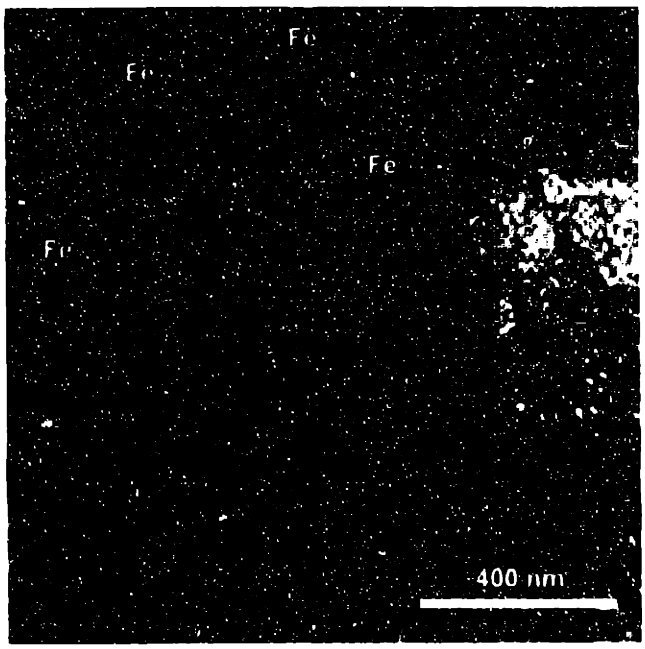

Figure 2.12: Associations among colloids released from the Georgetown sediment at pH 8.4. (a) (above) A STEM-EDX Si, Al and Fe composite map of a sample of embedded and ultramicrotomed colloids. Note the ubiquity of green pixels, indicating the abundance of a Si-rich phase. Clay particles (yellow) appear to be incorporated in the Si phase (indicated with arrows). The white and blue pixels in this area of the image represent an Fe-rich particle situated above the clay/Si aggregate. Some discrete iron oxyhydroxide particles (marked Fe) appear to be no longer specifically associated with the clays. The scale bar represents 400 nm. Each pixel represents approximately 12 x 12 nm of sample area. (b) (page 61) A TEM image of the embedded colloids with siliceous material (Si) and a kaolinite platelet (K) indicated. The scale bar represents 500 nm.

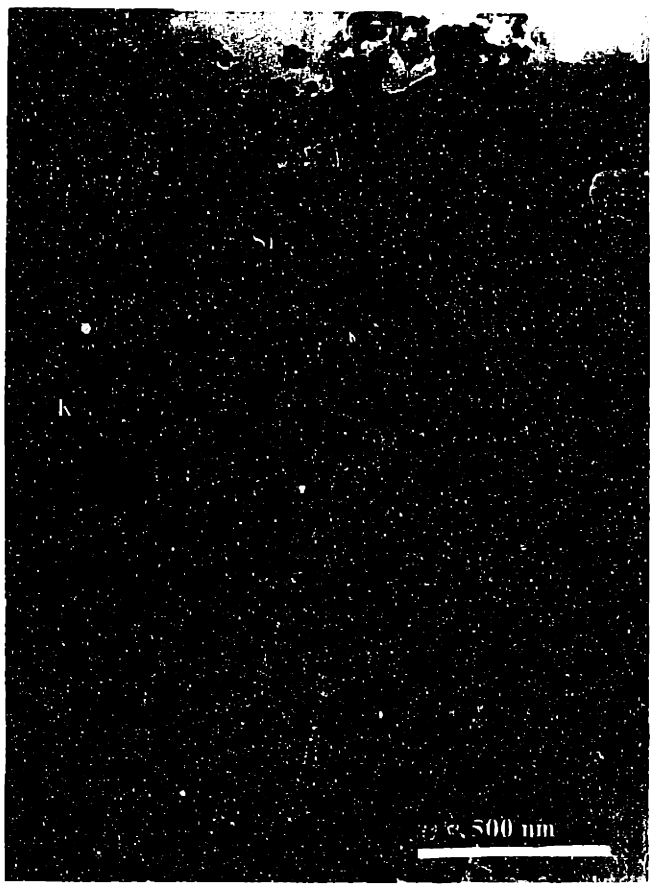
500 nm

aggregates (**Figure 2.12b**). These structures did not appear to be the result of the embedding process, as embedded aqueous samples of 1 μM to 1000 μM Si standards yielded Si maps with this element homogeneously distributed and unaggregated when analyzed by STEM-EDX. Note also that **Figure 2.12a** contains an amount of Si that does not correspond, in mass balance terms, to the amount of opaline Si extracted from the <63 μm fraction, as the images were recorded in a very Si-rich portion of a thin section of the column effluent where the Si-enriched structures were most microscopically apparent. Small iron oxyhydroxide particles (blue, marked Fe) mostly did not appear to be associated with the clay particles (**Figure 2.12a**), indicating that at least some of the iron oxyhydroxide/clay particles associations observed in the undisturbed matrix had been altered by mobilization. Thus, these observations appear to implicate the opal phase in a role as binding agent, possibly in tandem with the amorphous iron phase, in the Georgetown matrix.

2.4 Conclusions

Nanometer-scale spatial associations among clay-sized mineral particles in samples of sediment matrix were observed via TEM/HRTEM and STEM-EDX. Clay minerals were found to aggregate in face-associated domains. Two distinct populations of free iron oxyhydroxide phases were observed, supporting data derived from wet chemical, selective-extraction analysis of the sediment. A crystalline phase (goethite) was self-associative and thus unable to play a role in matrix binding. A second phase, probably composed of amorphous iron oxyhydroxide and adsorbed iron/iron polymers, was found to be distributed homogeneously throughout the matrix. It is this dispersed iron phase that would be the effective binding intermediary among the clay books. Furthermore, a siliceous phase, likely biogenic opal, was observed in the matrix and in colloid samples released from the sediment. The presence of this siliceous phase suggests that mechanical entrapment of colloids may inhibit their release. Thus, dissolution processes might play a role in mobilizing colloids in this aquifer.

2.5 References

Bachhuber K. and Frösch D. (1983) Melamine resins, a new class of water-soluble embedding media for electron microscopy. *J. Microsc.* **130**, 1-9.

Backhus D. A. Ryan J. N. Groher D. M. MacFarlane J. K. and Gschwend P. M. (1993) Sampling colloids and colloid associated contaminants in groundwater. *Groundwater* **31**, 466-479.

Banfield J. F. Jones B. F. and Veblen D. R. (1991) An AEM-TEM study of weathering and diagenesis, Abert Lake, Oregon: Diagenetic modification of the sedimentary assemblage. *Geochim. Cosmochim. Acta* **55**, 2795-2810.

Bartoli F. and Wilding L. P. (1980) Dissolution of biogenic opal as a function of its physical and chemical properties. *Soil Sci. Soc. Am. J.* **44**, 873-878.

Bell, D. C. (1996) personal communication, Center for Materials Science Electron Microscopy Facility, Massachusetts Institute of Technology.

Bennett R. H. Bryant W. R. and Keller G. H. (1981) Clay fabric of selected submarine sediments: Fundamental properties and models. *J. Sed. Pet.* **51**, 217-232.

Buddemeier R. W. and Hunt J. R. (1988) Transport of colloidal contaminants in groundwater: Radionuclide migration at the Nevada test site. *Appl. Geochem.* **3**, 535-548.

Cerda C. M. (1987) Mobilization of kaolinite fines in porous media. *Coll. Surf.* **27**, 219-241.

Collins K. and McGown A. (1974) The form and function of microfabric features in a variety of natural soils. *Geotechnique* **24**, 223-254.

Degueldre C. Baeyans B. Goerlich W. Riga J. Verbist J. and Stadelmann P. (1989) Colloids in water from a subsurface fracture in granitic rock, Grimsel test site, Switzerland. *Geochim. Cosmochim. Acta* **53**, 603-610.

Deshpande T. L. Greenland D. J. and Quirk J. P. (1968) Changes in soil properties associated with the removal of iron and aluminum oxides. *J. Soil Sci.* **19**, 123-126.

Dixon J. B. (1989) Kaolin and serpentine group minerals. In *Minerals in Soil Environments* (ed. J. B. Dixon and S. B. Weed), 2nd ed., pp. 467-526. Soil Science Society of America.

Douglas L. A. (1989) Vermiculites. In *Minerals in Soil Environments* (ed. J. B. Dixon and S. B. Weed), 2nd ed., pp. 635-674. Soil Science Society of America.

Drees L. R. Wilding L. P. Smeck N. E. and Senyaki A. L. (1989) Silica in soils: Quartz and disordered silica polymorphs. In *Minerals in Soil Environments* (ed. J. B. Dixon and S. B. Weed), 2nd ed., pp. 913-974. Soil Science Society of America.

Frösch D. and Westphal C. (1989) Melamine resins and their application in electron microscopy. *Elec. Micr. Rev.* **2**, 231-255.

Garrett-Reed A. J. (1995) personal communication. Center for Materials Science Electron Microscopy Facility, Massachusetts Institute of Technology.

Gee G. W. and Bauder J. W. (1986) Particle size analysis. In *Methods in Soil Analysis. Part 1-Physical and mineralogical methods* (ed. A. Klute), pp. 383-411. American Society of Agronomy, Inc.

Greenland D. J. Oades J. M. and Sherwin T. W. (1968) Electron microscopic observations of iron oxides in some red soils. *J. Soil Sci.* **19**, 123-126.

Gschwend P. M. Backhus D. A. MacFarlane J. K. and Page A. L. (1990) Mobilization of colloids in groundwater due to infiltration of water at a coal ash disposal site. *J. Contam. Hydrol.* **6**, 307-320.

Gschwend P. M. and Reynolds M. D. (1987) Monodisperse ferrous phosphate colloids in an anoxic groundwater plume. *J. Contam. Hydrol.* **1**, 309-327.

Hendershot W. H. and Lavkulich L. M. (1983) Effect of sesquioxide coatings on surface charge of standard mineral and soil samples. *Soil Sci. Soc. Am. J.* **57**, 1252-1260.

Herrington T. M. Clarke A. Q. and Watts J. C. (1992) The surface charge of kaolin. *Coll. Surf.* **68**, 161-169.

Holmén B. A. (1994) Polycyclic Aromatic Hydrocarbon Sorption Kinetics in Three Aquifer Sands. PhD. dissertation, Massachusetts Institute of Technology.

Holmén B. A. and Gschwend P. M. (1997) Estimating sorption rates of hydrophobic organic compounds in iron oxide- and aluminosilicate clay-coated aquifer sands. *Environ. Sci. Technol.* **31**, 105-113.

Jackson M. L. Lim C. H. and Zelazny L. W. (1986) Oxides, hydroxides and aluminosilicates. In *Methods in Soil Analysis. Part 1-Physical and mineralogical methods* (ed. A. Klute), pp. 101-150. American Society of Agronomy, Inc.

Jefferson D. A. Tricker M. J. and Winterbottom A. P. (1975) Electron-microscopic and Mössbauer spectroscopic studies of iron-stained kaolinite minerals. *Clays Clay Min.* **23**, 355-360.

Jones R. C. Hudnall W. H. and Sakai W. S. (1982) Some highly weathered soils of Puerto Rico. 2. Mineralogy. *Geoderma* **27**, 75-137.

Kaplan D. I. Bertsch P. M. and Adriano D. C. (1995) Facilitated transport of contaminant metals through an acidified aquifer. *Groundwater* **33**, 708-717.

Kaplan D. I. Bertsch P. M. Adriano D. C. and Miller W. P. (1993) Soil-borne mobile colloids as influenced by water flow and organic carbon. *Environ. Sci. Technol.* **27**, 1193-1200.

Kodama H. and Ross G. J. (1991) Tiron dissolution method used to remove and characterize inorganic components in soils. *Soil Sci. Soc. Am. J.* **55**, 1180-1187.

Lee S. Y. Hyder L. K. and Alley P. D. (1991) Microstructural and mineralogical characterization of selected shales in support of nuclear waste repository studies. In *Microstructure of Fine-grained Sediments* (ed. R. H. Bennett, W. R. Bryant and M. H. Hulbert), pp. 61-72. Springer-Verlag.

Leppard G. G. (1993) Evaluation of electron microscope techniques for the description of aquatic colloids. In *Environmental Particles* (ed. J. Buffle and H. P. vanLeeuwan), pp. 233-289. Int. Union of Pure and Applied Chemistry.

Liang L. McCarthy J. C. Jolley L. W. McNabb J. A. and Mehlhorn T. L. (1993) Iron dynamics: Transformation of Fe(II)/Fe(III) during injection of natural organic matter in a sandy aquifer. *Geochim. Cosmochim. Acta* **57**, 1987-1999.

Malengreau N. Muller J.-P. and Calas G. (1994) Fe-speciation in kaolins: A diffuse reflectance study. *Clays Clay Min.* **42**, 137-147.

McCarthy J. F. Williams T. M. Liang L. Jardine P. M. Jolley L. W. Taylor D. L. Palumbo A. V. and Cooper L. W. (1993) Mobility of natural organic matter in a sandy aquifer. *Environ. Sci. Technol.* **27**, 667-676.

McCarthy J. F. and Zachara J. M. (1989) Subsurface transport of contaminants. *Environ. Sci. Technol.* **23**, 496-502.

McDowell-Boyer L. M. (1992) Chemical mobilization of micron sized particles in saturated porous media under steady flow conditions. *Environ. Sci. Technol.* **26**, 586-593.

Morel F. M. M. and Hering J. G. (1993) *Principles and Applications of Aquatic Chemistry*. John Wiley and Sons, Inc.

Newman A. C. D. and Hayes M. H. B. (1990) Some properties of clays and of other soil colloids and their influence on soils. In *Soil Colloids and their Associations in Aggregates* (ed. M. F. DeBoodt), pp. 39-55. Springer Verlag.

Newman M. E. Elzerman A. W. and Looney B. B. (1993) Facilitated transport of selected metals in aquifer material packed columns. *J. Contam. Hydrol.* **14**, 233-246.

Oades J. M. (1984) Interactions of polycations of aluminum and iron with clays. *Clays Clay Min.* **32**, 49-57.

Penrose W. R. Polzer W. L. Essington E. H. Nelson D. M. and Orlandini K. A. (1990) Mobility of plutonium and americium through a shallow aquifer in a semiarid region. *Environ. Sci. Technol.* **24**, 228-234.

Perret D. Leppard G. G. Muller M. Belzile N. DeVitre R. and Buffle J. (1991) Electron microscopy of aquatic colloids: Non-perturbing preparation of specimens in the field. *Water Res.* **25**, 1333-1343.

Ronen D. Margaritz M. Weber U. and Amiel A. J. (1992) Characterization of suspended particle collected in groundwater under nautral gradient flow conditions. *Water Resourc. Res.* **28**, 1279-1291.

Ryan J. N. and Gschwend P. M. (1990) Colloid mobilization in two Atlantic Coastal Plain aquifers, field studies. *Water Resourc. Res.* **26**, 307-322.

Ryan J. N. and Gschwend P. M. (1991) Extraction of iron oxides from sediments using reductive dissolution by titanium(III). *Clays Clay Min.* **39**, 509-518.

Ryan J. N. and Gschwend P. M. (1992) Effect of iron diagenesis on the transport of colloidal clay in an unconfined sand aquifer. *Geochim. Cosmochim. Acta* **56**, 1507-1521.

Ryan J. N. and Gschwend P. M. (1994) Effect of solution chemistry on clay colloid release from an iron oxide-coated aquifer sand. *Environ. Sci. Technol.* **28**, 1717-1726.

Santos M. C. D. Mermut A. R. and Ribeiro M. R. (1989) Submicroscopy of clay microaggregates in an oxisol from Pernambuco, Brazil. *Soil Sci. Soc. Am. J.* **53**, 1895-1901.

Schahabi S. and Schwertmann U. (1970) Der einflus von synthetischen eisenoxiden auf die aggregation zweier losbodenhorizonte. *Z. Pflanzenernahr. Bodenkd.* **125**, 193-204.

Schindler P. W. and Stumm W. (1987) The surface chemistry of oxides, hydroxides, and oxide minerals. In *Aquatic Surface Chemistry* (ed. W. Stumm), pp. 83-110. John Wiley and Sons, Inc.

Schwertmann U. and Kampf N. (1985) Properties of goethite and hematite in kaolinitic soils of southern and central Brazil. *Soil Sci.* **139**, 344-350.

Schwertmann U. and Taylor R. M. (1989) Iron oxides. In *Minerals in Soil Environments* (ed. J. B. Dixon and S. B. Weed), 2nd ed., pp. 379-427.

Seaman J. C. Bertsch P. M. and Miller W. P. (1995) Chemical controls on colloid generation and transport in a sandy aquifer. *Environ. Sci. Technol.* **29**, 1808-1815.

Short S. A. Lowson R. T. and Ellis J. (1988) $^{234}U/^{238}U$ and $^{230}Th/^{234}U$ activity ratios in the colloidal phases of aquifers in lateritic weathered zones. *Geochim. Cosmochim. Acta* **52**, 2555-2563.

Sjörberg S. and Öhman L.-O. (1985) Equilibrium and structural studies of silicon (IV) and alumninum (III) in aqueous solution. Part 13. A potentiometric and ^{27}Al nuclear magnetic resonance study of speciation and equilibria in the aluminum(III)-oxalic acid-hydroxide system.

Smart P. and Tovey N. K. (1981) *Electron Microscopy of Soils and Sediments: Examples.* Clarendon Press.

Sposito G. (1984) *The Surface Chemistry of Soils.* Oxford University Press.

Thompson M. and Walsh J. N. (1989) *Handbook of Inductively Coupled Plasma Spectrometry.* Chapman and Hall.

Ulery, A. L. Unpublished data. Massachusetts Institute of Technology.

van Olphen H. (1977) *An Introduction to Clay Colloid Chemistry.* 2nd ed., John Wiley and Sons, Inc.

Wada K. (1989) Allophane and Imogolite. In *Minerals in Soil Environments* (ed. J. B. Dixon and S. B. Weed), 2nd ed., pp. 1051-1088. American Soil Science Society.

Wang H. D. White G. N. Turner F. T. and Dixon J. B. (1993) Ferrihydrite, lepidocrocite, and goethite in coatings from east Texas vertic soils. *Soil Sci. Soc. Am. J.* **57**, 1381-1386.

Wilding L. P. and Drees L. R. (1973) Scanning electron microscopy of opaque opaline forms isolated from forest soils in Ohio. *Soil Sci. Soc. Am. J.* **37**, 647-650.

Wilding L. P. Hallmark C. T. and Smeck N. E. (1979) Dissolution and stability of biogenic opal. *Soil Sci. Soc. Am. J.* **43**, 800-802.

Williams T. M. and McCarthy J. . (1991) Field-scale tests of colloid:facilitated transport. Proc. National Research and Development Conference on the Control of Hazardous Materials, 179-184.

Yariv S. and Cross H. (1979) *Geochemistry of Colloid Systems*. Springer-Verlag.

Chapter 3:

Mechanisms Controlling Release of Colloids to Groundwater in a Southeastern Coastal Plain Aquifer Sand*

*This chapter is an augmented version of C. H. Swartz and P. M. Gschwend, Mechanisms controlling release of colloids to groundwater in a Southeastern Coastal Plain aquifer sand, submitted to *Environmental Science and Technology*, September 8, 1997.

3.1 Introduction

The potential for colloid migration to facilitate the transport of contaminants in the subsurface motivates research focused on understanding the properties and generation of groundwater colloids (McCarthy and Zachara, 1989; Puls and Powell, 1992; Newman et al., 1993; Ryan and Elimelech, 1996). Inorganic constituents (e.g., clay minerals, iron, manganese and aluminum oxides, and quartz) have been implicated as the predominant colloidal phases in field observations and in other studies of groundwater colloids (Ronen et al., 1992; Ryan and Gschwend, 1992; Higgo et al., 1993; Kaplan et al., 1993; McCarthy and Degueldre, 1993). These inorganic colloids are thought to be generated by a variety of mechanisms, including precipitation of supersaturated phases (Gschwend and Reynolds, 1987; Bates et al., 1992; Liang et al., 1993) and by chemical perturbations which mobilize fines from interstitial matrices and coatings on framework grains (Kaplan et al., 1994; Ryan and Gschwend, 1994; Kaplan et al., 1995; Seaman et al., 1995).

Chemical perturbations must accomplish one or more of the following in order to mobilize these clay-size fines: (1) dissolution of a cemetitious phase which binds the fines mechanically (2a→3,2b→4 in **Figure 3.1**) or by cross-bonding among phases (1a→3,1b→4 in **Figure 3.1**) (Gschwend et al., 1990; Ryan and Gschwend, 1990; Ronen et al., 1992), (2) creation of like-charge on juxtaposed surfaces by altering the surface charge of variably charged constituents (e.g. iron and aluminum oxides, kaolinite edges) through changes in pH or the addition of surface potential altering sorbates to pore fluids (3→4 in **Figure 3.1**) (Kia et al., 1987; Ryan and Gschwend, 1994; Seaman et al., 1995), and (3) enhancement of electrostatic repulsion between juxtaposed surfaces of preexisting like-charge by lowering ionic strength (4→5 in **Figure 3.1**) (McDowell-Boyer, 1992; Roy and Dzombak, 1996). It necessarily follows that the preexisting mineral surface juxtapositions and associations dictate which sequence of chemical perturbations will mobilize colloids from a sediment.

As noted by Seaman et al. (1995), few studies exist which have examined colloid

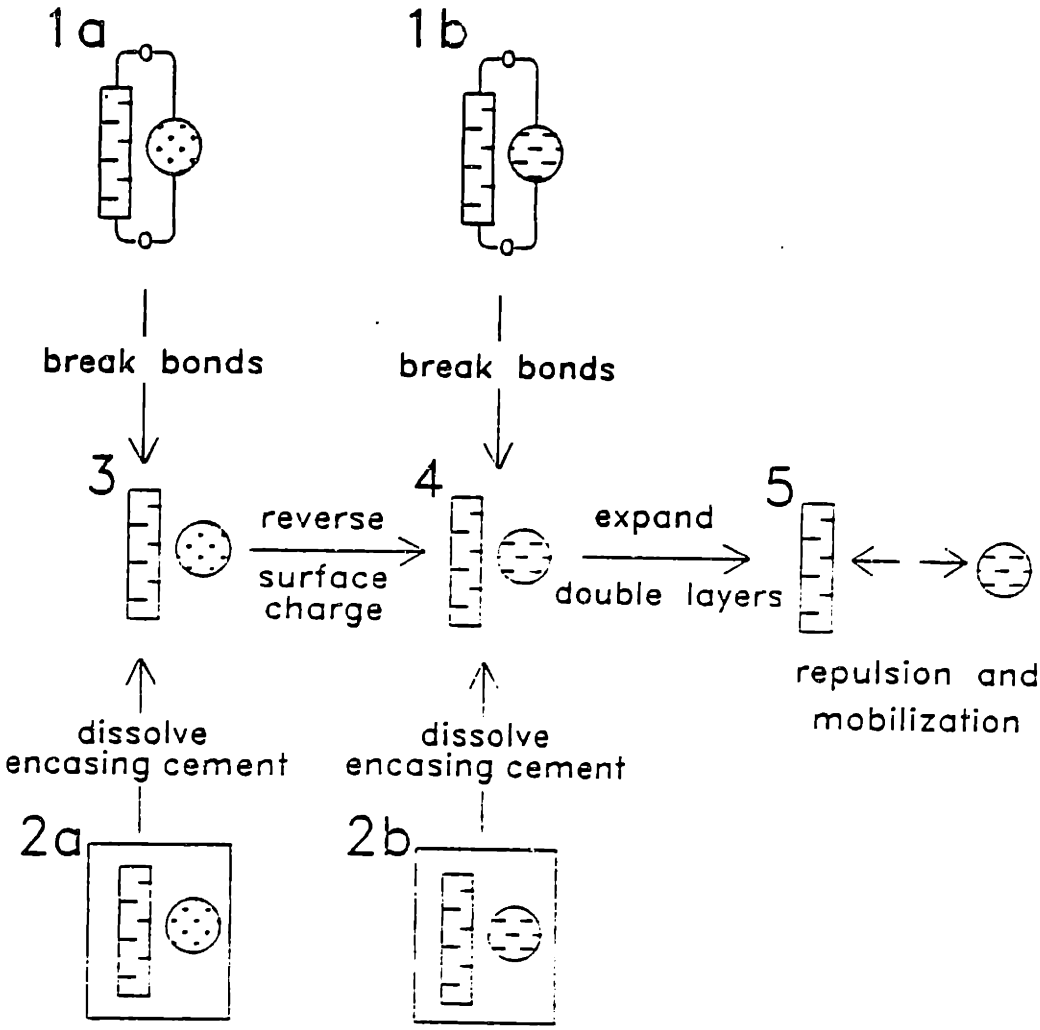

Figure 3.1: Schematic diagram of possible sequences of mechanisms inducing colloid mobilization. For the Georgetown sediment, the circles represent amorphous iron oxyhydroxides and the plates represent kaolinite. Positive or negative charge is represented within these shapes. The squares encompassing the amorphous iron and kaolinite (states 2a,b) represent an amorphous silica cement mechanically binding these constituents. Bonds between the amorphous iron oxyhydroxides and kaolinite are represented in states 1a, b. Although not represented, bonds could also exist among the amorphous silica and the matrix constituents.

mobilization behavior in relatively undisturbed sediments. Furthermore, the heterogeneity inherent in natural systems requires that a systematic characterization of sediment structure be coupled to studies of colloid release behavior if one is to elucidate the matrix constituents which play a key role in mobilization and if a broad understanding of the phenomenon is to be developed (Ryan and Elimelech, 1996). To this end, we previously analyzed a Scutheastern Coastal Plain aquifer sediment using analytical and transmission electron microscopy (AEM-TEM) to observe undisturbed associations among the inorganic matrix constituents and possible key binding agents (Chapter 2; Swartz et al., 1997). This AEM-TEM analysis indicated that an amorphous siliceous phase, biogenic opal (approximately 10% by weight of the <63 μm size fraction), appeared to be intimately associated with the matrix constituents and could cement the fines, either mechanically (i.e., 2a,b in **Figure 3.1**) or through bonds (i.e., 1a,b in **Figure 3.1**). In addition, a small amount (0.4% by weight of the <63 μm size fraction) of amorphous iron oxyhydroxides was found to be distributed among, and intimately associated with, the clay minerals in the matrix. Goethite, although constituting the majority (approximately 95%) of free iron in the sediment, occurred as discrete aggregates within the matrix. This observational evidence suggests that it is the small amount of amorphous iron oxyhydroxides which serve as the effective electrostatic (3 in **Figure 3.1**) and/or bonding intermediary (1a,b in **Figure 3.1**) among kaolinite plates, the predominant clay mineral in the sediment. It is improbable that the small amount of amorphous iron would act to mechanically bind the matrix constituents in this sediment.

Our objective in this study was to ascertain whether associations between the amorphous iron oxyhydroxides, amorphous silica, and clay minerals in the sediment matrix (a) were predominantly electrostatic in nature (3,4 in **Figure 3.1**) or (b) responded only to stronger perturbations which dissolved the amorphous iron oxyhydroxides or amorphous silica (1a→3, 1b→4, or 2a→3, 2b→4 in **Figure 3.1**). We subjected columns packed with the same relatively undisturbed sediment previously characterized by AEM-TEM (Chapter 2; Swartz et al., 1997) to appropriate perturbing solutions to test these possibilities. Information derived

from the dissolved and colloidal elemental composition of the column effluent was used to interpret mechanisms inducing mobilization and to differentiate various populations of matrix fines being mobilized.

3.2 Methodology

3.2.1 Sediment Characterization

The sediment is a 100,000-yr-old marine beach sand deposit that constitutes a shallow, approximately 3 m thick, coastal plain aquifer located at the Belle Baruch Forest Sciences Institute, Georgetown, SC (Williams and McCarthy, 1991). Dissolved organic carbon (DOC) mobility and iron redox chemistry have been studied previously in this aquifer (Liang et al., 1993; McCarthy et al., 1993; McCarthy et al., 1996). The sediment is approximately 95% quartz. The <63 μm and <2 μm size fractions represent 12% and 2.5% by weight of the sediment, respectively. The <2 μm size fraction is composed predominantly of kaolinite (45% by weight), with goethite, gibbsite, vermiculite and quartz present also (Chapter 2; Swartz et al., 1997). Organic carbon content is only 0.1% by weight of the bulk sediment (Holmén and Gschwend, 1997). Groundwater pH is typically 5.2-5.3 and conductivity is 43±6 μS cm^{-1}, which corresponds to an ionic strength of 0.4 mM calculated using the major cations and anions present in the groundwater (Chapter 2, Swartz et al., 1997).

A sample used for this study was obtained from the C horizon at a depth of 2.0-2.4 m during collection of a 5 cm diameter continuous core by hollow stem auger at the site in June, 1993. This sample consisted of the loose material collected from the auger flights. A later sample was collected at a depth of 2.2 m by hand auger in March, 1997, at a location 0.3 m away from the location of the earlier core. During both sampling events, the approximately 5 kg samples were stored in sealed plastic bags and refrigerated for later use. All experiments described in this study were initially conducted with the sediment collected in 1993 and analyzed by AEM-TEM (Swartz et al., 1997). Out of concern that the sample had lost too much moisture during storage, all experiments were reproduced using the fresh sample

collected in March, 1997. The elemental composition of the dissolved and colloidal constituents eluting from columns containing sediment collected in 1997 was found to be indistinguishable from that of the older samples when subjected to the same treatment solutions. All turbidity data presented herein were generated using the more recently collected sample.

Cations adsorbed on the sediment were determined by treating 0.1 g of the bulk sediment with 0.1 N $BaCl_2$ at pH 4. The sediment was placed in 50 mL centrifuge tubes with the $BaCl_2$ solution, shaken for 1 hr, then centrifuged at 3400 g for 20 min. The supernatant was carefully decanted, and the procedure was repeated three more times for a total of four equilibrations with 0.1 N $BaCl_2$ solution. One mL subsamples of the supernatant were passed through 30 nm pore-size polycarbonate membranes (Osmotics). Na, K, and Al were measured by graphite furnace atomic absorption (A.A.) spectroscopy (4100ZL, Perkin Elmer). Ca and Mg were quantified using inductively coupled plasma atomic emission spectroscopy (Thermo-Jarrel Ash).

3.2.2 Column Apparatus and Experimental Procedures

A column apparatus used in a previous study involving colloid mobilization (Ryan and Gschwend, 1994) was modified slightly. Argon was used to force prepared solutions from a pressure vessel (Millipore) to a 44 mm diameter filter cartridge containing approximately 5 g of moist sediment carefully packed within a 40 mm diameter o-ring (**Figure 3.2**). The 5 g sediment sample used to pack the column was taken directly from the plastic bag containing the field sample obtained during the coring procedure. No homogenization of the bag sample was attempted beforehand. PTFE tubing was used for all connections. This packing geometry produces a short flow path (approximately 2 mm) to minimize reattachment of colloids (Ryan and Gschwend, 1994). The void volume of this packed column was determined to be approximately 1 mL. Effluent turbidity (Hach Ratio X/R) and pH (Radiometer) were monitored in-line downstream, and data were recorded with a chart recorder. Turbidity measurements were calibrated in-line with formazin standards. A valve

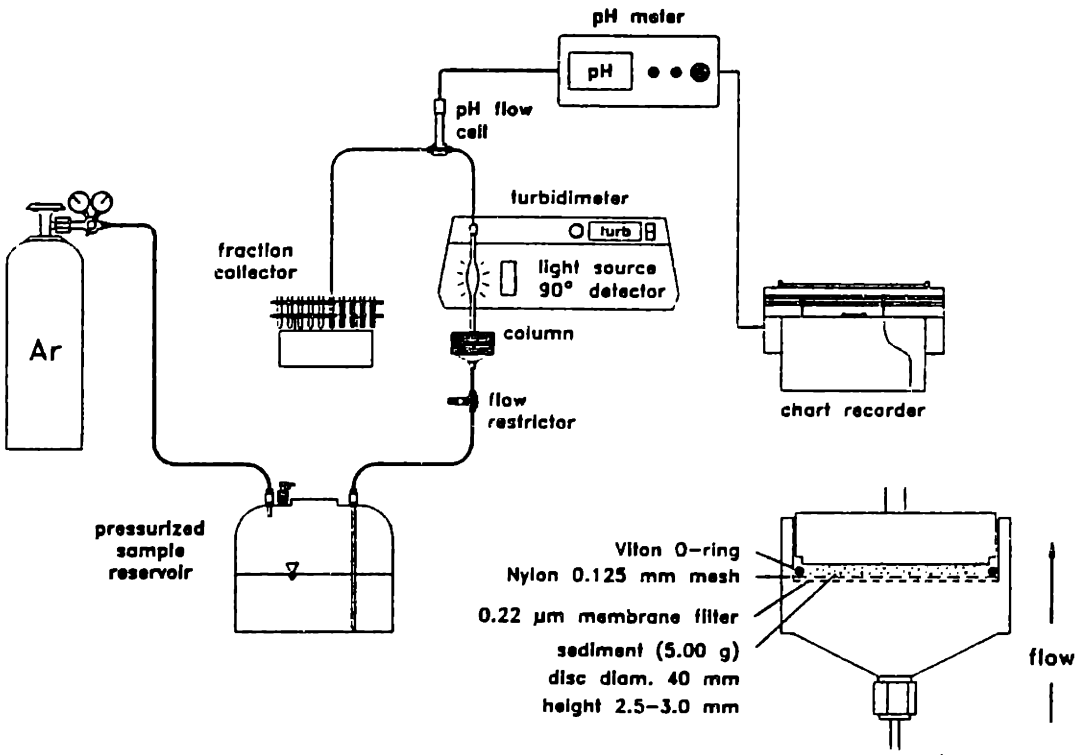

Figure 3.2: Schematic diagram of the column set-up used to study the colloid release mechanisms in the Georgetown. Argon was used to force prepared solutions from the stainless steel pressure bomb through the sediment-packed column.

placed upstream of the column maintained constant flow rates (approximately 0.35 to 0.40 mL min^{-1}), corresponding to seepage velocities of 1.5 m d^{-1} assuming a porosity of 0.30.

Each experiment was commenced with a column containing no sediment in order to record initial pH and baseline turbidity measurements (typically 0.09 NTU) of the prepared solutions at the prescribed flow rate and to collect samples for determining background levels of dissolved Fe, Al, and Si. The column was then isolated from upstream and downstream connections via stop valves, removed, and replaced with an identical column packed with sediment. The packed column was allowed to saturate before being reattached to the downstream portion of the apparatus. This procedure allowed the initial sediment response to be recorded with very minimal interference from any trapped air passing through the turbidity and pH flow cells. Column effluent was collected downstream in 2 mL microcentrifuge tubes (Marsh Biomedical).

For experiments in which a deionized water flush followed the initial solution treatment, flow was shut off at the upstream end of the column and the solutions were exchanged in the pressure bomb. Flow was then recommenced. This procedure generally took only 1 to 1.5 min. The brief flow interruption resulted in a short turbidity spike lasting 1 to 2 pore volumes after flow was restarted. Turbidity generally returned to near-baseline levels before the effect of the deionized water was manifest in the turbidity profiles (4 to 5 pore volumes after flow recommenced). The brief spike in turbidity due to flow interruption may have been caused by grain shifting within the column under the force that recommencing flow exerted on the sediment. The force applied to the cross sectional area of the wafer of sediment by recommencing flow, and concomitantly, the pressure drop across the column, was calculated to be approximately 5×10^{-3} kg m s^{-2}. This calculation was performed by using the Darcy equation to solve for the total change in head (as cm H_2O) across the column:

$$Q = KA\frac{dH}{dl} \qquad (1)$$

with Q equal to 0.35 mL min^{-1}, K estimated to be 3 x 10^{-5} m sec^{-1} (see section 4.2.1, Chapter 4), A equal to 14.5 cm^2 in the 4.0 cm diameter column, and dl equal to 0.25 cm. This pressure head was then integrated over the cross sectional area of the column to give the total force in kg m s^{-2} with the appropriate conversion factors. The gravitational force on the 5 g sample of sediment in the column was found to be approximately 5 x 10^{-2} kg m s^{-2}. Although the gravitational force appears to be ten times larger than the force caused by recommencing flow, possible underestimation of the K value by using a field derived estimate for K for the packed column would underestimate the pressure drop across the column as well. Grain shifting is a more probable cause for the turbidity spike than shearing of colloids from the sediment. Ryan (1992) demonstrated that the critical lift force required to overcome the intersurface potential energy of attachment of colloids to collector grains was exceeded only at a much larger flow rate (> 10 mL min^{-1}) for nearly identical column conditions to those used in our experiments. Others have also determined that hydrodynamic shear forces were negligible compared to electrostatic forces under laminar flow conditions (Khilar and Fogler, 1984, Cerda 1987).

Reagent grade L-ascorbic acid, oxalic acid, ammonium oxalate, hydroquinone (1,4-dihydroxybenzene), and sodium phosphate monobasic (NaH_2PO_4) were used with deionized water (" ponics) to prepare solutions. Surfactant solutions were prepared with ultrapure sodium dodecyl sulfate (SDS) (GibcoBRL), an anionic surfactant, and contained 10 mg L^{-1} $HgCl_2$ to inhibit biodegradation. Solution pH was modified with dilute HCl or NaOH solutions. A buffer, 0.2 mM sodium borate ($Na_2B_4O_7$), was used to help maintain elevated pH in some experiments (pH 8.0 and pH 8.8). All chemical treatments were performed in at least duplicate with fresh sediment to ensure reproducibility of the observed behaviors. All treatments performed are summarized in **Table 3.1**.

Table 3.1: Dissolved Fe in treatment solution effluents and Al/Fe mole ratios of mobilized colloids

Treatment	Dissolved Fe in treatment solution effluent (nmoles min^{-1})	Fe dissolved during treatment flush as percent of total amorphous Fe[1]	Al/Fe mole ratio of mobilized colloids[2]
DI water; pH 5.5	ND[3]	ND	NR[4]
0.1 N $CaCl_2$; pH 5.5	ND	ND	NR
0.1 N NaCl; pH 5.5	ND	ND	NR
1 mM $CaCl_2$; pH 2.6	0.16±0.03 (n=24)	0.05%	NR
0.2 mM $Na_2B_4O_7$; pH 8.8	ND	ND	1.5±0.5 (n=11)[5]
2 mM SDS, 1 mM NaCl; pH 5.4	ND	ND	NR
10 mM phosphate; pH 5.2	ND	ND	0.5±0.3 (n=22)[5]
10 mM oxalic; pH 4.1	9.0±0.5 (n=34)	2.9%	3.1±0.7 (n=19)[5]
10 mM ascorbic; pH 4.2	3.6±0.3 (n=51)	1.2%	NR
10 mM ascorbic; pH 5.2	1.4±0.1 (n=34)	0.5%	NR
10 mM hydroquinone; pH 4.6	0.13±0.03 (n=14)	0.05%	NR
10 mM ascorbic; pH 6.0	0.7±0.1 (n=51)	0.2%	2.5±1.4 (n=9)[5]
1 mM phosphate; pH 5.2	ND	ND	NR
1 mM ascorbic; pH 5.2	0.15±0.01 (n=19)	0.05%	NR
0.5 mM ascorbic + 0.5 mM phosphate; pH 5.2	0.06±0.02 (n=14)	0.02%	2.3±0.9 (n=23)[6]

[1]based on integration of dissolved Fe in 50 pore volumes of treatment effluent divided by total amorphous Fe present in column. Total amorphous Fe present calculated using 64 μmoles amorphous Fe g^{-1} <63 μm size fraction extracted by the ammonium oxalate method (Swartz et al., 1997)

[2]compare to Al/Fe mole ratio of bulk matrix 3.2±0.2 (measured from digestion of <63 μm size fraction (Swartz et al., 1997))

[3]ND= not detected (≤ 1ppb) or indifferentiable from background levels

[4]NR= no colloids released

[5]Al/Fe mole ratio for colloids released during deionized water flush following treatment flush

[6]Al/Fe mole ratio for colloids released during the treatment flush

3.2.3 Sample Analysis

Column effluent samples were prepared for analysis of dissolved concentrations of Fe, Al, Si first by centrifuging the 2 mL samples at 23,000 g for 20 min. A 1 mL aliquot of each sample was then passed through a 30 nm pore-size polycarbonate membrane (Osmotics). Fe, Al, and Si were quantified using a 4100Zl graphite furnace atomic absorption (A.A.) spectrometer (Perkin Elmer) calibrated with comparably dilute atomic absorption grade standards (Fisher) prepared in matrices as close to sample compositions as possible.

SDS was measured in the effluent from appropriate experiments using a total organic carbon analyzer (TOC-5000, Shimadzu). Background concentrations of TOC eluting from the columns were found to be equal to approximately 1% or less of the effluent SDS concentrations (as TOC). Integrated amounts of SDS sorbed in the column experiments were compared to amounts sorbed in batch equilibrations to determine if the packed columns were adequately adsorbing the SDS. For the batch experiments, 10 mL of a 2 mM SDS solution were added to 1 g of sediment in 22 mL glass vials with teflon lined caps. The vials were placed on a tumbler and periodically checked to ensure that pH remained constant at a value of 5.4. Dilute HCl and NaOH were sometimes added to maintain pH 5.4. At prescribed time points, samples were removed from the tumbler and centrifuged at 3400 g for 30 min before measuring the aqueous SDS concentration in the supernatant. The amount of SDS sorbed was determined by difference between the SDS concentration in control vials containing no sediment and that measured in sample supernatants after the prescribed contact time. The amount of SDS sorbed was corrected for dissolved organic carbon leached from the sediment using control vials which contained sediment suspended in deionized water only. An average value of the equilibrium amount of SDS sorbed was determined using samples sacrificed at time points beyond which the SDS concentrations in the sample supernatants attained a plateau.

Effluent samples containing colloids were sonicated (81 W) for 1 hr prior to addition of 50 μL of 3.0 M HF to 1 mL of each sample. The samples were then tumbled end over

end for 72 hr before subsamples were pipetted off for dilution and analysis of the Fe and Al content of the digested samples by A.A. The Al/Fe mole ratios of these colloids were compared to the Al/Fe mole ratio of the bulk matrix, which was calculated using the total Al and Fe measured by HF digestion of the <63μm size fraction of the Georgetown sediment (Chapter 2; Swartz et al., 1997).

3.2.4 Mobility Measurements

Mobility measurements were performed on model goethite colloids suspended in treatment solutions like those used in the column experiments to estimate the effects of these adsorbates on the surface potentials of the iron oxyhydroxides present in the Georgetown sediment. Although it is the amorphous iron oxyhydroxide, rather than goethite, which we believe is a potential key binding agent in the Georgetown sediment, goethite was chosen as the model colloid for the mobility studies because of its generally lower solubility in the presence of the sorbates analyzed.

The goethite was prepared according to the procedures outlined in Atkinson et al. (1968). The synthesized goethite suspension was dialyzed against deionized water until the conductivity of deionized water was equal to the initial conductivity. The goethite was stored in suspension for later use. X-ray diffraction (CuKα irradiation with a Rigaku RU300 diffractometer) verified the existence of goethite in the suspension. The surface area of the air-dried goethite was found to be 22 m^2 g^{-1} by N_2 adsorption (Porous Materials, Ithaca NY).

For each mobility measurement, a given volume of the goethite suspension was added to the appropriate solution made up in deionized water which had been brought to a specific pH using dilute NaOH or HCl solutions. NaCl was also added to some solutions so that all solutions studied possessed ionic strengths in the range of 5 to 20 mM. The final solids' concentration of the goethite suspensions was approximately 75 mg L^{-1}. The average particle size of the colloids in these suspensions was 350±110 nm, as measured by laser light scattering (Coulter model N4).

Mobilities were measured with a Mark II microelectrophoresis apparatus (Rank

Brothers, Bottisham, England) equipped with a four-electrode cylindrical cell and a 3 mW He/Ne laser. The mobilities of 15 to 20 particles measured at both stationary levels (mobilities at each level were found to be equal) were used to determine an average mobility for each solution condition.

3.3 Results and Discussion

3.3.1 Effect of ionic strength

The sediment did not release colloids in response to exchange of high ionic strength solutions (0.1 N NaCl or 0.1 N $CaCl_2$ at pH 5.5) for deionized water (**Figure 3.3**). Initial turbidity values of 1.0 to 3.0 NTU were probably due to release of loose material resulting from column packing. Turbidity generally fell to background levels (approximately 0.1 NTU) within five pore volumes after initiation of the high ionic strength treatment flushes (**Figure 3.3**). A treatment consisting of deionized water only produced similar initial turbidity levels (**Figure 3.3**).

Upon exchange of treatment solutions (0.1 N NaCl or 0.1 N $CaCl_2$) for deionized water, a brief, 1 to 2 pore volume, spike in turbidity occurred as the result of flow interruption necessary to exchange solutions in the pressure bomb (**Figure 3.3**). Only the deionized water flush following the 0.1 N $CaCl_2$ treatment resulted in slightly elevated and briefly sustained turbidity levels (to approximately 0.18 NTU, pore volumes 60 to 65, **Figure 3.3**) upon initial sediment contact with the deionized water. Length of contact time with the salt solutions was not a factor, as experiments were replicated to as many as 150 pore volumes of contact before following with a deionized water flush (data not shown).

These data suggest that binding mechanisms among the clay-size constituents in the Georgetown sediment do not respond to ionic strength perturbations causing electric double layer expansion (4 in **Figure 3.1**). As only juxtaposition of like-charged constituents would respond to such effects, the results imply that (1) surface charge repulsion among the negatively charged faces of the abundant kaolinite booklets observed in the sediment are

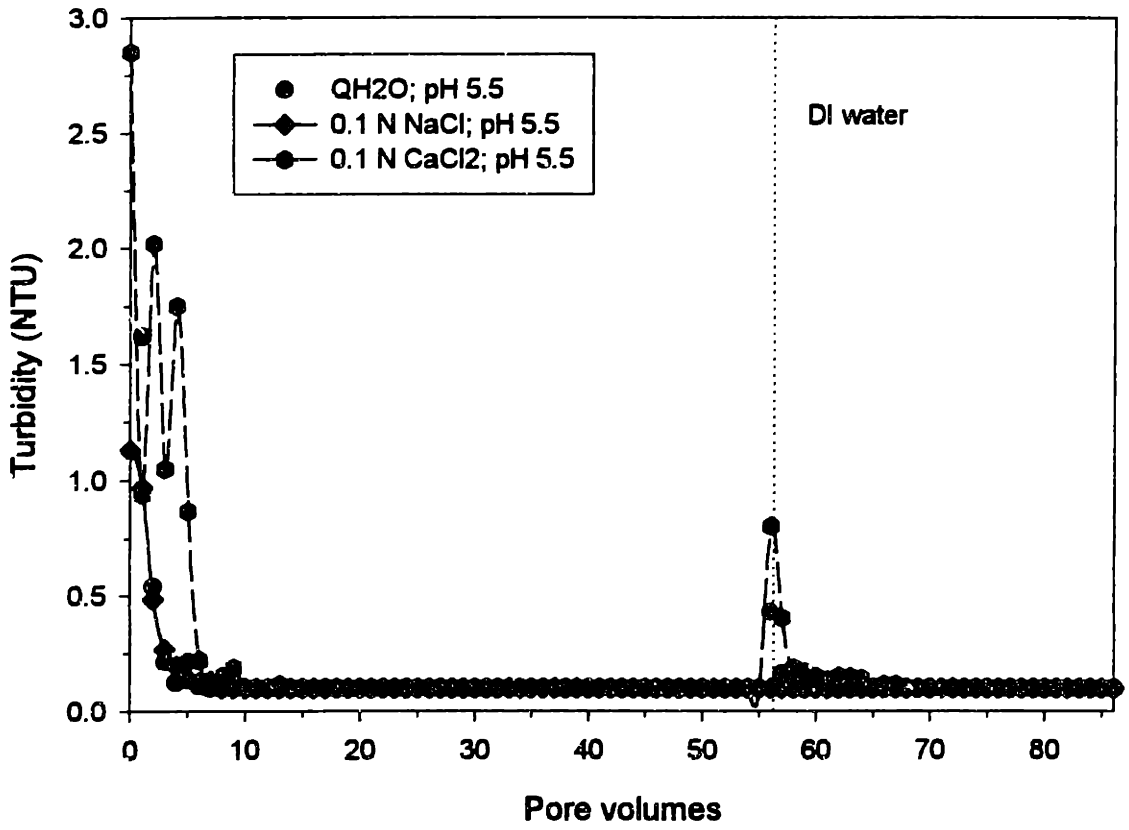

Figure 3.3: Turbidity profiles during experiments in which sediment was treated with either 0.1 N $CaCl_2$, 0.1 N NaCl, or deionized water only. The influent pH was approximately 5.5 for each case. Treatment solutions were flushed through the columns for 56 pore volumes and were followed with a 30 pore volume deionized water (DI) flush. The spike in turbidity positioned approximately at pore volume fifty seven was a result of flow interruption to change solutions in the pressure bomb.

effectively mitigated by *positively* charged amorphous iron oxyhydroxides distributed among them (i.e., 3 in **Figure 3.1**), and/or (2) the amorphous silica or amorphous iron oxyhydroxide phases chemically or mechanically bind the matrix (1a,b or 2a,b, respectively, in **Figure 3.1**) so that repulsive forces among the constituents can not induce mobilization. The goethite aggregates, although comprised of intimately associated 5 to 10 nm spheroids with assumedly similar surface charge (Chapter 2; Swartz et al., 1997), did not seem to be affected by the double layer perturbations either. This suggests that the goethite spheroids are chemically or mechanically bound, perhaps by amorphous Fe, so that the spheroids act predominantly as aggregate units. If this were the case, surface charge reversal of the presumably positively charged aggregates would have to occur to induce repulsive interactions between the aggregates and the surrounding, negatively charged kaolinite faces.

3.3.2 Effect of surfactant and phosphate

If the amorphous iron oxyhydroxide intermediaries among the kaolinite faces and the goethite aggregates were indeed positively charged under native groundwater conditions, reversing their surface charge and then lowering ionic strength might induce colloid release (i.e., 3→4→5 in **Figure 3.1**). However, if the matrix constituents are chemically or mechanically bound, rather than electrostatically, surface charge reversal of the iron oxyhydroxides would have no effect. Dissolution of the mechanical binding agent, in our case, the amorphous silica (i.e., 2a→3→4→5 in **Figure 3.1**), or breaking of bonds between the kaolinite and the amorphous iron or silica phases chemically binding these constituents (i.e., 1a→3→4→5 in **Figure 3.1**) would be required first.

To differentiate electrostatic binding from mechanical or chemical binding, we treated the sediment with 2 mM SDS in a 1 mM NaCl solution at pH 5.4 and a 10 mM phosphate solution at pH 5.2 in two separate experiments. Sufficiently concentrated SDS solutions have been shown to reverse the surface charge of oxides by forming admicelles on the initially positively charged surfaces (Böhmer and Koopal, 1992; Lee and Koopal, 1996). The mobilities of model goethite colloids suspended in 2 mM SDS (with 3 mM NaCl added to

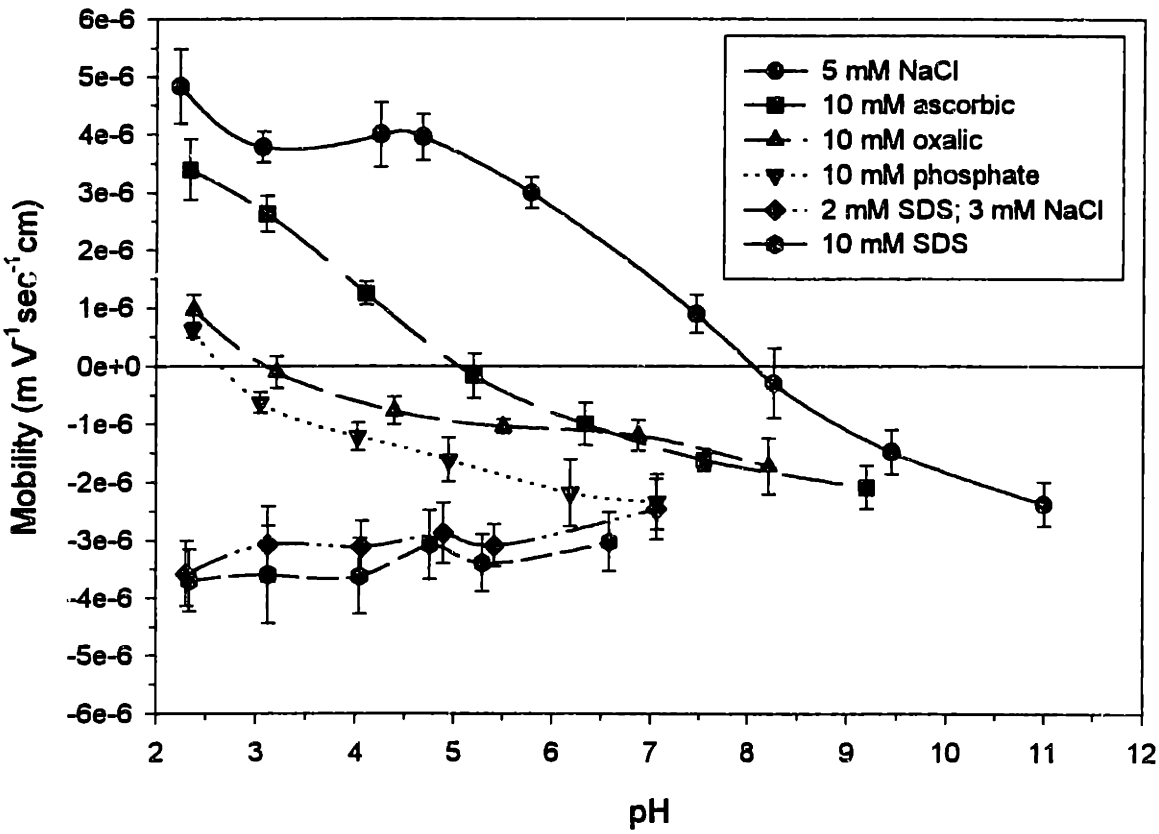

Figure 3.4: Electrophoretic mobilities (m V^{-1} sec^{-1} cm) of model goethite colloids suspended in various solutions like those used as treatment solutions in the column experiments. Each data point represents the average of 15 to 20 different particle measurements at both stationary levels. Error bars represent ± one standard deviation.

give a total ionic strength of 5 mM to the solution) clearly showed that this concentration of SDS was sufficient to reverse surface charge over a broad pH range (**Figure 3.4**). Phosphate also has been found to readily reverse the surface charge of iron oxides through strong specific adsorption (Hansmann and Anderson, 1985; Liang and Morgan, 1990). Indeed, the mobilities of the goethite colloids suspended in 10 mM phosphate solutions at various pH values indicated that the pH_{pzc} of the goethite under these conditions was shifted from a value of approximately 8.0 (5 mM NaCl) to 2.7 (**Figure 3.4**).

It was assumed that neither the sulfate head group of the SDS molecule nor phosphate could lyse bonds or dissolve amorphous iron oxyhydroxides or amorphous silica (Ognalaga et al., 1994). No dissolved Fe (<1 ppb, **Table 3.1**) was detected in the effluent during any of the SDS and phosphate treatments, supporting our presumption that dissolution was not occurring. Dissolved Si in even 10 mM SDS treatment effluent (**Figure 3.5**) was indifferentiable from average values calculated from dissolved Si levels measured in the effluent from a number of deionized water and 0.1 N $CaCl_2$ treatments (initial pH of 5.5). Dissolved Si eluting during these treatments was probably the result of partial leaching of adsorbed silicate and dissolved silicate present in residual pore fluids and not due to dissolution of the amorphous silica phase. Levels of dissolved Si in the 10 mM phosphate treatment effluent were elevated above those for the 10 mM SDS treatment and the average of the deionized water and 0.1 N $CaCl_2$ treatments (**Figure 3.5**). However, the elevated Si levels in the 10 mM phosphate effluent were probably due to anion exchange of the phosphate for adsorbed silicate on the surfaces of the matrix constituents and not due to dissolution of amorphous silica. Phosphate has been shown to readily displace adsorbed silicate on goethite due to its bidentate chelating structure (Torrent et al., 1992). SDS was not able to displace adsorbed silicate probably because the sulfate head group lacks a bidentate chelating structure.

From solutions containing 2 mM SDS and 1 mM NaCl, approximately 1.5±0.1 μmoles SDS g sediment^{-1} were lost to the sediment in 100 pore volume treatment flushes (**Figure 3.6**). Approximately 70% of this amount was sorbed in the first 50 pore volumes (**Figure**

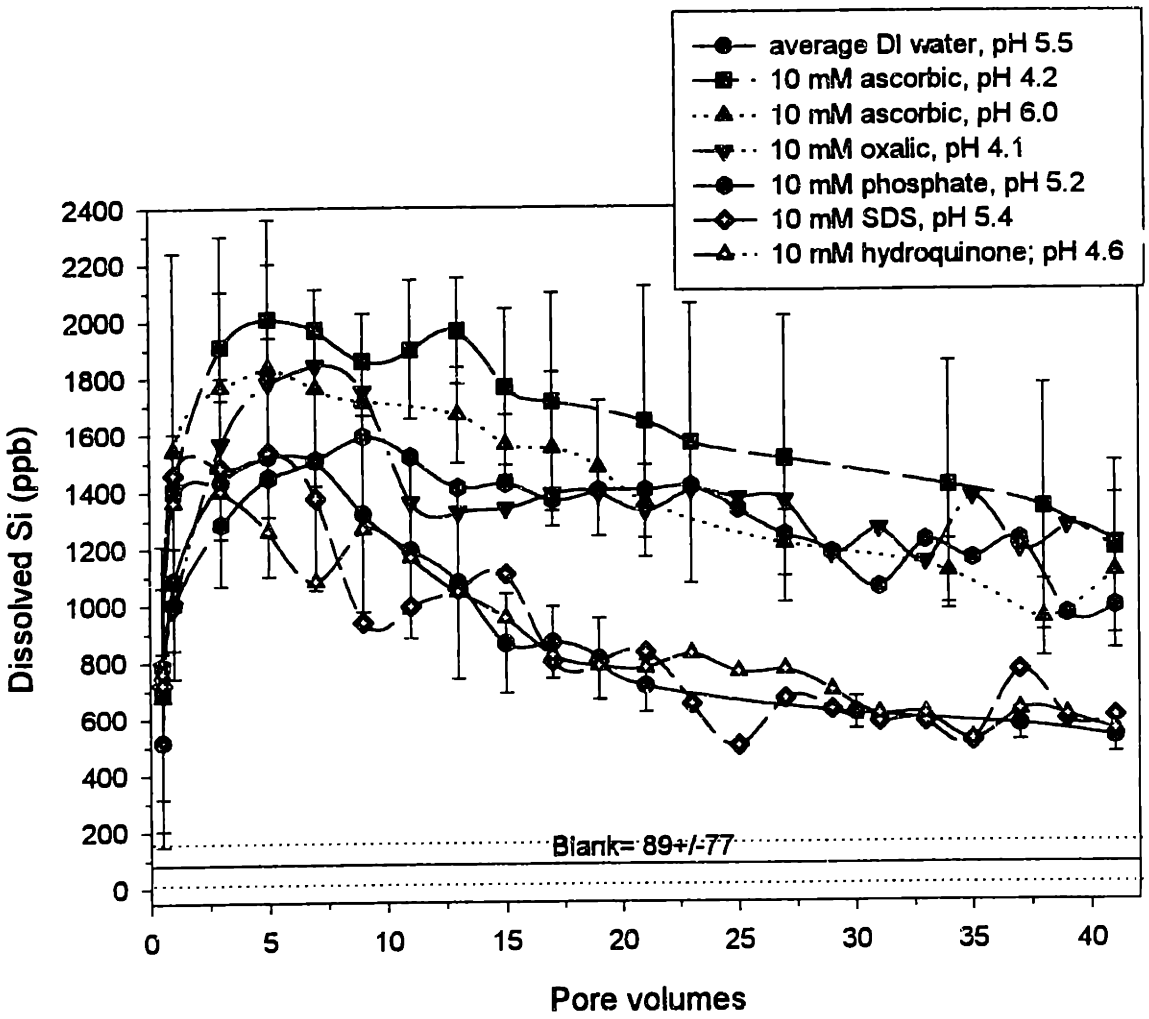

Figure 3.5: Profiles of dissolved Si (ppb) in effluent from columns subjected to treatments used in this study. Each data point represents a measurement from a 2 mL sample of collected effluent, or the average of several 2 mL samples collected from replicate experiments, at the respective pore volume. Each data point constituting the "DI water, pH 5.5" profile is the average of the dissolved Si in samples from five deionized water treatments and one 0.1 N $CaCl_2$ treatment, all at an initial pH of 5.5. Error bars represent ± one standard deviation. For the 10 mM ascorbic acid pH 4.2 and pH 6.0 treatments, n=3. The background Si was 89±77 ppb.

3.6). From the elution profiles of the SDS solutions (**Figure 3.6**), it is evident that near equilibrium was reached (i.e., effluent SDS concentration was within several percent of the influent concentration) with the sediment within the 100 pore volume contact time. Curiously, in conducting batch equilibration experiments with the bulk sediment, 2.4±0.1 μmoles SDS g sediment^{-1} (n=11, **Figure 3.7**) were sorbed with a final equilibrium aqueous concentration of 1.3 mM SDS. A comparison of this batch result to the integrated amount sorbed after 100 pore volumes of contact with 2 mM SDS (1.5±0.1 μmoles SDS g sediment^{-1}) suggests that only approximately 63% of the sites accessible under batch conditions were accessed within the 100 pore volumes contact time of the 2 mM SDS column experiments. The removal inefficiency for SDS in the column relative to the batch experiments was probably due to the presence of immobile zones in the sediment in which diffusive transport limited the accessibility of sites. The behavior of a conservative tracer (acetone) in column studies of polycyclic aromatic hydrocarbon to this sediment suggested the presence of physical nonequilibrium transport effects as well (Holmén, 1994; Holmén and Gschwend, 1997).

Despite the ability of 2 mM SDS to reverse surface charge of model goethite colloids (**Figure 3.4**) and the indication that 2 mM SDS solutions had come to sorptive equilibrium with the accessible sites in the sediment (**Figure 3.6**), we did not observe any colloid release during the 2 mM SDS treatment (**Figure 3.8**). No colloids were released during the subsequent deionized water flush either (**Figure 3.8**).

Note that mobilization experiments were conducted with more highly concentrated (10 mM) SDS solutions as well (data not shown). However, these solutions appeared to physically disrupt the sediment due to the formation of bubbles as the solution contacted the sediment. The higher surfactant concentration, above the critical micelle concentration of 8.0 mM SDS (Mysels and Mysels, 1965; Chandar et al., 1987), likely promoted the formation of bubbles as the solution contacted the sediment. The addition of 0.1 M NaCl to 10 mM SDS solutions appeared to partially inhibit bubble formation by counteracting the decrease in

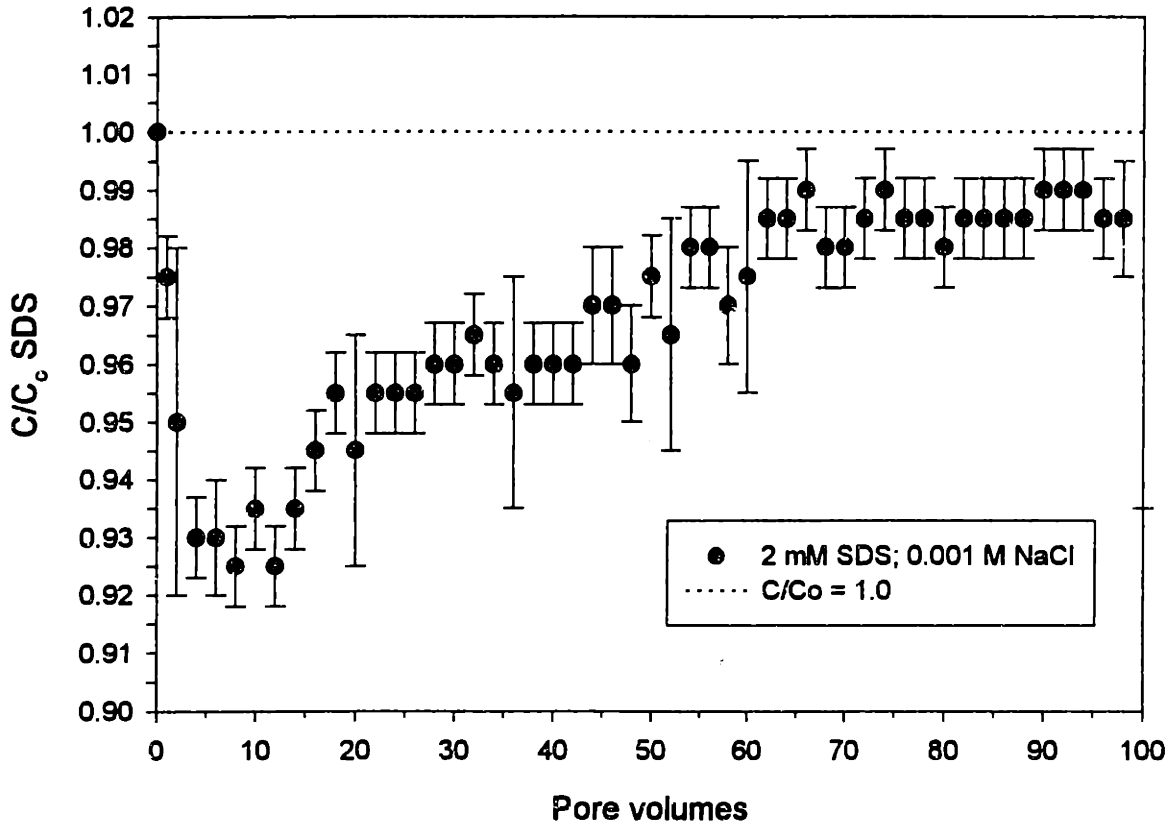

Figure 3.6: Average elution profile for the aqueous phase concentration of SDS in the effluent from columns treated with 2 mM SDS. Note that near equilibrium with accessible sites (effluent concentration approached influent concentration within 1 to 2%) was attained within approximately 100 pore volumes of contact. Error bars represent ± 1 standard deviation (n=3).

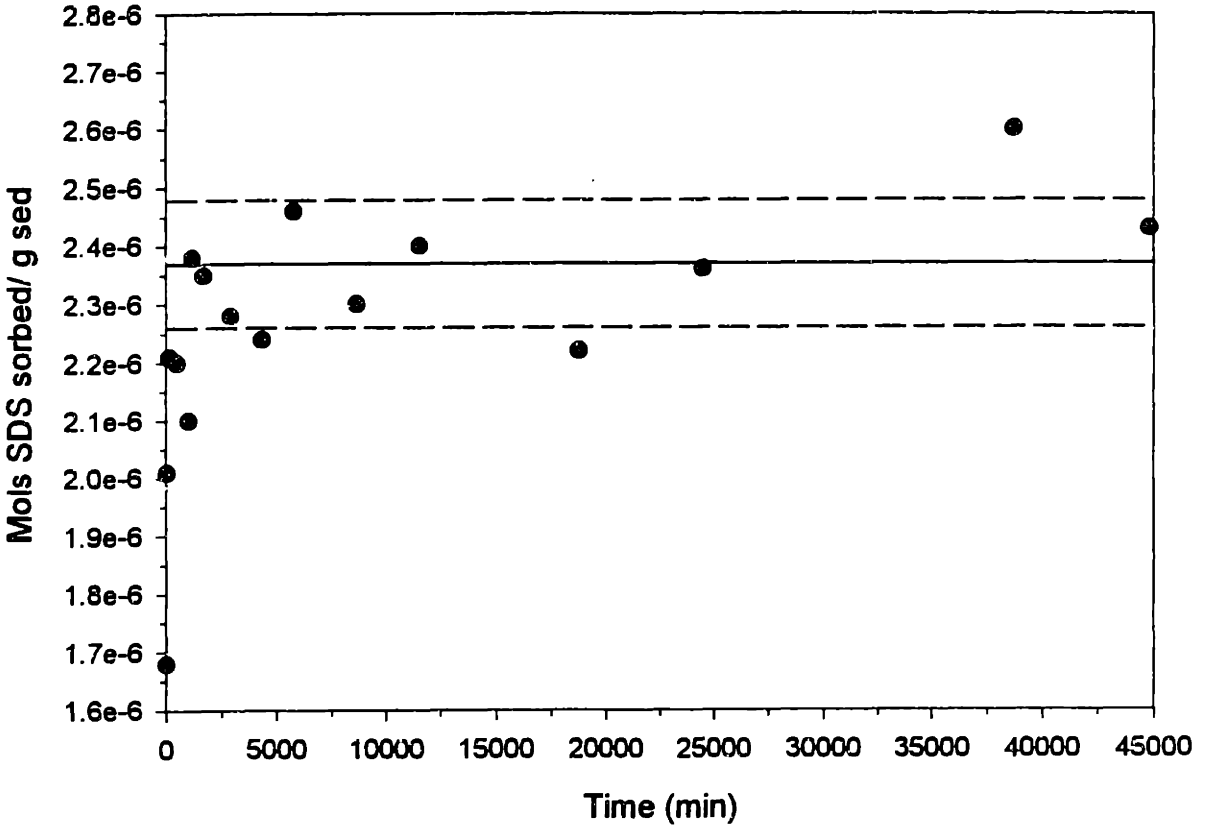

Figure 3.7: Results from batch kinetics experiment to determine the time needed to attain equilibrium sorption between a 1.5 mM SDS solution and the bulk Georgetown sediment. The final aqueous phase concentration in the plateau was approximately 1.3 mM SDS. The average amount sorbed was 2.4±0.1 μmoles SDS g^{-1} sediment. The last eleven data points, in which no further losses of SDS to the sediment were observed with increased contact time, were used to calculate this average value.

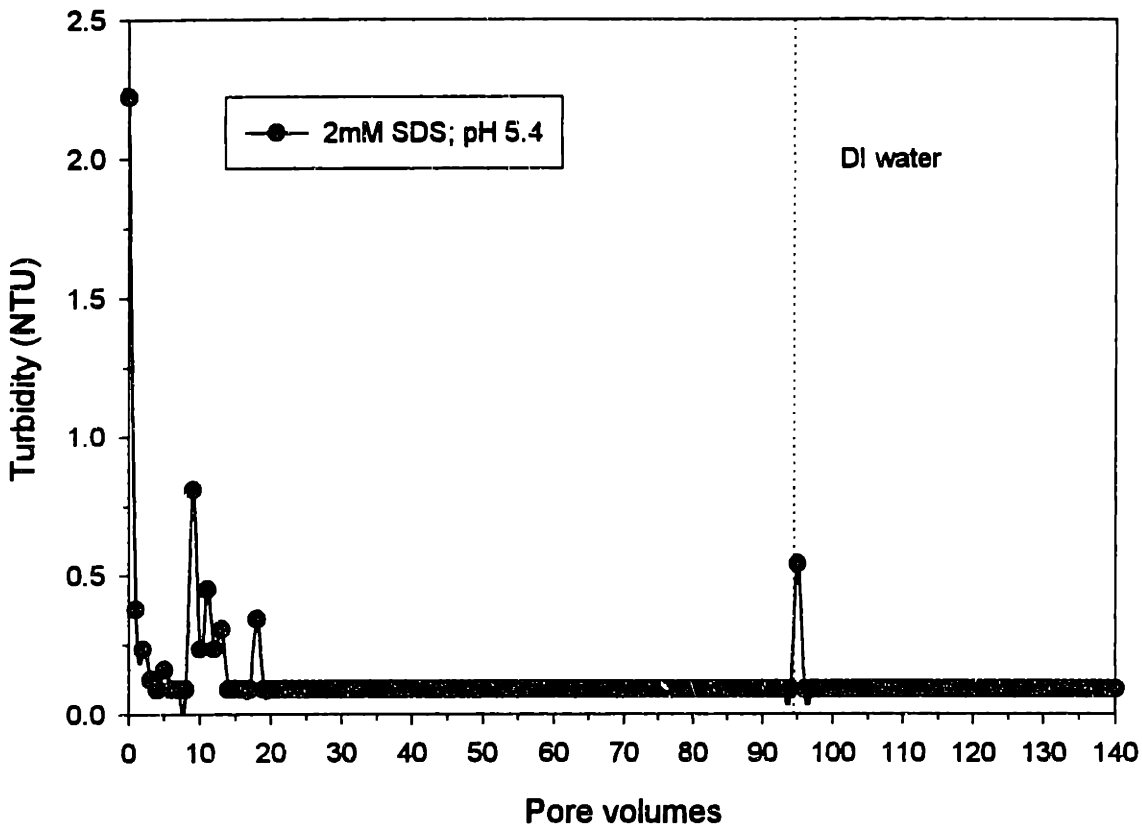

Figure 3.8: Turbidity profile for experiment in which sediment was treated with 2 mM SDS (pH 5.4) for 95 pore volumes followed by a 35 pore volume deionized (DI) water flush. The spike in turbidity at pore volume ninety five was caused by flow interruption required to change solutions in the pressure bomb.

surface tension of water caused by addition of the surfactant. However, brief (1 to 2 pore volume) spikes of turbidity were still preceded by visual observation of bubbles passing from the column with 10 mM SDS solutions containing 0.1 M NaCl, confounding the analysis of colloid release behavior.

In contrast to the 2mM SDS results, colloids were mobilized in the deionized water flush following a 56 pore volume treatment with 10 mM phosphate (**Figure 3.9**). The mobilization event occurred as a pulse which began as the deionized water contacted the sediment (approximately pore volume 60, **Figure 3.9**). This pulse peaked at approximately 1 NTU and subsequently declined within the 30 pore volume deionized water flush (**Figure 3.9**). No mobilization occurred during the 10 mM phosphate treatment flush itself except for the initial release of loose material which occurred at the beginning of the treatment (**Figure 3.9**).

When the elemental composition of the colloids mobilized in the deionized water flush following the 10 mM phosphate treatment were analyzed, it was found that the average Al/Fe mole ratio of the colloids (0.5±0.3, **Table 3.1**) differed greatly from that of the bulk matrix (3.2±0.2, **Table 3.1**) and was weighted more strongly by iron than was the bulk matrix. The lower Al/Fe ratio of the colloids suggests that predominantly goethite aggregates and proportionately lesser amounts of kaolinite, vermiculite and gibbsite were mobilized by the 10 mM phosphate treatment and subsequent deionized water flush. Apparently, the goethite aggregates were more free to respond (i.e., be mobilized) to the repulsive interactions with neighboring kaolinite books than were the rest of the bulk matrix constituents. The fact that mobilization occurred in the deionized water flush and not during the phosphate treatment suggests that a decrease in ionic strength, and concomitant expansion of electric double layers, was necessary to induce this mobilization. Although the average Al/Fe mole ratio of these detached colloids was very similar to that of the amorphous iron oxyhydroxides (0.7; Swartz et al., 1997), it is unlikely that only the amorphous iron oxyhydroxides would be mobilized because of their intimate association with the clay minerals in the bulk matrix

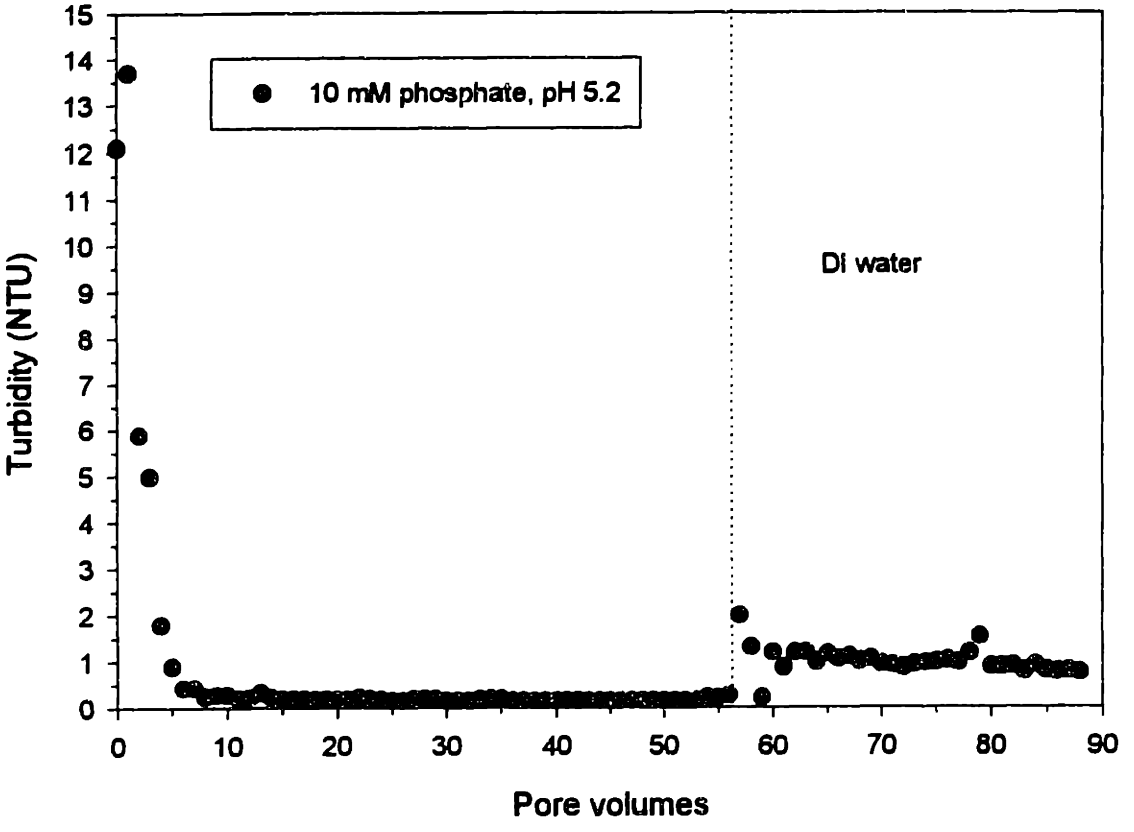

Figure 3.9: Turbidity profile for experiment in which sediment was treated with 10 mM phosphate (pH 5.2) for 56 pore volumes followed by a 30 pore volume deionized (DI) water flush. The spike in turbidity at pore volume fifty seven was caused by flow interruption required to change solutions in the pressure bomb. The pulse of turbidity beginning approximately at pore volume sixty occurred concomitantly with contact of the deionized water with the sediment.

(Swartz et al., 1997).

That treatment of the sediment with 10 mM phosphate, and not 2 mM SDS, was able to induce preferential mobilization of the goethite during the subsequent deionized water flush does not correlate with the mobility data obtained for the model goethite colloids (**Figure 3.4**). The mobility data suggest that, at a pH of approximately 5.2, 2 mM SDS would be able to impart greater negative potential to the iron oxyhydroxides in the Georgetown sediment than does 10 mM phosphate. Thus, one would expect 2 mM SDS to induce mobilization, given the mobility data. The observed release behavior was probably due to the immediate decay of the SDS admicelle upon flushing with deionized water, which would destroy the surface charge reversal effect imparted by SDS adsorption during the treatment flush. In contrast, phosphate desorption has been shown to be generally slow (Djafer et al., 1991). Thus, the surface charge reversal of goethite (and amorphous iron oxyhydroxides) in the sediment imparted by phosphate adsorption during the treatment flush would be left intact upon flushing subsequently with deionized water. As a result, repulsion between the goethite aggregates and surrounding kaolinite was sufficient to induce mobilization of predominantly the goethite when double layer expansion occurred upon contact with the decreased ionic strength of the deionized water.

It may also be likely that competitive adsorption effects inhibited the ability of the SDS molecule to sufficiently sorb and impart negative charge to matrix constituents. Note that elevated levels of dissolved Si were detected in the effluent from the 10 mM phosphate treatments, while Si in effluent from even 10 mM SDS treatments was indifferentiable from experiments in which only deionized water or 0.1 N $CaCl_2$ solutions were flushed through the sediment (**Figure 3.5**). This indicates that the phosphate ligand was able to displace adsorbed silicate while the SDS head group could not. Other preadsorbed anions (e.g., sulfate, carbonate species) not measured in the effluents from these column experiments may also have hindered SDS sorption. Further evidence suggesting that competitive adsorption effects may play a role in determining which adsorbates will induce mobilization in this

sediment was gathered from *in situ* mobilization experiments (Chapter 4) and is discussed in detail in Chapter 5.

3.3.3 Effect of organic acids

Given the mobilization behavior observed for the phosphate and surfactant treatments, perhaps stronger treatments were needed to mobilize colloids more representative of the bulk composition of the sediment matrix. To this end, the sediment was treated with the reductants, l-ascorbic acid and hydroquinone, and a complexant (in the absence of light), oxalic acid (Zinder et al., 1986; Banwart et al., 1989; Suter et al., 1991). These organic adsorbates dissolve iron oxyhydroxides (Zinder et al., 1986; Banwart et al., 1989). Thus, treatment of the sediment with these organic acids would be expected to break bonds between the amorphous iron oxyhydroxides and the kaolinite books in the Georgetown sediment (1→3 in **Figure 3.1**). In addition, these adsorbates might impart negative charge to the amorphous iron oxyhydroxides and goethite by specific adsorption, depending on the ligand surface speciation (3→4 in **Figure 3.1**).

Treatment of the sediment with oxalic acid at pH 4.1 resulted in an extended initial release of colloids to 15 pore volumes, as well as continued release at approximately 0.5 to 1.0 NTU (**Figure 3.10**) over the 56 pore volume duration of the treatment. During the deionized water flush which followed, turbidity peaked initially at approximately 8 NTU, then leveled off at 5 to 6 NTU for 15 pore volumes (pore volumes 60 to 75, **Figure 3.10**) before gradually declining.

During the ascorbic acid treatments at pH values of 4.2, 5.2, and 6.0, no sustained turbidity was observed after the initial release during the treatment flushes (56 pore volumes), although the initial pulse at the beginning of the pH 6.0 ascorbic acid treatment was notably larger than occurred during the pH 4.2 and pH 5.2 treatments (**Figure 3.10**). No turbidity was observed for the deionized water flushes following the pH 4.2 and 5.2 ascorbic acid treatments. Only during the deionized water flush following the pH 6.0 ascorbic acid treatment was a pulse of turbidity observed (**Figure 3.10**). This pulse peaked at

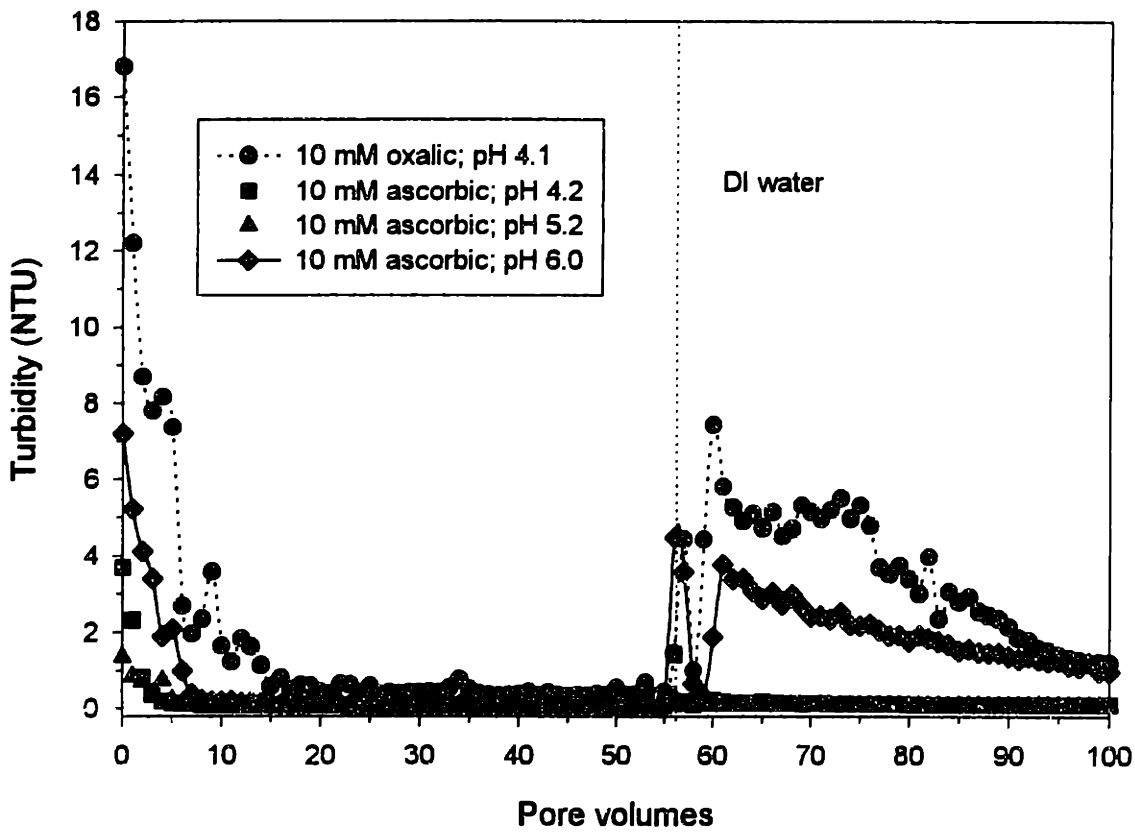

Figure 3.10: Turbidity profiles for experiments in which sediment was treated with10 mM oxalic acid, pH 4.1, or 10 mM ascorbic acid, pH 4.2, 5.2, and 6.0. Treatment solutions were flushed through the columns for 56 pore volumes before exchange with deionized (DI) water. The spike in turbidity at pore volume fifty seven was the result of flow interruption to change solutions in the pressure bomb.

approximately 4 NTU and declined similarly as that which occurred for the pH 4.1 oxalic acid treatment (**Figure 3.10**).

Treatments containing 10 mM hydroquinone at pH 4.6 did not result in any colloid release (data not shown). No release was observed in the subsequent deionized water flush either.

The Al/Fe mole ratios of the colloids released in the deionized water flushes following the oxalic acid (3.1±0.7, **Table 3.1**) and pH 6.0 ascorbic acid (2.5±1.4, **Table 3.1**) treatments differed greatly from those released by the 10 mM phosphate treatments (0.5±0.3, **Table 3.1**). Indeed, oxalic acid and pH 6 ascorbic acid treatments promoted mobilization of colloidal material whose Al/Fe mole ratios were very similar to that of the bulk matrix (3.2±0.2, **Table 3.1**).

Mobilization of colloids compositionally representative of the entire bulk matrix does not appear to be correlated with dissolution of the amorphous silica acting as a mechanical binding agent. If the amorphous silica were mechanically binding the fines (2a,b in **Figure 3.1**), one would expect that relatively large amounts (at least several weight percent) of the amorphous silica cement would be required to "free" the fines. Oxalic acid has been found to enhance the solubility of silicon-rich mineral phases (Bennett et al., 1988; Bennett, 1991; Ohman et al., 1991). Thus, dissolved Si in the oxalic acid and possibly the ascorbic acid treatments would be significantly elevated above the dissolved Si levels in the 10 mM phosphate treatment if dissolution of amorphous silica phase were required to mobilize colloids representative of the bulk matrix. However, levels of dissolved Si in the 10 mM ascorbic acid and 10 mM oxalic acid treatment effluents (**Figure 3.5**) were not significantly different from the levels produced by the 10 mM phosphate treatment. The similar levels of dissolved Si in the ascorbic acid, oxalic acid, and phosphate treatments suggest that these elevated Si levels were the result of exchange of the specifically adsorbing ligands for adsorbed silicate on the surfaces of the matrix constituents and were not due to dissolution of the amorphous silica phase. The five-member ring chelation structures possessed by each of

these ligands would promote such exchange. On the other hand, hydroquinone has no such chelating ability. Correspondingly, dissolved Si levels in the effluent from the 10 mM hydroquinone treatment were indifferentiable from the levels measured for the 10 mM SDS and average of the deionized water and 0.1 N $CaCl_2$ treatments.

The absence of significantly elevated levels of dissolved Si levels in the ascorbic and oxalic acid treatments relative to the phosphate treatment, however, does not preclude the possibility that the organic acids only broke bonds among the amorphous silica and other matrix constituents (e.g., kaolinite). Breaking of bonds would then allow the bulk matrix constituents to respond to repulsive electrostatic effects imparted by specific adsorption of the oxalic and ascorbic acid (i.e., 1a→3→4→5).

The oxalic acid and all ascorbic acid treatments did result in elevated levels of dissolved Fe in the effluent during these treatment flushes (**Table 3.1**). Thus, dissolution of the iron oxyhydroxides in the Georgetown sediment may be correlated with mobilization of colloids representative of the bulk matrix. The pH-dependent colloid release behavior observed for the ascorbic acid treatments (only pH 6.0 ascorbic acid treatment resulted in mobilization, even though dissolved Fe was lowest in the pH 6.0 treatment effluent, **Table 3.1**) suggests that, although initiating dissolution of the amorphous iron oxide intermediaries was necessary for mobilization of the bulk matrix, this dissolution alone was not sufficient to induce mobilization (i.e., 1b→4 in **Figure 3.1** is not viable).

The likely explanation for the pH dependent release observed for the ascorbic acid treatments is that sufficient negative charge had to be imparted to the amorphous iron oxyhydroxides through specific adsorption of sorbates before lowering ionic strength in order to induce mobilization of the bulk matrix (i.e., 1a→3→4→5 in **Figure 3.1**). Apparently, the pH value at which specifically adsorbed ascorbic acid was able to reverse the surface charge of the amorphous iron oxyhydroxide intermediaries lay between pH 4 and pH 6, as suggested by the pH-dependency of colloid release observed in the ascorbic acid treatments. In comparison, specific adsorption of oxalic acid at pH 4.1 was sufficient to reverse surface

charge of the amorphous iron oxyhydroxides. The ability of oxalic acid to impart greater repulsive forces than ascorbic acid through specific adsorption correlates with the comparatively lower aqueous acidity constants (pK_1= 1.5 and pK_2= 4.2; *Merck Index*, (1996)) of oxalic acid versus those of ascorbic acid (pK_1= 4.28, pK_2=11.5; *Merck Index*, (1996)). The mobilities of model goethite colloids suspended in 10 mM oxalic acid and 10 mM ascorbic acid were in qualitative agreement with this trend (**Figure 3.4**). 10 mM oxalic acid was able to reverse the surface charge of goethite colloids at a much lower pH value (approximately pH_{pzc}= 3) than was 10 mM ascorbic acid (approximately pH_{pzc}= 5) (**Figure 3.4**). The pH_{pzc} of the model goethite colloids suspended in 10 mM ascorbic acid was also in good agreement with the colloid release data, in which mobilization of the bulk matrix was observed after treatment with 10 mM ascorbic at pH 6, but no release at all was observed at pH 4 or 5.2 (**Figure 3.10**). Note, though, that it is the surface charge reversal of the *amorphous iron oxyhydroxides* which we believe induces mobilization of the bulk matrix in the Georgetown sediment. The colloid release data suggests that surface charge reversal of the amorphous iron oxyhydroxides occurred near pH 5 in the presence of 10 mM ascorbic acid as well.

3.3.4 Effect of elevated pH

The integrated amounts of Fe released in any of the organic acid treatment represented only a very small percentage of the total amorphous Fe present (**Table 3.1**), even if one assumes that all of the dissolved Fe was derived from the amorphous iron oxyhydroxides (as opposed to both the amorphous iron and goethite phases). For example, the small percentage of amorphous iron dissolved during the pH 6.0 ascorbic acid treatment (0.2%, **Table 3.1**) suggests that dissolution of only very small amounts of amorphous iron oxyhydroxide were required to mobilize colloids compositionally representative of the bulk matrix. Certainly, altering juxtapositions from clay mineral-iron oxide-clay mineral to clay mineral-clay mineral by dissolving the amorphous iron oxyhydroxide intermediaries did not occur in our experiments with the Georgetown sediment. This mechanism has been proposed to explain colloid release behavior in another study in which coastal plain sediments were treated with

ascorbic acid (Ryan and Gschwend, 1994). Rather, our data suggests that perhaps only bond-breaking among the amorphous iron oxyhydroxides and kaolinite was required (i.e., 1a in **Figure 3.1**).

Mobilization behavior upon treatment of the sediment with elevated pH (pH 8.0 and 8.8 solutions) supports the bond-breaking mechanism. At pH 8.0, only limited, sporadic release above a value of 0.5 NTU occurred (**Figure 3.11a**). At pH 8.8, sustained colloid mobilization began only after approximately eighty pore volumes and grew to values of several NTU by the end of the experiment at 190 pore volumes (**Figure 3.11a**). The delayed release at pH 8.8 could have been due to the observed strong buffering capacity of the sediment, which caused effluent pH to fall initially before approaching the influent pH after approximately 60 pore volumes (**Figure 3.11b**). Perhaps sustained release was delayed until pore fluid pH remained high enough (e.g., pH 8.8) to sufficiently hydrolyze bonds among the amorphous iron oxyhydroxides and kaolinite and reverse the surface charge of goethite aggregates and the amorphous iron oxyhydroxide intermediaries among the kaolinite faces to promote detachment. The pH_{pzc} of synthetic goethite can fall in the range of 7.0 to 9.7 depending on the amount and charge of specifically adsorbed ions (Sigg and Stumm, 1980; Borgaard, 1983; Zeltner and Anderson, 1988), and the pH_{pzc} of naturally occurring goethite and amorphous iron oxyhydroxides would be expected to be at the lower end of the range (Schwertmann and Fechter, 1982).

The average Al/Fe mole ratio of these colloids (1.5±0.5, **Table 3.1**), although half that determined for the bulk matrix (3.2±0.2, **Table 3.1**), was higher than the average Al/Fe mole ratio for the colloids mobilized in the deionized water flush following the 10 mM phosphate treatment (0.5±0.3, **Table 3.1**). This suggests that the pH 8.8 treatment was capable of inducing mobilization of colloids more compositionally representative of the bulk matrix than was the 10 mM phosphate treatment.

The lack of detectable Fe (<1 ppb, **Table 3.1**) in the effluent from the pH 8.8 treatment would imply that only bond breaking (i.e., hydrolysis) among the amorphous iron

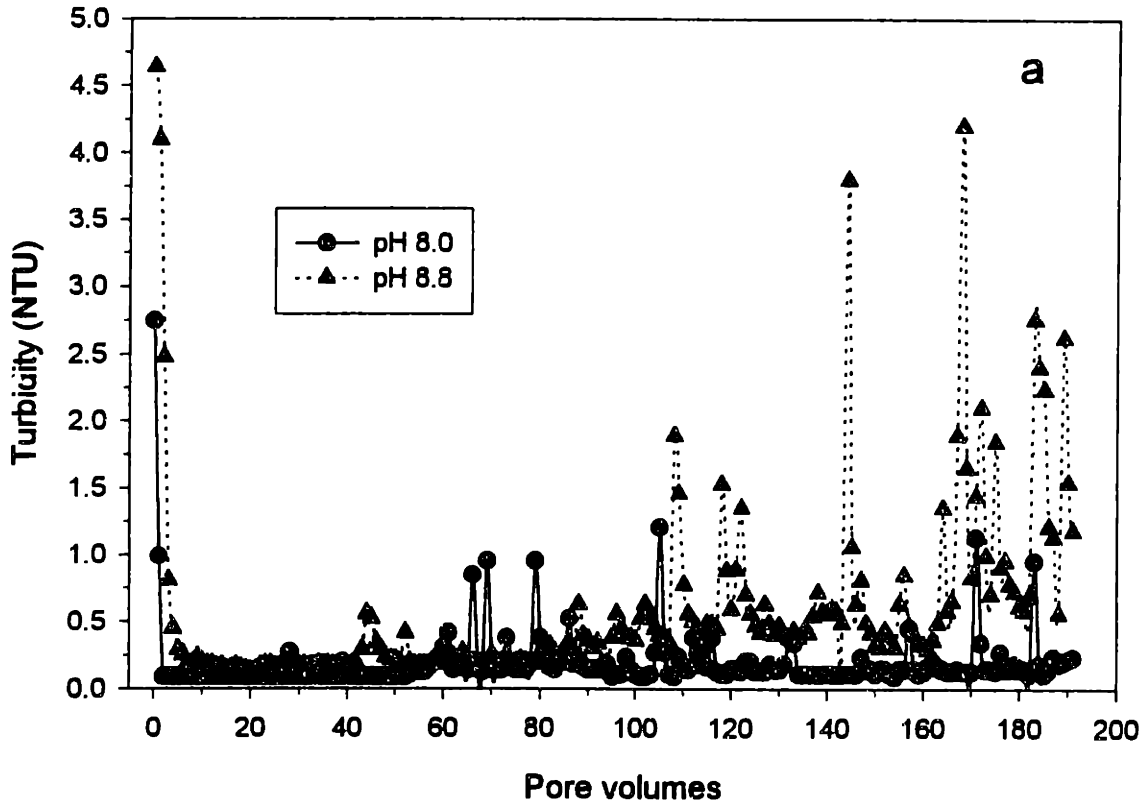

Figure 3.11: (a) (above) Turbidity profiles for experiments in which sediment was subjected to pH 8.0 and pH 8.8 solutions. (b) (next page) pH profiles for the elevated pH treatments. After 10 pore volumes, pH for only every third pore volume is represented. Note the initially lower pH of the effluents for both experiments and the gradual rise to the influent pH. Both treatment solutions were buffered with 0.2 mM $Na_2B_4O_7$ to minimize this titration effect. (c) Profiles of dissolved Si (ppb) measured in the effluents from columns subjected to treatment solutions at various pH and ionic strength values. Each data point represents a measurement of a 2 mL sample of the collected effluent. Background Si was 89±77 ppb. Note that the dissolved Si in the tails of the profiles for the elevated pH treatments is indistinguishable from that for treatments at pH 5.5.

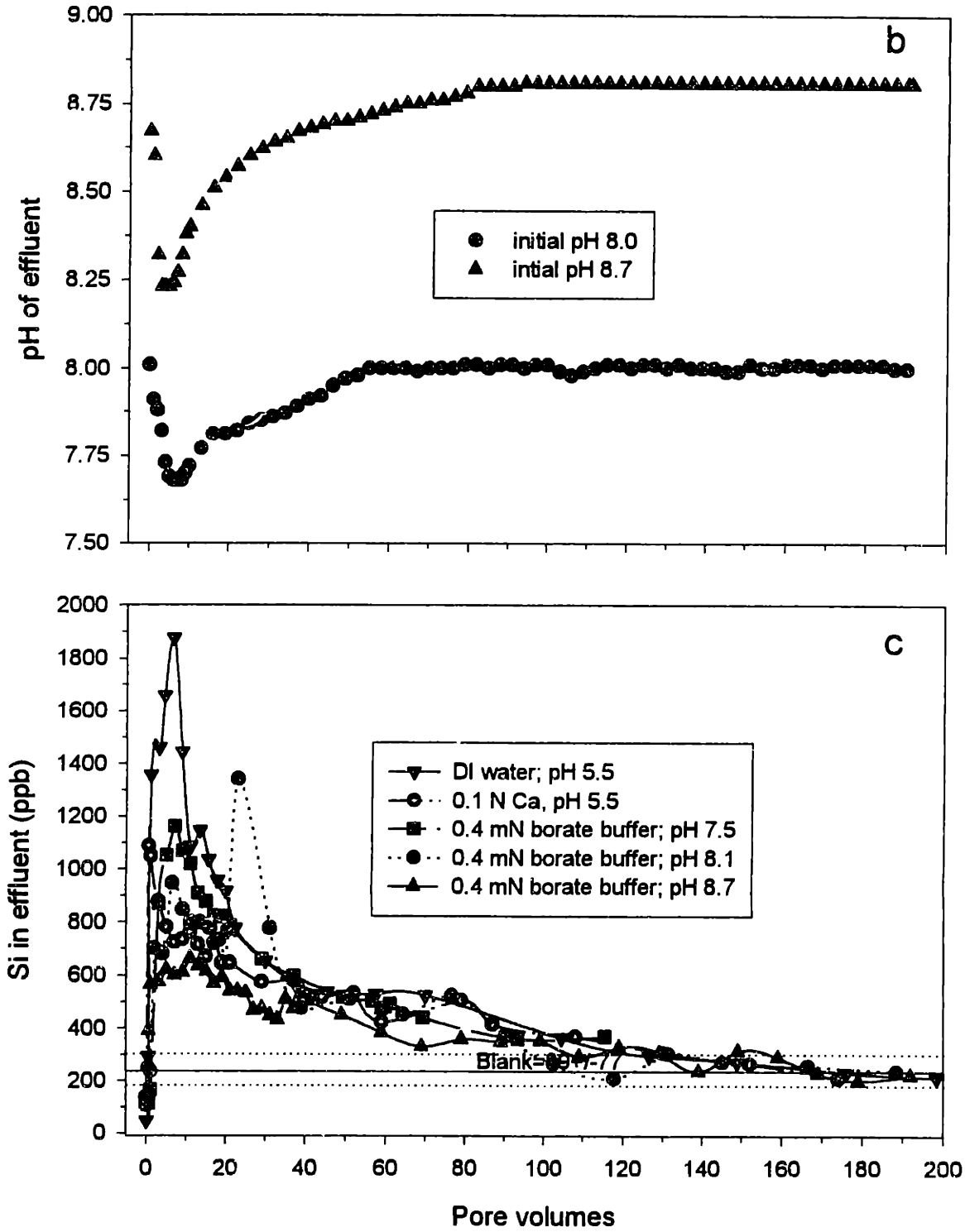
b
pH of effluent
9.00
8.75
8.50
8.25
8.00
7.75
7.50
initial pH 8.0
intial pH 8.7
c
Si in effluent (ppb)
2000
1800
1600
1400
1200
1000
800
600
400
200
0
DI water; pH 5.5
0.1 N Ca, pH 5.5
0.4 mN borate buffer; pH 7.5
0.4 mN borate buffer; pH 8.1
0.4 mN borate buffer; pH 8.7
0
20
40
60
80
100
120
140
160
180
200
Pore volumes

oxyhydroxides and kaolinite was required in order to begin mobilizing colloids more representative of the entire bulk matrix. Similarly, the indifferentiability of dissolved Si in the pH 8.8 treatment relative to dissolved Si levels in treatments at lower pH (**Figure 3.11c**) indicates that, although dissolution of mechanically binding amorphous silica is not playing a role in colloid mobilization, bond breaking among the amorphous silica and other matrix constituents can not be ruled out as a possible mobilization mechanism. In either case, both 10 mM phosphate and pH 8.8 solutions would impart comparable negative charge to the iron oxyhydroxides in the sediment based on surface charge considerations alone (**Figure 3.4**), and both should have been able to mobilize colloids representative of the bulk matrix if only electrostatic binding mechanisms needed to be overcome. Thus, the delayed release behavior exhibited during the pH 8.8 treatment discussed above can not be attributed only to pore fluid pH surpassing the pH_{pzc} of the amorphous iron oxyhydroxide intermediaries, but also to lysing of bonds among the kaolinite and amorphous iron oxyhydroxides.

3.3.5 Effect of acidic pH

If the juxtaposition of positively charged amorphous iron oxyhydroxide and negatively charged kaolinite face is predominant in the Georgetown sediment (i.e., 3 in **Figure 3.1**), dissolution of the amorphous iron oxyhydroxides and concomitant enhancement of *positive* charge on the amorphous iron oxyhydroxides would not be expected to induce mobilization. Acidic pH levels (< 5), induced by hydrolysis of Al^{3+} exchanged for Ca^{2+} when the sediment was subjected to 1 mM $CaCl_2$ solutions (initial pH of approximately 5.5), have been associated with colloid mobilization in other coastal plain sediments (Seaman et al., 1995). Enhancement of positive charge on variably charged constituents (e.g., iron oxides) by the acidic pH were thought to induce mobilization of positively charged colloids in that study (Seaman et al., 1995).

We subjected the Georgetown sediment to 1 mM $CaCl_2$ and 1 mM NaCl solutions with influent pH values of 5.5 before flushing with deionized water to see if the same effect induced colloid release in our sediment (**Figure 3.12**). Decreases in initial pH (5.5) to

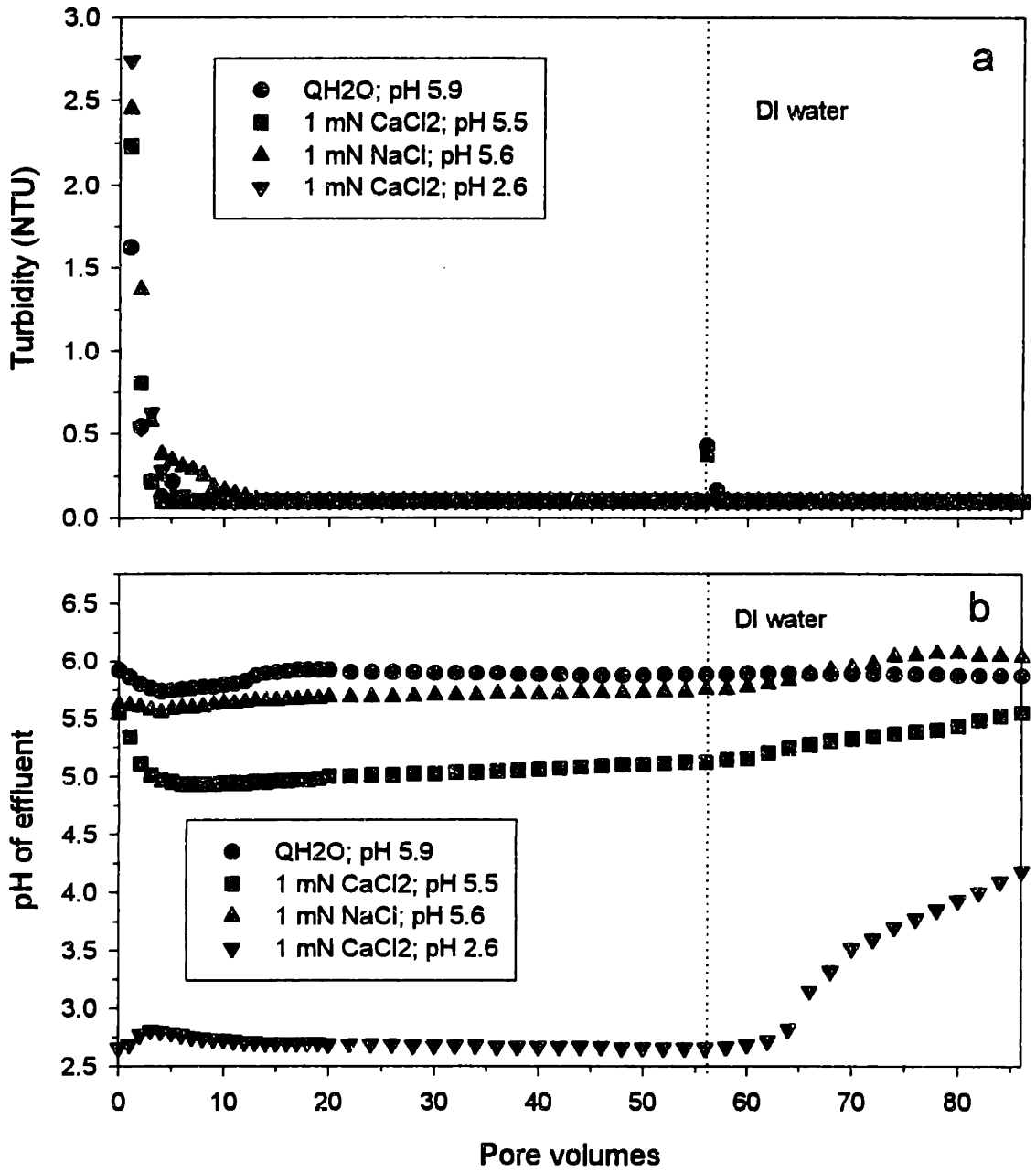

Figure 3.12: (a)Turbidity profiles and (b) effluent pH profiles for experiments in which the sediment was treated with either 1 mN $CaCl_2$, 1 mN NaCl, or deionized water, all at an influent pH of 5.5-6.0, or 1 mN $CaCl_2$ at an influent pH of 2.6. Treatment flushes occurred for 56 pore volumes and were followed by a 30 pore volume deionized (DI) water flush. The spike in turbidity at pore volume fifty seven was due to flow interruption to change solutions in the pressure bomb.

approximately pH 4.5 (**Figure 3.12b**) were observed when the Georgetown sediment was flushed with 1 mN $CaCl_2$. However, no colloid release was observed, as expected (**Figure 3.12a**). Indeed, only the 1 mM NaCl treatment resulted in a slightly elevated turbidity for up to the first 10 pore volumes (**Figure 3.12a**). As stated above, enhancement of positive charge should not induce colloid release if positively charged amorphous iron oxyhydroxide-negatively charged kaolinite face associations dominate in our sediment.

One might argue that hydrolysis of exchanged Al^{3+} perhaps was not strong enough to drive pH low enough to induce mobilization in the Georgetown sediment. Ba^{2+}-exchangeable Al^{3+} was only approximately 8.0% (0.14±0.02 mEq $100g^{-1}$, **Table 3.2**) of the total exchangeable cations in this sediment, whereas Ca^{2+} (1.03±0.09 mEq 100 g^{-1}, **Table 3.2**) and Mg^{2+} (0.50±0.03 meq 100 g^{-1}, **Table 3.2**) made up 78% of the total exchangeable cations. However, no colloid release was observed even when pH 2.6 solutions containing 1 mN $CaCl_2$ were flushed through the sediment (**Figure 3.12a**) before following with deionized water, even though dissolved Fe was detected in the effluent during this treatment (**Table 3.1**). The same treatment taken to 150 pore volumes responded similarly (data not shown).

If the goethite spheroids were chemically bound by amorphous iron and acted in aggregate, as proposed above (effect of ionic strength section), dissolution of the amorphous Fe would allow the spheroids to respond individually to the overall positive repulsive forces acting among them. That no mobilization at all was observed suggests either (1) the attractive forces created between the positively-charged spheroids and surrounding negatively-charged kaolinite by the acidic environment were stronger than spheroid-spheroid repulsion, or (2) amorphous Fe mechanically bound the spheroids, and dissolution of larger amounts of Fe would be required before the spheroids could respond to the spheroid-spheroid repulsive forces generated by the acidic pH.

TABLE 3.2: Cation exchange data[1]

Ion	Average[2] (meq 100 g^{-1})	Standard Deviation	Percent of total[3]
Ca	1.03	0.09	52%
Mg	0.52	0.06	26%
Na	0.20	0.01	14%
Al	0.14	0.02	5%
K	0.03	0.02	3%

[1] by four successive equilibrations with 0.1N $BaCl_2$
[2] based on three replicates
[3] as moles g^{-1}

3.4 Summary: Mechanisms of Colloid Detachment

It appears that effective mobilization of the bulk matrix constituents in this sediment can occur when subjected to a *combination* of solutes (a) which attack the surfaces of the amorphous iron oxyhydroxides, breaking bonds between the amorphous iron phase and the kaolinite (e.g., ascorbic acid, oxalic acid), and (b) impart sufficient negative charge to the amorphous iron oxyhydroxides (e.g., phosphate, oxalic acid, ascorbic acid at pH>5) to repulse the amorphous iron oxyhydroxides and kaolinite faces. In addition, the aqueous concentration of the sorbates must be low enough to permit sufficiently thick double layers among the neighboring phases to allow electrostatic repulsions to exceed van der Waals attractions. Sediment response to relatively low (1 mM) levels of ascorbic acid and phosphate at pH 5.2 (the pH of the native groundwater at the Georgetown site) further supports this mechanism (**Figure 3.13**). Neither 1 mM ascorbic acid nor 1 mM phosphate treatments alone at pH 5.2 induced mobilization of colloids (**Figure 3.13**). However, when 0.5 mM ascorbic and 0.5 mM phosphate were added together at pH 5.2, sustained release of colloids occurred at levels of 2 to 3 NTU over the 40 pore volume duration of the treatment. The Al/Fe mole ratio of the colloids was 2.3±1.0 (**Table 3.1**), indicating that mobilization of colloids representative of the entire bulk matrix was occurring.

Others have observed iron oxide-kaolinite interactions which do not respond only to electrostatic perturbations (Golden and Dixon, 1985). Mixtures of kaolinite and iron oxyhydroxides, formed by oxidation in the presence of the kaolinite, did not respond to electrostatic perturbations, whereas mechanical mixtures of the two constituents did (Golden and Dixon, 1985). These workers hypothesized that bonds held the iron oxide-clay mineral aggregates intact, inhibiting electrostatic dispersion.

The mineralogical composition and structural associations existing in any sediment are dictated, in large part, by the diagenetic processes which act on the sediment. For example, the degree of crystallinity of iron oxides in the sediment is a function of the age and diagenetic history of the deposit. Recurrent oxidation and reduction reactions, as well as the

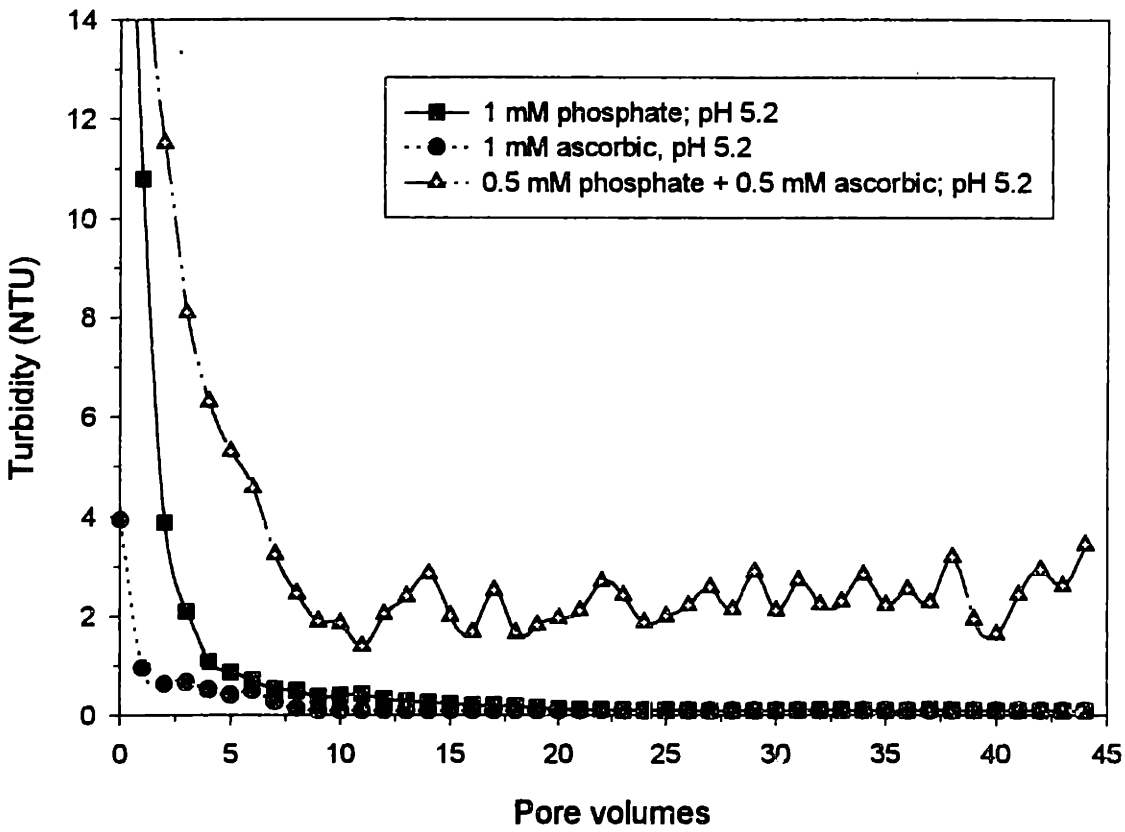

Figure 3.13: Turbidity profiles for experiments in which sediment was treated with either 1 mM phosphate, 1 mM ascorbic acid, or 0.5 mM phosphate and 0.5 mM ascorbic acid. The influent pH in all cases was approximately 5.2. Note that sustained colloid mobilization occurred only when the sediment was treated with the phosphate-ascorbic acid mixture.

presence of solutes which interfere with crystallization (Cornell and Schwertmann, 1979; Anderson and Benjamin, 1985), can promote amorphous or weakly crystalline phases which might become intimately associated with the other constituents of the sediment fines, e.g. clay minerals. As this study demonstrates, these phases may inhibit the effects of chemical perturbations which might mobilize substantially colloids in older, more crystalline (and by inference less "cross-bonded") deposits. Recognition of such differences in behavior among deposits of differing age and diagenetic history is important in developing an understanding of the various mechanisms which generate colloids in the subsurface.

3.5 References

Anderson P. R. and Benjamin M. M. (1985) Effects of silicon on the crystalization and adsorption properties of ferric oxides. *Environ. Sci. Technol.* **19**, 1048-1053.

Atkinson R. J., Posner A. M., and Quirk J. P. (1968) Crystal nucleation in Fe(III) solutions and hydroxide gels. *J. Inorg. Nucl. Chem.* **30**, 2371-2381.

Banwart S., Davies S., and Stumm W. (1989) The role of oxalate in accelerating the reductive dissolution of hematite (α-Fe_2O_3) by ascorbate. *Coll. Surf.* **39**, 303-309.

Bates J. K., Bradley J. P., Teetsov A., Bradley C. R., and Brink M. B. t. (1992) Colloid formation during waste form reaction: Implications for nuclear waste disposal. *Science* **256**, 649-651.

Bennett P. C. (1991) Quartz dissolution in organic-rich aqueous systems. *Geochim. Cosmochim. Acta* **55**, 1781-1797.

Bennett P. C., Melcer M. E., Siegel D. I., and Hasset J. P. (1988) The dissolution of quartz in dilute aqueous solutions of organic acids at 25°C. *Geochim. Cosmochim. Acta* **52**, 1521-1530.

Böhmer M. R. and Koopal L. K. (1992) Adsorption of ionic surfactants on variable-charge surfaces. 1. Charge effects and structure of the adsorbed layer. *Langmuir* **8**, 2649-2659.

Borgaard O. K. (1983) Effect of surface area and mineralogy of iron oxides on their surface charge and anion-adsorption properties. *Clays Clay Min.* **31**, 230-232.

Cerda C. (1987) Mobilization of kaolinite fines in porous media. *Coll. Surf.* **27**, 219-241.

Chandar P., Somasundaran P., and Turro N. J. (1987) Fluorescence probe studies on the structure of the adsorbed layer of sodium dodecyl sulfate at the alumina-water interface. *J. Colloid Int. Sci.* **117**, 31-46.

Cornell R. M. and Schwertmann U. (1979) Influence of organic anions on the crystallization of ferrihydrite. *Clays Clay Min.* **27**, 402-410.

Djafer M., Khandal R. K., and Terce M. (1991) Interactions between different anions and the goethite surface as seen by different methods. *Coll. Surf.* **54**, 209-218.

Golden D. C. and Dixon J. B. (1985) Silicate and phosphate influence on Kaolin-iron oxide interactions. *Soil Sci. Soc. Am. J.* **49**, 1568-1576.

Gschwend P. M., Backhus D. A., MacFarlane J. K., and Page A. L. (1990) Mobilization of colloids in groundwater due to infiltration of water at a coal ash disposal site. *J. Contam. Hydrol.* **6**, 307-320.

Gschwend P. M. and Reynolds M. D. (1987) Monodisperse ferrous phosphate colloids in an anoxic groundwater plume. *J. Contam. Hydrol.* **1**, 309-327.

Hansmann D. D. and Anderson M. A. (1985) Using electrophoresis in modeling sulfate, selenite, and phosphate adsorption onto goethite. *Environ. Sci. Technol.* **19**, 544-551.

Higgo J. J. W., Williams G. M., Harrison I., Warwick P., Gardiner M. P., and Longworth G. (1993) Colloid transport in a glacial sand aquifer. Laboratory and field studies. *Coll. Surf. A.* **73**, 179-200.

Holmén B. A. (1994) Polycyclic Aromatic Hydrocarbon Sorption Kinetics in Three Aquifer Sands. PhD. dissertation, Massachusetts Institute of Technology.

Holmén B. A. and Gschwend P. M. (1997) Estimating sorption rates of hydrophobic organic compounds in iron oxide- and aluminosilicate clay-coated aquifer sands. *Environ. Sci. Technol.* **31**, 105-113.

Kaplan D. I., Bertsch P. M., and Adriano D. C. (1995) Facilitated transport of contaminant metals through an acidified aquifer. *Groundwater* **33**, 708-717.

Kaplan D. I., Bertsch P. M., Adriano D. C., and Miller W. P. (1993) Soil-borne mobile colloids as influenced by water flow and organic carbon. *Environ. Sci. Technol.* **27**, 1193-1200.

Kaplan D. I., Bertsch P. M., Adriano D. C., and Orlandini K. A. (1994) Actinide association with groundwater colloids in a coastal plain aquifer. *Radiochimica Acta* **66/67**, 189-195.

Khilar K. C. and Fogler H. S. (1984) The existence of a critical salt concentration for particle release. *J. Colloid Int. Sci.* **101**, 214-224.

Kia S. F., Fogler H. S., and Reed M. G. (1987) Effect of pH on colloidally induced fines migration. *J. Colloid Int. Sci.* **118**, 158-168.

Lee E. M. and Koopal L. K. (1996) Adsorption of cationic and anionic surfactants on metal oxide surfaces: Surface charge adjustment and competition effects. *J. Colloid Int. Sci.* **177**, 478-489.

Liang L., McCarthy J. C., Jolley L. W., McNabb J. A., and Mehlhorn T. L. (1993) Iron dynamics: Transformation of Fe(II)/Fe(III) during injection of natural organic matter in a sandy aquifer. *Geochim. Cosmochim. Acta* **57**, 1987-1999.

Liang L. and Mc gan J. J. (1990) Chemical aspects of iron oxide coagulation in water: Laboratory studies and implications for natural systems. *Aquatic Sci.* **52**, 32-55.

McCarthy J. F. and Degueldre C. (1993) Sampling and characterization of colloids and particles in groundwater for studying their role in contaminant transport. In *Environmental Particles*, Vol. 2 (ed. H. P. v. Leeuwen and J. Buffle)2-64.

McCarthy J. F., Gu B., Liang L., Mas-Pla J., Williams T. M., and Yeh T.-C. J. (1996) Field tracer tests on the mobility of natural organic matter in a sandy aquifer. *Water Resourc. Res.* **32**, 1223-1238.

McCarthy J. F., Williams T. M., Liang L., Jardine P. M., Jolley L. W., Taylor D. L., Palumbo A. V., and Cooper L. W. (1993) Mobility of natural organic matter in a sandy aquifer. *Environ. Sci. Technol.* **27**, 667-676.

McCarthy J. F. and Zachara J. M. (1989) Subsurface transport of contaminants. *Environ. Sci. Technol.* **23**, 496-502.

McDowell-Boyer L. M. (1992) Chemical mobilization of micron sized particles in saturated porous media under steady flow conditions. *Environ. Sci. Technol.* **26**, 586-593.

The Merck Index. (1996) Merck and Co.

Mysels E. K. and Mysels K. J. (1965) Conductimetric determination of the critical micelle concentration of surfactants in salt solutions. *Journal of Colloid Science* **20**, 315-321.

Newman M. E., Elzerman A. W., and Looney B. B. (1993) Facilitated transport of selected metals in aquifer material packed columns. *J. Contam. Hydrol.* **14**, 233-246.

Ognalaga M., Frossard E., and Thomas F. (1994) Glucose-1-phosphate and Myo-inositol hexaphosphate adsorption mechanisms on goethite. *Soil Sci. Soc. Am. J.* **58**, 332-337.

Ohman L.-O., Nordin A., Sedeh F. I., and Sjoberg S. (1991) Equilibrium and structural studies of silicon (IV) and aluminum (III) in aqueous solution. 28. Formation of soluble silicic acid-ligand complexes as studied by potentiometric and solubility measurements. *Acta Chem. Scand.* **45**, 335-341.

Puls R. W. and Powell R. M. (1992) Transport of inorganic colloids through natural aquifer material: Implications for contaminant transport. *Environ. Sci. Technol.* **26**, 614-621.

Ronen D., Margaritz M., Weber U., and Amiel A. J. (1992) Characterization of suspended particle collected in groundwater under nautral gradient flow conditions. *Water Resourc. Res.* **28**, 1279-1291.

Roy S. B. and Dzombak D. (1996) Colloid release and transport processes in natural and model porous media. *Coll. Surf.* **107**, 245-262.

Ryan J. N. (1992) Clay Colloid Mobilization in an Iron Oxide-Coated Sand. PhD. dissertation. Massachusetts Institute of Technology.

Ryan J. N. and Elimelech M. (1996) Colloid mobilization and transport in groundwater. *Coll. Surf. A.* **107**, 1-56.

Ryan J. N. and Gschwend P. M. (1990) Colloid mobilization in two Atlantic Coastal Plain aquifers, field studies. *Water Resourc. Res.* **26**, 307-322.

Ryan J. N. and Gschwend P. M. (1992) Effect of iron diagenesis on the transport of colloidal clay in an unconfined sand aquifer. *Geochim. Cosmochim. Acta* **56**, 1507-1521.

Ryan J. N. and Gschwend P. M. (1994) Effect of solution chemistry on clay colloid release from an iron oxide-coated aquifer sand. *Environ. Sci. Technol.* **28**, 1717-1726.

Schwertmann U. and Fechter H. (1982) The point of zero charge of natural and synthetic ferrihydrite and its relation of adsorbed silicate. *Clay Min.* **17**, 471-476.

Seaman J. C., Bertsch P. M., and Miller W. P. (1995) Chemical controls on colloid generation and transport in a sandy aquifer. *Environ. Sci. Technol.* **29**, 1808-1815.

Sigg L. and Stumm W. (1980) The interaction of anions and weak acids with the hydrous goethite (α-FeOOH) surface. *Coll. Surf.* **2**, 101-117.

Suter D., Banwart S., and Stumm W. (1991) Dissolution of hydrous iron (III) oxides by reductive mechanisms. *Langmuir* **7**, 809-813.

Swartz C. H., Ulery A. L., and Gschwend P. M. (1997) An AEM-TEM study of nanometer-scale mineral associations in an aquifer sand: Implications for colloid mobilization. *Geochim. Cosmochim. Acta* **61**, 707-718.

Torrent J., Schwertmann U., and Barron V. (1992) Fast and slow phosphate sorption by goethite-rich natural materials. *Clays Clay Min.* **40**, 14-21.

Williams T. M. and McCarthy J. F. (1991) Field-scale tests of colloid:facilitated transport. *National Research and Development Conference on the Control of Hazardous Materials*, 179-184.

Zeltner W. A. and Anderson M. A. (1988) Surface charge development at the goethite/aqueous solution interface: Effects of CO_2 adsorption. *Langmuir* **4**, 469-474.

Zinder B., Furrer G., and Stumm W. (1986) The coordination chemistry of weather: II. Dissolution of Fe(III) oxides. *Geochim. Cosmochim. Acta* **50**, 1861-1869.

Chapter 4:

Field Studies of *in situ* Colloid Mobilization in a shallow, Southeastern Coastal Plain aquifer

4.1 Introduction

The mobilization of aquifer fines due to perturbations in pore fluid chemistry is increasingly acknowledged as an important factor which must be accounted for in contaminant transport models (McCarthy and Degueldre, 1993; Ryan and Elimelech, 1996; Roy and Dzombak, 1997). Because toxic metals (Puls and Powell, 1992), actinides (Bates et al., 1992) and hydrophobic organic contaminants (Gounaris et al., 1993) have been shown to strongly associate with the clay-size solids which constitute aquifer fines, mobilization of aquifer fines may complicate prediction of transport of the associated contaminants.

For example, Kaplan et al. (1995) found various heavy metals to be associated with groundwater colloids consisting of quartz, aluminosilicates, and iron-titanium oxides at the Savannah River site near Aiken, South Carolina. Their observations suggest that colloids have the potential to facilitate the transport of heavy metals. They proposed that the highly acidic waste plume generated by nuclear materials processing caused mobilization of the colloids by decreasing the pore fluid pH below the net pH_{pzc} of the aquifer sediment, producing net repulsive forces among the charged surfaces of the sediment constituents. Laboratory column studies simulating waste plumes moving through aquifer material collected at the Savannah River site have also indicated the potential for colloids mobilized from this sediment to facilitate transport of heavy metals (Newman et al., 1993). In addition, actinides have been shown to associate with groundwater colloids at a variety of sites, suggesting facilitated transport of these contaminants as well (Short et al., 1988; Penrose et al., 1990; Kaplan et al., 1994).

Understanding the chemical processes which induce mobilization of aquifer fines is an important step in predicting colloid-facilitated transport of contaminants. Dissolution of carbonate (Gschwend et al., 1990; Ronen et al., 1992) and iron oxide (Ryan and Gschwend, 1990) cements has been suggested to explain the presence of colloids in some groundwaters. In addition, numerous laboratory studies on natural and synthetic aquifer materials have found

that chemical perturbations which promote particle-particle repulsive interactions among the fines can mobilize colloids. These perturbations include changes in ionic strength (Goldenberg and Margaritz, 1983; McDowell-Boyer, 1992; Roy and Dzombak, 1996) and pH (Cerda, 1987; Kia et al., 1987; Ryan and Gschwend, 1994; Roy and Dzombak, 1996). In addition, surfactants (Ryan and Gschwend, 1994) and subtle changes in cation chemistry (Seaman et al., 1995) have also been show to induce mobilization in iron oxide-rich aquifer sediments.

Although a large number of laboratory columns studies of colloid mobilization behavior have been conducted, field-based verification of the chemical perturbations which mobilize colloids in aquifer materials has not been attempted to date. Only Kaplan et al. (1993) have attempted field-based studies by investigating the effects of percolation rate and dissolved organic carbon on colloid generation in large scale (several meter dimensions) lysimeters containing sediment collected from the Savannah River site.

In the study detailed herein, we attempted to induce mobilization of colloidal fines *in situ* in a Southeastern Coastal Plain aquifer sand. The composition and intimate associations among fine-grained matrix constituents in this sediment have been characterized previously using analytical electron microscopy techniques to identify which constituents may play a key role in binding the fines (Chapter 2, Swartz et al., 1997). In addition, laboratory columns packed with the same sand were subjected to various perturbing solutions to determine the mechanisms which induce mobilization of the matrix in this sediment (Chapter 3). The results of these studies suggested that solutes which break bonds between amorphous iron oxyhydroxides and the clay minerals, among which the amorphous iron oxyhydroxides are intimately associated (Chapter 2, Swartz et al., 1997), can induce mobilization of the bulk matrix if sufficient electrostatic repulsive forces among these constituents are generated concomitantly (Chapter 3).

Using a single well, injection-withdrawal method, we treated sediment *in situ* with groundwater amended with solutes that were found to either induce or not induce mobilization

in the laboratory columns. The single well injection-withdrawal methodology has been used for over twenty years in the petroleum reservoir engineering field, particularly to determine residual oil saturation in these reservoirs (Tomich et al., 1973; Deans and Carlisle, 1986). More recently, the method has been applied to the in situ study of microbial processes (Trudell et al., 1986; Istok et al., 1997). In addition, single well tests have been used to estimate hydraulic properties of aquifers (Gelhar and Collins, 1971; Capuano et al., 1983; Lessoff and Konikow, 1997).

In our single well injection-withdrawal experiments, known volumes of amended groundwater were slowly injected into the aquifer via wells screened and packed-off at a discrete depth. The injected slugs of amended groundwater were then immediately retrieved by reversing flow. The groundwater amendments were chosen to test our hypothesis that dissolution of the amorphous iron oxyhydroxides and generation of sufficient repulsive forces among the matrix constituents were required to induce mobilization in this sediment. "Control" experiments were also performed with unamended groundwater to determine "baseline" turbidity produced by the flow reversal process inherent in the injection-withdrawal procedure. In general, the results of these *in situ* experiments qualitatively verified the mobilization behavior exhibited by the sediment in the packed-column studies (Chapter 3). We suggest that the single well, injection-withdrawal method can be useful in quickly and efficiently testing the colloid mobilization behavior of sediments in response to various chemically perturbing solutions.

4.2 Methodology

4.2.1 Site Characterization

The *in situ* colloid mobilization experiments were conducted in a shallow, unconfined, Southeastern Coastal plain aquifer located on the grounds of Clemson University's Belle Baruch Forest Science Institute in Georgetown, SC. The aquifer is composed of an approximately 100,000 yr old marine beach sand deposit (Williams and McCarthy, 1991).

This approximately 3 m thick aquifer is underlain by a 1 m thick clay layer (Williams and McCarthy, 1991). Previous studies have sought to characterize the two and three dimensional variations in hydraulic conductivity which occur in this distinctly layered aquifer (Mas-Pla et al., 1992; Yeh et al., 1996) in order to more accurately interpret the transport behavior of dissolved organic matter (DOM) observed from forced gradient injection experiments conducted in the aquifer (McCarthy et al., 1993; McCarthy et al., 1996) (**Figure 4.1**). This site was also used to investigate *in situ* iron transformation reaction dynamics in a forced gradient injection experiment (Liang et al., 1993).

The gradient in the aquifer is approximately 0.02 to 0.03 m m^{-1} (McCarthy et al., 1993; Yeh et al., 1996). Values of hydraulic conductivity determined by slug test analyses vary with depth by about one order of magnitude in the aquifer, from approximately 7.9×10^{-6} m sec^{-1} at a depth of 1.15 m to approximately 7.6×10^{-5} m sec^{-1} at 2.65 m below surface (Yeh et al., 1996). The location chosen for our colloid mobilization experiments was approximately 50 m hydraulically upgradient from, and 0.4 m topographically higher than, the test site used for the DOM transport and iron transformation studies discussed above (**Figure 4.1**). The injection depth for all of our experiments was centered at approximately 2.65 m below surface. Slug test analyses to deduce the hydraulic conductivity at the depth of injection were not performed. However, taking into account the topographic difference between our location and that of Yeh et al. (1995) and McCarthy et al. (1996), the hydraulic conductivity at a depth of 2.65 m at our location can be roughly estimated to be 3×10^{-5} m sec^{-1} based on the data of Yeh et al. (1995).

A sediment sample taken from a depth of approximately 2.2 m in June, 1993, was previously characterized for grain-size distribution and mineralogy and studied to deduce the intimate associations among the clay-size constituents making up the interstitial matrix among the primary grains (Chapter 2, Swartz et al., 1997). Microporosity and organic carbon measurements have also been performed on this sediment sample during studies of polycyclic aromatic hydrocarbon sorption (Holmén and Gschwend, 1997). The colloid release behavior

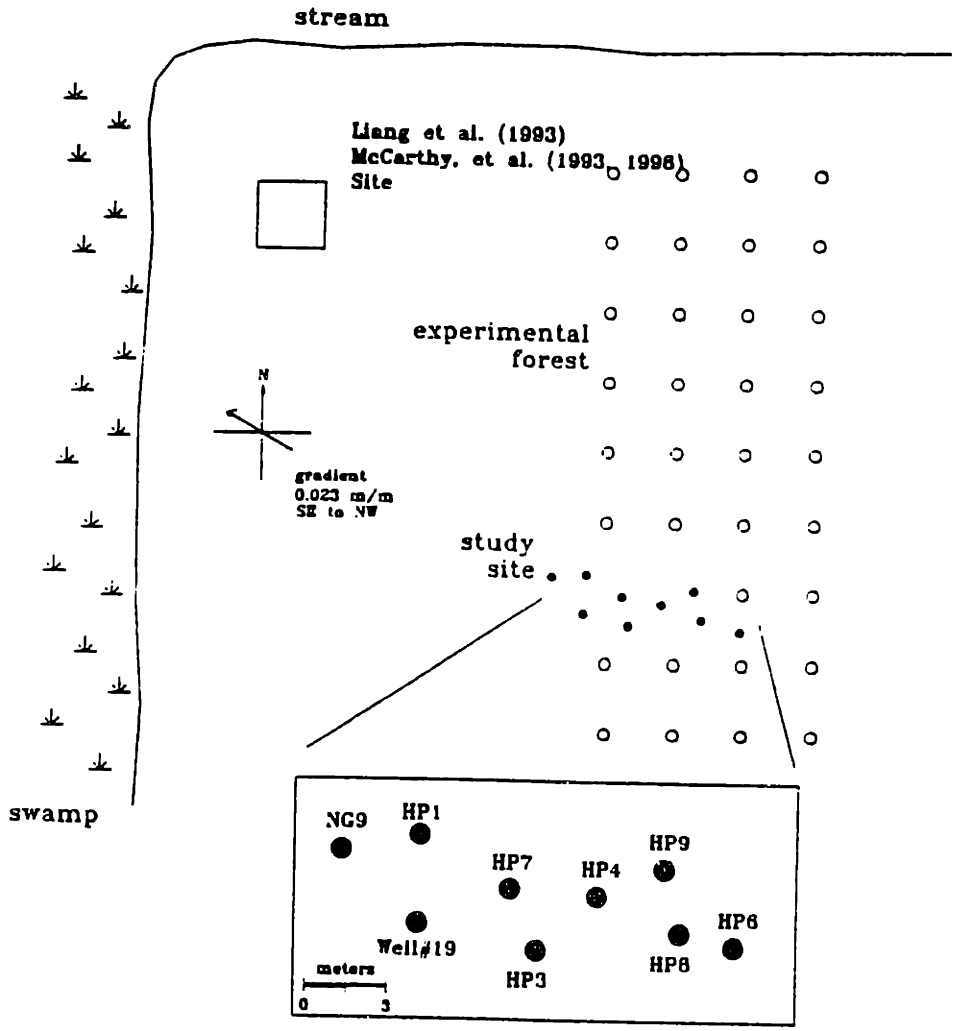

Figure 4.1: Map of the site on the grounds of the Baruch Forest Sciences Institute in Georgetown, SC. Depicted are the array of wells emplaced for the injection-withdrawal experiments, as well as the location of the wells used in the studies of Liang et al. (1993) and McCarthy et al. (1993). NG9 marks the location where the samples for microscopy analysis (Chapter 2) and the packed-column experiments (Chapter 3) were collected. The grid of open circles represents positions of pine trees in a experimental forest plot.

of the sediment in response to various perturbing solutions was investigated using the June, 1993, sample and a second sample collected in March, 1997, from a depth of 2.2 m at a location approximately 0.3 m from the first sample (location NG9 in **Figure 4.1**) (Chapter 3).

The sediment is composed predominantly (approximately 95%) of quartz sand. The <63 μm (silt) and <2 μm (clay) size fractions constitute 12% and 2.5% by weight of the sediment, respectively. Quartz, phyllosilicate minerals (kaolinite and vermiculite), crystalline (goethite) and amorphous iron oxyhydroxides, gibbsite, and amorphous silica phases have been identified in the silt- and clay- size fractions by x-ray diffraction, thermo-gravimetric analysis, selective extraction, and analytical transmission electron microscopy (AEM) techniques (Swartz et al., 1997).

The depth of 2.65 m was chosen for the *in situ* mobilization experiments so that the injection depth would be approximately 1 m below the water table, which was located at about 1.7 m below surface. Although this depth differs from that in which samples were collected for detailed AEM characterization and laboratory colloid mobilization studies (2.2 m), mineralogical and grain-size distribution analysis of intact cores obtained by split-tube sampling at the site indicates that the sediment is relatively mineralogically homogeneous from a depth of 2.0 to 3.0 m (see **Table 2.2**, Chapter 2; Ulery, unpublished data). Visual observation of these cores suggests macroscopic homogeneity of the sediment over this depth range as well.

4.2.2 General organization of injection-withdrawal experiments

Injection-withdrawal experiments were conducted on three occasions at the site (**Table 4.1**). The first set of experiments was conducted in well HP3 in October, 1994 (**Figure 4.1**). On this occasion, the pH of the injected groundwater was sequentially increased from the unamended value of 5.2 (see **Tables 4.2** and **4.3** for ambient groundwater conditions) up to pH 9.5 in a series of six injection-withdrawal experiments (**Table 4.1**). In March, 1997, two wells were emplaced. In the first well, HP4 (**Figure 4.1**), the effect of amending the groundwater with a mixture of 0.5 M phosphate and 0.5 M ascorbic acid was tested (**Table**

Table 4.1: Experimental Parameters

Well	Date	Experiment	Groundwater alteration	Mass Br recovered	Volume injected (ml)
HP3	10/94	A	control (pH_i= 5.19)	0.99*	11500
		B	pH_i= 6.88	1.00	11500
		C	pH_i= 7.68	0.97	11500
		D	pH_i= 8.41	1.02	11500
		E	control (pH_i= 5.13)	0.99*	11300
		F	pH_i= 9.59	0.97	11500
		G	control (pH_i= 5.40)	0.98*	11500
HP4	3/97	A	control (pH_i= 5.42)	0.99*	11275
		B	control (pH_i= 5.42)	0.98*	11400
		C	0.5 mM NaH_2PO_4 and 0.5 mM ascorbic acid (pH_i= 5.78)	0.97	11485
		D	control (pH_i= 5.25)	0.96*	11285
HP6	3/97	A	control (pH_i= 5.33)	1.02	11275
		B	2 mM SDS (pH_i= 5.33)	0.93	11375
		C	10 mM SDS (pH_i= 5.28)	ND	11500
		D	control (pH_i= 5.28)	0.99	11500
HP7	10/97	A	control (pH_i= 5.25)	0.97	11475
		B	pH_i= 2.50	ND	11525
HP8	10/97	A	control (pH_i= 5.38)	0.94	11475
		B	1 mM ascorbic acid (pH_i= 5.30)	0.96	11525
HP9	10/97	A	control (pH_i= 5.35)	0.97	11550
		B	1 mM NaH_2PO_4 (pH_i= 5.25)	0.96	11500

*Helium and neon saturated groundwater used
ND= not determined

4.1). The pH of this mixture was similar to the ambient pH of the groundwater. In the second well, HP6 (**Figure 4.1**), two different concentrations of an anionic surfactant, sodium dodecyl sulfate (SDS), were added to groundwater in a series of two injection-withdrawal experiments (**Table 4.1**). Again, the pH each of these two amended groundwater injectates was similar to the prevailing groundwater pH. For wells HP3, HP4 and HP6, control injection-withdrawal experiments using unamended groundwater (except for the addition of conservative tracers) were carried out both before and after the sequence of amended groundwater injection-withdrawal experiments (**Table 4.1**). In October, 1997, three additional sets of experiments were conducted (**Figure 4.1**). In well HP7 (**Figure 4.1**), the groundwater pH was lowered to approximately 2.5 (**Table 4.1**). In well HP8 (**Figure 4.1**), 1 mM ascorbic acid was added to the groundwater, and in well HP9 (**Figure 4.1**), the groundwater was amended with 1 mM phosphate, added as NaH_2PO_4 (**Table 4.1**). In the latter two experiments, the pH of the amended groundwater was similar to the prevailing pH (**Table 4.1**). For each of the wells HP7, HP8, and HP9, only a "before" control experiment was conducted.

4.2.3 Injection Well Construction and Emplacement

The injection wells were designed to minimize the dead volume contained in the well apparatus between the screened interface with the sediment and the sampling apparatus at ground surface. Most of the decrease in dead volume came from a design feature which alleviated a large, packed off well-bore volume. Rather than use a traditional packer system to isolate a particular screened depth within a casing, we designed a well system in which a very thin, screened annulus was created and packed off (**Figure 4.2**).

Two basic structural components constituted each well. A 4" i.d. PVC pipe with a 3" long slotted screen (slot width equal to 1/1000") centered at the appropriate depth (2.65 m) acted as a traditional well casing emplaced in a hand-augered hole. From some holes, intact cores were obtained during augering by hammering a split-tube sampler a depth of one foot below the position of the bottom of the 4" i.d. PVC casing before advancement of the casing.

Table 4.2: Groundwater Chemical Parameters[1]

pH	5.26±0.13
alkalinity (μM)[2]	26±10
conductivity (μMHOS cm^{-1})[3]	38±5
NP-DOC (μM)[4]	92±21
Dissolved Fe (nM)[5]	130±100
Dissolved Al (nM)[5]	170±120
Dissolved Si (μM)[5]	370±120
SO_4^{2-} (μM)	54±7
Dissolved Oxygen (μM)	140±9
Dissolved Bromide (μM)	0.44±0.06

[1]the average±one standard deviation for n=7 to 10 samples, with at least 1 sample from each of 7 wells included (see **Table4.3** for breakdown of individual values for each well)

[2]measured by Gran titration

[3]corresponds to an ionic strength of approximately 0.4 mM, calculated using the concentrations of the major groundwater ions (Chapter 2)

[4]non-purgeable dissolved organic carbon

[5]defined as passing through a 30 nm pore size filter

Table 4.3: Breakdown of chemical parameters for each of the wells sampled

Chemical Parameter	Well Designation							
	Well#19[1]	HP1[1]	HP3[2]	HP4[3]	HP6[3]	HP7[4]	HP8[4]	HP9[4]
pH		5.50	5.54	5.27	5.38	5.16	5.20	5.20
Alkalinity (μM)		15	35, 23, 36	31, 44, 20	23, 25	32		13,17
Conductivity (μMHO cm^{-1})	40.0	37.2	33.0	32.3		48.6	35.8	36.1
NP-DOC[5] (μM)		130	72	98,72	72, 81	117	100	100, 75
Dissolved Fe[6] (nM)	340	35	130	150	160	160	57	160, 18
Dissolved Al[6] (nM)	120	120	40	63	390	110	260	220
Dissolved Si[6] (μM)	460	550	510	350	270	230	350	350
SO_4^{2-} (μM)			46	51	62	48	52	64
Dissolve O_2 (μM)		140	140	125	160	140	140	
Dissolved Br (μM)	0.39	0.30	0.48	0.52, 0.48	0.41, 0.49	0.46, 0.41	0.54	0.43

[1]Sampled 6/94 or 10/94
[2]Sampled 10/94
[3]Sampled 3/97
[4]Sampled 10/97
[5] Non-purgeable dissolved organic carbon
[6]defined as passing through a 30 nm pore-size filter

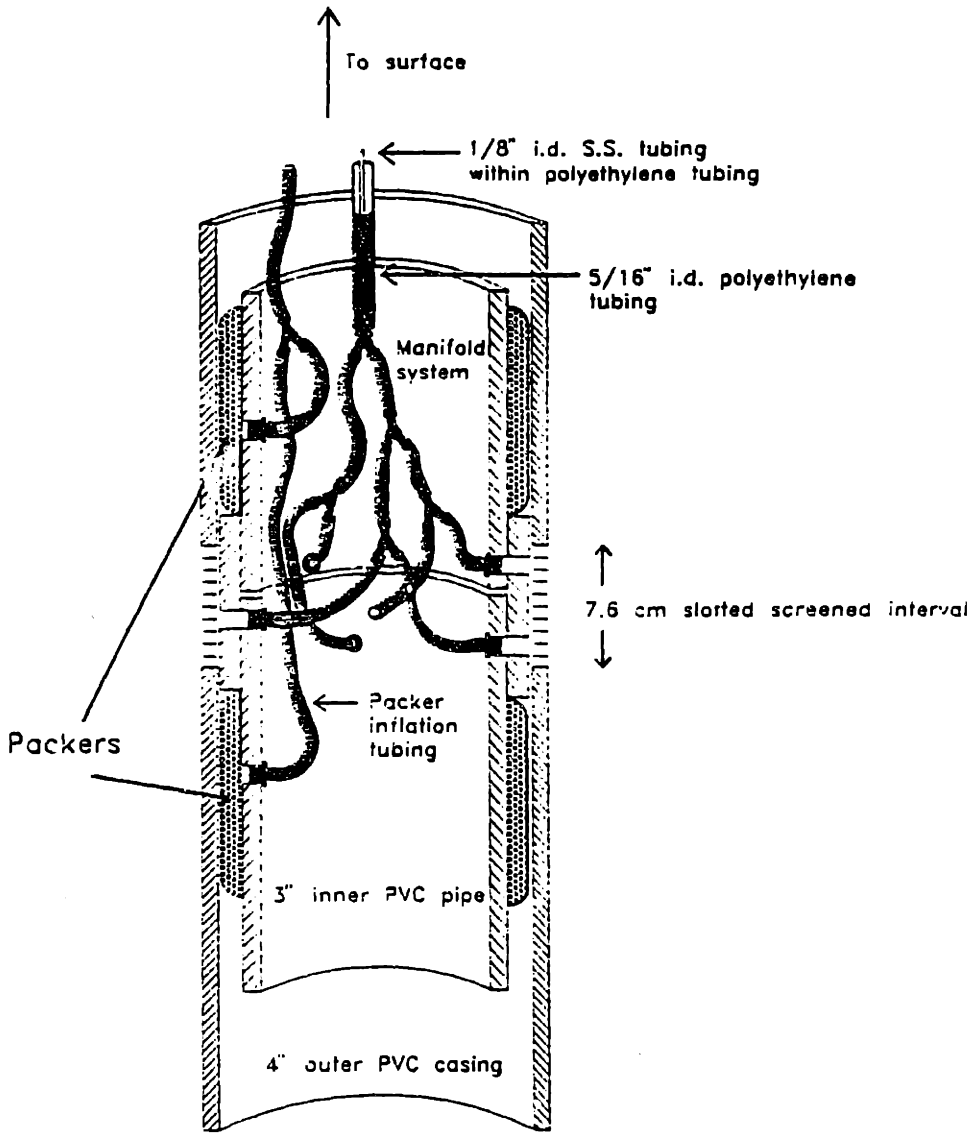

Figure 4.2: Schematic diagram of the well construction. Each well consisted of (1) a 4" i.d. pvc outer casing with a 3" long slotted screen (1/1000") and (2) a 3" i.d. inner well apparatus which included a tubing manifold distribution system (i.e., the "screened interval") for injection and withdrawal of water from the aquifer and an upper and lower inflatable packer. See text for details of construction of the inner well apparatus.

The split tube sampler was retrieved from the hole, and the casing was then advanced one foot concomitantly as the hole was cleaned out with a hand auger to that incremental depth. For all wells augered for this study, the bottom of the 4" i.d. casing was advanced to approximately 3.2 m.

A 3" i.d. PVC pipe with a 4" long "screened" interval centered at 2.65 m and bounded by inflatable, rubber sleeves was inserted into the 4" i.d. casing after the casing was emplaced to the appropriate depth in the aquifer (**Figure 4.2**). The length of the 3" i.d. pipe allowed the "screened" interval of the 3" i.d. pipe to be centered at 2.65 m below ground surface, in line with the screened interval of the 4" i.d. casing. The end result was a very thin well-bore annulus that served as the injection zone when the two screened intervals were aligned (**Figure 4.2**). The 3" i.d. pipe constituting the inner well apparatus could be removed and reinserted in other wells.

The "screened" zone on the 3" i.d. pipe was created by drilling six holes in the surface of a 4" long PVC coupling of the correct size to join 3" i.d. PVC pipe. The holes were tapped with 1/4" threads and 1/4" i.d. barbed hose fittings were threaded into the holes from the inside surface of the coupling. The holes were staggered vertically around the centerline of the 4" long coupling to promote even distribution of flow out of the well (**Figure 4.2**). A length of 1/8" i.d. tubing (tygon) was then fitted onto each of the barbs, and all six pieces of tubing were joined together by barbed fittings to create a branched manifold distribution system for the "screened" interval. A short, 17" long piece of 3" i.d. PVC pipe was then joined to one end of the coupling.

The packers were obtained by cutting a rubber inner tube into two sleeves. One of these sleeves was applied to the 17" long piece of 3" i.d. PVC pipe with contact cement and telephone wire so that the packer would inflate directly against the edge of the coupling where it joined the 3" i.d. pipe (**Figure 4.2**). A barbed fitting had previously threaded into this piece of pipe from the inside surface of the pipe. A similar fitting was applied to the inside surface of a longer piece (10') of 3" PVC pipe to which the upper packer was applied

(**Figure 4.2**). A length of 1/8 " i.d. tygon tubing was applied to each of the packer fittings. Both lengths of tubing were then connected together by a barbed "T" fitting (**Figure 4.2**). A 15' length of tygon tubing was also joined to this "T" fitting. This length of tubing extended up through the 10' long piece of 3" i.d. pipe, and would later be connected to an air tank to inflate the packers once the apparatus was emplaced in the casing. A single length of 5/16" i.d. tygon tubing was also connected to the manifold distribution system for screened interval. This length of tubing extended up through the interior of the longer (10') length of 3" i.d. PVC pipe, where it would later be connected to the sampling apparatus and a peristaltic pump at ground surface (**Figure 4.3**). Upon installing all of the plumbing and making the necessary connections, the longer (10') section of 3" PVC pipe was joined to the coupling with PVC cement.

The use of the coupling reduced the volume of the screened interval annulus to a greater degree than by merely inserting a 3" i.d. pipe inside a 4" i.d. pipe. The surface of the coupling actually had to be filed down somewhat so that the 3" i.d. inner well apparatus would slide easily down the 4" i.d. casing. The clearance between the outer surface of the coupling attached to the 3" i.d. pipe and the inner surface of the 4" i.d. casing was approximately 1/32", producing a volume of approximately 25 mL in the annulus upon inflation of the packers around the edges of the coupling (**Figure 4.2**).

Within the 5/16" i.d. sample line tubing was a length of 1/8" o.d. stainless steel tubing (HPLC grade, Alltech Associates) which extended from the screened interval manifold to ground surface (**Figure 4.2**). At the ground surface, a brass "T" fitting allowed the stainless steel line to be separated from the plastic line so that samples could be taken to determine initial concentrations of the tracers, amendment solutes and other dissolved solutes (e.g., Fe and Al), and pH of the injectate during the injection phase of the experiments (**Figure 4.3** inset). The stainless steel line was also used to sample for He and Ne tracers added to several of the injection slugs (**Table 4.1**) in a related study on diffusion-limited transport in the aquifer (Sanford et al., unpublished data). The stainless line allowed these gases to be

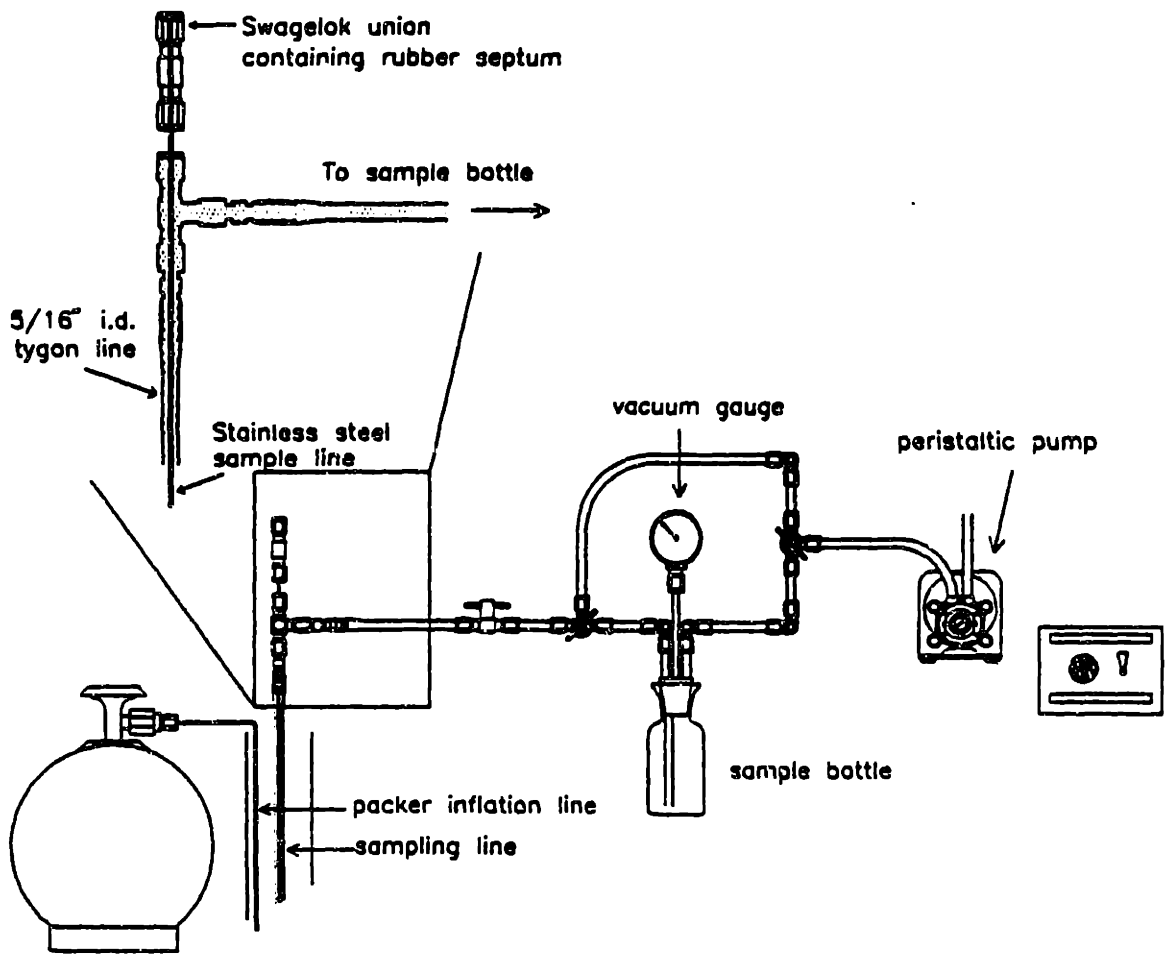

Figure 4.3: Schematic diagram of the sampling apparatus at ground surface. Discrete samples were obtained from the sample bottle during the withdrawal phase of experiments. Sample were obtained by syringe from the swagelok port truncating the stainless steel sample line during the injection phase (see inset). The stainless steel sample line was within the 5/16" plastic tubing, both of which extended to the manifold distribution system at the well screen.

sampled independently from the samples collected for measurement of turbidity, pH, and concentrations of amendment solutes and other appropriate dissolved solutes during the withdrawal phase of the experiments.

4.2.4 Experimental procedures

Injectate Preparation. After a well had been emplaced, but before injection-withdrawal experiments could begin, enough groundwater had to be pumped (at 100 mL min^{-1}) from the well to complete the experiments designated for that well. Collection of this groundwater was begun only after determining that baseline turbidity (approximately 0.08 NTU) had been reached. For each new well, the volume of groundwater pumped before attainment of background turbidity was approximately 5 to 6 liters.

The volume of groundwater collected and prepared for reinjection was generally about 20 L, although only approximately 11.5 L were injected once the dead volume in the well and sampling apparatus (approximately 225 mL) was accounted for. This injection volume was chosen to provide a volume of the aquifer to be "affected" by the injection of the amended groundwater which would be much larger than any disturbed zone around the well screen created by emplacement of the well. We surmised that this disturbed zone might extend several centimeters into the aquifer in a radius around the well screen. The zone affected by the injection would extend approximately 40 cm in a radius around the well screen if radial (disk-shaped) flow was assumed and 21 cm if spherical flow was assumed (see Appendix B). A porosity of 0.30 was assumed in calculating the volumes, and radii of extent, of the aquifer affected by the injections. Thus, the radius of the zone of influence of the injectates would be at least ten times greater than the radius of any disturbed zone around the well screen.

A conservative tracer (sodium bromide, NaBr) was added to each injectate volume. NaBr was added to produce approximately 500 uM Br^-, approximately three orders of magnitude greater than the ambient concentration of Br in the groundwater (**Table 4.2**). In several experiments, helium and neon were also added to study diffusion-limited transport in the aquifer (Sanford et al., unpublished data). Details of the procedure used to saturate the

slugs of groundwater with helium and neon prior to injection are presented elsewhere (Sanford et al., unpublished data).

Depending on the experiment, various chemically perturbing solutes were added to the groundwater as well. Reagent grade sodium bromide, l-ascorbic acid, sodium phosphate monobasic (NaH_2PO_4), and ultrapure sodium dodecyl sulfate (SDS) (GibcoBRL) were added to the groundwater. NaOH and HCl were used to adjust the pH of the collected groundwater.

Well preparation. The first well in which experiments were conducted (HP3, **Table 4.1**) was not developed first before commencing with the first injection-withdrawal experiment (HP3-A; **Table 4.1**) for that well. We believe this led to artificially high initial values of turbidity upon commencing with the withdrawal phase of HP3-A, as initial turbidity values for subsequent injection-withdrawal sequences (a series of higher pH injectates) sequentially declined before increasing dramatically in HP3-F (see results below). This effect was probably due to the presence of loose material near the well screen that was not adequately purged from around the well screen before commencing with the actual experiments. In future wells, we decided to first develop each new well by conducting three to four short (2 L volume) injection-withdrawal sequences (at 100 mL min^{-1}) in succession. Each well was then pumped overnight at 100 mL min^{-1} before beginning the first control experiment. This procedure appeared to stabilize the initial turbidity readings in the actual "before" control experiments.

Injection-withdrawal Procedure. The injection was commenced by stopping the pump (discharge of groundwater from a well was maintained continuously once the developing sequence discussed above had been carried out), connecting the pump to tubing feeding from the carboy, and switching the pump back on in reverse (injection) mode. All experiments were conducted at a pumping rate of 100 mL min^{-1}, which corresponded to a seepage velocity of approximately 2.0 m day^{-1} at the well screen calculated using the area of the well screen and a porosity of 0.30. Depletion of the carboy was monitored until the appropriate volume of groundwater had been injected. Approximately five 10 mL samples were taken from the

stainless steel line by syringe during the course of the injection in order to obtain initial concentrations of the conservative tracers and other added solutes and to monitor pH of the injectate close to the point of injection. Flow was then stopped, and the pump was disconnected from the carboy feed tubing and turned back on in forward (discharge) mode. The dead volumes of the well and sampling apparatus were allowed to pass through the system before commencement of sample collection for turbidity, pH and Br^- measurement.

Sampling apparatus. The sampling apparatus allowed discrete samples to be obtained. The airtight system consisted of teflon stopcocks and tubing, a vacuum gauge, and a 125 ml polyethelene sample bottle (**Figure 4.3**). This system was constructed to allow flow to be stopped so that the filled sample bottle could be replaced with an empty one without losing the column of water held in the line from the screen up to the ground surface. Once bottles had been exchanged, the pump was restarted and the vacuum gauge was monitored until the system approached the appropriate vacuum. The upstream stopcock was then reopened and discharge commenced. The entire exchange procedure required approximately 30-40 s. The acquired sample was then analyzed for turbidity, pH and Br^-, and a subsample was archived for subsequent analysis.

This procedure was repeated after every 500 mL of discharge up to 25,000 mL total discharge. Samples were taken every 2000 mL up to 31,000 mL total discharge, then every 5 L to 10 L thereafter until background levels of the conservative tracers were reattained (usually 45,000 to 50,000 mL for attainment of background Br^-, or four to five times the amount injected). After that, pumping was maintained at 100 mL min^{-1} until the next injection experiment in the sequence was commenced (usually after approximately 120,000 mL, or ten times the previous injection volume, had been discharged).

Sample Analysis. The initial groundwater chemistry was determined from samples obtained from each well before any injection-withdrawal experiments were conducted in that well. To determine dissolved Fe, Al, and Si, approximately 2 mL of each groundwater sample was passed through a 30 nm pore size membrane (Osmotics) which had first been

soaked in a 5% nitric acid solution. Concentrations of these metals were determined using graphite furnace atomic absorption spectroscopy (4100ZL, Perkin Elmer). Anion concentrations (Br^-, SO_4^{2-}, total phosphate) were measured by ion chromatography (Dionex model 16 ion chromatograph with an anion self-regenerating suppressor column). Dissolved O_2 was measured colorimetrically (Chemets) and alkalinity was determined by Gran titration with 0.001 N HCl. Nonpurgeable dissolved organic carbon (NP-DOC) was determined by high temperature (680°C) combustion and detection by a non-dispersive infrared gas analyzer (TOC-5000, Shimadzu). Samples were first acidified with dilute phosporic acid, followed by purging with N_2 for approximately 5 min, before measurement.

For the samples collected during the injection-withdrawal experiments, turbidity (Ratio X/R, Hach) was measured in subsamples (approximately 30 mL) poured from the 125 mL sample bottle into a turbidity sample cell. Because the groundwater was oxic (see **Table 4.2**), there was little danger of creating artifactual turbidity by briefly exposing the samples to the atmosphere in transferring them to the turbidity sample cell (Backhus et al., 1993). Br^- was measured in the field with a specific ion electrode (Corning). pH was measured with a combination electrode (Orion). A temperature compensation probe (Orion) was used with the Br^- concentration and pH measurements.

A 35 mL portion of each collected 125 mL sample was archived for later laboratory measurement of Br^- concentration, dissolved metal concentrations, concentrations of appropriate anions, and colloidal elemental composition when appropriate. Dissolved metal concentrations (Fe, Al, and Si) in the experimental samples were determined in the same manner as was used to determine their concentrations in the unaltered groundwater samples. The Br^- concentrations of some samples were measured again using an ICP-MS (VG Plasmaquad KP-20, Visons Inst.) or ion chromatograph (Dionex model 16 with an anion self-regenerating suppressor column) because the specific electrode did not reliably measure Br^- below levels of approximately 10 μM. A 1.8 mM Na_2CO_3/ 1.7 mM $NaHCO_3$ buffer was used in the ion chromatography. SDS was measured in appropriate archived samples in the same

manner as was used to determine NP-DOC in the ambient groundwater (TOC-5000, Shimadzu).

In samples from experiments in which colloids were mobilized, colloidal Al/Fe mole ratios were determined by first digesting a 1 mL subsample of the archived sample with 0.15 to 0.30 M HF for 72 h, followed by quantification of Fe and Al by A.A. analysis. To get an idea of the variability in the Al/Fe mole ratio for the colloids mobilized in each experiment, subsamples from each of at least the first eight archived samples were analyzed. Whether more archived samples were analyzed depended on how many samples possessed high enough turbidity to permit the analysis. A cut off of approximately 1 NTU was used in this determination.

4.3 Results

4.3.1 Prevailing Groundwater Chemistry

Groundwater samples were collected from each well to determine the ambient chemical conditions in the aquifer and to provide an idea of the spatial and temporal variablity of these parameters (**Tables 4.2** and **4.3**). Note that the pH and dissolved concentrations of O_2, and SO_4^{2-} concentrations were fairly similar among the wells, while dissolved Fe, Al and Si were more variable (**Table 4.2**). The relatively high levels of dissolved Si (approximately 370 μM) suggested that the water was in equilibrium with an amorphous silica phase, possibly biogenically produced opal (Wilding et al., 1979; Drees et al., 1989). Indeed, selective extraction revealed that the <63 μm size fraction of the sediment contained approximately 10% by weight amorphous silica (Chapter 2, Swartz et al., 1997). The dissolved Al concentration (170±120 nM, **Table 4.2**) was somewhat larger than that expected for a groundwater in equilibrium with gibbsite (approximately 80 nM), which was detected in x-ray diffraction patterns of the < 2 μm size fraction (Chapter 2, Swartz et al., 1997).

The O_2 concentration was less than that predicted by its solubility (294 μM) at 18°C

(the approximate ambient groundwater temperature). The observed oxygen depletion may have been the result of subsurface microbial respiration, as the dissolved CO_2 concentration (320 μM as $H_2CO_3^*$), calculated assuming all alkalinity exists as the HCO^{1-} anion, was approximately a factor of 27 larger than predicted by atmospheric equilibration with the groundwater (12 μM). Approximately 160 μM $H_2CO_3^*$ should have been present to satisfy the 1:1 stoichiometry between CO_2 overabundance and O_2 depletion predicted by microbial respiration (Morel and Hering, 1993). The predicted concentration was half that which was present, but the large observed variation in alkalinity may partially explain this discrepancy.

4.3.2 Injection-Withdrawal Experimental Results

Amendments to the groundwater were designed to test whether dissolution of amorphous iron oxyhydroxides, found to be distributed among the kaolinite platelets in the clay-size fraction (Swartz et al., 1997), was required to mobilize colloids representative of the bulk matrix. Laboratory column experiments suggested that merely electrostatic perturbations (treatment with phosphate) mobilized predominantly only goethite aggregates from the sediment, if mobilization occurred at all (Chapter 3). Goethite was found to occur in discretely organized aggregates in the sediment matrix (Swartz et al., 1997), which may explain why they would be preferentially mobilized by electrostatic perturbations. Colloids representative of the entire matrix mobilized were mobilized only when reductants (ascorbic acid) or complexing ligands (oxalic acid), which dissolved the iron oxyhydroxides in the sediment, were added to the flushing solutions (Chapter 3). It was hypothesized that bonds among the amorphous iron oxyhydroxides and kaolinite platelets had to be broken before electrostatic perturbations could act to mobilize the bulk matrix constituents. Rather than present the results of the *in situ* experiments in chronological order of completion, the results are discussed with the development of the bond-breaking hypothesis in mind.

Amendment of groundwater with surfactant. In laboratory column experiments, the Georgetown sediment was flushed with an anionic surfactant, SDS, to determine if reversing the surface charge of positively charged particles through adsorption of the surfactant would

mobilize colloids from the sediment (Chapter 3). The objective in exposing the sediment to an anionic surfactant was to impart a strongly negative surface potential to the amorphous iron oxyhydroxide intermediaries distributed among the kaolinite platelets. The basal plane faces of kaolinite platelets possess a permanent negative charge. Thus, if the surface charge of the amorphous iron oxyhydroxide intermediaries became negative as well, sufficiently strong repulsive electrostatic interactions might induce mobilization if only electrostatic mechanisms bound these constituents.

The sulfate head group of the SDS molecule would not be capable of hydrolyzing bonds. Thus, the effects of treating the sediment with a purely electrostatic perturbation could be studied with the surfactant. Because the goethite aggregates were discretely organized in the matrix, adsorption of SDS onto the goethite would be expected to cause repulsive interactions among its surfaces and surrounding kaolinite faces as well. As no bonds were thought to hold the goethite aggregates immobile, they would be free to respond to such electrostatic perturbations, resulting in their preferential mobilization.

Surfactant experiments were conducted in a sequence of two injections, one at a concentration of 2 mM SDS (HP6-B), and the other at a concentration of 10 mM SDS (HP6-C). Both concentrations of SDS have been found to completely reverse the surface charge of model goethite colloids across a broad pH range (Chapter 3). Thus, injection of groundwater amended with SDS at these concentrations would be expected to induce mobilization of matrix constituents if purely electrostatic binding mechanisms prevailed. However, injection of 2 mM SDS into the aquifer did not produce turbidity in the retrieved injectate that was significantly different from that of the "before" (HP6-A) or "after" (HP6-D) controls (**Figure 4.4a**). This behavior is in correspondence with that observed in packed-columns subjected to 2 mM SDS solutions (Chapter 3).

In contrast, injection of 10 mM SDS (HP6-C) did result in a large, prolonged mobilization event (**Figure 4.4b**). However, given that both 2 mM and 10 mM concentrations of SDS were both equally capable of reversing surface charge of model

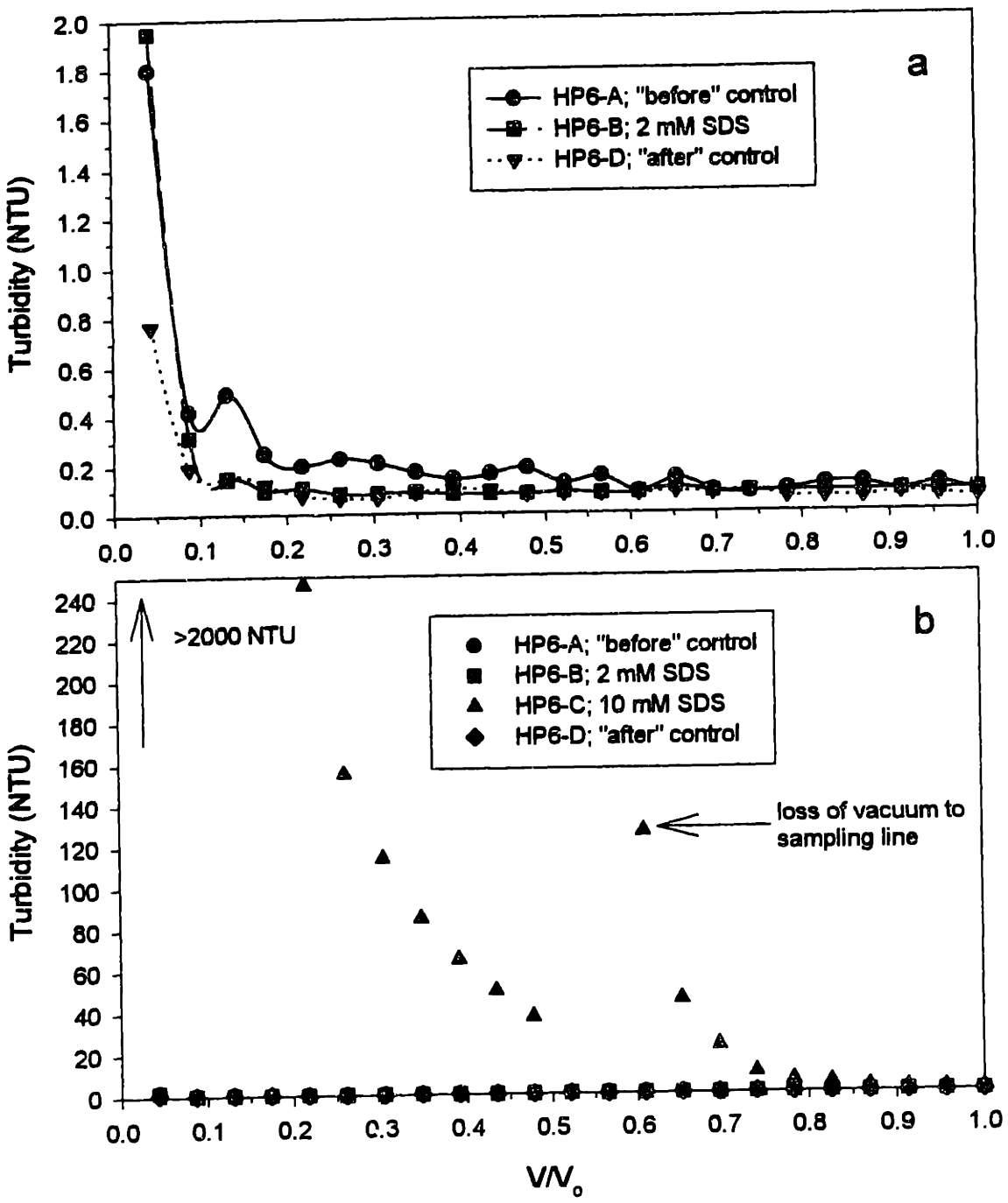

Figure 4.4: Turbidity in each 500 mL sample of retrieved injectate (up to V/V_o= 1.0) for experiments conducted in well HP6. The x axis (V/V_o) is the ratio of volume discharged (retrieved) to volume recharged. (a) Turbidity in discharge during HP6-A, the "before" control, HP6-B (2 mM SDS amended groundwater at pH 5.33), and HP6-D, the "after" control, and (b) Turbidity in discharge for HP6-C (10 mM SDS amended groundwater at pH 5.28). Data for HP6-A,B and D is present again in for comparison.

goethite colloids (**Figure 3.4**, Chapter 3), it appears that the mobilization event caused by the 10 mM SDS injection was due to some additional variable besides electrostatic interactions.

Rather, observation suggested that physical perturbation of the sediment by the surfactant-laden groundwater resulted in the mobilization event. Physical disruption was most likely caused by bubble formation generated by contact of the 10 mM surfactant solution with the sediment. Note that the critical micelle concentration (CMC) of SDS is approximately 8 mM in a 1 mM NaCl solution (Mysels and Mysels, 1965). It appears that the peristaltic, vacuum action of the pump used to inject and withdraw the groundwater aggravated the foaming tendency of this concentrated SDS solution. Intense foaming was observed in the injection line leading from the peristaltic pump to the well screen. Upon reversing flow, the water in the sampling line surged as the peristaltic pump "pulled" on the foaming solution (now containing a fair amount of air). The resulting surging action induced by the pump only added to the physical perturbation created by contact of the foaming solution with the aquifer solids. The result was a substantial mobilization event, with turbidity levels in the retrieved injectate initially greater (≥2000 NTU) than the measurable range of the turbidimeter.

Bubbles were also observed emanating from the packed-columns flushed with 10 mM SDS (Chapter 3). Concomitant with bubble formation, abundant turbidity was measured in the effluent from these columns. In the column experiments, flow was initiated by a relatively gentle process, that is, the surfactant solution was forced through the column under a constant argon pressure of 3 psi (Chapter 3). One would expect that the harsher action of the peristaltic pump, combined with the flow reversal inherent in the injection-withdrawal method, would generate greater physical disruption of the sediment matrix *in situ*.

Note, though, that even after such a large mobilization event, turbidity in the retrieved injectate in the subsequent control experiment (HP6-D) was not significantly different from either HP6-A (the "before" control) or the 2 mM SDS injection (HP6-B) (**Figure 4.4a**). This indicated that the mobilization event that occurred in HP6-C did not produce a large amount of loose material that could be readily flushed in the subsequent control experiment (HP6-D).

Amendment of the groundwater with phosphate. Phosphate has been shown to possess a strong affinity for iron oxyhydroxide surfaces, reversing their surface charge in a manner much like SDS (Sigg and Stumm, 1980; Liang and Morgan, 1990a). We injected 1 mM phosphate amended groundwater into the aquifer (HP9-B) to observe whether this adsorbate induced mobilization. Turbidity in the retrieved samples of the 1 mM phosphate amended groundwater was somewhat elevated in comparison to the control experiment (HP9-A) (**Figure 4.5**). The first sample withdrawn from the phosphate injection (HP9-B) had a turbidity of 12.3±0.2 (error represents one standard deviation on sample measurement), whereas the first sample withdrawn in HP9-A had a turbidity of 4.6±0.1. By the third sample (1,500 mL discharged), the turbidity of the discharge from the phosphate injection had decreased to 2.83±0.1, whereas control values had decreased to 0.33±0.02.

After approximately 8000 mL discharged (i.e., V/V_o=0.75), the turbidity in HP9-B rose again, from approximately 0.5 NTU to 5.7±0.1 NTU. Turbidity then declined, and rose again to values near 2 NTU before finally falling again to 0.6 NTU at V/V_o= 1.1 (**Figure 4.5**). It is possible that these two short pulse of turbidity which occurred at V/V_o> 0.7 were a manifestation of the influx of lower ionic strength water as the dispersively mixed injectate front move into the injectate-affected zone around the well. These later turbidity pulses were perhaps similar in origin to the pulse of turbidity commonly seen in column experiments when deionized water flushes follow treatment with a chemically perturbing solution (Ryan and Gschwend, 1994; Seaman et al., 1995). The dispersion front, a mixture of injectate with ambient groundwater, would possess a lower ionic strength which might have induced expansion of the electric double layers of matrix constituents. The ambient ionic strength of the groundwater was approximately 0.4 mM, calculated using the Debye-Hückel approximation and the concentration of major ions measured in the water (Chapter 2; Morel and Hering, 1993). This effect would magnify any repulsive electrostatic interactions induced by specific adsorption of the phosphate in the zone of influence around the well. Note that these secondary turbidity pulses occurred in samples in which the normalized concentration of

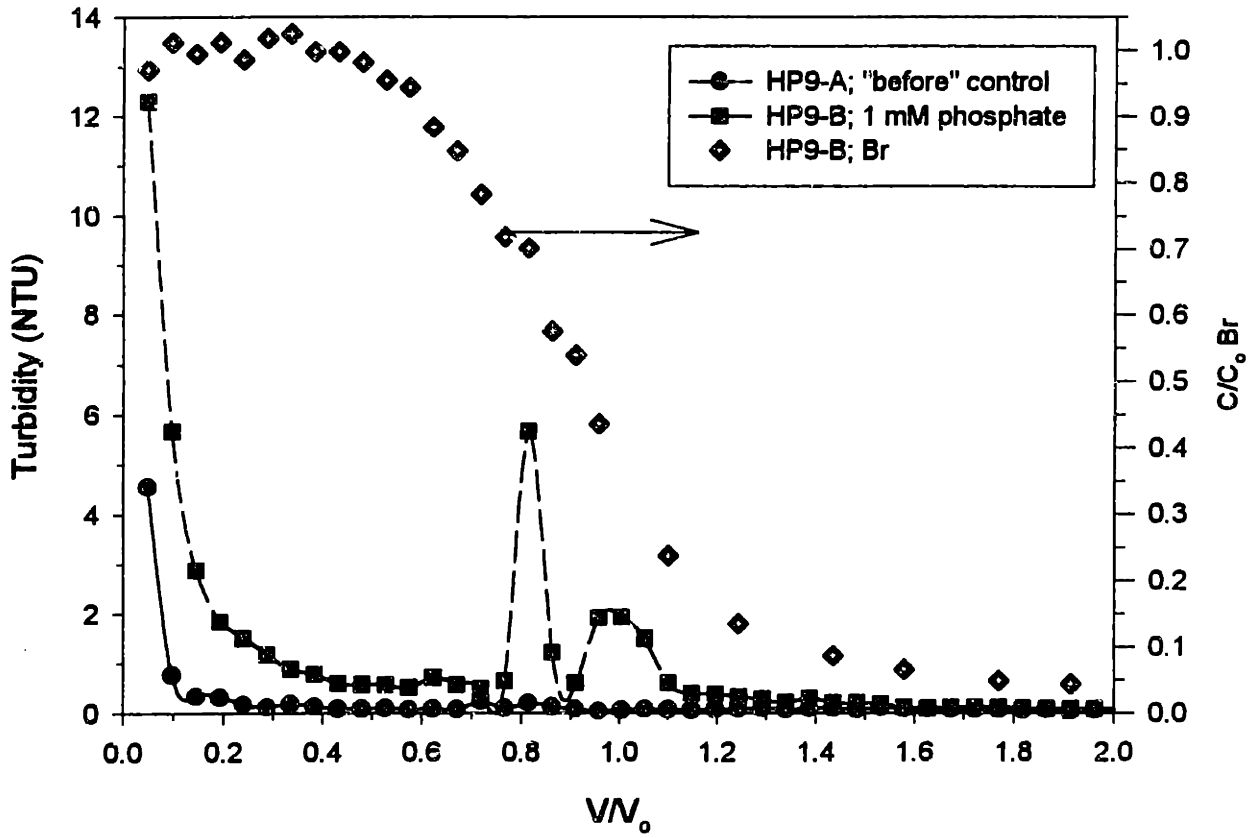

Figure 4.5: Turbidity in each 500 mL sample of retrieved injectate for HP9-A (the control experiment) and HP9-B (1 mM phosphate amended groundwater at pH 5.25). The normalized concentration of Br^- for HP9-B corresponds to the right y axis.

the tracer (Br^-) had begun to decrease sharply (**Figure 4.5**). The sharp decrease in the tracer concentration indicated that these samples were withdrawn from the dispersively mixed injectate front, which had reached the well screen.

In contrast to this *in situ* behavior, laboratory columns subjected to 1 mM phosphate did not release colloids, even after forty pore volumes of contact time (Chapter 3). Only a brief, initial pulse of turbidity, elevated with respect to control experiment levels, was observed in the laboratory columns, and this pulse was thought to be due to mobilization of loose material caused by column packing. No deionized water flush followed the 1 mM phosphate treatments conducted in the columns. Solutions containing 10 mM phosphate did not induce mobilization either, although a sustained pulse of turbidity was observed during the deionized water flush following the 10 mM phosphate treatment (Chapter 3). This turbidity pulse peaked at 1 NTU and subsequently decreased over the 30-pore-volume deionized water flush (Chapter 3).

It is difficult to compare the magnitudes of the mobilization events which occurred in the laboratory column experiments to those which occurred in the field experiments. The flow reversal inherent in the single well procedure may have produced larger turbidity values than would have been produced by uniform flow conditions. Note that the "before" control (HP9-A) exhibited comparatively higher initial turbidity levels than occurred in any of the control experiments conducted in HP6 (or HP7, discussed below). Thus, the discrepancy between the column and *in situ* behavior may have been due to the presence of a disturbed zone near the well screen of HP9, which would result in more easily mobilized material.

What is strikingly consistent between the column and laboratory results is the chemical makeup of the colloids mobilized by phosphate treatment. HF digestion of the colloids mobilized in HP9-B revealed that their Al/Fe mole ratio was 0.8±0.2 (n= 8). Colloids mobilized in the deionized water flush following treatment with 10 mM phosphate possessed an Al/Fe mole ratio of 0.5±0.3 (Chapter 3). These Al/Fe mole ratios are much more similar to that of the goethite aggregates (0.24±0.8, Swartz et al., 1997, Chapter 2) than to the Al/Fe

mole ratio of the bulk matrix (3.2±0.2, Chapter 3), suggesting that preferential mobilization of the goethite occurred in both the *in situ* and column experiments. The much lower Al/Fe mole ratio of the colloids in comparison to the bulk indicates that the amorphous iron oxyhydroxides and kaolinite platelets remained predominantly immobile during the phosphate treatment.

Others have recently observed preferential mobilization of goethite in a similar Southeastern Coastal Plain sediment. Seaman et al. (1997) examined colloids mobilized in columns packed with aquifer material taken from the Savannah River Site near Aiken, South Carolina. The columns were subjected to various $CaCl_2$ solutions. In these experiments, exchange of Ca^{2+} for Al^{3+} resulted in lowering of the pore fluid pH to a point where net positive charge, and apparently significant repulsive interactions, was generated and induced colloid release (Seaman et al., 1995; Seaman et al., 1997). Using transmission electron microscopy, they observed that as much as 77% of the total colloids released from the sediment was composed of goethite (Seaman et al., 1997). We performed some calculations to estimate what percent of the mobilized colloids was goethite for our experiments. Based on the Al/Fe mole ratios we measured, we found goethite to represent > 90% by weight of the colloids mobilized *which contain Al and Fe* (see Appendix A). This value corresponds well to that found by Seaman et al., 1997, for their sediment, when only Al and Fe contributing phases are considered in their percent calculation (85%).

Given that solutions containing 2 mM SDS were able to lower the surface charge of model goethite colloids to a greater degree than solutions containing even 10 mM phosphate (Chapter 3), the question remains as to why 1 mM phosphate addition to the groundwater induced mobilization of predominantly goethite aggregates (HP9-B), while amendment of the groundwater with 2 mM SDS (HP7-B) did nothing. The same behavior was exhibited in the column experiments as well (Chapter 3). The answer may lie in competitive adsorption effects involving the added adsorbate and ambient adsorbates in the subsurface system (Chapter 5).

Amendment of Groundwater with Ascorbic acid. Bonds between the homogeneously distributed amorphous iron oxyhydroxides and kaolinite platelets may render electrostatic perturbations ineffective which would otherwise mobilize these constituents in this sediment (Chapter 3). Lysing of these bonds through initiation of iron oxyhydroxide dissolution by a reductant, ascorbic acid, induced mobilization only when pH and the concentration of ascorbic acid were sufficient to promote surface charge reversal of the iron oxyhydroxides (Chapter 3). For example, 10 mM ascorbic acid was found to reverse the surface charge of model goethite colloids only at pH values above approximately 5.2 (Chapter 3), which is the approximate pH of the groundwater pH at the Georgetown site (**Table 4.2**). Columns containing the Georgetown sediment did not release colloids in response to 1 mM ascorbic acid solutions at pH 5.2, even while dissolution of the iron oxyhydroxides was taking place (Chapter 3). This behavior supported the conclusions drawn from the electrophoretic mobility data.

Injection of 1mM ascorbic acid was conducted (HP8-B) to determine if this behavior could be reproduced *in situ*. Specifically, we sought to determine if adding a reductant to the groundwater would induce mobilization at a concentration which would dissolve iron oxyhydroxides, but would not be expected to impart sufficient electrostatic repulsion among the matrix constituents. Initial turbidity in the retrieved injectate for HP8-B was approximately twice (27.8±0.1) that in the retrieved injectate from the 1 mM phosphate injection (HP9-B) (**Figure 4.6**) and was much greater than the control values. Turbidity remained at values of 2 to 3 NTU up to approximately 6000 mL discharged (V/V_o=0.52; **Figure 4.6**), in contrast to the 1 mM phosphate treatment (HP9-B), where turbidity values fell below 1 NTU by 3000 mL discharged (V/V_o= 0.26; **Figure 4.5**). At 6900 mL discharged (V/V_o= 0.6; **Figure 4.6**), turbidity began to rise again as a second pulse of turbidity appeared in the discharge. This second pulse reached a peak of 36.8±0.2 NTU at 8000 mL discharged (V/V_o= 0.69) before falling to approximately 1 NTU by 12,000 mL discharged (V/V_o= 1.04; **Figure 4.6**). The second turbidity pulse which occurred in HP8-B peaked at a somewhat lower value of V/V_o (0.69) than the second, but comparably much smaller, turbidity pulse

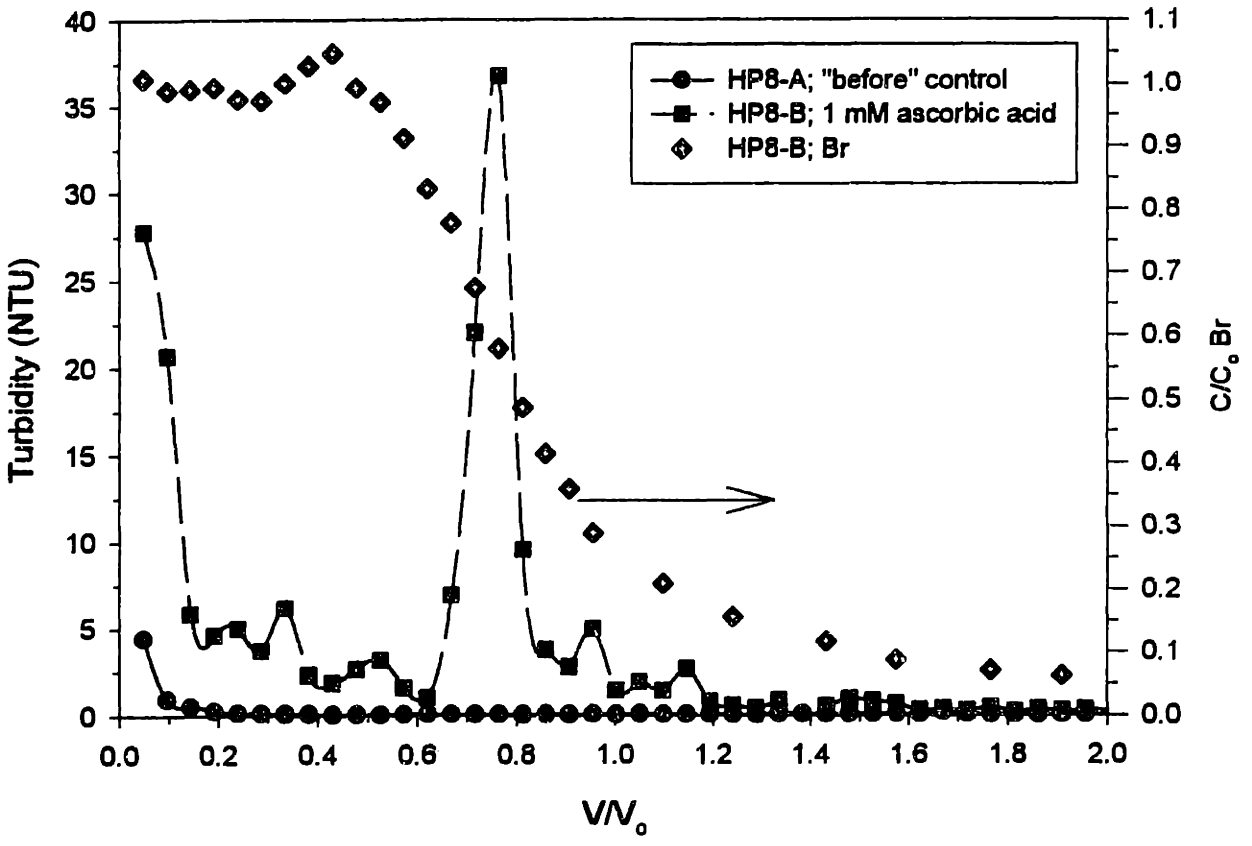

Figure 4.6: Turbidity in each 500 mL sample of retrieved injectate for HP8-A (the control experiment) and HP8-B (1 mM ascorbic acid amended groundwater at pH 5.30). The normalized concentration of Br^- for HP8-B corresponds to the right y axis.

which occurred in HP9-B (V/V_o = 0.73). The shift represented a difference in V/V_o of approximately 0.05 (about 600 mL, or one sample volume). However, if one compares the positions of these secondary turbidity peaks for both HP8-B and HP9-B with respect to values of the normalized concentration of the Br^- tracer, they appeared at very similar values of C/C_o Br^- (approximately 0.60). The shift in the Br^- concentration profiles with respect to V/V_o between the two wells probably reflected subsurface spatial heterogeneity (see Appendix B). As suggested above, the origin of the secondary turbidity peaks was probably due the drop in solution ionic strength as injectate-mixed formation water flushed the affected solids.

In contrast to the colloids mobilized by the 1 mM phosphate injectate (HP9-B), the colloids mobilized by 1 mM ascorbic acid treatment appeared to be more chemically representative of the bulk matrix. The Al/Fe mole ratio of these colloids was 1.9±0.2 (n= 12), more similar to that of the bulk matrix (3.2±0.2) than were the colloids mobilized by the 1 mM phosphate treatment (0.8±0.2). Thus, the 1 mM ascorbic acid treatment, which increased dissolved Fe considerably above ambient levels (**Figure 4.7**), appears to have been able to mobilize a larger fraction of the amorphous iron oxyhydroxide-kaolinite platelet assemblages in addition to goethite. Note that the calculation of the Al/Fe mole ratio of the colloids was performed using a correction for the dissolved Fe and Al that were present in the samples. This *in situ* behavior is in agreement with the bonding mechanism believed to control the mobilization behavior of the amorphous iron oxyhydroxide-kaolinite platelet components of the matrix.

However, the *in situ* mobilization behavior in response to 1 mM ascorbic acid treatment is in disagreement with the laboratory column behavior. In the column experiments, no release of colloids was observed with 1 mM ascorbic acid solutions at pH 5.2 (Chapter 3). At pH 5.2, one would not expect 1 mM ascorbic acid to impart sufficient negative charge to matrix constituents to induce repulsion and mobilization based on the electrophoretic mobility studies with model goethite colloids (Chapter 3). The initial pH of the injectate (5.30, **Table 4.1**), did rise to approximately 5.5 as the result of exchange and dissolution processes (see

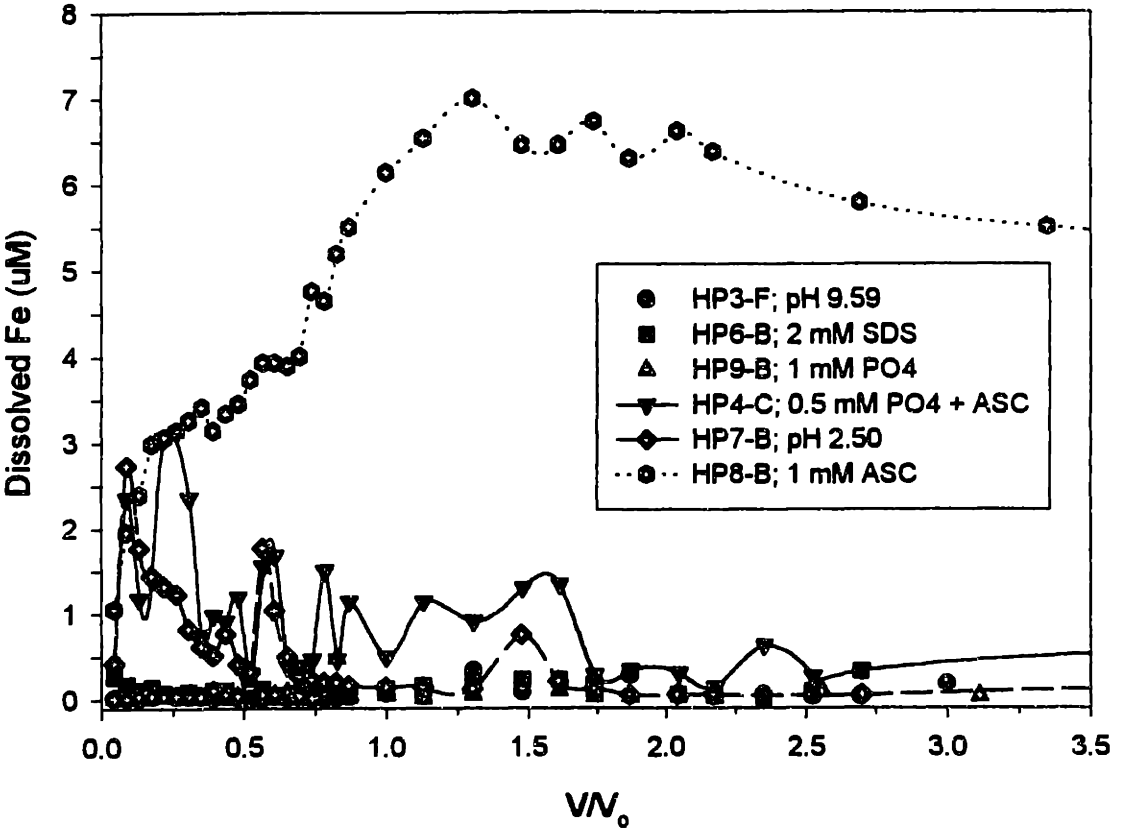

Figure 4.7: Dissolved Fe (μM) in each 500 mL sample of retrieved injectatate (up to V/V_o= 3.5) for the experiments in which the aquifer was chemically perturbed. Data for experiments HP3-F (pH_i= 9.59), HP4-C (0.5 mM phosphate and 0.5 mM ascorbic acid, pH 5.78), HP6-B (2 mM SDS, pH 5.33), HP7-B (pH 2.50), HP8-B (1 mM ascorbic acid, pH 5.30), and HP9-B (1 mM phosphate, pH 5.25) are represented. Note that the dissolved Fe in the samples from experiments HP3-F, HP6-B, and HP9-B are indistinguishable from ambient (130±100 nM) levels.

Chapter 5) upon contact with the sediment. Perhaps this rise in pH was enough to allow adsorbed ascorbic acid molecules to impart sufficient repulsive forces among the matrix constituents to induce mobilization.

Another possible cause of the discrepancy between the *in situ* and column behavior might have been the presence of additional adsorbates in the groundwater which acted synergistically with the added ascorbic acid to induce mobilization in the *in situ* experiments. These additional sorbates would not have been present in the deionized water used to prepare the ascorbic acid solutions for the laboratory column experiments. Dissolved organic matter (DOM), naturally containing carboxyl groups, has been shown to shift the pH_{pzc} of iron oxyhydroxides to lower values (Tipping, 1981; Tipping and Cooke, 1982; Liang and Morgan, 1990b). The pH_{pzc} of hematite colloids was shifted from a value of 8.5 to 6.9 when the colloids were suspended in approximately 0.1 mg L^{-1} Suwannee River humic acid (Liang and Morgan, 1990b). Tipping (1982) found similar concentrations of humic material in lakewater samples to shift the pH_{pzc} of goethite from a value of 7.4 to 6.7. Although we measured *DOC* in the Georgetown groundwater (92±21 μM C or approximately 1.0 mg L^{-1} C; **Table 4.2**), this amount of dissolved organic carbon would represent at least ten times the concentration of dissolved organic matter present in the studies of Liang and Morgan (1990) and Tipping (1982). Thus, it is possible that carboxyl groups present in adsorbed DOM acted in concert with the adsorbed ascorbic acid to impart sufficient repulsive interactions among the matrix constituents to induce mobilization in the *in situ* experiments.

It might also be possible that flow reversal contributed sufficient physically disruptive forces to mobilize colloids once the bonding mechanisms among the matrix constituents had been altered. In other words, lysed bonds between the amorphous iron oxyhydroxides and kaolinite platelets made them more susceptible to mobilization by physical disruption.

Amendment of Groundwater with Phosphate and Ascorbic Acid. In laboratory columns containing the Georgetown sediment, a treatment solution containing 0.5 mM phosphate and 0.5 mM ascorbic acid was found to induce sustained, low levels (2 - 3 NTU)

of colloid release when passed through the sediment, in contrast to solutions containing 1 mM levels of either of these two solutes (Chapter 3). By adding adsorbates (1) capable of breaking bonds between the amorphous iron oxyhydroxides and the kaolinite platelets, (i.e., ascorbic acid), and (2) imparting repulsive interactions among the constituents, (i.e., phosphate), mobilization of colloids representative of the bulk matrix was achieved (Chapter 4).

Injection of groundwater amended with 0.5 mM phosphate and 0.5 mM ascorbic acid (HP4-C) induced *in situ* mobilization as well (**Figure 4.8**). Turbidity in the first 500 mL sample withdrawn was > 600 NTU (**Figure 4.8**), indicating that a much larger mobilization event was achieved by injecting the phosphate-ascorbic acid amended groundwater than occurred with either the 1 mM phosphate (HP9-B) or 1 mM ascorbic acid (HP8-B) injectates. Turbidity fell rapidly, but remained at 2 to 3 NTU before falling below 1 NTU at 7000 mL discharged (V/V_o= 0.61; **Figure 4.8**). Turbidity of the first samples from the control experiments conducted before (HP4-B) and after (HP4-D) the mobilization experiment consistently reached only values of approximately 4.5 NTU, similar to the "before" controls conducted for HP8 and HP9. Curiously, no secondary peak of turbidity occurred in HP4-C, even though the initial mobilization event was much stronger than that which occurred in HP8-B or HP9-B (**Figure 4.8**). This suggested that the affected solids were not sensitive to contact with the lower ionic strength formation water coming in behind the injectate dispersion front.

The Al/Fe mole ratio of the colloids mobilized by the 0.5 mM phosphate and ascorbic acid addition was 2.5±0.6 (n= 8), indicating that colloids closely resembling the make up of the bulk matrix (3.1±0.2) were mobilized by the treatment. The Al/Fe mole ratio for the colloids mobilized in packed-columns subjected to 0.5 mM phosphate and 0.5 mM ascorbic acid was very similar (2.3±0.9, **Table 3.1**, Chapter 3) to those mobilized by *in situ* treatment. The Al/Fe mole ratios of the colloids is congruent with the hypothesis that the presence of solutes which (1) break bonds among the amorphous iron oxyhydroxides and kaolinite, and

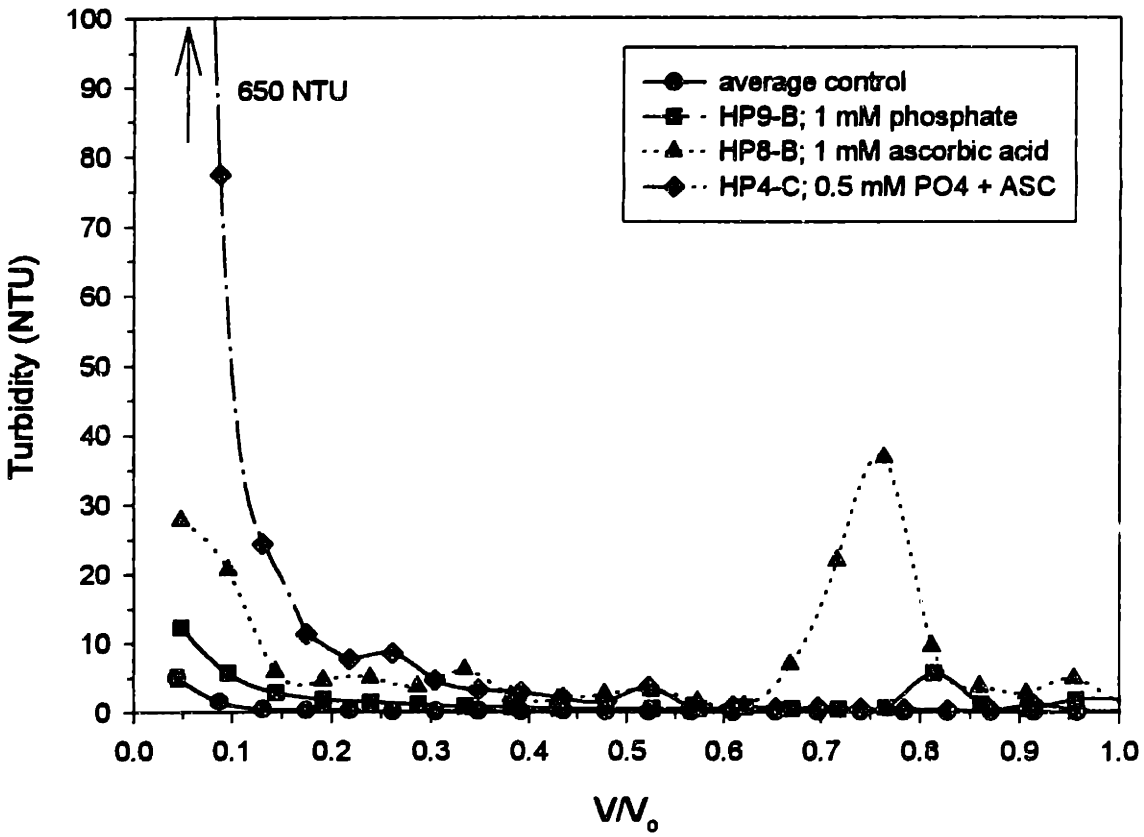

Figure 4.8: Turbidity in each 500 mL sample of retrieved injectate for HP4-C (0.5 mM phosphate and 0.5 mM ascorbic acid, pH 5.78). Data for HP8-B (1 mM ascorbic acid, pH 5.30) and HP9-B (1 mM phosphate, pH 5.25) are presented also for comparison.. The control data represent averaged values of turbidity incorporating samples (at the same value of V/V_o) from HP4-A, HP4-D, HP8-A, and HP9-A. Error bars are generally smaller than symbol size for these average values.

(2) impart sufficient repulsive interactions among these constituents would induce mobilization of the bulk matrix of this sediment.

Again, the magnitude of release observed *in situ* in HP4-C was much larger compared to what was observed in the laboratory columns (only a sustained level of 2 to 3 NTU was generated in the columns subjected to the phosphate-ascorbate treatment, see Chapter 3). Assuming that similar solid-to-water ratios apply for both types of experiments, it appears that scaling-up of the turbidity from the laboratory to the field may be difficult, possibly due to the added effect of shearing forces produced by the injection-withdrawal scheme.

Amendment of Groundwater with Base. Elevation of pH may be expected to result in (1) surface charge reversal and an increasingly negative surface charge of the goethite and amorphous iron oxyhydroxides in the sediment, and (2) possible hydrolysis of bonds among the amorphous iron oxyhydroxides and kaolinite platelets. As the pH_{pzc} of naturally occurring iron oxyhydroxides is in the range of 6.0 to 8.0 (Schwertmann and Fechter, 1982), raising pH to levels of 8.0-9.0 would be expected to induce mobilization of the goethite aggregates in the sediment at the very least, as net negative repulsive interactions among the aggregates and negatively charged kaolinite faces and edges would occur (the pH_{pzc} of kaolinite edges is approximately 7; Herrington et al., 1992). Given our hypothesis of the existence of bonds among the amorphous iron oxyhydroxides and kaolinite, hydrolysis of these bonds at elevated pH would also allow the net negative repulsive interactions among the amorphous iron oxyhydroxides and kaolinite to induce mobilization of these constituents as well. Colloids mobilized in column experiments at pH values of 8.8 had Al/Fe mole ratios of 1.5±0.5 (**Table 3.1**, Chapter 3), suggesting that at least partial mobilization of the amorphous iron oxyhydroxide-kaolinite constituents had occurred in addition to mobilization of goethite aggregates.

Elevating the pH of the groundwater to 9.59 (HP3-F) appeared to produce the same result *in situ* (**Figure 4.9**). Because a sequence of injections with successively increasing pH were conducted in one well (HP3, **Table 4.1**), the turbidity of the first 500 mL sample taken

Figure 4.9 appears on the next page

Figure 4.9: Turbidity in the retrieved samples of injectate for experiments conducted in wells HP3 and HP7 (basic and acidic pH experiments, respectively). (a) Turbidity in the first 500 mL sample retrieved from HP3-A (pH_i= 5.19), HP3-B (pH_i= 6.79) , HP3-C (pH_i= 7.68), HP3-D (pH_i= 8.41), HP3-E (pH_i= 5.12), HP3-F (pH_i= 9.59), HP3-G (pH_i= 5.60), and HP7-B (pH_i=2.50). Note the "peak" in turbidity at approximately pH 7.0. The artifacts causing this peak are discussed in the text. (b) Turbidity in each 500 mL discharge sample for the same experiments presented in (a) except for HP7-B. The normalized concentration of Br^- for HP3-G corresponds to the right y axis.

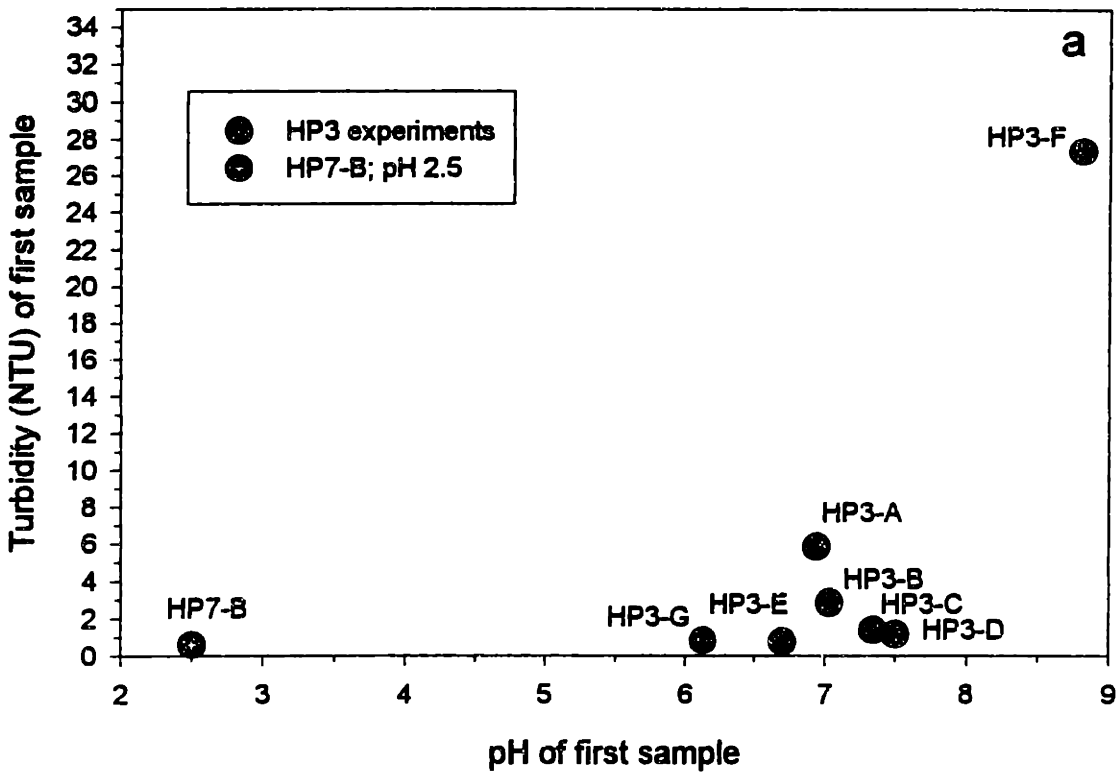
a
HP3 experiments
HP7-B; pH 2.5
HP3-F
HP3-A
HP3-B
HP3-C
HP3-D
HP3-E
HP3-G
HP7-B
Turbidity (NTU) of first sample
pH of first sample

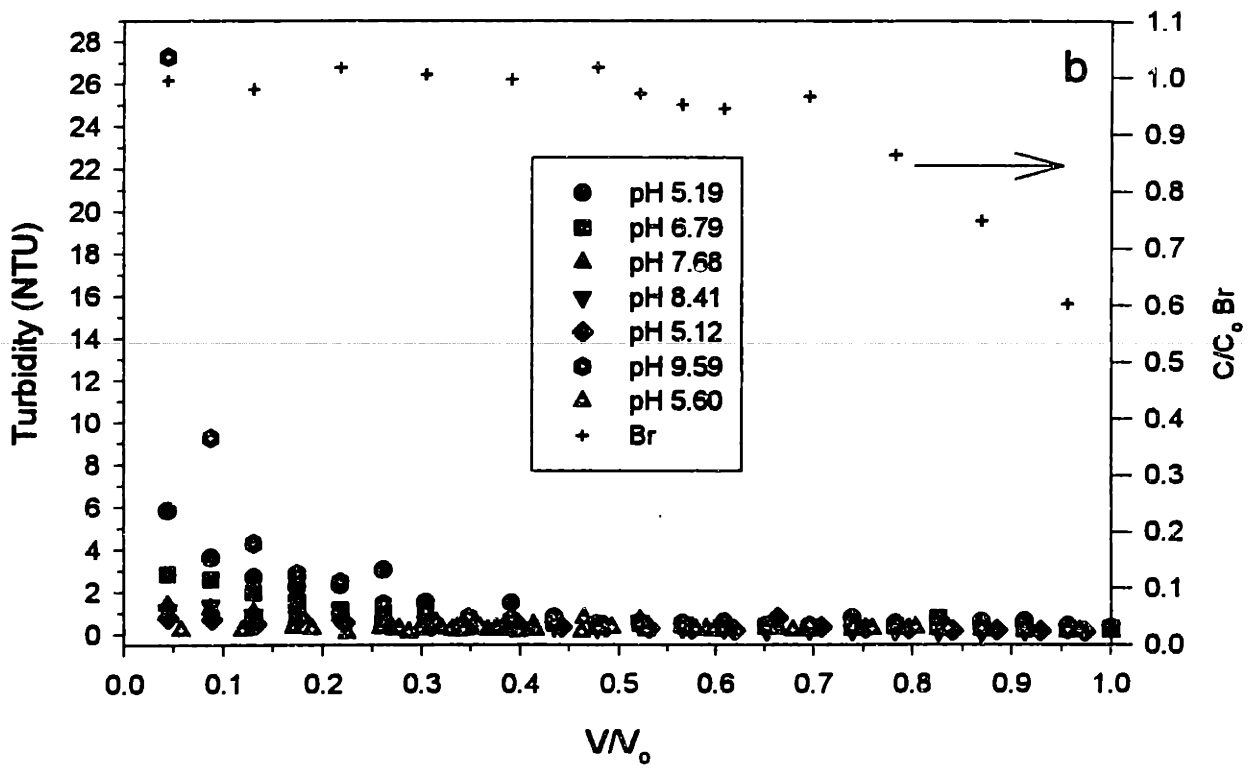
b
pH 5.19
pH 6.79
pH 7.68
pH 8.41
pH 5.12
pH 9.59
pH 5.60
Br
Turbidity (NTU)
C/C0 Br
V/V0

upon commencing with the withdrawal phase in each experiment is plotted against the pH of that 500 mL sample to summarize and clarify the behavior observed (**Figure 4.9a**). Greatly elevated turbidity (27.3±.1) occurred in the first sample retrieved in HP3-F (pH_i= 9.59, **Table 4.1**) in comparison to the control experiment (HP3-E, pH_i = 5.12) performed immediatedly before it. The Al/Fe mole ratio (1.8±0.7, n=9) of the colloids mobilized in HP3-F was very similar to the Al/Fe mole ratio for colloids mobilized at pH 8.8 in the column experiments (1.5±0.5; **Table 3.1**, Chapter 3).

The Al/Fe mole ratio of the colloids mobilized in HP3-F was also similar to the Al/Fe mole ratio of the colloids mobilized in the 1 mM ascorbic acid injection (HP8-B), indicating colloids of similar composition were mobilized by the two different treatments. In contrast to HP8-B samples, however, dissolved Fe concentrations in HP3-F samples were indistinguishable from ambient levels (**Figure 4.7**). This suggests that only hydrolysis of bonds, and not dissolution of the amorphous iron oxyhydroxides, was required to initiate mobilization of colloids more representative of the bulk matrix. A similar interpretation was made from observations of the sediment behavior in the column experiments (Chapter 3).

Note that turbidity values for the first samples withdrawn from experiments HP3-A through HP3-E systematically declined (**Figure 4.9a**). The "peak" in turbidity observed near pH 7.0 is an artifact of two confounding factors. First, because well HP3 was not primed before commencing with the first injection-withdrawal sequence (HP3-A), this experiment had artificially high initial turbidity values. As stated in the methods section, loose material may not have been adequately flushed from near the well screen of HP3 before beginning HP3-A. HP3-B suffered to a lesser extent from the same effect, as evidenced by the lower, but still elevated turbidity level of the first sample collected (**Figure 4.9a**). By the time HP3-C (pH_i = 7.68, **Table 4.1**) and HP3-D (pH_i=8.41, **Table 4.1**) were performed, it appeared that initial turbidity induced by loose material and the flow reversal procedure had stabilized at low levels (near 1.1 NTU). Thus, the turbidity value (0.77±0.05) of the first sample from HP3-E (pH_i= 5.13, **Table 4.1**) probably represented the true baseline value of turbidity from which to

judge the magnitude of the mobilization event which occurred in HP3-F (pH_i = 9.59, **Table 4.1**) (**Figure 4.9a**).

The second confounding factor is apparent when one notes that HP3-A was meant to be a control experiment with pH_i = 5.19, approximately equal to the ambient pH of the groundwater. However, the pH of the injected groundwater never matched the pH of the groundwater upon withdrawal of the first sample for any of the experiments in HP3 (**Figure 4.10a**). When amended groundwater with a pH less than approximately 7 was injected (HP3-A,B,E,G), the pH of the retrieved samples was initially elevated above the pH of the injectate before it had contacted the sediment (**Figure 4.10a**). Correspondingly, when amended groundwater with a pH above 7 was injected (HP3-C,D,F), the pH of the samples retrieved was less than that before contact with the sediment (**Figure 4.10a**). Note that this discrepancy in pH between injected and withdrawn waters was not due to alteration of the water by the sample line, as the pH of subsamples of the injectate extracted from the stainless steel sample line during the injection phase of the experiments was the same as the pH of the injectate in the carboy.

The decrease in pH observed for the injectates with an initial pH > 7.0 was most likely due to titration of the injectate as the surfaces of the sediment constituents deprotonated in an attempt to equilibrate with the elevated aqueous OH^- concentration. The predominate matrix constituents, goethite and kaolinite, both probably have pH_{pzc} values near 7.0 to 8.0. The surface chemistry of these constituents would titrate solution pH toward their pH_{pzc} values. This titration effect probably drove the pH of the injectate down in the *in situ* experiments utilizing injectates with elevated pH. A similar titration effect was observed in the column experiments with the Georgetown sediment (Chapter 3).

The increase in pH of injectates with a pH_i of 5.2 to 5.5 (HP3-A,E,G; **Figure 4.10a**) upon contact with the sediment, however, was opposite to the effect observed in the laboratory, where initial declines in pH were observed when pH 5.5 deionized water was passed through the Georgetown sediment (Chapter 3). In the column experiments, the

Figure 4.10 appears on the next page

Figure 4.10: pH of the samples of retrieved injectate for experiments conducted in well HP3 (a) in the first 500 mL sample retrieved in each of the experiment, and (b) in each 500 mL sample retrieved up to $V/V_o = 3.0$ for each experiment. The normalized Br^- concentration profile for HP3-G corresponds the right y axis. Note in (a) that the pH of the first sample retrieved was less than the injectate initial pH when the initial pH was greater than approximately 7.0. Conversely, the pH of the retrieved samples were greater than the injectate initial pH when the initial pH was less than 7.0. Note in (b) that a significant titration of the injectate pH occurs in the zone where no dispersive mixing with ambient groundwater occurs (i.e., C/C_o $Br^- = 1.0$).

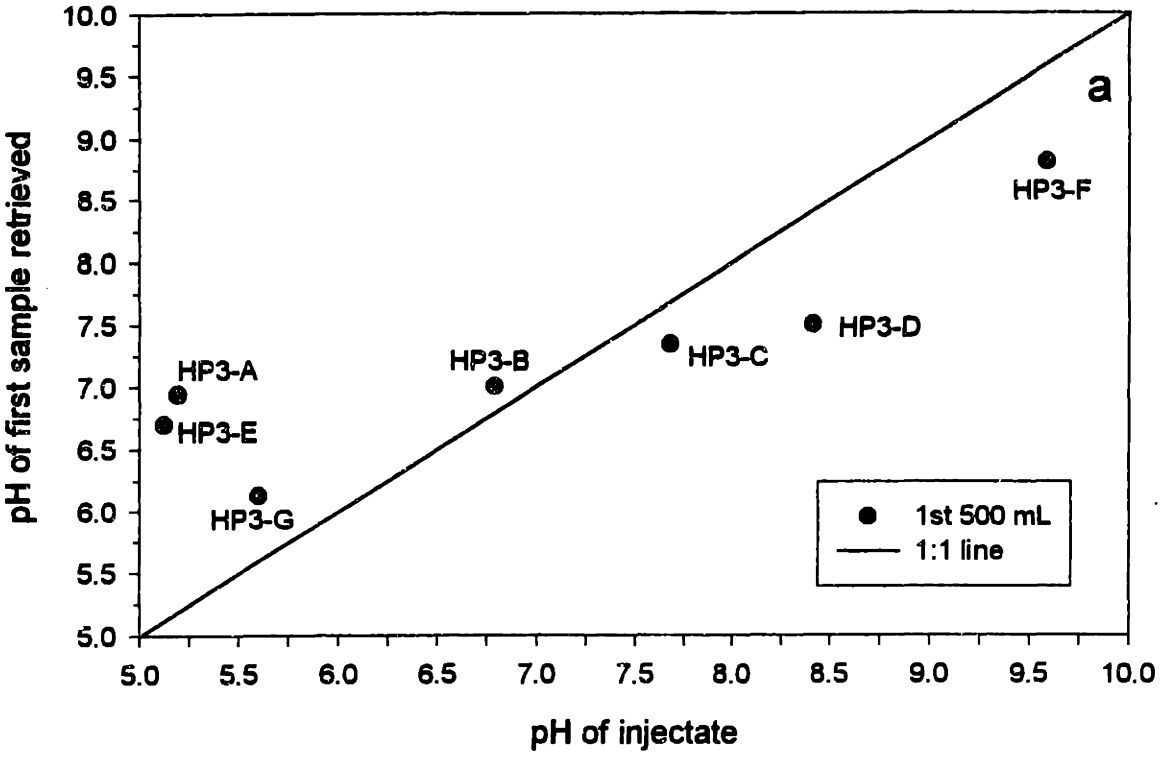
a
pH of first sample retrieved
pH of injectate
HP3-A
HP3-B
HP3-C
HP3-D
HP3-E
HP3-F
HP3-G
1st 500 mL
1:1 line

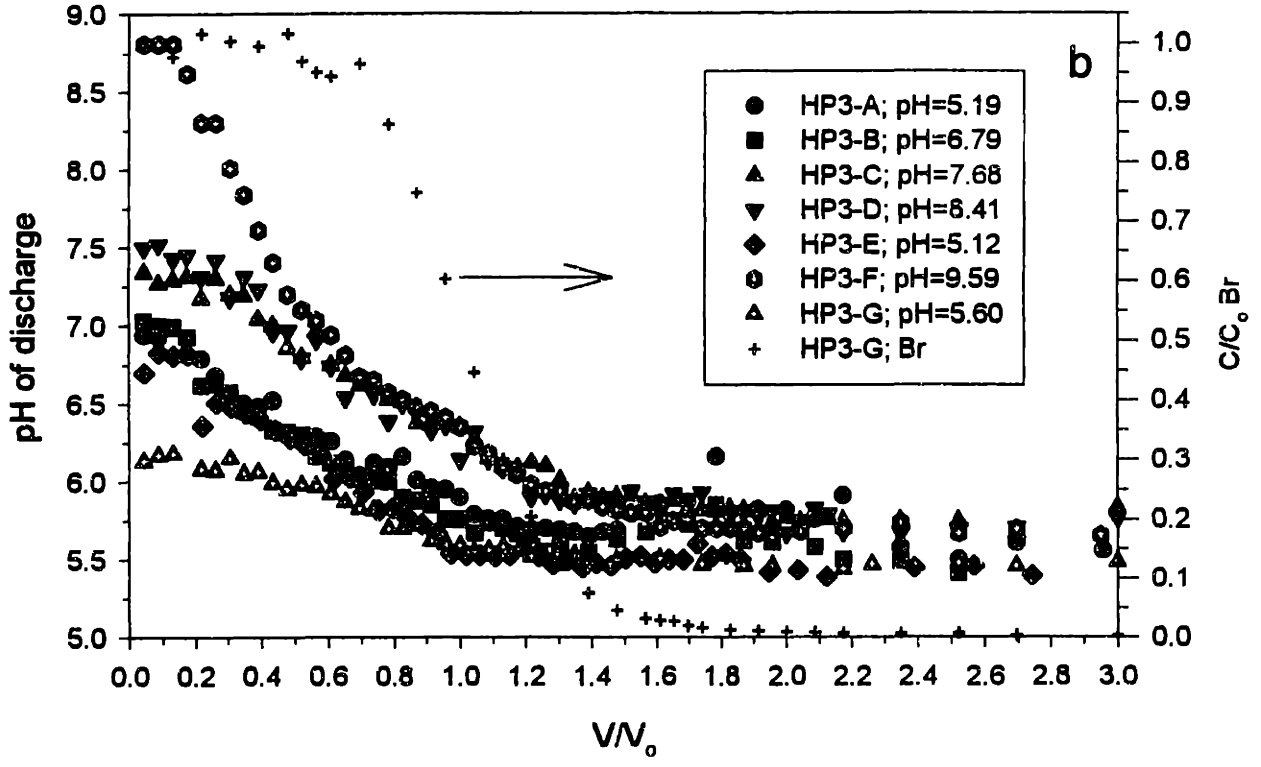
b
pH of discharge
C/C$_o$ Br
V/V$_o$
HP3-A; pH=5.19
HP3-B; pH=6.79
HP3-C; pH=7.68
HP3-D; pH=8.41
HP3-E; pH=5.12
HP3-F; pH=9.59
HP3-G; pH=5.60
HP3-G; Br

declines in pH in this pH range were thought to be due mostly to the desorption and hydrolysis of exchangeable Al present in the sediment, as hypothesized by other workers who have observed similar effects in Coastal Plain aquifer sediments (Seaman et al., 1995; Seaman et al., 1997). As freshly extracted groundwater was used for the field experiments, one would expect that the injectates used in HP3-A,E, and G were preequilibrated with respect to exchangeable Al at the *in situ* pH (5.26, **Table 4.2**). Thus, one would not expect *declines* in pH to occur when the injectate contacted the aquifer.

However, no attempt was made to keep the groundwater equilibrated with the ambient subsurface partial pressure of CO_2. Because the ambient pCO_2 was 27 times the level which would be in equilibrium with the atmosphere (**Table 4.2**), one would expect the groundwater to degas CO_2 in the time during which the groundwater was stored at the ground surface. In addition, the injectates used in HP3-A,E, and G had been purged of ambient dissolved gases during saturation with the tracer gases (helium and neon), which were added to study diffusion-limited transport in the aquifer (Sanford et al., unpublished data). Indeed, dilute HCl had to be added to the groundwater to bring it back down to its initial pH (approximately 5.2 to 5.3) before injection. Thus, the elevation in pH observed upon retrieval of the groundwater in HP3-A,E, and G might have been due to desorption of bicarbonate adsorbed on surfaces of aquifer constituents, particularly the iron oxyhydroxides. The desorption of sorbed bicarbonate would be necessary to establish equilibrium with the injected groundwater, which had been stripped of CO_2 (and, correspondingly, the HCO_3^- anion) during the helium and neon saturation process. Desorbed into water of pH initially at 5.26, the HCO_3^- anion would protonate to become $H_2CO_3^*$ (pK_{a1}=6.35), producing an hydroxyl ion (OH^-) in the process and driving up pH. Note that a somewhat lesser elevation of pH (with respect to pH_i of the injectate) was seen in the initial samples withdrawn from HP4-A and B, where pH increased from an injected value of 5.42 to 5.90 and 5.60, respectively, upon retrieval. These injectates had undergone the helium and neon saturation process as well.

In the HP3 experiments, the pH of the samples fell rapidly to background levels as the

injectate was progressively withdrawn (**Figure 4.10b**). This trend was greatest in HP3-F, the injectate with the highest initial pH (**Figure 4.10b**). These rapid decreases can not be explained by mixing of the injectate with the *in situ* groundwater, as the declines occurred between $V/V_o = 0.0$ and $V/V_o = 0.5$. In this portion of the discharge cycle, the normalized concentration of Br^- remained near a value of 1.0, indicating that dispersive mixing with the ambient groundwater had not affected these samples (**Figure 4.10b**). Rather, the pH declines in the portion of the discharge cycle prior to $V/V_o = 0.5$ reflect the rapid titration of the injectate pH, as discussed above.

Amendment of Groundwater with Acid. A well (HP7) was also emplaced to test whether acidified (pH_i=2.50) groundwater induced mobilization of colloids. Seaman et al. (1995) observed turbidity pulses concomitant with pH declines in a similar Coastal Plain sediment. They hypothesized that these mobilization events were caused by exchange processes which decreased the pore fluid pH below the net pH_{pzc} of the sediment. This effect in turn induced mobilization of colloids due to net repulsive interactions generated by the positive surface charge on some matrix constituents. They found the colloids mobilized by this mechanism to be predominantly (77% of total colloids released) goethite (Seaman et al., 1997).

In column experiments with the Georgetown sediment, we found no colloid mobilization occurred at acidic pH values as low as 2.5 (Chapter 3). The injection of pH 2.5 amended groundwater (HP7-B) verified this behavior *in situ* in the Georgetown sediment (**Figure 4.9a**). Indeed, the turbidity of the first sample of injected retrieved (0.59±0.05; **Figure 4.9a**) was less than that of the control (HP7-A) (0.78±0.04), as were turbidity levels in subsequent samples (data not shown). As discussed in Chapter 3, one would not expect mobilization of the goethite aggregates to occur at acidic pH if goethite-kaolinite face juxtapositions existed predominately in the matrix. Given these juxtapositions, the electrostatic interactions among these two constituents would be attractive at acidic pH. In addition, amorphous iron oxyhydroxide-kaolinite face juxtapositions would be attractive as

well. Although the breaking of bonds among the amorphous iron oxyhydroxides and the kaolinite would be expected to occur at low pH as proton-promoted dissolution of iron oxyhydroxides occurred (Zinder et al., 1986), the acidic pH would not impart the repulsive electrostatic conditions necessary to induce mobilization. Indeed, elevated levels of dissolved Fe as compared to background levels were observed in the retrieved injectate of HP7-B (**Figure 4.7**), but no concomitant mobilization of colloids occurred (**Figure 4.9a**). Note that only if an adsorbate had been added to the injectate which was able to impart negative charge to the iron oxyhydroxides *at pH 2.5* would the electrostatic interactions between the iron oxyhydroxides and the kaolinite faces have become repulsive and mobilization would have occurred.

4.3.4 Transport of the mobilized colloids

Theory Development Colloid transport has been studied recently in packed-column systems (Saiers et al., 1994; Kretzschmar et al., 1997). Using either a step or pulse input of a known concentration of synthetic colloids, the elution profiles for the colloids were analyzed with solutions for the advective-dispersive-reaction equation containing a reaction term incorporating first and/or second order assumptions for the colloid interactions with the immobile collector phase (the aquifer).

Saiers et al. (1994) found that colloid transport and deposition behavior, as monitored throught the aqueous phase colloidal concentration, was best described using a first order kinetics assumption when studying the transport of negatively-charged colloidal silica through quartz sand. In these systems, repulsive electrostatic interactions between colloids and collector surfaces dominated. However, when systems in which attractive electrostatic interactions prevailed, i.e., systems in which positively-charged boehmite and anatase were flushed through the quartz sand, the colloid concentration in the effluent was best fit when a second order kinetics assumption was included in the model.

Kretzschmar et al. (1997) studied the transport of two types of colloids (negatively charged latex, humic-coated hematite) in columns packed with glass beads, a sample from the

EB horizon of a sandy alluvial soil, or a carbonate aquifer material. They found the transport behavior to be described well using a first order kinetics expressions. Note that, for all cases investigated by Kretzschmar et. al. (1997), the electrostatic interactions were net repulsive either due to the type of colloid used and/or the high pH values used for the influent solutions (pH 8.4 for the carbonate material). Therefore, the first order behavior observed in the systems studies by Kretzschmar et al. (1997) were in agreement with the work of Saiers et al. (1994).

We wondered if the turbidity data obtained from our *in situ* mobilization experiments could be analyzed in such a manner. Specifically, we sought to determine if the reaction order describing the mobilized colloid concentration in the retrieved injectate with respect to residence time in the aquifer varied depending on the amendment performed. If such variations did occur, we wanted to know if they corresponded to, or could be interpreted as due to, changes in the electrostatic interactions in the subsurface system. Several assumptions underlie the basis for this analysis.

First, one must view the single well injection-withdrawal sequence as a system in which the injectate mobilized an amount of colloids (if chemical conditions permit) upon contacting the sediment around the well screen. This volume of injectate, carrying a parcel of mobilized colloids, moved radially outward into the aquifer as recharge continued. The colloidal load was subject to deposition and entrainment effects along this outwardly radiating flow path. This colloidal load was subject to the same effects during the journey back to the well screen when flow was reversed and the discharge phase was begun (under the same pumping rate conditions as during injection).

The contact time of the mobilized colloidal load contained in a parcel of injectate with the stationary aquifer solids was calculated by dividing the volume discharged by the discharge rate and multiplying by two (to correct for time spent in the aquifer during the injection phase *and* withdrawal phase). In this manner, the analysis was viewed as monitoring the concentration of colloidal solids (turbidity) at one coordinate along the

transport transect, just as effluent from column experiments is usually analyzed at the endpoint of the column. For the single-well case, this coordinate happens to correspond to the coordinate of origin of the colloids (i.e., initial mobilization is assumed to occur near the well screen and mobilized colloids "backtrack").

The second assumption involved the use of turbidity measurements as analogs for the concentrations of colloidal solids per unit volume of water. A turbidity measurement is actually a measurement of the amount of light scattered by the solids suspended in an aqueous sample, and the magnitude of scatter depends on the amount and size of the suspended solids. If the size distribution of the suspended solids remain constant as turbidity changes, then turbidity remains proportional to the mass, and concentration, of the suspended solids. Thus, turbidity can be linearly correlated to a concentration (in mg L^{-1}) of the colloids when the size distribution remains constant. Ryan and Gschwend (1994) used such an assumption to correlate turbidity (in NTU) in effluent from packed-columns containing a coastal plain sand to mg L^{-1} kaolin, the most abundant clay-size constituent in that sand.

To determine if turbidity and concentration of colloidal solids were linearly proportional, we used the measurement of total Fe in a 1 mL subsample of the archived samples saved from each of the *in situ* experiments as an analog for the concentration of colloidal solids in the samples. Total Fe in the 1 mL subsamples had been obtained previously by HF digestion of the colloids in each of the subsamples for the purpose of determining the Al/Fe mole ratios of the colloids' composition (see section 4.2.4, sample analysis above). The turbidity values had been measured in the field upon discharge of each sample from the aquifer (see section 4.2.4). For each experiment, total Fe in each of the subsamples was regressed against the corresponding turbidities of the samples from which the subsample was obtained (**Figure 4.11**).

Total digested Fe varied linearly (R^2 values ranged from 0.96 to 0.99) with turbidity across the entire range of turbidity exhibited for most of the experiments (HP3-F, HP4-C, HP8-B, and HP9-B; **Figure 4.11a**). The samples representing these experiments were all

Figure 4.11 appears on the next page

Figure 4.11: Correlation of total digested Fe in retrieved samples (by HF digestion) with the turbidity of each sample (a) for experiments HP3-F (pH_i= 9.59), HP4-C (0.5 mM phosphate and 0.5 mM ascorbic acid), HP6-C (10 mM SDS), HP8-B (1 mM ascorbic acid), and HP9-B (1 mM phosphate). The regression slopes and correlation coefficients are noted beside each regression line, and (b) for the same experiments as in (a), but with the x axis expanded to show all of the data points for HP6-C. Note that the slope of the regression for the HP4-C data (0.071 mg Fe L^{-1} sample/ mg L^{-1} colloidal solids) can be expressed as 1270 μM Fe g^{-1} colloidal solids, which compares very well to the total Fe present in the <63 μm size fraction (1360±95 μM Fe g^{-1} <63 μm size fraction, Swartz et. al., 1997). Note also that the regression line through the HP6-C data in (a) and (b) includes only those samples having turbidities between 50 and 1000 NTU.

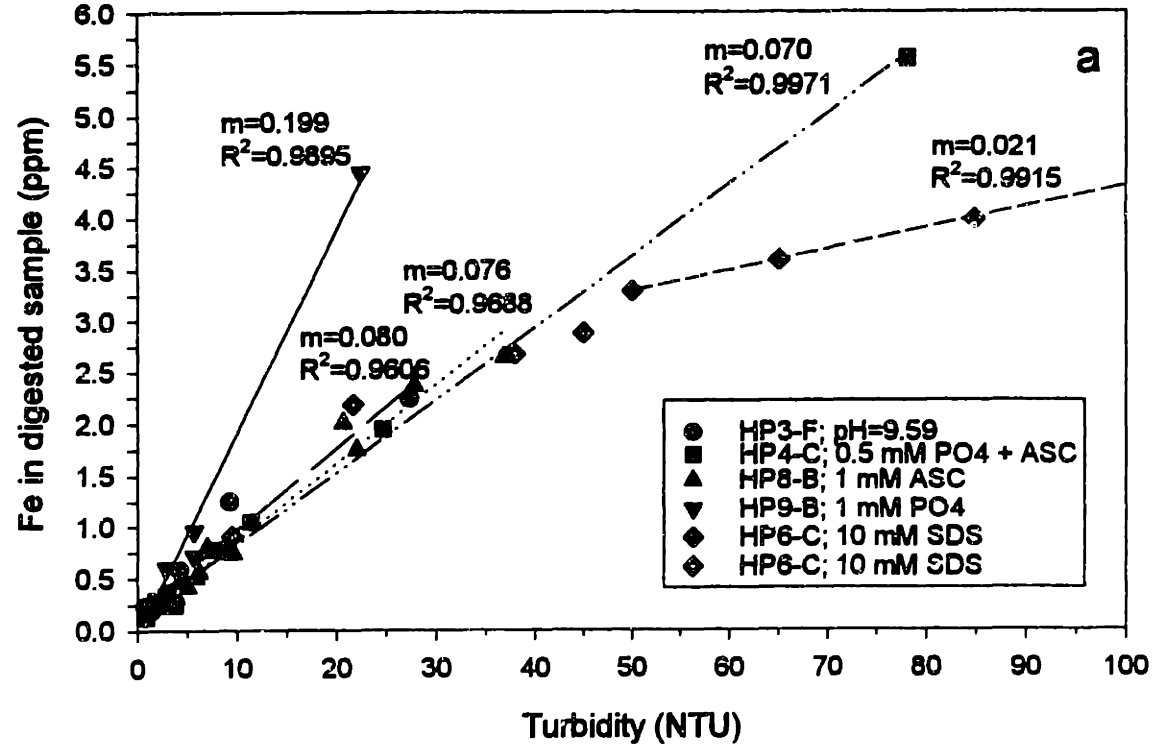
a
m=0.070
R²=0.9971
m=0.199
R²=0.9895
m=0.021
R²=0.9915
m=0.076
R²=0.9688
m=0.080
R²=0.9606
HP3-F; pH=9.59
HP4-C; 0.5 mM PO4 + ASC
HP8-B; 1 mM ASC
HP9-B; 1 mM PO4
HP6-C; 10 mM SDS
HP6-C; 10 mM SDS
Fe in digested sample (ppm)
Turbidity (NTU)

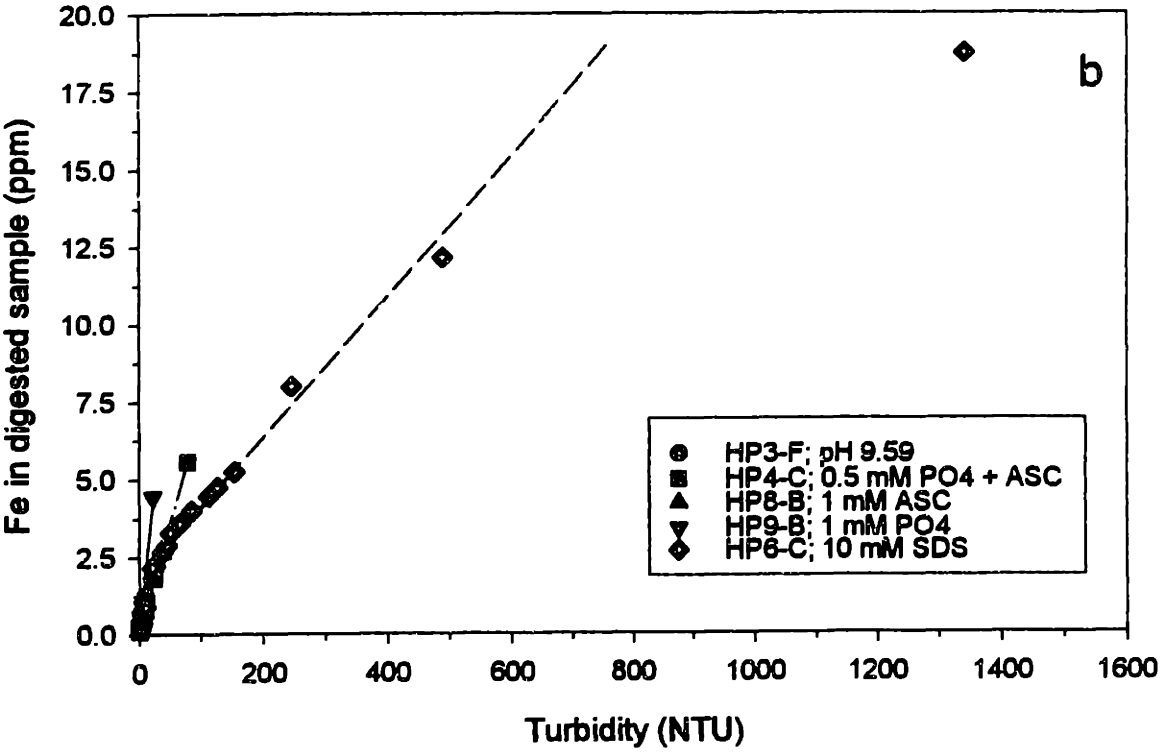
b
HP3-F; pH 9.59
HP4-C; 0.5 mM PO4 + ASC
HP8-B; 1 mM ASC
HP9-B; 1 mM PO4
HP6-C; 10 mM SDS
Fe in digested sample (ppm)
Turbidity (NTU)

discharged from the aquifer in the portion of the recovered injectate which experienced no dispersive mixing with the ambient groundwater. Note that not all of the data for HP6-C (amendment with 10 mM SDS) could be described with a single regression line. Values of total Fe in samples from HP6-C with turbidities below 50 NTU appeared to vary similarly with turbidity as the data for HP3-F, HP4-C, and HP8-B, whose regression slopes (m) possessed values between 0.08 and 0.071 (**Figure 4.11a**). The HP6-C samples with turbidities less than 50 NTU represent total volumes withdrawn of 5500 mL to 8500 mL (V/V_o equal to 0.48 to 0.74). The normalized concentration of Br^- tracer indicated that the portion of the injectate represented by these samples had experienced dispersive mixing with the ambient groundwater (i.e. C/C_o $Br^- < 1.0$). However, samples from HP6-C which correspond to turbidity in the range 50 to 600 NTU (the samples which experienced no dispersive mixing with the ambient groundwater) were described well (R^2=.9915) with a different slope (m=0.021). A data point representing a sample from HP6-C with even higher turbidity (1340 NTU) deviated significantly from this regression (**Figure 4.11b**). This data represents the third sample discharged from HP6-C (1500 mL total discharge). The first two samples discharged during HP6-C possessed turbidities above the measurable range of the turbidimeter (≤ 2000 NTU), and thus were not included in the analysis. Possible explanations for the total Fe-turbidity behavior exhibited by HP6-C are discussed below.

The regression slope for the HP9-B data (0.198) differed significantly from the slopes for HP3-B, HP4-C and HP8-B (and for HP6-C data less than 50 NTU), which were all very similar. These differences in slopes reflect the fact that different subsets of the bulk matrix were mobilized by the different chemical perturbations which acted on the sediment in each of the experiments. Remember that the Al/Fe mole ratio for the colloids mobilized in HP9-B was 0.8±0.2, whereas the Al/Fe mole ratios of the colloids were 1.8±0.7, 1.9±0.2, and 2.5±0.6 for HP3-F, HP8-B, and HP4-C, respectively. These Al/Fe mole ratios suggested that goethite aggregates were mobilized predominantly in HP9-B, whereas, colloids more representative of the entire bulk matrix (with respect to Al and Fe) were mobilized in HP3-F and HP8-B.

Colloids very close to the chemical composition of the bulk matrix were mobilized in HP4-C.

Note that the regression slopes in **Figures 4.11a, b** represent mg total Fe L^{-1} sample over mg colloidal solid L^{-1} sample, or more simply, mg total Fe mg^{-1} colloidal solid. Therefore, one would expect the regression slope to change as a function of the composition of the colloids mobilized by the experiments. Indeed, the regression slope increased as the proportion of goethite making up the colloidal solids increased (HP9-B, **Figure 4.11a, b**). Note also that the regression slope (0.071 mg total Fe mg^{-1} colloidal solid) for the HP4-C data is equivalent to 1270 μmoles Fe g^{-1} colloidal solid. If one assumes that one gram of colloidal solid is equivalent to one gram of the <63 μm size fraction for the HP4-C case (the Al/Fe mole ratio of the colloids did suggest that colloids representative of the entire bulk matrix, or <63 μm size fraction, were mobilized) then the regression slope corresponds to 1270 μmoles Fe g^{-1} <63 μm size fraction. This number is within the range of error of the measurement of total Fe in the <63 μm size fraction obtained by HF digestion (1360±95 μmoles Fe g^{-1} <63 m size fraction, **Table 2.1**, Chapter 2). In other words, the regression slope reflects that fact that near constant mobilization of colloidal solids representing the chemical composition of the *entire* bulk matrix (expressed as the amount of total Fe in the <63 μm size fraction in the regression slope) occurred in the mobilization event in HP4-C. The regression slope is, therefore, in agreement with colloidal Al/Fe mole ratio (2.5±0.6) for HP4-C, which indicates that mobilization of colloids representative of the entire bulk matrix occurred in this experiment.

The Al/Fe mole ratio for the colloids mobilized in HP6-C (3.1±1.7, n=10) indicated that colloids representative of the bulk matrix were mobilized in this experiment as well. However, the regression slope for turbidity values greater than approximately 50 NTU (m= 0.021 in **Figure 4.11a, b**) suggested that colloids containing proportionally less total Fe g^{-1} colloidal solid than the bulk matrix (m≈0.071) were present in the samples initially discharged from the aquifer (these samples possessed the highest turbidity). Note that, for HP4-C, the data could be described well by one regression slope even though samples with turbidity

greater than 50 NTU were present. Thus, artifacts that might be caused by large amounts of solids in the samples, such as incomplete digestion of the solids, can not explain the behavior of the data in HP6-C.

That the colloids mobilized in HP6-C possessed less total Fe g^{-1} colloidal solid than is representative of the entire the bulk matrix (i.e., the colloids mobilized in HP4-C) could indicate that iron containing phases (i.e., goethite) were left unmobilized in the first samples retrieved in HP6-C. However, the Al/Fe mole ratio for the HP6-G samples (3.1±1.7) indicates that Fe and Al containing phases were mobilized in proportion to that which exists in the <63 μm size fraction. Rather, the regression slope for HP6-G data greater than > 50 NTU (Figure **4.11a, b**) probably indicates that the mobilized colloidal population was diluted with some phase that did not contain Fe or Al and which was mobilized from a size fraction larger than the <63 μm size fraction. The obvious choice would be very fine quartz or possibly titanium oxides present in the 125-63 μm size fraction. One would expect that larger constituents would have been mobilized by the physical perturbation created by the foaming surfactant solution as it was injected into the aquifer. These larger solids would have been mobilized in greater abundance in initial samples discharged from the aquifer (i.e., data represented by the data points > 50 NTU in **Figures 4.11a, b**) where the injectate was not affected by dispersive mixing with the ambient groundwater.

The data presented in **Figure 4.11a, b** indicate that turbidity did vary linearly with a measurement of the concentration of colloidal solids (total Fe) across the entire range of turbidities measured for most of the *in situ* experiments. Only the data of HP6-C (the 10 mM SDS experiment) needed to be described by more than one regression slope. Thus, turbidity can be used as a surrogate for concentration of colloids in the samples in determining the reaction order of the transport behavior exhibited by the colloids mobilized in the *in situ* experiments. Note that, for all of the experiments, only data obtained from samples discharged in the portion of the injectate unaffected by dispersive mixing with the ambient groundwater was used in the following analysis. For HP3-F, HP4-C, and HP8-B, and HP9-

B, this means that all data appearing in **Figures 4.11a, b** could be included. For HP6-C, only the data described by the regression slope equal to 0.021 was used.

Possessing both a pseudo-concentration (turbidity in NTU) and pseudo-contact time with the aquifer (the volume discharged divided by the flow rate, all multiplied by two) for each 500 mL sample withdrawn from each well, a reaction order plot can be created using the the intergrated form of the following relation:

$$\frac{dC}{dt} = -kC^n \qquad (1)$$

where k is an overall rate coefficient incorporating all effects which determine the aqueous phase colloid concentration and n is the reaction order with respect to C, the aqueous phase colloid concentration. Logarthymic transformation of the integrated form of (1) provides the linearized form:

$$\ln C = \frac{\ln[-k(1-n)]}{1-n} + \frac{1}{1-n}\ln t \qquad (2)$$

where n can be calculated from the slope 1/(1-n). Note that t, the contact time, can be replaced with V/V_o in (2) for ease of calculation; the proportionality between t and V/V_o would only add an additional term to the y intercept and would not affect the slope and calculation of the reaction order n.

Discussion of Transport Behavior. Linear regression of ln (turbidity) versus ln (contact time in the aquifer) provided the slope (m in **Figure 4.12**) from which the order (n in **Figure 4.12**) of the colloid behavior with respect to turbidity (the analog for C in equation 4) was calculated for all *in situ* experiments in which colloids were mobilized (HP3-F, HP4-C, HP6-G, HP8-B, and HP9-B) (**Figure 4.12a**). The R^2 values for most of these regressions were 0.98 or higher. In each of these experiments, the turbidity of the first samples withdrawn was significantly greater than the respective control experiments for that well, indicating that the injectate chemistry had induced mobilization.

Figure 4.12 appears on the next page

Figure 4.12: Reaction order plot for determining the value of n (the reaction order) of the colloid-collector interaction during transport of the colloids mobilized in (a) experiments HP3-F (pH_i= 9.59), HP4-C (0.5 mM phosphate and 0.5 mM ascorbic acid), HP6-C (10 mM SDS), HP8-B (1 mM ascorbic acid), and HP9-B (1 mM phosphate), and (b) the corresponding control experiments HP3-G, HP4-D, HP6-D, HP7-A, HP8-A, and HP9-A. The value of n was determined for each experiment from the slope of the regression of ln (turbidity) versus ln (residence time in aquifer) for each 500 mL sample of the retrieved injectate which was not affected by dispersive mixing. See text for derivation of the logarithmic expression and the calculation of residence time.

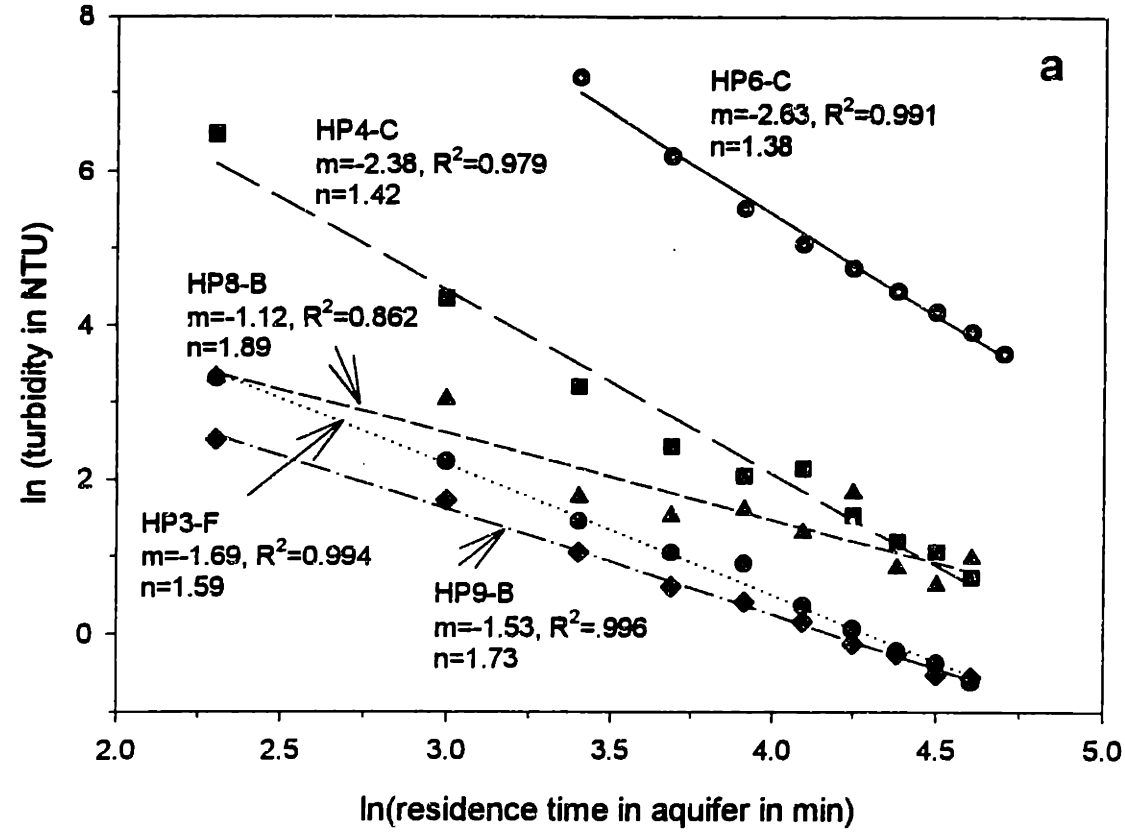
a
HP6-C
m=-2.63, R2=0.991
n=1.38
HP4-C
m=-2.38, R2=0.979
n=1.42
HP8-B
m=-1.12, R2=0.862
n=1.89
HP3-F
m=-1.69, R2=0.994
n=1.59
HP9-B
m=-1.53, R2=.996
n=1.73
ln (turbidity in NTU)
ln(residence time in aquifer in min)

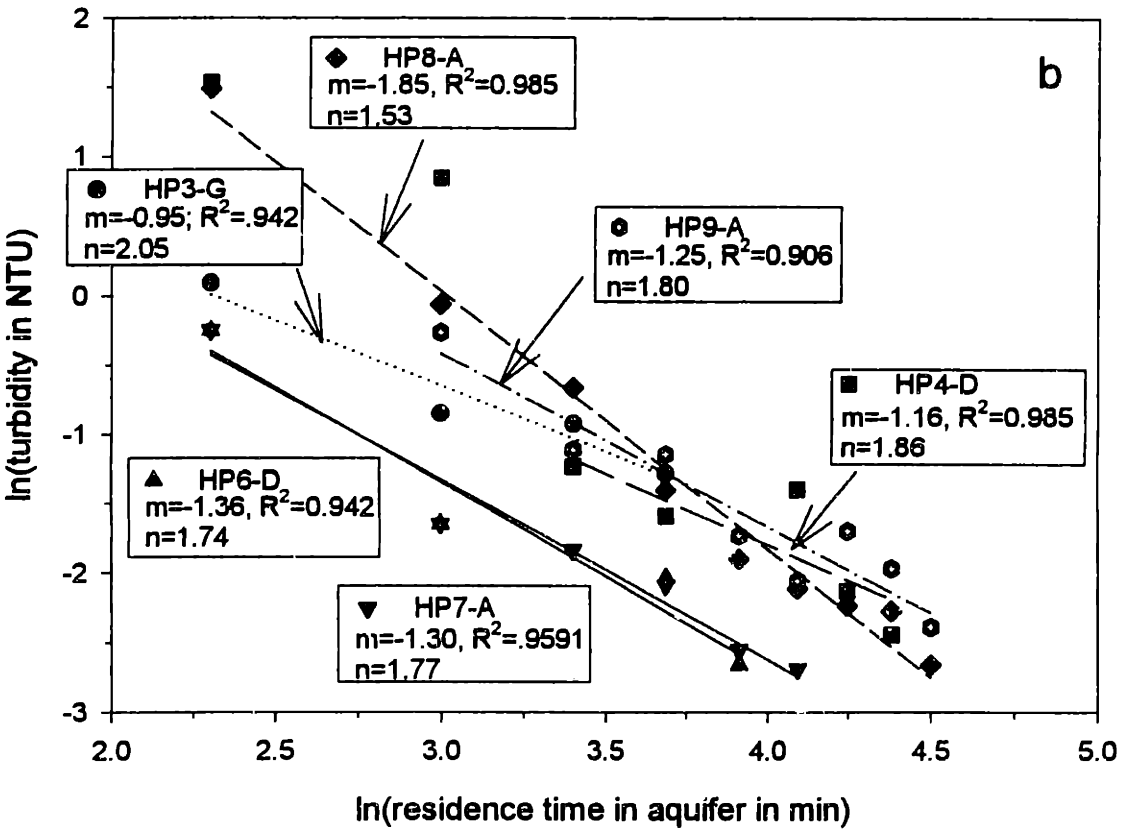
b
HP8-A
m=-1.85, R2=0.985
n=1.53
HP3-G
m=-0.95; R2=.942
n=2.05
HP9-A
m=-1.25, R2=0.906
n=1.80
HP4-D
m=-1.16, R2=0.985
n=1.86
HP6-D
m=-1.36, R2=0.942
n=1.74
HP7-A
m=-1.30, R2=.9591
n=1.77
ln(turbidity in NTU)
ln(residence time in aquifer in min)

The data for the control experiments HP3-G, HP4-D, HP6-H, HP7-A, HP8-A, and HP9-A, are plotted for comparison in **Figure 4.12b**. For control experiments HP3-G, HP6-H, and HP7-A, turbidity values reached baseline levels before the dispersive mixing zone reached the well screen. Therefore, only samples with turbidity levels greater than baseline values were used in the regression analysis. The turbidity data for control experiments HP4-D and HP9-A suffered from greater scatter in turbidity, probably due to the presence of loose material near the well screen. Turbidity values in the first sample for each of these controls, as well as HP8-A, were significantly elevated above those for the first samples in the controls for HP3-G, HP6-H, and HP7-A. The high turbidity levels in the first samples for HP4-D and HP9-A appeared to significantly bias the regression for these cases. For this reason, the first two samples for HP4-D and the first sample for HP9-A were excluded from the regression calculation. This resulted in a substantial increase in the R^2 value (0.9853 versus 0.9247) for the HP4-D regression in particular.

The values of n for all of the mobilization and control experiments fell between 1.0 and 2.0 (**Figure 4.12a, b**). A distinct trend in the slopes of the regressions, and concomitantly, the reaction order constant (n), was apparent. For the control experiments HP3-G, HP4-D, HP6-H, HP7-A, and HP9-A, the values of n (n = 2.05, 1.86, 1.77, 1.77, and 1.80, respectively) were all close to 2.0, suggesting that second order kinetic behavior controlled the transport of the mobilized colloids in these injection-withdrawal sequences. The average value of n for these control experiments was 1.85±0.12. Note, however, that the n value for HP8-A (1.53) is anomalously low compared to the n values for all of the other control experiments.

In the experiments in which a mobilization event occurred due to injectate chemistry, the value of n appeared to decrease systematically as the magnitude of the mobilization event increased (HP9-B< HP3-F < HP4-C < HP6-C). The value of n decreased from 1.65 and 1.42 for HP9-B and HP4-C, respectively, to n= 1.38 for HP6-C. Thus, the larger the mobilization event, the closer the transport of the colloids followed first order behavior with respect to the

turbidity. Note again that the data for HP8-B (1 mM ascorbic acid amendment) does not appear to fit the trend discussed above, as a comparatively higher value of n (1.90) was calculated for the data even though the mobilization event was somewhat higher than either HP9-B or HP3-F. Note also that more scatter (producing a lower R^2 value) was exhibited by the data for HP8-B. Possible reasons for the behavior exhibited by HP8-B are discussed below.

Recall that the colloids mobilized in each of the experiments represented in **Figure 4.12a** differed in composition from that of the bulk matrix to varying degrees. In HP9-B (1 mM phosphate amendment), colloids with an Al/Fe ratio (0.8±0.2) more similar that of the goethite aggregates were mobilized. In HP3-F (pH_i=9.5 amendment), the Al/Fe mole ratio of the colloids was 1.8±0.7, and in HP4-C (0.5 mM phosphate and 0.5 mM ascorbic acid) the ratio was 2.5±0.6. The Al/Fe mole ratio of HP6-G (10 mM SDS) was found to be 3.1±1.7. Thus, the magnitudes of the mobilization events were positively correlated with the Al/Fe mole ratios of the colloids, with the larger events releasing colloids more representative of the entire bulk matrix. For this reason, the values of n in **Figure 4.12a** are inversely correlated with the Al/Fe ratio of the mobilized colloids. It appears that the closer the Al/Fe mole ratio of the colloids approached that of the bulk matrix, the closer the transport behavior approached first order kinetics. Note that the Al/Fe mole ratio of the colloids in the control experiments were not measured because the turbidity, i.e, the amount of colloidal solids in the samples, was generally too low (< 1 NTU).

The work of Saiers et al. (1994) and Kretzschmar et al. (1997) indicated that colloid transport followed first order behavior with respect to the aqueous phase concentration of the colloids when interactions among the colloids and collector surface were repulsive. On the other hand, transport behavior was modeled more closely by second order behavior when interactions were attractive (Saiers et al., 1994). The data generated by the *in situ* experiments can perhaps be interpreted using these generalities. The presence of small amounts of mobilized colloids in the initial discharge from the control experiments most

likely resulted from physical perturbations, like shear forces, created by the reversal of flow inherent in the injection-withdrawal procedure. For the control experiments, no apparent chemical perturbations to the sediment occurred upon injection, as only groundwater amended with the bromide tracer was injected. Thus, it can be assumed that prevailing electrostatic interactions among matrix constituents were not altered by the injectate during the control experiments. The ambient electrostatic interactions among the matrix constituents would be expected to be more attractive than repulsive, as very low baseline turbidity levels in the groundwater (not significantly different from stray light) indicated that the matrix was obviously stable. Thus, the "loose" material mobilized in the control experiments would be expected to follow a second order transport behavior based on the work of Saiers et al. (1994), as no chemical perturbations were superimposed on the physical disturbance created by the injection-withdrawal process.

Indeed, considering the control experiments HP3-H, HP4-D, HP6-D, HP7-A, and HP9-B, the average value of n (1.85±0.12) was close to 2.0, suggesting that the transport behavior of the colloids mobilized in these control experiments could be described better with a second order reaction. In other words, the electrostatic interactions acting in the control systems appeared to be more attractive than repulsive. Perhaps only small amounts of loose goethite were mobilized by flow reversal in these control experiments. Goethite colloids mobilized by physical disturbances would still be attracted to the abundant quartz and kaolinite collector surfaces in the Georgetown sediment. Note that the colloids and collectors in this system can be the same phase, as the colloids are a mobilized subset of the collectors (the portion of the matrix which remains stationary).

The anomalously low value of n (1.53) observed for the HP8 control experiment (HP8-A) data suggests that the colloids mobilized by the physical disturbance produced by this injection-withdrawal sequence experienced greater repulsive interactions than the colloids mobilized in the control experiments for wells HP3, HP4, HP6, HP7, and HP9. Perhaps more loose material around the well screen in HP8 included phases such as kaolinite, which

would experience repulsive interactions with quartz and stationary kaolinite acting as collector surfaces. The amount and composition of loose material generated by emplacement of the wells may be due to aquifer heterogeneity.

Based on the findings of Saiers et al. (1994) and Kretschmar et al. (1997), one would expect the transport behavior of mobilized colloids to be described better by first order reaction kinetics when groundwater amended to enhance electrostatic repulsion in the subsurface system was injected. Indeed, when groundwater amended with NaOH to pH 9.5 (HP3-F) was injected and withdrawn, not only did turbidity levels rise significantly with respect to control levels (see **Figure 4.9**), but the reaction order decreased from n= 1.05 to 1.59 (**Figure 4.12a, b**). Elevated pH would be expected to enhance electrostatic repulsion by reversing the surface charge of goethite, the amorphous iron oxyhydroxides, and kaolinite edges. In addition, it is suspected that elevated pH caused hydrolysis of bonds among the amorphous iron oxyhydroxides and kaolinite. This allowed electrostatic repulsions to act on these constituents to induce mobilization of colloids more representative of the bulk matrix (i.e., kaolinite), as evidenced by the Al/Fe mole ratio of 1.8±0.7 for the colloids. With the mobilized colloids (kaolinite, amorphous iron oxhydroxides, and goethite) and potential collector surfaces (quartz, kaolinite, goethite) all possessing a negative charge, one would expect the system produced to be more electrostatically repulsive, and the reaction order describing the aqueous colloid concentration would shift closer toward first order behavior.

In HP4-C (amendment with 0.5 mM phosphate and 0.5 mM ascorbic acid), the reaction order decreased to n=1.42 when an electrostatically perturbing solute (phosphate) was injected together with ascorbic acid. Presumably, the ascorbic acid broke bonds among the kaolinite and amorphous iron oxyhydroxides, and the phosphate provided the electrostatic perturbation by imparting negative charge to the constituents. Together, these effects mobilized an even larger population of the bulk matrix than occurred in HP3-F (i.e., a larger mass of kaolinite platelets per gram colloidal solid). Thus, one would expect even greater net repulsive interactions in this system. Indeed, the reaction order n=1.42 for HP4-C, compared

to n=1.59 for HP3-F, suggests the transport behavior of the colloids mobilized in HP4-C could be described more closely by first order kinetics.

In HP9-B, 1 mM phosphate amended groundwater was injected. The resulting mobilization was somewhat larger than that which occurred in the control for that well (see **Figure 4.5**). The value of n for HP9-B (1.72) and its control (1.86) did not differ greatly, suggesting that electrostatic interactions did not change significantly by adding the 1 mM phosphate to the groundwater. Remember that the Al/Fe mole ratio (0.8±0.2) of the colloids mobilized in HP9-B indicated that the composition of those colloids differed greatly from that of the bulk matrix, probably reflecting mobilization of goethite preferentially. That the reaction order describing the transport behavior of these colloids does not differ greatly from the reaction order for the control experiment perhaps suggests a relatively weak mobilization event occurred in HP9-B. This interpretation would support the observations made in the packed-column studies (Chapter 3). In these column experiments, 1 mM phosphate caused only a brief mobilization of material upon saturating the column with the 1 mM phosphate solution. This pulse was interpreted to be due to loose material flushed from the system in the first one to five pore volumes. However, the 1 mM phosphate solution did not induce sustained mobilization of colloids, even after flushing with 40 pore volumes of the solution (Chapter 3).

Greater scatter in the data for HP8-B makes interpretation of the regression slope for this experiment more difficult. In fact, the value of n (1.90) calculated from the slope is larger than that calculated for the appropriate control (n=1.53, HP8-A), suggesting that the addition of ascorbic acid made electrostatic interactions *more attractive*. Excluding the first data point of HP8-B (which may have strongly biased the regression, see **Figure 4.12a**) only decreased the value of n to 1.72. However, if one assumes that the average value of n (1.85±0.12) obtained from all of the other control experiments is more representative of the mobilization behavior imparted by just the flow reversal process, the colloid transport behavior exhibited by colloids mobilized by 1 mM ascorbic acid was not significantly

different from "control" behavior. This finding would be congruent with the electrophoretic mobility studies with model goethite colloids, which indicated that even 10 mM ascorbic acid at pH 5.2 would not generate significant negative charge to the iron oxyhydroxides in the Georgetown sediment to induce mobilization, even though bonds among the amorphous iron oxyhydroxides and kaolinite would be broken by the ascorbic acid (Chapter 3). The lack of significant difference in the reaction order for the colloids mobilized with 1 mM ascorbic acid and colloids mobilized by the majority of the control experiments would also be in line with the packed-column behavior, which indicated that 1 mM ascorbic acid did not generate a chemical perturbation significant enough to mobilize colloids (Chapter 3).

However, the 1 mM ascorbic acid injectate *did* generate significant turbidity in the *in situ* experiment (see **Figure 4.6**). In addition, the Al/Fe mole ratio of the colloids (1.8±0.2) mobilized in HP8-B suggests that they were similar in composition to those mobilized in HP3-F (1.7±0.7). One would expect that the *potential* for mobilization of similarly composed colloids in both of these experiments would exist because both treatments would lyse bonds holding constituents like kaolinite immobile. However, only elevated pH would be expected to provide the repulsive electrostatic component needed to induce mobilization, based on electrophoretic mobility data and packed-column behavior (Chapter 3). Indeed, in contrast to HP8-B, the transport behavior of the colloids mobilized in HP3-F suggests that electrostatic interactions in the elevated pH system were made repulsive, as indicated by the lower value of n (1.59).

Why colloids were mobilized in HP8-B without the necessary electrostatic perturbation may be explained perhaps by the combined influence of the physical perturbation inherent in the flow reversal process and the dissolution of iron oxyhydroxides and concomitant breaking of bonds among matrix constituents. Such dissolution processes, evident in the highly elevated dissolved Fe concentrations in the discharge from HP8-B (**Figure 4.7**), would "loosen" matrix constituents, making them susceptible to physical disturbances produced by flow reversal in the aquifer. As the physical perturbation inherent in the *in situ* method

would not occur in the packed-columns treated with 1 mM ascorbic acid, this interpretation may explain the discrepancy in behavior observed between the two methods.

Similar physical perturbation would have acted on "loosened" matrix constituents in HP3-F, so perhaps the magnitude of turbidity generated in HP3-F was actually a manifestation of superposition of physical and chemical perturbations as well. Determination of the reaction order of the transport behavior of the mobilized colloids in both experiments (HP3-F and HP8-B) appears to allow one to at least partially discriminate when chemical perturbations producing significant repulsive interactions were superimposed on the physical perturbation omnipresent in the *in situ* experiments.

For the case of HP6-G (10 mM SDS amendment), it is believed that the very large mobilization event which occurred was induced by physical perturbation of the sediment upon injecting the foaming surfactant solution. The surfactant may not have been able to alter the surface charge of the goethite aggregates (or other constituents) by adsorbtion due to competitive blocking by prevailing adsorbed anions (see Chapter 5). Thus, the SDS may not have greatly altered electrostatic interactions in the system. The physical perturbation caused by the foaming solution did mobilize colloids compositionally representative of the entire bulk matrix (as defined by Al and Fe in the <63 μm size fraction) during this experiment, as indicated by the Al/Fe mole ratio (3.1±1.7) of the colloids. Indeed, the relation between total Fe and turbidity suggests that very fine size quartz or other mineral phases in larger size fractions were mobilized by the physical disturbance as well (see discussion of **Figure 4.11a, b** above). Perhaps the foaming solution stabilized the colloidal suspension. Imparting net repulsive electrostatic interactions to the system would result in similar stabilization of the colloidal suspension. Thus, one would expect that the colloid transport behavior which occurred in this system would more closely follow a first order kinetic description. Indeed, the value of n (1.38) for HP6-C indicated that this system was the closest of all the experiments to being described by first order behavior.

4.3.3 Effect of mobilization on aquifer properties

Although differences in the normalized concentration profiles of Br^- were observed among the wells (**Figure 4.13**), the Br^- profiles obtained from multiple experiments in any one well were very similar (see **Figures 4.14-4.16** for examples). Note that the Br^- profiles for the multiple experiments conducted in HP3 (**Figure 4.14**), HP4 (**Figure 4.15**), and HP6 (**Figure 4.16**) did not differ significantly, even though mobilization events occurred in each of these wells. Large colloid releases might be expected to clog pores and alter the permeability of the sediment (Goldenberg and Margaritz, 1983; Khilar and Fogler, 1984). For the cases of HP4 and HP6, the mobilization events were rather large (initial turbidity > 500 NTU). However, based on the similarity of the Br^- profiles for these wells, it does not appear that the mobilization events which occurred altered the aquifer transport properties noticeably around these wells. Furthermore, the profiles for the helium and neon tracers added to the groundwater in HP4-A,B and D did not differ significantly (Sanford, 1997). The helium and neon tracer studies conducted in HP3 suffered from large variability in initial concentration, making the data difficult to interpret. Because the behavior of the helium and neon tracers would be much more sensitive to alterations in the diffusive properties, the unchanged behavior of these tracers indicated the mobilization event that occurred in HP4-C did not alter the transport properties of the aquifer around the well. Thus, it appears that controlled *in situ* mobilization was accomplished without clogging pores and decreasing permeability of the affected region near the well.

4.4 Conclusions

A single well injection-withdrawal method for determining *in situ* colloid mobilization behavior was tested in an aquifer. Previous laboratory colloid mobilization studies involving columns packed with the aquifer material provided a reference for comparison with the *in situ* behavior. Generally, the trends in mobilization behavior exhibited by the two methods were comparable, although the magnitudes of the releases for corresponding treatments were greater

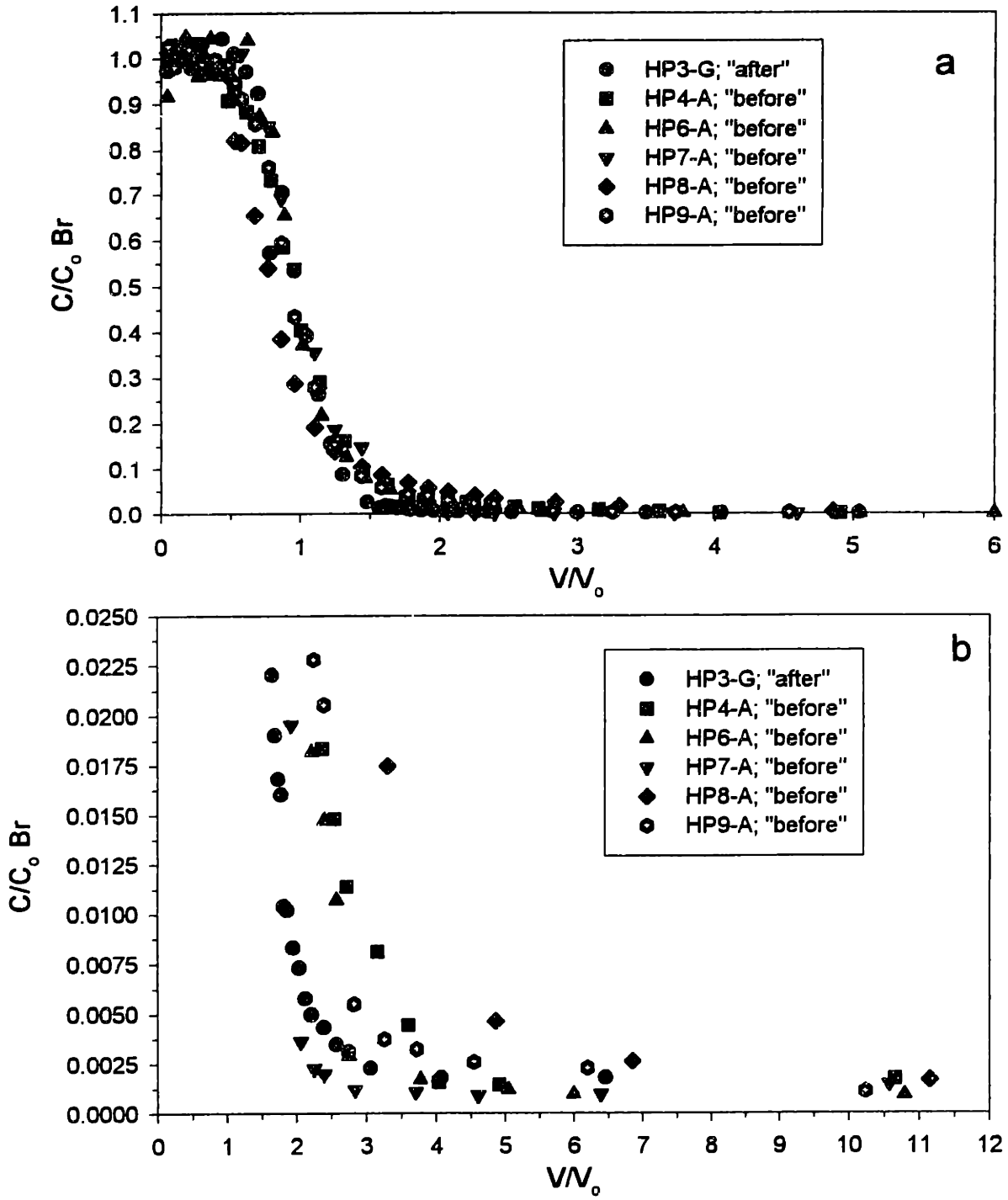

Figure 4.13: Normalized Br^- concentration profiles for various control experiments conducted in each of the wells HP3, HP4, HP6, HP7, HP8, and HP9. In (a) all data is presented, and in (b) only data less than C/C_0 equal to 0.25 is presented. Each well is represented by one "before" or "after" profile.

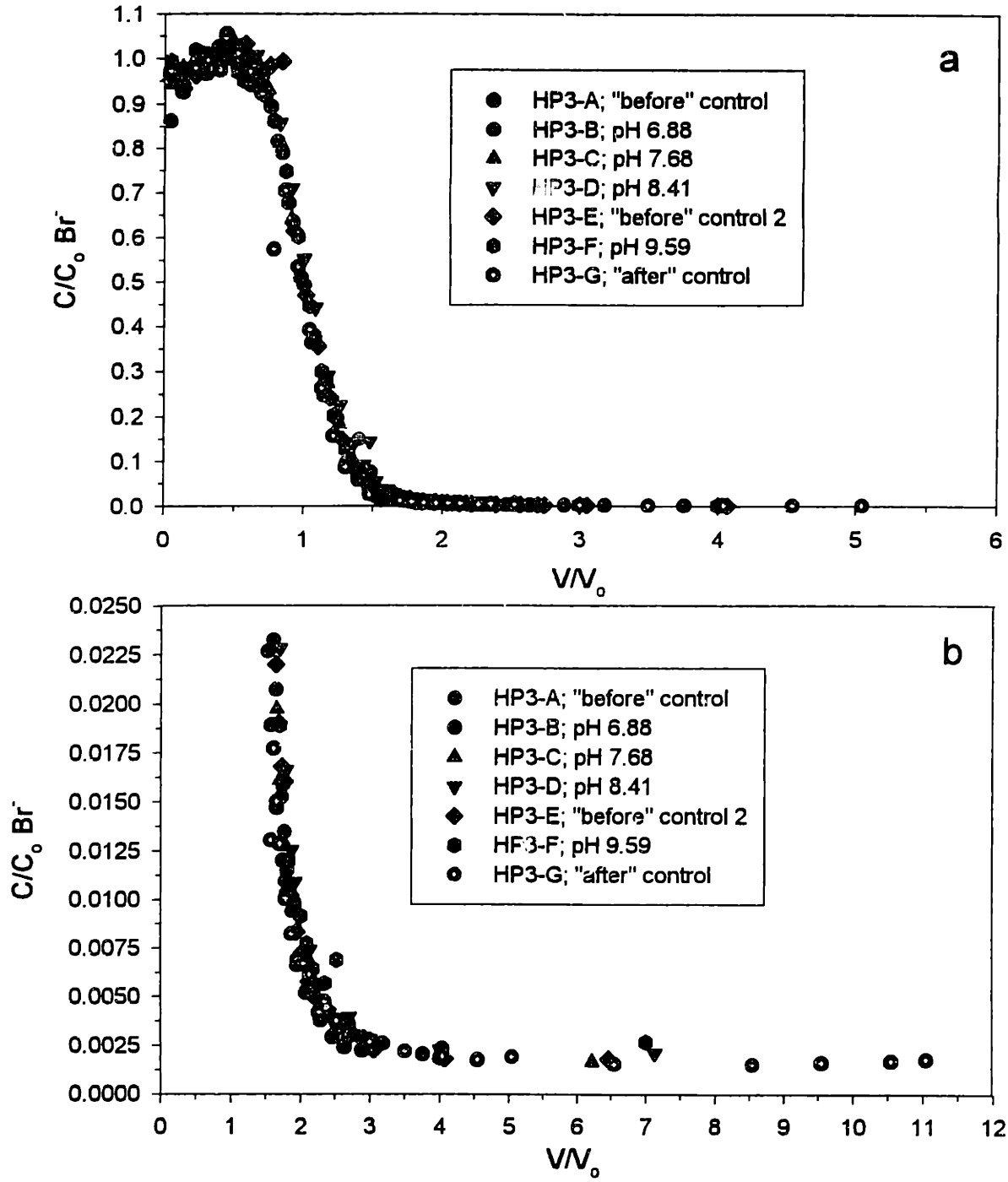

Figure 4.14: Normalized Br^- concentration profiles for all of the experiments conducted in well HP3. In (a) all data is presented, and in (b) only data less than C/C_0 equal to 0.25 is presented. Note the similarity in profiles for the different experiments.

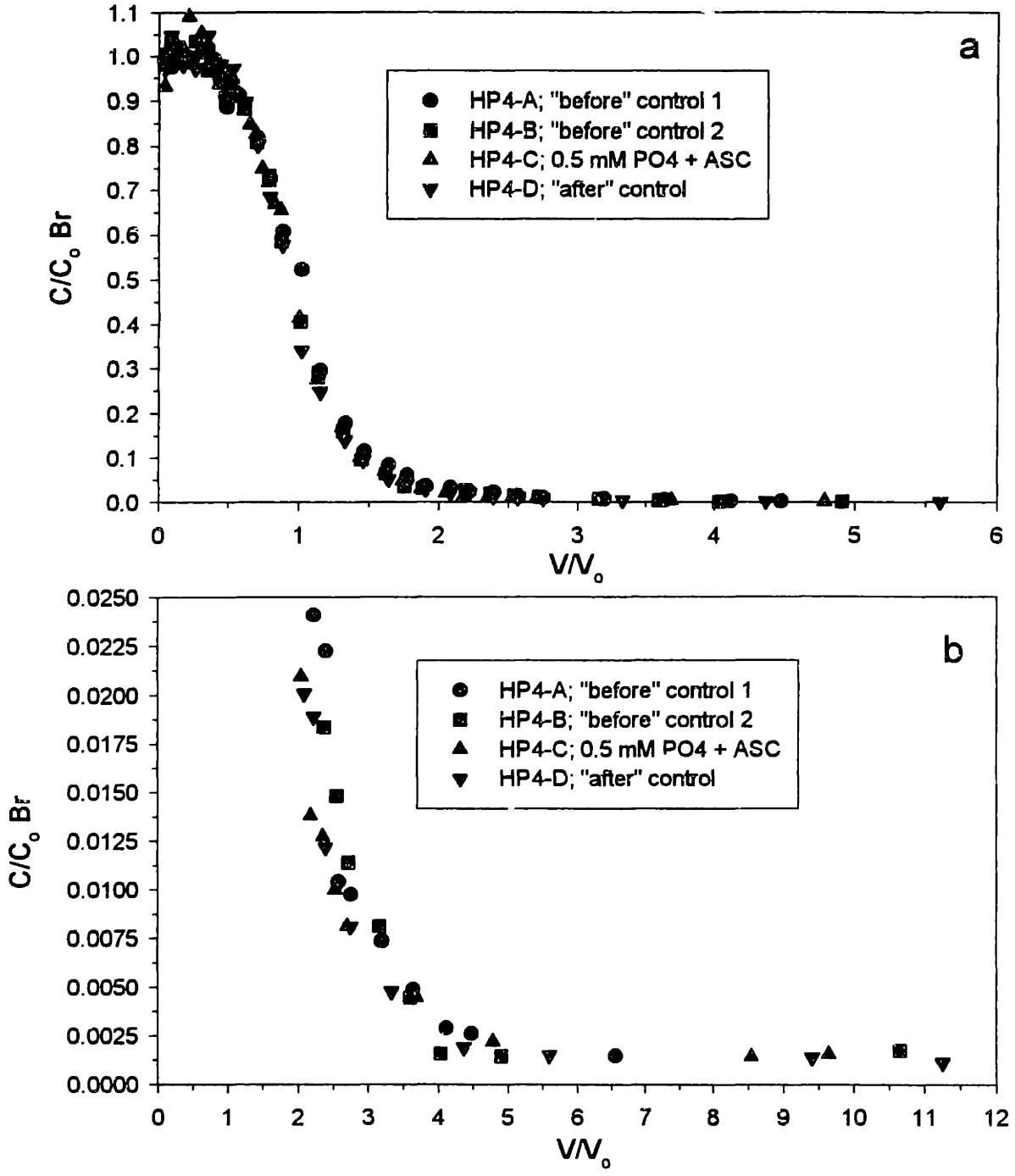

Figure 4.15: Normalized Br^- concentration profiles for all of the experiments conducted in well HP4. In (a) all data is presented, and in (b) only data less than C/C_0 equal to 0.25 is presented. Note the similarity in profiles for the different experiments, even though a large mobilization event (turbidity > 500 NTU in first sample) occurred in HP4-C.

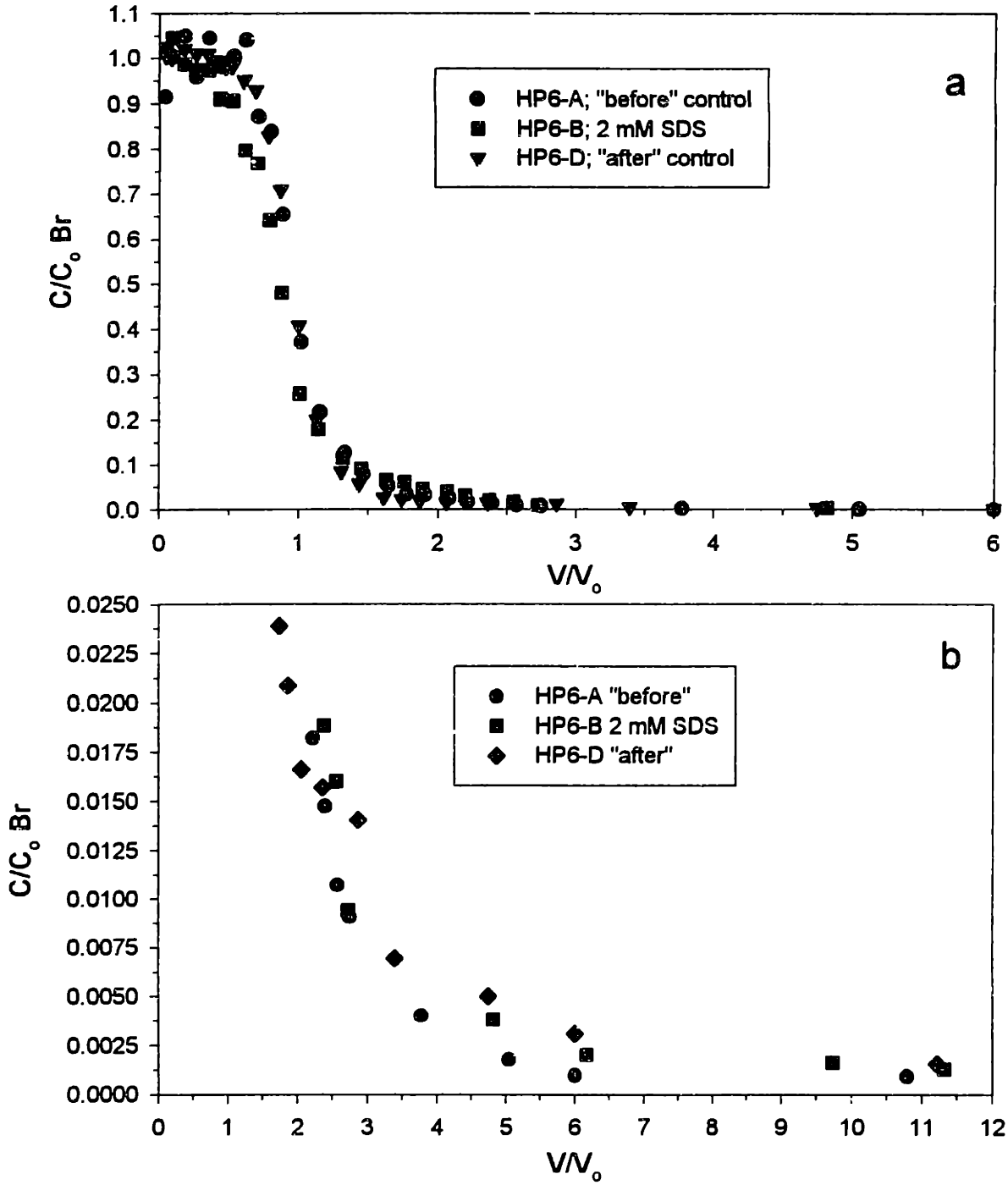

Figure 4.16: Normalized Br^- concentration profiles for all of the experiments conducted in well HP6. In (a) all data is presented, and in (b) only data less than C/C_o equal to 0.25 is presented. Note the similarity in profiles for the different experiments, even though a large mobilization event (turbidity > 2000 NTU in first sample) occurred in HP6-C.

in the field than in the column experiments.

In the *in situ* experiments, preferential mobilization of goethite aggregates occurred, as indicated by Al/Fe mole ratios of the colloids mobilized, when the sediment was treated with specifically adsorbing adsorbates (phosphate) which only reversed surface charge of the matrix constituent phases (particularly iron oxyhydroxides). No mobilization occurred when an anionic surfactant, 2 mM SDS, was introduced into the aquifer, probably because this ligand could not compete with the ambient adsorbed species (Chapter 5). Injectate amended with 10 mM SDS did result in a very large release of colloids, but foaming of the surfactant due to the peristaltic action of the pump was thought to cause physical disruption of the sediment upon introduction into the aquifer. Only when a reductant (ascorbic acid) and phosphate were both added to the injectate were colloids chemically mobilized that were more compositionally representative of the bulk matrix. An injectate with elevated pH also was more effective than injectate containing just phosphate at mobilizing colloids representative of the bulk matrix, although this treatment was not as effective as adding both ascorbic acid and phosphate to the injectate.

The colloid mobilization behavior exhibited *in situ* by the aquifer supported the hypothesis developed from mobilization behavior observed in the laboratory column experiments. These observations led to development of the hypothesis that bonds among the amorphous iron oxyhydroxides and kaolinite platelets in the sediment matrix had be broken before electrostatic repulsion could induce mobilization of colloids representative of the bulk matrix. These bonds could be broken either through hydrolysis (i.e., basic pH) or by reductates which dissolved iron oxyhydroxides (i.e., ascorbic acid). Goethite was thought to be preferentially mobilized when only electrostatic perturbations were introduced by pore fluids because this phase occurs as discrete aggregates among the matrix (Swartz et al., 1997).

Analysis of the decay in turbidity as a function of contact time, or distance traveled, in the aquifer during the experiments suggested that the behavior of the suspended colloid concentration could be described by reactions between that of first and second order.

Colloids mobilized by chemical perturbations causing increasingly repulsive interactions in the subsurface system more closely followed first order kinetic behavior. In contrast, the "loose" colloidal material mobilized in control experiments followed a second order behavior. In this case, it was assumed that subsurface electrostatic interactions remained attractive, as no chemically perturbing solute was added to the groundwater. The *in situ* colloid transport behavior was in general correspondence with published studies of colloid transport kinetic behavior in packed-column systems (Saiers et al., 1994; Kretzschmar et al., 1997). The analysis of the colloid transport process also allowed us to differentiate, in part, mobilization due to physical perturbations imparted by the flow reversal process from mobilization induced by chemical amendment of the groundwater. This differentiation aided in explaining discrepancies between the *in situ* and packed-column observations of colloid mobilization behavior in this sediment.

These experiments demonstrate the usefulness of the single well injection-withdrawal system for *in situ* determination of aquifer response to various chemically perturbing injectates. The method could be used in a variety of applications. For example, prior to chemically enhanced remediation efforts, like introduction of surfactant solutions to solubilize organic contaminants, test solutions could be introduced via the single well method to determine whether large colloid releases would result from exposure of the aquifer solids to the solution. Such releases could result in clogged pores and concomitantly reduced hydraulic conductivities, hindering the remediation effort. The single well injection-withdrawal method also provides valuable geochemical information on such phenomena as competitive sorption among aqueous species (see Chapter 5), an effect which may determine whether or not a particular adsorbate is able to effect changes in the electrostatic interactions among aquifer matrix constituents.

4.5 References

Backhus D. A., Ryan J. N., Groher D. M., MacFarlane J. K., and Gschwend P. M. (1993) Sampling colloids and colloid associated contaminants in groundwater. *Groundwater* **31**, 466-479.

Bates J. K., Bradley J. P., Teetsov A., Bradley C. R., and Brink M. B. t. (1992) Colloid formation during waste form reaction: Implications for nuclear waste disposal. *Science* **256**, 649-651.

Cerda C. M. (1987) Mobilization of kaolinite fines in porous media. *Coll. Surf.* **27**, 219-241.

Capuano R. M., Adams M. C., and Wright P. M. (1983) Tracer recovery and mixing from two geothermal injection-backflow studies. In: Proceedings Ninth Workshop Geothermal Reservoir Engineering, Stanford University, December, 1983, 299-304.

Deans H. A. and Carlisle C. T. (1986) Single-well tracer test in complex pore systems. Paper SPE 14886, SPE/DOE 5th Symposium on Enhanced Oil Recovery, Tulsa, OK, April 20-23, 1986. **1**, 61-76.

Drees L. R., Wilding L. P., Smeck N. E., and Senyaki A. L. (1989) Silica in soils: Quartz and disordered silica polymorphs. In *Minerals in Soil Environments* (ed. J. B. Dixon and S. B. Weed),2nd ed., pp. 913-974. Soil Science Society of America.

Gelhar L. W. and Collins M. A. (1971) General analysis of longitudinal dispersion in nonuniform flow. *Water Resourc. Res.* **7**, 1511-1521.

Goldenberg L. C. and Margaritz M. (1983) Experimental investigation on irreversible changes of hydraulic conductivity on the seawater-freshwater interface in coastal aquifers. *Water Resourc. Res.* **19**, 77-85.

Gounaris V., Anderson P. R., and Holsen T. M. (1993) Characteristics and environmental significance of colloids in landfill leachate. *Environ. Sci. Technol.* **27**, 1381-1387.

Gschwend P. M., Backhus D. A., MacFarlane J. K., and Page A. L. (1990) Mobilization of colloids in groundwater due to infiltration of water at a coal ash disposal site. *J. Contam. Hydrol.* **6**, 307-320.

Herrington T. M., Clarke A. Q., and Watts J. C. (1992) The surface charge of kaolin. *Coll. Surf.* **68**, 161-169.

Holmén B. A. and Gschwend P. M. (1997) Estimating sorption rates of hydrophobic organic compounds in iron oxide- and aluminosilicate clay-coated aquifer sands. *Environ. Sci. Technol.* **31**, 105-113.

Istok J. D., Humphrey M. D., Schroth M. H., Hyman M. R., and O'Reilly K. T. (1997) Single-well, "push-pull" test for in situ determination of microbial activities. *Groundwater* **35**, 619-631.

Kaplan D. I., Bertsch P. M., and Adriano D. C. (1995) Facilitated transport of contaminant metals through an acidified aquifer. *Groundwater* **33**, 708-717.

Kaplan D. I., Bertsch P. M., Adriano D. C., and Miller W. P. (1993) Soil-borne mobile colloids as influenced by water flow and organic carbon. *Environ. Sci. Technol.* **27**, 1193-1200.

Kaplan D. I., Bertsch P. M., Adriano D. C., and Orlandini K. A. (1994) Actinide association with groundwater colloids in a coastal plain aquifer. *Radiochimica Acta* **66/67**, 189-195.

Khilar K. C. and Fogler H. S. (1984) The existence of a critical salt concentration for particle release. *J. Colloid Int. Sci.* **101**, 214-224.

Kia S. F., Fogler H. S., and Reed M. G. (1987) Effect of pH on colloidally induced fines migration. *J. Colloid Int. Sci.* **118**, 158-168.

Kretzschmar R., Barmettler K., Grolimund D., Yan Y.-d., Borkovec M., and Sticher H. (1997) Experimental determination of colloid deposition rates and collision efficiencies in natural porous media. *Water Resourc. Res.* **33**, 1129-1137.

Lessoff S. C. and Konikow L. F. (1997) Ambiguity in measuring matrix diffusion with single-well injection/recovery tracer tests. *Groundwater* **35**, 166-176.

Liang L., McCarthy J. C., Jolley L. W., McNabb J. A., and Mehlhorn T. L. (1993) Iron dynamics: Transformation of Fe(II)/Fe(III) during injection of natural organic matter in a sandy aquifer. *Geochim. Cosmochim. Acta* **57**, 1987-1999.

Liang L. and Morgan J. J. (1990a) Chemical aspects of iron oxide coagulation in water: Laboratory studies and implications for natural systems. *Aquatic Sci.* **52**, 32-55.

Liang L. and Morgan J. J. (1990b) Coagulation of iron oxide particles in the presence of organic materials. *American Chemical Society Symposium Series* **No. 146**, 293-308.

Mas-Pla J., Yeh T.-C. J., McCarthy J. F., and Williams T. M. (1992) A forced gradient tracer experiment in a coastal sandy aquifer, Georgetown Site, South Carolina. *Groundwater* **30**, 958-964.

McCarthy J. F. and Degueldre C. (1993) Sampling and characterization of colloids and particles in groundwater for studying their role in contaminant transport. In *Environmental Particles*, Vol. 2 (ed. H. P. v. Leeuwen and J. Buffle)2-64.

McCarthy J. F., Gu B., Liang L., Mas-Pla J., Williams T. M., and Yeh T.-C. J. (1996) Field tracer tests on the mobility of natural organic matter in a sandy aquifer. *Water Resourc. Res.* **32**, 1223-1238.

McCarthy J. F., Williams T. M., Liang L., Jardine P. M., Jolley L. W., Taylor D. L., Palumbo A. V., and Cooper L. W. (1993) Mobility of natural organic matter in a sandy aquifer. *Environ. Sci. Technol.* **27**, 667-676.

McDowell-Boyer L. M. (1992) Chemical mobilization of micron sized particles in saturated porous media under steady flow conditions. *Environ. Sci. Technol.* **26**, 586-593.

Morel F. M. M. and Hering J. G. (1993) *Principles and Applications of Aquatic Chemistry*. John Wiley and Sons, Inc.

Mysels E. K. and Mysels K. J. (1965) Conductimetric determination of the critical micelle concentration of surfactants in salt solutions. *Journal of Colloid Science* **20**, 315-321.

Newman M. E., Elzerman A. W., and Looney B. B. (1993) Facilitated transport of selected metals in aquifer material packed columns. *J. Contam. Hydrol.* **14**, 233-246.

Penrose W. R., Polzer W. L., Essington E. H., Nelson D. M., and Orlandini K. A. (1990) Mobility of plutonium and americium through a shallow aquifer in a semiarid region. *Environ. Sci. Technol.* **24**, 228-234.

Puls R. W. and Powell R. M. (1992) Transport of inorganic colloids through natural aquifer material: Implications for contaminant transport. *Environ. Sci. Technol.* **26**, 614-621.

Ronen D., Margaritz M., Weber U., and Amiel A. J. (1992) Characterization of suspended particle collected in groundwater under nautral gradient flow conditions. *Water Resourc. Res.* **28**, 1279-1291.

Roy S. B. and Dzombak D. (1996) Colloid release and transport processes in natural and model porous media. *Coll. Surf.* **107**, 245-.

Roy S. B. and Dzombak D. A. (1997) Chemical factors influencing colloid-facilitated transport of contaminants in porous media. *Environ. Sci. Technol.* **31**, 656-664.

Ryan J. N. and Elimelech M. (1996) Colloid mobilization and transport in groundwater. *Coll. Surf. A.* **107**, 1-56.

Ryan J. N. and Gschwend P. M. (1990) Colloid mobilization in two Atlantic Coastal Plain aquifers, field studies. *Water Resourc. Res.* **26**, 307-322.

Ryan J. N. and Gschwend P. M. (1994) Effect of solution chemistry on clay colloid release from an iron oxide-coated aquifer sand. *Environ. Sci. Technol.* **28**, 1717-1726.

Saiers J. E., Hornberger G. M., and Liang L. (1994) First- and second-order kinetic approaches for modeling the transport of colloidal particles in porous media. *Water Resourc. Res.* **30**, 2499-2506.

Sanford W. (1997) personal communication. Colorado State University, Fort Collins, Colorado.

Sanford W., Hall D., and Solomon K. Unpublished data. Colorado State University, Fort Collins, Colorado, and University of Utah, Salt Lake City, Utah.

Schwertmann U. and Fechter H. (1982) The point of zero charge of natural and synthetic ferrihydrite and its relation of adsorbed silicate. *Clay Min.* **17**, 471-476.

Seaman J. C., Bertsch P. M., and Miller W. P. (1995) Chemical controls on colloid generation and transport in a sandy aquifer. *Environ. Sci. Technol.* **29**, 1808-1815.

Seaman J. C., Bertsch P. M., and Strom R. N. (1997) Characterization of colloids mobilized from Southeastern Coastal Plain sediments. *Environ. Sci. Technol.* **31**, 2782-2790.

Short S. A., Lowson R. T., and Ellis J. (1988) $^{234}U/^{238}U$ and $^{230}Th/^{234}U$ activity ratios in the colloidal phases of aquifers in lateritic weathered zones. *Geochim. Cosmochim. Acta* **52**, 2555-2563.

Sigg L. and Stumm W. (1980) The interaction of anions and weak acids with the hydrous goethite (α-FeOOH) surface. *Coll. Surf.* **2**, 101-117.

Swartz C. H., Ulery A. L., and Gschwend P. M. (1997) An AEM-TEM study of nanometer-scale mineral associations in an aquifer sand: Implications for colloid mobilization. *Geochim. Cosmochim. Acta* **61**, 707-718.

Tipping E. (1981) The adsorption of aquatic humic substances by iron oxides. *Geochim. Cosmochim. Acta* **45**, 191-199.

Tipping E. and Cooke D. (1982) The effects of adsorbed humic substances on the surface charge of goethite (α-FeOOH) in freshwaters. *Geochim. Cosmochim. Acta* **46**, 75-80.

Tomich J. F., Dalton R. I., Deans H. A., and Shallenberger I. K. (1973) Single-well tracer test method to measure residual oil saturation. *J. Petrol. Tech.* **Feb** , 211-218.

Trudall M. R., Gillham R. W., and Cherry J. A. (1986) An in situ study of the occurrence and rate of denitrification in a shallow unconfined sand aquifer. *J. Hydrol.* **83**, 251-268.

Ulery, A. L. Unpublished data. Massachusetts Institute of Technology.

Wilding L. P., Hallmark C. T., and Smeck N. E. (1979) Dissolution and stability of biogenic opal. *Soil Sci. Soc. Am. J.* **43**, 800-802.

Williams T. M. and McCarthy J. F. (1991) Field-scale tests of colloid:facilitated transport. *National Research and Development Conference on the Control of Hazardous Materials*, 179-184.

Yeh T.-C. J., Mas-Pla J., Williams T. M., and McCarthy J. F. (1995) Observation and three-dimensional simulation of chloride plumes in a sandy aquifer under forced-gradient conditions. *Water Resourc. Res.* **31**, 2141-2157.

Zinder B., Furrer G., and Stumm W. (1986) The coordination chemistry of weather: II. Dissolution of Fe(III) oxides. *Geochim. Cosmochim. Acta* **50**, 1861-1869.

Chapter 5:

Competitive Adsorption Effects on Colloid Mobilization

5.1 Introduction

Studies of adsorption on amphoterically, or variably, charged oxide surfaces have repeatedly demonstrated the ability of various inorganic and organic anions and to influence the surface charge of these surfaces (Hingston et al., 1972; Anderson and Malotky, 1979; Sigg and Stumm, 1980; Liang and Morgan, 1990a). Amphoteric oxides, particularly those of iron (e.g., goethite, amorphous iron oxyhydroxides) and aluminum (e.g., gibbsite), are ubiquitous in environmental systems like surface waters and aquifer sediments, often coating clay minerals and quartz grains and acting as electrostatic intermediaries among these phases. Clay minerals possess a permanent negative charge on their basal plane faces, and quartz is negatively charged above pH 2.0. The pristine point of zero charge (pH_{pzc}) of many of the amphoteric oxides is greater than 7.0, indicating that their surfaces would be positively charged in many natural aquatic environments in the absence of specific adsorbates. However, the specific adsorption of many anionic species can lower the point of zero charge, imparting significant negative charge to the surfaces at pH values of 4.0 or lower. As the surface charge of these oxides plays a pivotal role in determining whether their electrostatic interactions with the surfaces of neighboring clay minerals and quartz are attractive or repulsive, the presence of specific adsorbing solutes can control the electrostatic stability of the colloidal system.

For example, the adsorption of dissolved organic matter from various lake waters onto goethite, amorphous iron oxyhydroxides, and aluminum oxides has been found to reverse the surface charge of these solids (Davis and Gloor, 1981; Tipping, 1981; Tipping and Cooke, 1982). The adsorption of various organic acids, used as analogs for natural dissolved organic matter, has been found to dramatically alter the coagulation kinetics of hematite (Liang and Morgan, 1990b). Thus, by altering surface charge, the specific adsorption of solutes can affect the residence time of such colloidal solids in the water column, and subsequently, the cycling of metals in these systems.

Simple organic acids have been found to induce colloid mobilization in aquifer sediments, presumably due to destabilization of goethite-kaolinite electrostatic interactions by specific adsorption of the organic acid onto goethite and concomitant surface charge reversal of goethite (Ryan and Gschwend, 1994). Common inorganic constituents of natural waters like phosphate, sulfate, and silicate (Hohl et al., 1980; Sigg and Stumm, 1980; Djafer et al., 1991) as well as toxic adsorbates like selenite (Hansmann and Anderson, 1985), arsenate (Anderson and Malotky, 1979), and chromate (Davis and Leckie, 1980) can also modify the surface charge of amphoteric surfaces. The destabilization of the electrostatic interactions among colloidal solids by adsorbing contaminants can have serious implications for the fate of those contaminants. In aquifer systems, adsorption of the contaminant to immobile solids would result in retardation of the transport of the contaminant in the aquifer. However, if adsorption of the contaminant destabilized electrostatic interactions and mobilized aquifer solids, the transport of the contaminant would be enhanced.

A particular adsorbate can only affect the surface charge of the adsorbent if it is able to specifically adsorb (Pyman et al., 1979). For natural systems, this means that the adsorbate must compete with other naturally occurring ligands for sites on the adsorbent surface. In natural waters, a variety of inorganic ligands, e.g., sulfate, phosphate, silicate, carbonate species, and organic ligands (e.g., humic substances) can be present. Competition between these ligands and other adsorbates of interest (e.g., contaminants such as selenite and chromate) for surface sites on well-characterized materials like goethite have been increasingly investigated (Hingston et al., 1971; Balistrieri and Murray, 1987; Hawke et al., 1989; Ali and Dzombak, 1996). The competition for sites among adsorbates appears to be controlled by the relative affinities of the adsorbates for the surface sites and the relative concentrations of adsorbates present (Mesuere and Fish, 1992b; Ali and Dzombak, 1996).

Competitive adsorption phenomena appear to be manifest in data obtained from an *in situ* method used to investigate colloid mobilization in a Southeastern Coastal plain aquifer (see Chapter 4). In these experiments, various adsorbates, e.g., phosphate, ascorbate, and

sodium dodecyl sulfate (SDS, an anionic surfactant), were added to groundwater pumped from wells emplaced in the aquifer. A prescribed volume of the amended groundwater was then reinjected into the aquifer, and subsequently retrieved by reversing flow. Levels of dissolved solutes were measured in the retrieved injectate.

The results indicated that competitive adsorption effects could aid in explaining why SDS failed to induce preferential mobilization of goethite aggregates *in situ* (and in laboratory columns packed with the sediment), while phosphate did induce preferential mobilization of goethite aggregates in the *in situ* and column experiments. This mobilization behavior does not correspond to electrophoretic mobility studies using model goethite colloids, which indicated that SDS would impart greater repulsive interactions among goethite aggregates and kaolinite present in the aquifer matrix than would phosphate. We believe that competitive inhibition of adsorption of the anionic surfactant (SDS) to the aquifer solids (e.g., goethite) by ambiently adsorbed sulfate, silicate, and possibly carbonate species, appeared to prevent the surfactant from inducing mobilization of the goethite aggregates. The data obtained from the single well injection-withdrawal method suggest that this method can provide valuable information regarding *in situ* competitive adsorption phenomena.

5.2 Methodology

The *in situ* colloid mobilization experiments were conducted on the grounds of the Baruch Forest Science Institute, Georgetown, SC. The aquifer is shallow, unconfined, and composed of an iron oxide-coated quartz sand deposited in a marine beach environment approximately 100,000 yrs ago (Williams and McCarthy, 1991). The mineralogy of the matrix components and mineral phase associations within the matrix of this sediment were analyzed using analytical and transmission electron microscopy (see Chapter 2, Swartz et. al., 1997). The colloid mobilization behavior of the sediment was studied initially using columns packed with the sediment (see Chapter 3). Samples obtained from a depth of 2.2 m in the aquifer (see **Figure 4.1**, Chapter 4, for the location of these samples) were used for the

microscopy and column investigations.

The *in situ* mobilization experiments were conducted in six different wells emplaced over a period of three years (see **Table 4.1**, Chapter 4). These experiments were designed to test the mobilization behavior of the aquifer material *in situ* in response to various chemically perturbing adsorbates which had been used to test the colloid mobilization behavior of the sediment in packed-column experiments (Chapter 3). These adsorbates, which included reagent grade phosphate (added as NaH_2PO_4), ascorbic acid, and ultrapure sodium dodecyl sulfate (an anionic surfactant), were added to groundwater pumped from the aquifer. The effects of acidifying and elevating the pH of the groundwater, with HCl and NaOH, respectively, were also investigated. A conservative tracer, NaBr, was added to all injectates at a concentration of 0.5 mM.

Well Construction. Each well was constructed of a 4" i.d. PVC casing advanced into the aquifer by hand augering a hole to a total depth of approximately 3.2 m. Each casing was screened over a 7.6 cm interval which was centered at a depth of 2.65 m. Inserted into each casing was an apparatus composed of a 3" i.d. PVC pipe plumbed with tygon tubing to create a discrete injection-withdrawal system centered at a depth of 2.65 m upon insertion into the casing. The objective of the system design was to minimize the dead volume in the well bore by creating a packed-off annulus between the 4" i.d. casing and the 3" i.d. inner well apparatus (see **Figure 4.2** and section 4.2.4, Chapter 4 for details). The dead volume in this annulus was approximately 25 mL.

Experimental Procedure. The single well injection-withdrawal method for studying colloid mobilization *in situ* involved pumping ambient groundwater from each well via a peristaltic pump, amending it with the prescribed solutes, and reinjecting a known volume (approximately 11.5 L) of the amended groundwater back into the aquifer. The injectate was then retrieved by reversing the flow direction of the peristaltic pump. Details of this procedure can be found in Chapter 4 (section 4.2.4). In most cases, only one chemical perturbation experiment was conducted in each well, along with "control" experiments

conducted before and after the chemical perturbation experiment. The control experiments involved an injection-withdrawal sequence using unamended groundwater (except for the presence of the Br^- tracer).

Sampling Apparatus. The sampling apparatus at ground surface was designed to allow collection of discrete samples of the retrieved injectate during the withdrawal phase of the experiments (see **Figure 4.2**, Chapter 4). A 125 mL sample was obtained for every 500 mL of retrieved injectate up to 25,000 mL discharged (approximately 2.5 times the injectate volume). A 125 mL sample was obtained thereafter upon discharge of every 5,000 to 10,000 mL discharged until background levels of the bromide tracer were attained (usually approximately 50,000 mL). Samples were then obtained every 25,000 to 50,000 mL until the next injection-withdrawal sequence for that well was begun (after approximately 120,000 mL discharged). A 35 mL subsample of each 125 mL sample obtained was archived for later chemical analysis.

The initial chemistry of the injectate was obtained from samples collected by syringe from a sampling port truncating a 1/8" o.d. stainless steel line emplaced within the main 5/16" i.d. plastic line (see **Figure 4.3**, Chapter 4). Both of these lines extended to the distribution and collection system at the well screen (see **Figure 4.2**, Chapter 4). The stainless steel line allowed sampling of the injectate during the injection phase of the experiment.

Sample Analysis. The pH (Orion) and turbidity (Ratio X/R, Hach) of each 125 mL sample were measured in the field upon discharge of the sample from the well. All anion analyses (Br^-, sulfate, phosphate) were conducted with the 35 mL archived samples upon returning to the laboratory. Br^- was measured either by inductively coupled plasma mass spectrometry (VG Plasmaquad KP-20, Visons Inst.) or by ion chromatography (Dionex model 16 ion chromatograph with an anion self-regenerating suppressor column). Sulfate and phosphate were also measured by ion chromatography. The buffer consisted of 1.8 mM Na_2CO_3 and 1.7 mM $NaHCO_3$. SDS was measured in appropriate samples by combustion of total organic carbon (subsamples were acidified and bubbled with N_2 to remove inorganic

carbon) and detection by infrared absorption (TOC-5000, Shimadzu). Dissolved silicate was measured colorimetrically using the molybdosilicate method (*AWWA Standard Methods*, 1992) and a spectrophotometer (Beckman DU 640) set at a wavelength of 410 nm.

5.3 Results and Discussion

5.3.1 Ambient Groundwater Chemistry

The prevailing groundwater chemistry was determined from analysis of one to two samples obtained from each well emplaced over the three year period of the project. These samples were obtained before the first injection-withdrawal sequence (**Table 5.1**) in each well. The groundwater pH and concentrations of O_2 (by Chemets), SO_4^{2-}, and total dissolved Si concentrations were all fairly constant over the three year period in which they were monitored. Phosphate was not detected in the groundwater (i.e., <1 μM). Note that the concentration of molybdate-reactive silicate (160± 10 μM) was approximately half the value of total dissolved Si (370±120 μM) determined by graphite furnace atomic absorption (A.A.) spectrometry (See Chapter 4). Both measurements were performed on samples which had passed through 30 nm pore-size membranes. The molybdate-reactive form of the dissolved Si species is assumed to be silicate, i.e., H_4SiO_4. The difference between the molybdate reactive silicate concentration and the total dissolved Si determined by A.A. suggests either some very small (< 30 nm) colloidal silica particles were present in the groundwater (these particles would be molybdate unreactive) or that all of the measured Si was truly dissolved, but that half of it was molybdate unreactive. Issues regarding molybdate reactivity of dissolved species in natural waters have not been resolved in the literature (*AWWA Standard Methods*, 1992).

Alkalinity varied to a greater degree. Note that the $H_2CO_3^*$ concentration of the groundwater (320 μM), calculated assuming alkalinity was composed entirely of HCO_3^{1-}, is approximately 37 times the value which would be predicted based on equilibration with the atmosphere at pH 5.26. The elevated levels of $H_2CO_3^*$ probably originated from subsurface

Table 5.1: Groundwater Chemical Parameters[1]

pH	5.26±0.13
alkalinity (μM)[2]	26±10
conductivity (μMHOS cm^{-1})[3]	38±5
NP-DOC (μM)[4]	92±21
Dissolved Fe (nM)[5]	130±100
Dissolved Al (nM)[5]	170±120
Dissolved Si (μM)[5]	370±120
Dissolved silicate (μM)[6]	160±10
Dissolved sulfate (μM)	54±7
Dissolved Oxygen (μM)	140±9
Dissolved Bromide (μM)	0.44±0.06

[1]the average±one standard deviation for n=7 to 10 samples, with at least 1 sample from each of 7 wells included

[2]measured by Gran titration

[3]corresponds to an ionic strength of approximately 0.4 mM, calculated using the concentrations of the major groundwater ions (Chapter 2)

[4]non-purgeable dissolved organic carbon

[5]defined as passing through a 30 nm pore size filter

[6]molybdate-reactive silicate

microbial respiration.

5.3.2 Mobilization Behavior in Response to Phosphate and SDS

The chemical amendments to the groundwater were chosen to test our hypothesis that bonds thought to exist among amorphous iron oxyhydroxides and kaolinite platelets prevented electrostatic perturbations (e.g., surface charge reversal of the iron oxyhydroxides in the sediment through specific adsorption) from inducing mobilization of these components of the bulk matrix. This hypothesis was developed after observing the response of the sediment to various treatment solutions in packed-column experiments (see Chapter 3). These experiments indicated that only adsorbates which (1) promoted dissolution of the iron oxyhydroxides in the sediment, and (2) generated sufficient repulsive forces among matrix constituents (e.g., the iron oxyhydroxides) through specific adsorption would mobilize colloids compositionally representative of the bulk matrix (see Chapter 3).

Goethite was found to occur as discrete aggregates in the matrix (Chapter 2, Swartz et al., 1997), suggesting that this phase was able to respond freely to electrostatic perturbations such as surface charge reversal. Indeed, when the sediment was treated with a sufficiently concentrated phosphate solution (10 mM) at pH 5.2, colloids with an Al/Fe mole ratio (0.5±0.3, Table 3.1, Chapter 3) similar to that of the goethite aggregates (0.24±0.08, Chapter 2, Swartz et al., 1997) were mobilized in a subsequent deionized water flush. Mobilization during the phosphate treatment was apparently hindered by compression of the electric double layers of the goethite aggregates due to the relatively high ionic strength of the treatment solution. A solution containing only 1 mM phosphate induced no colloid mobilization during the treatment flush either (**Figure 3.13**, Chapter 3).

When the sediment was treated with a 2 mM SDS solution (pH 5.4) and a subsequent deionized water flush, no colloids were released in either flush (see **Figure 3.8**, Chapter 3). However, results from electrophoretic mobility studies using model goethite colloids indicated that a solution containing 2 mM SDS at pH 5.2 would impart greater negative charge to the surfaces of the goethite than would a 10 mM phosphate solution at pH 5.2 (see **Figure 3.4**

Chapter 3).

To verify this colloid release behavior *in situ*, we injected groundwater amended with 2 mM SDS (pH = 5.33) into the aquifer in injection-withdrawal experiment HP6-B (Chapter 4). In a manner similar to that of the packed-column behavior, turbidity in the retrieved injectate was not significantly different from the control experiment (HP6-A) conducted prior to HP6-B (**Figure 4.4**, Chapter 4).

In contrast to the results obtained by injecting SDS amended groundwater, groundwater amended with 1 mM phosphate (HP9-B) did result in somewhat elevated turbidity of the retrieved injectate as compared to the control experiment (HP9-A) (**Figure 4.5**, Chapter 4). The Al/Fe ratio of the mobilized colloids (0.8±0.2) suggested that treatment of the sediment with phosphate had resulted in preferential mobilization of the goethite aggregates.

Thus, the *in situ* colloid mobilization experiments confirmed the inability of SDS to induce mobilization in the Georgetown sediment, while phosphate appeared to be capable of inducing mobilization. Such results contradict electrophoretic mobility measurements of model goethite colloids suspended in comparable SDS and phosphate solutions, which indicated that 2 mM SDS would be more effect than even 10 mM phosphate at reversing the surface charge of the iron oxyhydroxides in the Georgetown sediment (**Figure 3.4**, Chapter 3). We believe that the behavior of major anions in the groundwater, measured in the *in situ* experiments detailed in Chapter 4, provides an explanation for this discrepancy.

5.3.3 Evidence for Competitive Adsorption by Phosphate and Ascorbate

Anion Behavior in Response to Phosphate Injection. When 1 mM phosphate amended groundwater was injected (HP9-B) and then withdrawn from the aquifer, the retrieved samples exhibited large losses of phosphate with respect to the initial concentration injected (**Figure 5.1a**). The normalized concentration of phosphate after every 500 mL discharged (determined from the 35 mL archived subsample of each 125 mL collected) is represented on the left y axis of **Figure 5.1a**, as is the normalized concentration of the Br^- tracer. Note that these

Figure 5.1 appears on the next page

Figure 5.1: Normalized concentrations of bromide and phosphate (left y axis) and sulfate, silicate, and OH^- (right y axis) as a function of V/V_c for experiments (a) HP9-B, in which 1 mM phosphate amended groundwater was injected, and (b) HP9-A, the control experiment.

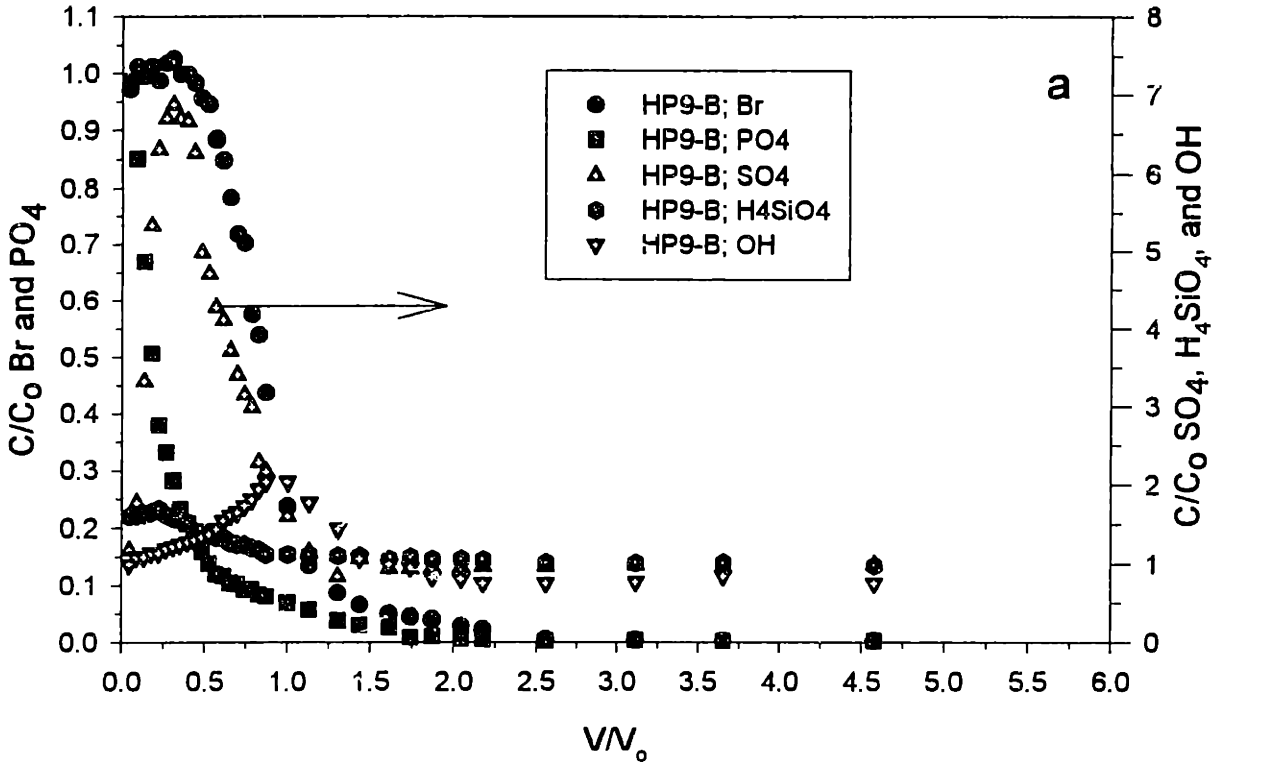
a
HP9-B; Br
HP9-B; PO4
HP9-B; SO4
HP9-B; H4SiO4
HP9-B; OH
C/Co Br and PO4
C/Co SO4, H4SiO4, and OH
V/Vo

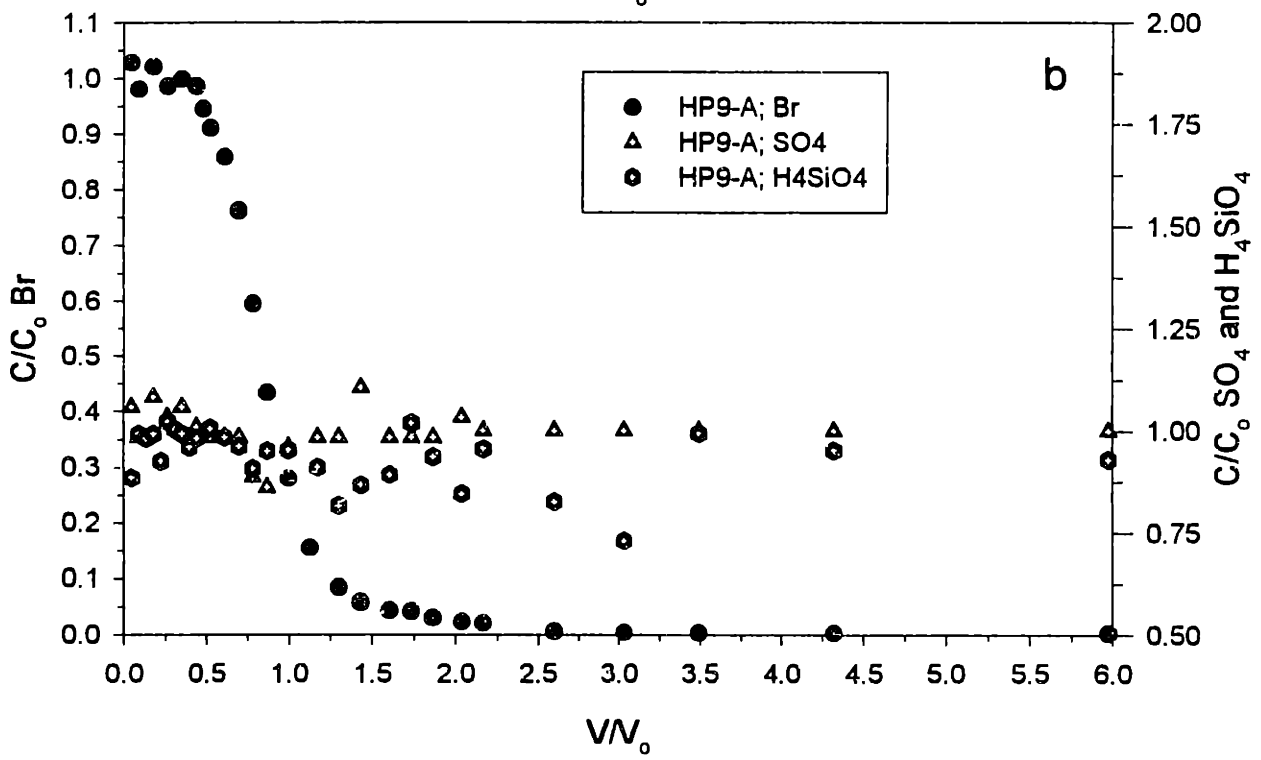
b
HP9-A; Br
HP9-A; SO4
HP9-A; H4SiO4
C/Co Br
C/Co SO4 and H4SiO4
V/Vo

losses could not be explained by dilution due to mixing with the ambient groundwater, as the precipitous drop in the value of C/C_0 for phosphate occurred in the samples which were not effected by dispersive mixing (as indicated by C/C_0 values for Br^- equal to 1.0) (**Figure 5.1a**).

This loss of phosphate was first order with respect to the aqueous phosphate concentration in the samples, as indicated by the high correlation coefficients (0.98) obtained for the regressions of ln (C/C_0) versus V/V_0 (volume discharged/volume recharged) for phosphate (**Figure 5.2**). The data representing phosphate loss could be separated into two distinct regression slopes. Values of V/V_0 were used in the reaction order plot to facilitate comparison with the data in **Figure 5.1**. Note that values of V/V_0 are a linearly proportional analog for residence time in the aquifer, as the quantity V/V_0 can be multiplied by V_0 and divided by the pumping rate (100 mL min^{-1}) to obtain the value of one half the total time (min) that the sample spends in the aquifer. This value is one half the total time because the sample is injected *and* withdrawn (at the same pumping rate) in the course of contact with the aquifer. Thus, the use of V/V_0 as the independent variable in the regression analysis does not effect the slope of the regression, but rather, only the y intercept value.

Concomitant with phosphate loss from the injectate, the concentration of SO_4^{2-} in the injectate *increased by a factor of seven* (the normalized concentration of SO_4^{2-} is represented with the right y axis in **Figure 5.1a**). The concentration of sulfate peaked and then began to fall (as did the Br^- concentration) as dispersive mixing with the ambient groundwater affected these samples. The ambient SO_4^{2-} concentration was reattained in samples retrieved at a V/V_0 value of approximately 1.3 (**Figure 5.1a**). Similarly, the concentration of molybdate-reactive silicate grew to approximately 1.5 times its initial concentration before decreasing to ambient levels in the samples affected by dispersive mixing with ambient groundwater (the normalized concentration of silicate is represented with the right y axis in **Figure 5.1a**). Note that no such increases in the concentrations of SO_4^{2-} and silicate occurred upon retrieval of the injectate in the control experiment, in which groundwater amended with only NaBr was

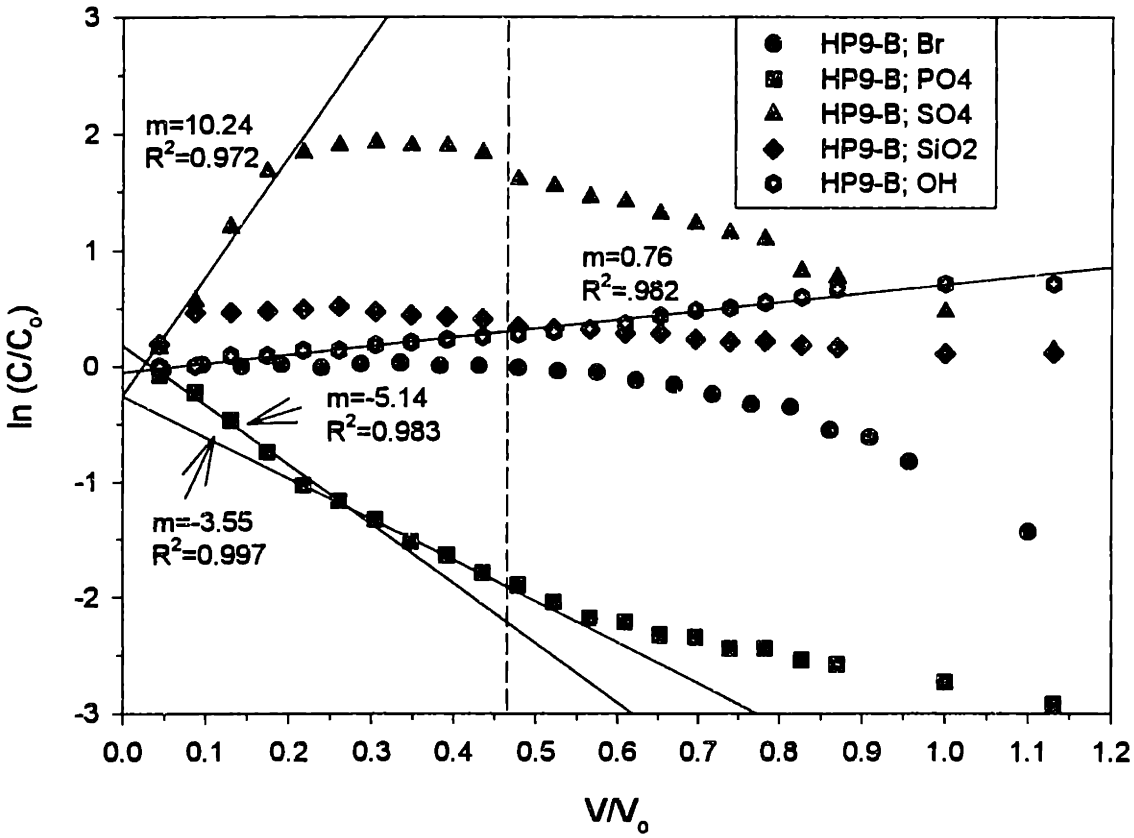

Figure 5.2: Plot of $\ln(C/C_o)$ bromide, phosphate, sulfate, silicate, and OH^- versus V/V_o for the samples retrieved during HP9-B (1 mM phosphate amended groundwater injected). The relatively high R^2 values obtained from regression of the data suggest that these solutes behaved first order with respect to their respective aqueous phase concentrations during retrieval of the injectate. For the sulfate data R^2=0.972, for OH^- R^2=0.982, for the first 5 data points of the phosphate data, R^2=0.983, and for the second five points of phosphate date, R^2=0.997.

injected (HP9-A, **Figure 5.1b**). The absence of any increase in the concentration of SO_4^{2-} or silicate in the retrieved injectate in the control experiment indicated that the concentration of Br^- (0.5 mM) in the injectate, although ten times greater than the SO_4^{2-} concentration (approximately 50 μM) and four times greater than the molybdate-reactive silicate concentration (160 μM), was not large enough to drive displacement of preadsorbed SO_4^{2-} and silicate from the matrix constituent surface sites.

The growth of sulfate in the samples retrieved in HP9-B appeared to be first order with respect to the aqueous phase concentration of sulfate (R^2=0.972) due to the displacement processes which linked the aqueous phase sulfate and phosphate concentrations (**Figure 5.2**). Only the first four samples retrieved from the aquifer were considered in the sulfate regression analysis (**Figure 5.2**). In the next six samples retrieved, the values of ln (C/C_o) for sulfate remained essentially constant, indicating that little change in the concentration of sulfate occurred in samples of injectate which had been "pushed out" further from the well screen (**Figure 5.2**). Values of ln (C/C_o) for sulfate then began to decrease as the effect of dispersive mixing with ambient groundwater occurred (the onset of which is indicated by the dashed line in **Figure 5.2**). Values of ln C/C_o for silicate showed an increase only between the first and second sample, and therefore, no regression was attempted (**Figure 5.2**). Thereafter, the silicate concentration of the retrieved samples remained unchanged until samples affected by dispersive mixing were subsequently drawn to the well screen and retrieved (sample data to the right of the dashed line in **Figure 5.2**).

The behavior observed for dissolved phosphate, sulfate, and silicate in the HP9-B samples is indicative of competitive adsorption for surface sites on the matrix constituents, probably predominantly on goethite, kaolinite, and amorphous iron oxyhydroxide found to be present in the sediment (Chapter 2, Swartz et al., 1997). We attempted a simple mass balance of the displaced sulfate and silica surface species by phosphate by plotting the amount of phosphate lost from the injectate (as μmoles per 500 mL sample retrieved), and the amounts of sulfate and silicate (i.e., H_4SiO_4) gained in the injectate (also as μmoles per 500 mL sample

retrieved) as a function of V/V_o (**Figure 5.3**). For this analysis, only the data representing samples of retrieved injectate unaffected by dispersive mixing, i.e., those samples appearing to the left of the dashed line in **Figure 5.2a**, were used.

In this analysis, we made no assumptions concerning the speciation of the adsorbed forms of these ligands. Such assumptions are beyond the scope of this work. The speciation and bonding structure (e.g., monodentate, bidentate, mononuclear or binuclear) of *adsorbed* sulfate, silicate, and phosphate on adsorbents of concern in this study (i.e., goethite, amorphous iron oxyhydroxide, and kaolinite) have either not been studied or are currently debated in the literature. Studies of surface speciation of such ligands involving fitting adsorption edge data with surface complexation models might not realistically portray the true surface species, but which allow net adsorption predictions to be made (Sigg and Stumm, 1980; Zachara et al., 1987; Mesuere and Fish, 1992a). Spectroscopic studies may determine surface species more realistically, but such studies are difficult and rare (Tejedor-Tejedor and Anderson, 1990). We merely made a simple comparison of phosphate lost from the aqueous phase, and sulfate and silicate gained in the aqueous phase, all on a μmolar basis. Of course, to maintain conservation of charge in the aqueous phase (i.e., a mass balance on a μEquivalent basis), various protonation, deprotonation and hydrolysis reactions might have to be included in the overall displacement reactions between phosphate, silicate, and sulfate.

Note, though, that the aqueous phase species can be defined readily. Phosphate would exist predominantly in the monobasic form ($H_2PO_4^{1-}$) in the aqueous phase at pH 5.26 (pK_{a2}= 7.2, Morel and Hering, 1993). The aqueous phase speciation of the silicate molecule would be H_4SiO_4 at pH 5.26 (the ambient groundwater pH), as its pK_{a1} equals 9.71 (Faure, 1991). Sulfate would exist as SO_4^{2-}at pH 5.26 (pK_{a2}= 1.92, *CRC Handbook*, 1990).

The resulting data could be separated into three distinct zones (**Figure 5.3a**). In the first zone, the total phosphate lost (35 μmoles) and sulfate and silicate gained (5 and 18 μmoles, respectively) represent the chemistry of the first 500 mL sample of the injectate retrieved (**Figure 5.3a**). Note that the total ligands gained (22 μmoles) accounted for only

Figure 5.3 appears on the next page

Figure 5.3: (a) The amounts (in μmoles) of phosphate lost from the injectate, and sulfate and silicate gained in the injectate in the first ten 500 mL samples retrieved from HP9-B (1 mM phosphate amended groundwater). The samples were not affected by dispersive mixing with the formation water. The plot is broken into zones based on changes in behavior of the three solutes with respect to V/V_o. Sulfate and silicate account for approximately 70% of the phosphate lost in zones 1 and 2, as indicated by comparing the regression slope incorporating the first 5 samples for phosphate lost (1690 μmoles V/V_o^{-1}) versus the slope for total sulfate and silicate gained obtained using the first five samples (1190 μmoles V/V_o^{-1}). (b) Total sulfate and silicate gained (in μmoles) per sample as a fraction of total phosphate lost (in μmoles) per sample with increasing V/V_o.

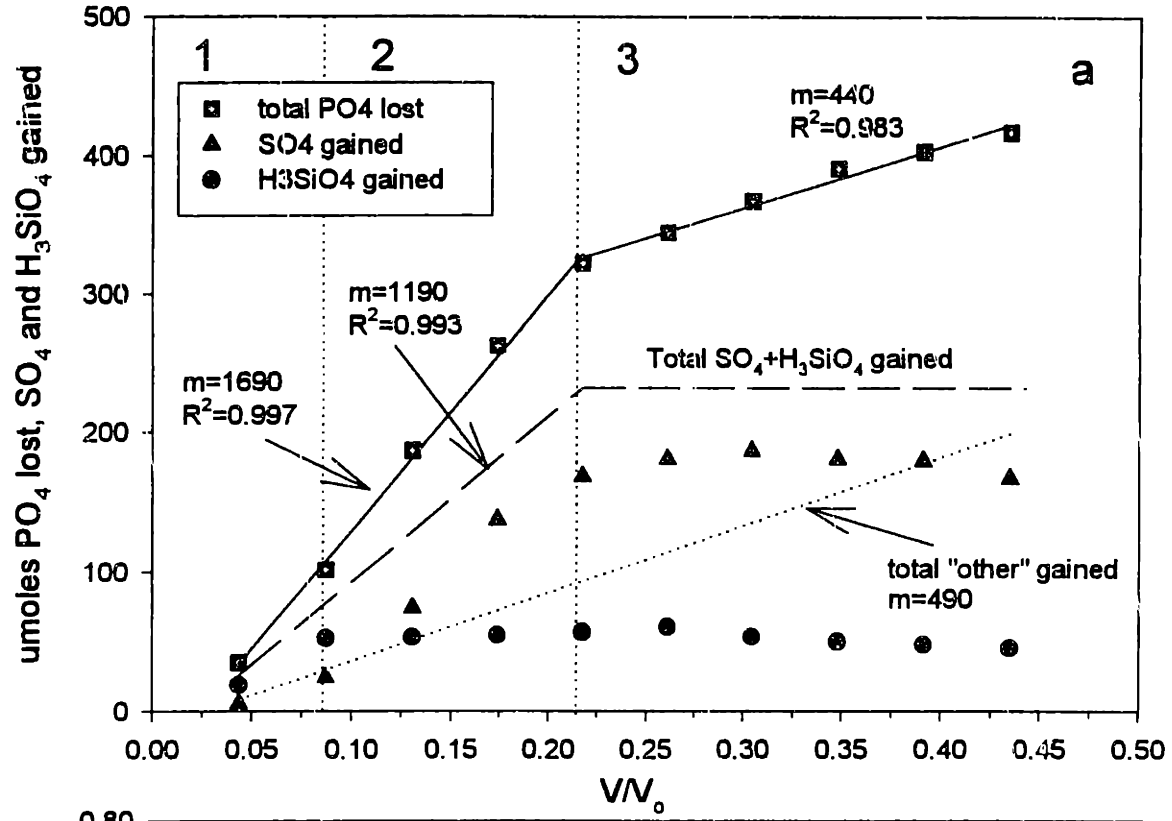
1
2
3
a
total PO4 lost
SO4 gained
H3SiO4 gained
m=440
R2=0.983
m=1190
R2=0.993
m=1690
R2=0.997
Total SO4+H3SiO4 gained
total "other" gained
m=490
umoles PO4 lost, SO4 and H3SiO4 gained
V/Vo

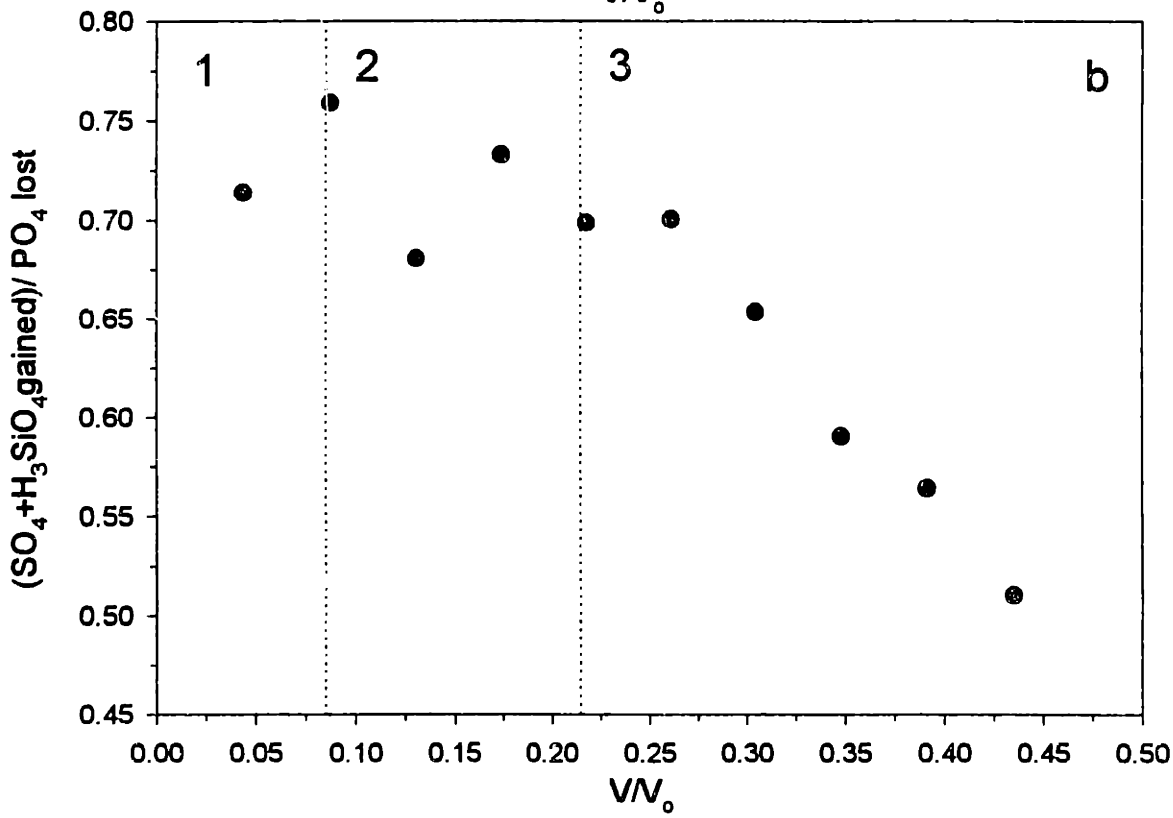
1
2
3
b
(SO4+H3SiO4gained)/ PO4 lost
V/Vo

approximately 70% of the phosphate lost. Although error in the measurement of the initial concentrations of the anions in the injectate (about ±5% for phosphate) may preclude exact assessment of the mass balance of ligands lost and gained for this first sample, it appears that the total amount of measured ligands (i.e., sulfate and silicate) gained in the injectate did not correspond to the total amount of ligand lost (i.e., phosphate).

In the second zone, one notes that the silicate gained in each sample attained a constant level (approximately 50 μmoles per 500 mL sample) (**Figure 5.3a**). However, the amount of sulfate gained per sample continued to rise linearly in zone 2 for each successive sample of the injectate withdrawn. The amount of phosphate lost per sample continued to rise linearly as well (slope equal to 1690 μmoles V/V_o^{-1}). When data points representing the sum of the sulfate and silicate gained per sample in zones 1 and 2 were regressed, a slope of 1190 μmoles V/V_o^{-1} was obtained. Note that the value of this slope, which represents the total sulfate and silicate gained per sample with increasing V/V_o, is only approximately 70% of the slope representing phosphate lost per sample with increasing V/V_o. Thus, this mole balance exercise indicates that approximately 30% of the displaced ligands were not being accounted for (i.e., measured) in the exchange processes that occurred in the experiment.

In zone 3, the amount of sulfate gained per sample attained a constant value (approximately 180 μmoles per 500 mL sample) as successive samples of the injectate were withdrawn, and the amount of silicate gained per sample still remained at the level which prevailed in zone 2 (approximately 50 μmoles) (**Figure 5.3a**). However, the amount of phosphate lost per sample continued to rise in each sample successively retrieved (i.e., with increasing V/V_o). As the total amounts of both sulfate and silicate gained per sample retrieved in zone 3 did not rise further, the continued increase in the amount of phosphate lost per sample (440 μmoles V/V_o^{-1}) must have been due to displacement processes with other ligands which were not measured in the samples. Note that the slope representing phosphate lost per sample (i.e., with increasing V/V_o) in zone 3 shifted to a value (440 μmoles V/V_o^{-1}) that was approximately 30% of the value of the slope representing the phosphate data in

zones 1 and 2 (1690 μmoles V/V_o^{-1}). This 70% decrease in the value of the slope representing phosphate loss corresponds to the amount of phosphate loss which could be explained by total sulfate and silicate gained in zones 1 and 2. This indicates that a line representing "other" displaced ligands can be drawn in zones 1, 2, and 3 in **Figure 5.3a** with a constant slope equal to approximately 30% of the value of the slope representing phosphate loss per sample in zones 1 an 2 (i.e., 1690 μmoles V/V_o^{-1} multiplied by 0.3 to obtain 507 μmoles V/V_o^{-1}). The sum of this line, which represents ligands other than sulfate and silicate that were displaced by phosphate in each sample, and the line representing total sulfate and silicate gained per sample would correspond to total phosphate lost per sample in all three zones in **Figure 5.3a**.

One can view the data represented in **Figure 5.3a** in a more concise way by plotting the total μmoles sulfate and silicate gained per sample as a fraction of the total μmoles phosphate lost per sample with increasing V/V_o^{-1} (**Figure 5.3b**). With the same three zones represented, one notes that total μmoles sulfate and silicate gained represents approximately 70% of the total μmoles phosphate lost per sample in zones 1 and 2 (**Figure 5.3b**). However, total μmoles sulfate and silicate gained represents a successively lower fraction of total μmoles phosphate lost per sample in zone 3 (**Figure 5.3b**) because the values for μmoles sulfate and silicate gained had both attained near constant levels in the samples represented in zone 3. The fraction of total phosphate lost represented by gains in "other" ligands not measured in this study would have to increase concomitantly as the fraction represented by gains in sulfate and silicate decreased to achieve an overall ligand balance.

Various ligands could be included in this pool of unidentified adsorbates being displaced by phosphate. The most obvious ligand would be the OH^- anion. At pH 5.2, neutral surface sites occupied by bound OH^- groups would be expected to be present on iron oxyhydroxide surfaces. Note though, that if OH^- was responsible for 30% of the displaced sites, considerable elevation in pH of the samples would have occurred. For example, in the tenth sample in **Figure 5.3a** (V/V_o =0.435), 30% of the phosphate lost (417 μmoles) would

equal 125 μmoles. A gain of this amount of OH^- in the aqueous phase would have raised the pH of the 500 mL sample to above a value of 10. The pH of this sample was only 5.36. Certainly, hydroxyl groups were displaced by phosphate, but buffering by the aqueous phase and the surface reactions make quantification of the exact quantity of hydroxyl ions displaced impossible.

Other possible candidates would be various humic substances, as approximately 90 μM dissolved organic carbon was present in the groundwater (**Table 5.1**). In addition, carbonate species may also occupy surface sites on the Georgetown sediment. Carbonate levels produced by atmospheric contamination have been identified as a culprit in confounding the measurement of the pristine point of zero charge (pH_{pzc}) in goethite (Evans et al., 1979; Zeltner and Anderson, 1988). As the concentration of $H_2CO_3^*$ in the groundwater is elevated by a factor of 27 above that which would exist for water in equilibrium with the atmosphere, one might expect carbonate species to be bound on surface sites on the aquifer solids. Carbonate has been found to strongly adsorb on goethite surfaces (Russell et al., 1975), for example.

The plateaus observed, first in μmoles silicate gained, and then in sulfate gained, suggest that the initial injected amount of phosphate (500±24 μmoles in each 500 mL sample, or 1 mM) in each 500 mL parcel of water eventually attained some type of equilibrium with the sulfate and silicate occupied sites. The incremental rise and plateau in sulfate and silicate gained per sample indicates that eventually, a point was reached where phosphate could no longer displace silicate and sulfate because the aqueous phase concentration of phosphate was being lowered by adsorption. Concomitant with the lowering of the aqueous phase phosphate concentration, the aqueous phase concentrations of sulfate and silicate were driven up by their by displacement from the solids' surfaces by phosphate. Such a combination of effects would hinder the ability of the remaining phosphate in the aqueous phase to compete for further sulfate and silicate sites.

From the trend in the data in **Figure 5.3a**, it appears that some kinetic constraint or

site limitation kept each 500 mL parcel from attaining equilibrium immediately with the sediment surfaces when it was injected. Otherwise, the first 500 mL sample retrieved would have gained the same amounts of silicate, sulfate, and unidentified ligands, and lost the same amount of phosphate as the tenth 500 mL sample retrieved (i.e., the sample represented by data points at V/V_o approximately equal to 0.44 in **Figure 5.3a**).

One can view the displacement reactions that occurred during the injection-withdrawal experiment in two ways. One could view all displacement reactions as having occurred immediately upon contact with the aquifer solids around the well screen, with no kinetic constraints acting. In this way, site limitation would be the cause of the change in amount of phosphate lost per sample with increasing V/V_o that is observed in the data. Note that increasing values of V/V_o represent contact with an increasing amount of aquifer solids, i.e., the 500 mL sample withdrawn at V/V_o=0.5 contacted more solids than the 500 mL sample withdrawn at V/V=0.2. In other words, a particular parcel of water would have to advance further into the aquifer (i.e., V/V_o increases) to lose enough phosphate to surface sites to reach the point where the aqueous phase concentration of phosphate could no longer compete with any ligands for sites (the point where plateau values are reached). This view would suggest that site limitation of the surface sites ascribed to the unidentified ligands was manifest in phosphate loss for all of the samples represented in **Figure 5.3a**. That a plateau was observed in the data for sulfate (**Figure 5.3a**) would indicate that surface sites ascribed initially to sulfate only became limiting after a larger volume of injectate had passed through the affected zone in this view.

In the second view, the number of surface sites for phosphate to exchange with near the well screen would not be limiting, but a time constraint induced by flow velocity would inhibit reaching equilibrium with these sites immediately upon contact with the aquifer. Hence, an injected parcel of water would advance into the aquifer still containing a high enough concentration of phosphate in the aqueous phase to drive exchange with surface sites. Viewing the data in this way would suggest that the unidentified ligand exchange sites were

relatively the weakest, and that the aqueous phase concentration of phosphate in the samples represented in **Figure 5.3a** maintained a high enough level to drive displacement of these more weakly-held ligands.

A rough estimate of the number of sites available for adsorption in a representative mass of aquifer solids adjacent to the well screen would indicate if site limitation could impose the trend seen in the data in **Figure 5.3a**. The number of sites available in the first 3000 g of sediment around the well screen (this is the amount of sediment contacted by a 500 mL pore volume, which is the sample size obtained in the experiments, using a solid-to-water ratio of 6 g mL^{-1}) if considering only the goethite present in the sediment would be approximately 7 mmoles. This calculation was performed using 1190 μmoles Fe g^{-1} <63 μm size fraction (i.e., the amount of crystalline Fe in the <63 μm size fraction, Swartz et al., 1997), 0.12 g <63 μm size fraction g^{-1} bulk sediment, and 0.016 moles of sites $mole^{-1}$ Fe incorporated in goethite (Ali and Dzombak, 1996). If kaolinite were considered also, the total sites available for exchange would rise to approximately 15 mmoles. The number of sites available on kaolinite was estimated using 0.45 g kaolinite g^{-1} < 2 μm size fraction, 0.025 g < 2 μm size fraction g^{-1} bulk sediment, a surface area of 12 m^2 g^{-1} for kaolinite, and an anion exchange capacity of 2 x 10^{-5} moles m^{-2}, Schwarzenbach et al., 1993). The contribution of surface sites by the amorphous iron oxyhydroxide phase would only add approximately 1 mmole to the total. This estimate was obtained using 0.005 g amorphous Fe g^{-1} <63 μm size fraction, 0.12 g <63 μm size fraction g^{-1} bulk sediment, a surface area of 600 m^2 g^{-1} for amorphous iron oxyhydroxide, and an anion exchange capacity of 5 x 10^{-8} moles m^{-2}, Schwarzenbach et al., 1993). The amount of phosphate which was not retrieved in the HP9-B injection was approximately 7.9 mmoles. Thus, the total number of exchange sites present in a representative mass of aquifer solids around the well screen appears to be twice the amount of phosphate lost during the entire injection and withdrawal sequence.

However, all of these sites may not have been immediately accessible under the flow conditions operating during the injection-withdrawal cycle. Perhaps the linear flow velocity

induced by the 100 mL min^{-1} pumping rate, which was approximately 1.4 m day^{-1}, calculated using a porosity of 0.3 and the surface area of the screened interval, did not allow each 500 mL parcel of injectate to equilibrate with only the first block of aquifer solids contacted (approximately 3000 g for a 500 mL pore volume using a solid to water ratio of 6 g mL^{-1}). The presence of immobile pore water and kinetic limitations to sorption have been observed in this sediment (Holmén and Gschwend, 1997). Thus, kinetic constraints may have imparted a site limitation effect on trend in the observed data in **Figure 5.3a**.

Anion Behavior in Response to Ascorbate Injection. The anion behavior observed in samples retrieved from experiments conducted with 1 mM phosphate-amended groundwater also was manifest when 1 mM ascorbic acid-amended groundwater (experiment HP8-B, Chapter 4) and groundwater amended with 0.5 mM phosphate and 0.5 mM ascorbic acid (experiment HP4-C, Chapter 4). Both sulfate and silica grew into the samples as both of these injectates were retrieved from the aquifer (**Figure 5.4a**). Note that the normalized concentrations of sulfate and silicate did not increase as dramatically in the 1 mM ascorbic acid experiment (**Figure 5.4a**) as they did when 1 mM phosphate amended groundwater was injected (**Figure 5.1a**). The levels of sulfate and silicate attained when a mixture of 0.5 mM phosphate and 0.5 mM ascorbic acid (HP4-C) was injected (**Figure 5.4b**) were intermediate between those attained when either 1 mM phosphate or 1 mM ascorbic acid was injected.

The relative amounts of sulfate and silicate gained (in μmoles) with respect to V/V_o for each of these injection-withdrawal experiments is summarized in **Figure 5.5**. It appears that 1 mM levels of ascorbic acid were approximately half as efficient as similar levels of phosphate in displacing sulfate and silicate from surface sites on the sediment, based on comparison of the plateau levels of these anions gained during the 1 mM ascorbic acid and 1 mM phosphate injections (**Figure 5.5**). Apparently, phosphate was able to compete more effectively with sulfate and silicate for surface sites than was ascorbic acid due to its stronger affinity for the surface sites. Note that the amounts of sulfate and silicate gained upon injection of the 0.5 mM phosphate and 0.5 mM ascorbic acid mixture were approximately

Figure 5.4 appears on the next page

Figure 5.4: Normalized concentrations of bromide and phosphate (left y axis) and sulfate, silicate, and OH^- (right y axis) as a function of V/V_o for experiments (a) HP8-B, in which 1 mM ascorbic acid amended groundwater was injected, and (b) HP4-C, in which a mixture of 0.5 mM phosphate and 0.5 mM ascorbic acid amended groundwater was injected.

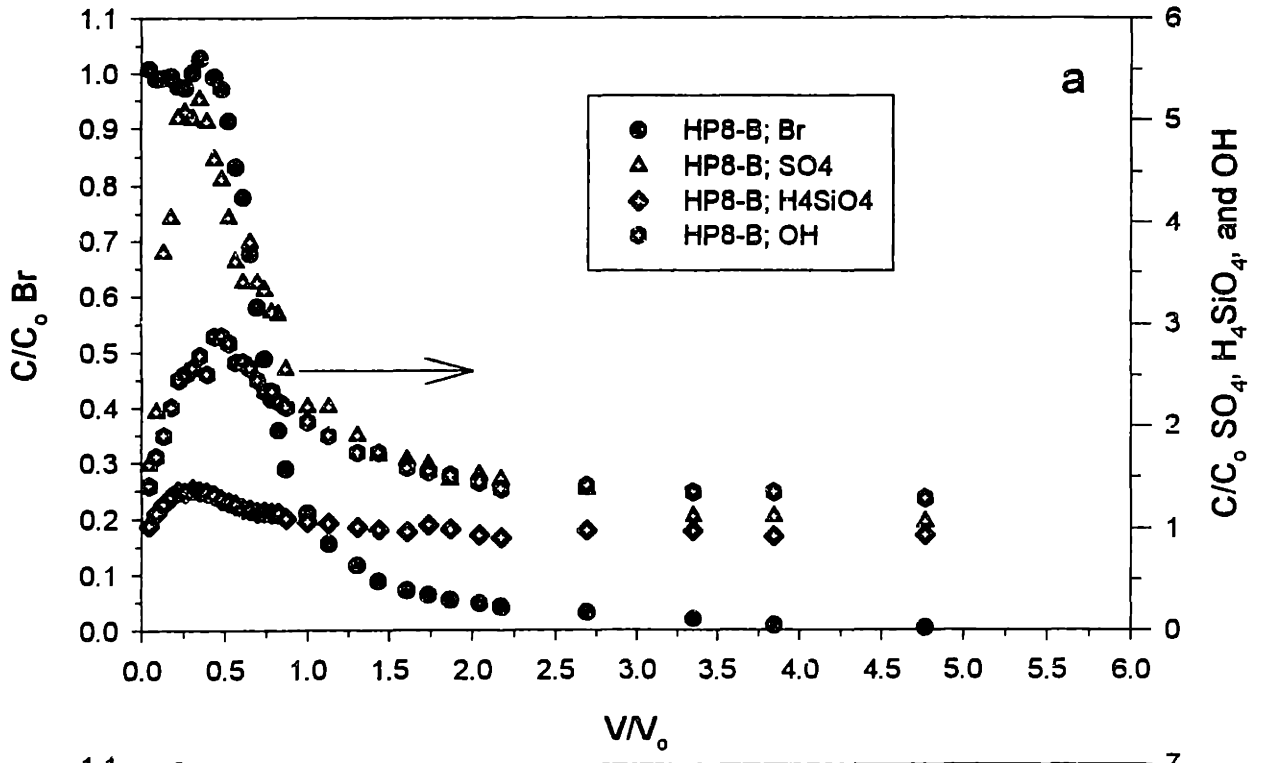
a
HP8-B; Br
HP8-B; SO4
HP8-B; H4SiO4
HP8-B; OH
C/C$_o$ Br
C/C$_o$ SO$_4$, H$_4$SiO$_4$, and OH
V/V$_o$

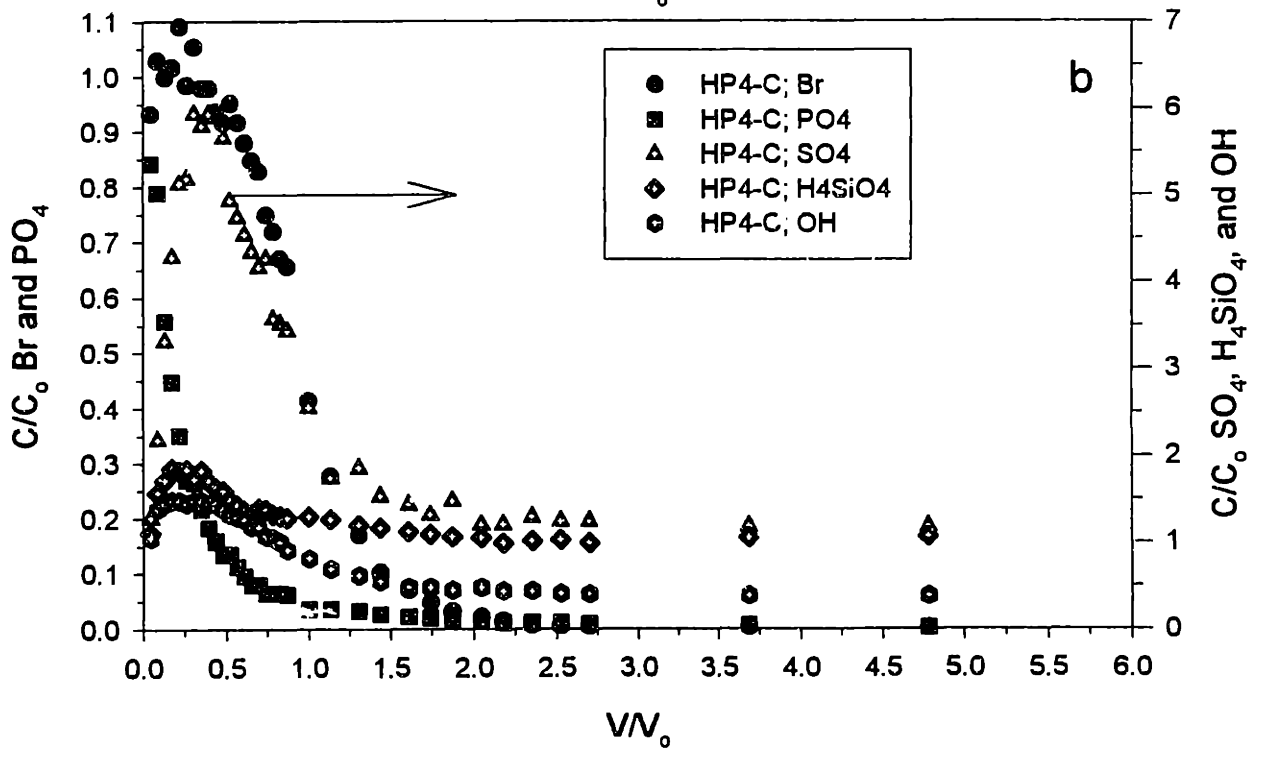
b
HP4-C; Br
HP4-C; PO4
HP4-C; SO4
HP4-C; H4SiO4
HP4-C; OH
C/C$_o$ Br and PO$_4$
C/C$_o$ SO$_4$, H$_4$SiO$_4$, and OH
V/V$_o$

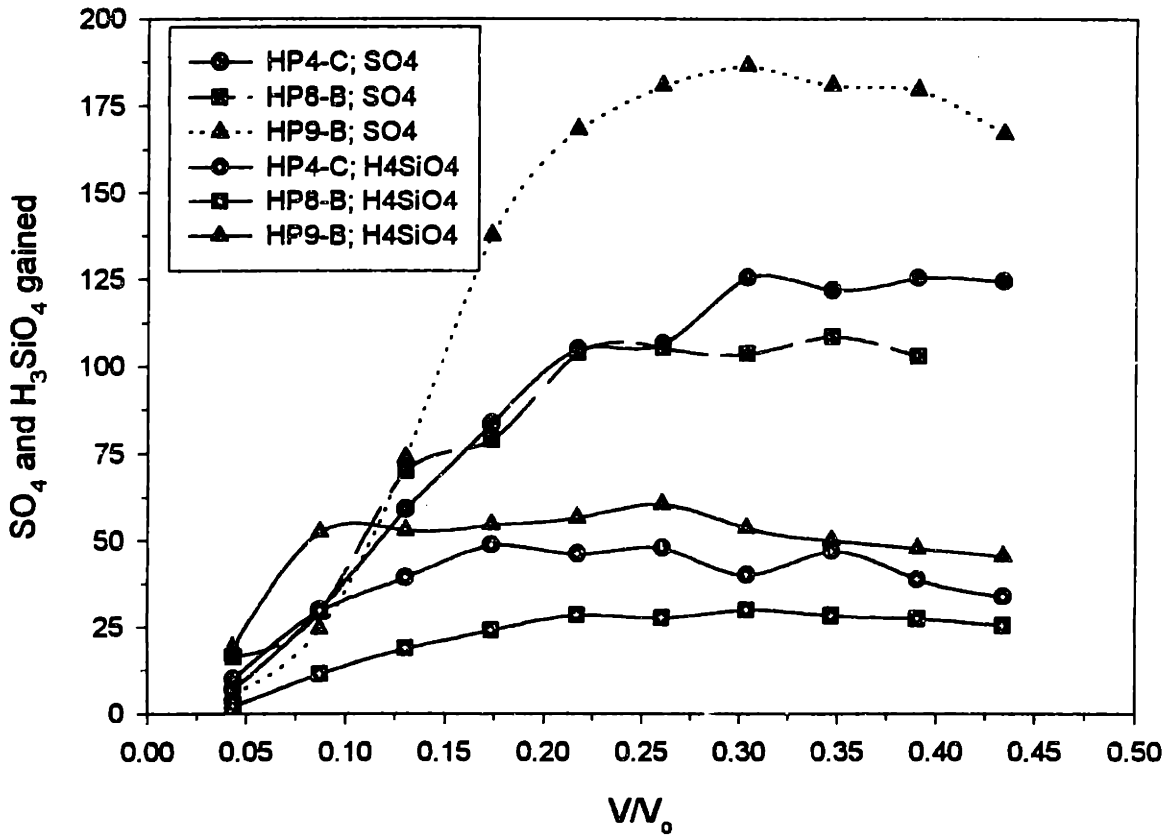

Figure 5.5: Summary plot of amounts of sulfate and silicate gained (in μmoles) in each 500 mL sample retrieved from experiments HP4-C (0.5 mM phosphate and 0.5 mM ascorbic acid amended groundwater injection), HP8-B (1 mM ascorbic acid amended groundwater injection), and HP9-B (1 mM phosphate amended groundwater injection). The plateaus for silicate had average plateau values of 53±5 (HP9-B), 42±6 (HP4-C), and 28±2 (HP8-B). The average plateau values for sulfate were 180±7 (HP9-B), 124±2 (HP4-C), and 105±2 (HP8-B).

75% of the levels attained when 1 mM phosphate was injected (**Figure 5.5**). If only 0.5 mM phosphate had been injected, one would have expected the amounts of sulfate and silicate gained to be 50% of the levels gained when 1 mM phosphate was injected. Because 0.5 mM ascorbic acid was also added to the groundwater along with 0.5 mM phosphate, one would expect the levels of sulfate and silicate gained with this mixture to be greater than 50% of the levels attained with the 1 mM phosphate injection. As the ability of ascorbate to displace sulfate and silicate is only half as strong as the ability of phosphate to displace these ligands, injecting 0.5 mM ascorbic acid only would produce levels of sulfate and silicate that would be half that achieved by injecting 0.5 mM phosphate only (or 25% of the levels achieved by 1 mM phosphate). Thus, one would expect that injecting 0.5 mM phosphate and 0.5 mM ascorbic acid would produce levels of sulfate and silicate approximately 75% of the levels attained with the 1 mM phosphate injection, as indeed appears to have occurred (**Figure 5.5**).

Correspondence of Anion Behavior to their Intrinsic Affinities for Surface Sites. One would expect that the relative plateau levels for silicate and sulfate gained in the retrieved injectates would be in correspondence with the intrinsic affinity constants of these ligands for the surface sites involved in the adsorption process (e.g., sites on goethite, kaolinite, and amorphous iron oxyhydroxides). Studies of competition among sulfate, silicate, and other anions like selenite for surface sites on goethite and amorphous iron oxyhydroxides have repeatedly demonstrated the greater affinity of silicate for these sites as compared to sulfate (Balistrieri and Chao, 1987; Balistrieri and Chao, 1990). Indeed, the relative magnitudes of the intrinsic affinity constants of silicate and sulfate (log K equal to 28.4 and 7.8 for silicate and sulfate, respectively, Dzombak and Morel, 1990) for amorphous iron oxyhydroxide surface sites indicate that silicate binds more strongly than sulfate to iron oxyhydroxides. The intrinsic affinity constant for sulfate was derived from potentiometric titration data and the intrinsic affinity constant for silicate was estimated using a linear free energy relationship between measured intrinsic affinity constants and the corresponding equilibrium constants for analogous solution complexes (Dzombak and Morel, 1990).

The relative plateau levels of silicate and sulfate gained thus appear to correspond with the relative affinities of these two ligands for surface sites, as the weaker ligand (sulfate) was displaced to a greater extent by phosphate and ascorbic acid (**Figure 5.5**). Although phosphate is considered to be a strongly binding anion (Dzombak and Morel, 1990; Mesuere and Fish, 1992b), its intrinsic affinity constant for amorphous iron oxyhydroxide (log K equal to 31.3) is only slightly larger than that of silicate (log K equal to 28.4). However, the difference between the intrinsic affinity constants of phosphate (log K_1 equal to 10.43) and silicate (log K_1 equal to 3.82) for goethite was found to be much larger based on adsorption envelope studies (Goldberg, 1985). The elevated levels of silicate measured in retrieved samples of the 1 mM phosphate injectate (HP9-B) indicated that phosphate was able to displace silicate in the Georgetown aquifer. Others have observed displacement of adsorbed silicate on goethite by even 30 μM phosphate solutions (Torrent et al., 1992).

It was hypothesized that carbonate species accounted for at least some of the unidentified, displaced ligands in mass balance conducted for the data of HP9-B (**Figure 5.3**). No studies of carbonate species displacement by phosphate on goethite could be found in the literature. However, intrinsic affinity constants derived for use in triple layer modeling of carbonate and sulfate species to amorphous iron oxyhydroxide indicated that sulfate (log K equal to 11.6) had a somewhat larger affinity for iron oxyhydroxide surfaces than the $H_2CO_3^*$ (log K equal to 3.32) and HCO_3^{1-} species (log K equal to 10.37) (Zachara et al., 1987). Thus, it appears that phosphate would have a much stronger affinity for surface sites on the aquifer solids than would carbonate species, and displacement of carbonate species would be expected.

5.3.4 Evidence for Competitive Inhibition of SDS Adsorption

When groundwater amended with 2 mM SDS was injected into the aquifer and retrieved, some retardation of the SDS profile with respect to that of the bromide tracer was observed (HP6-B, **Figure 5.6a**). Retardation of the SDS was indicated by the slightly earlier drop off from C/C_o values equal to 1.0 and the greater tailing of the SDS profile at a given

Figure 5.6 appears on the next page

Figure 5.6: Normalized concentrations of bromide and SDS (left y axis) and sulfate and silicate (right y axis) as a function of V/V_o for experiments (a) HP6-B, in which 2 mM SDS amended groundwater was injected, and (b) HP6-A, the control experiment.

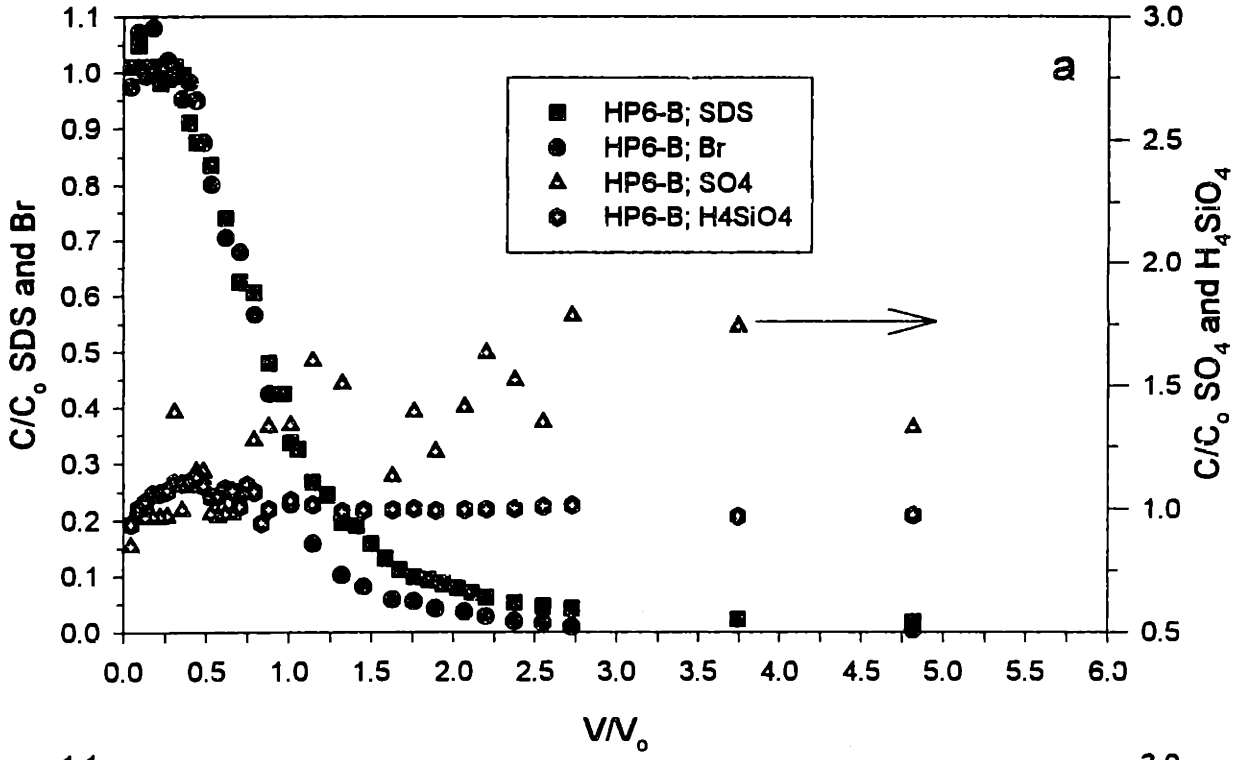
a
HP6-B; SDS
HP6-B; Br
HP6-B; SO4
HP6-B; H4SiO4
C/C$_o$ SDS and Br
C/C$_o$ SO$_4$ and H$_4$SiO$_4$
V/V$_o$

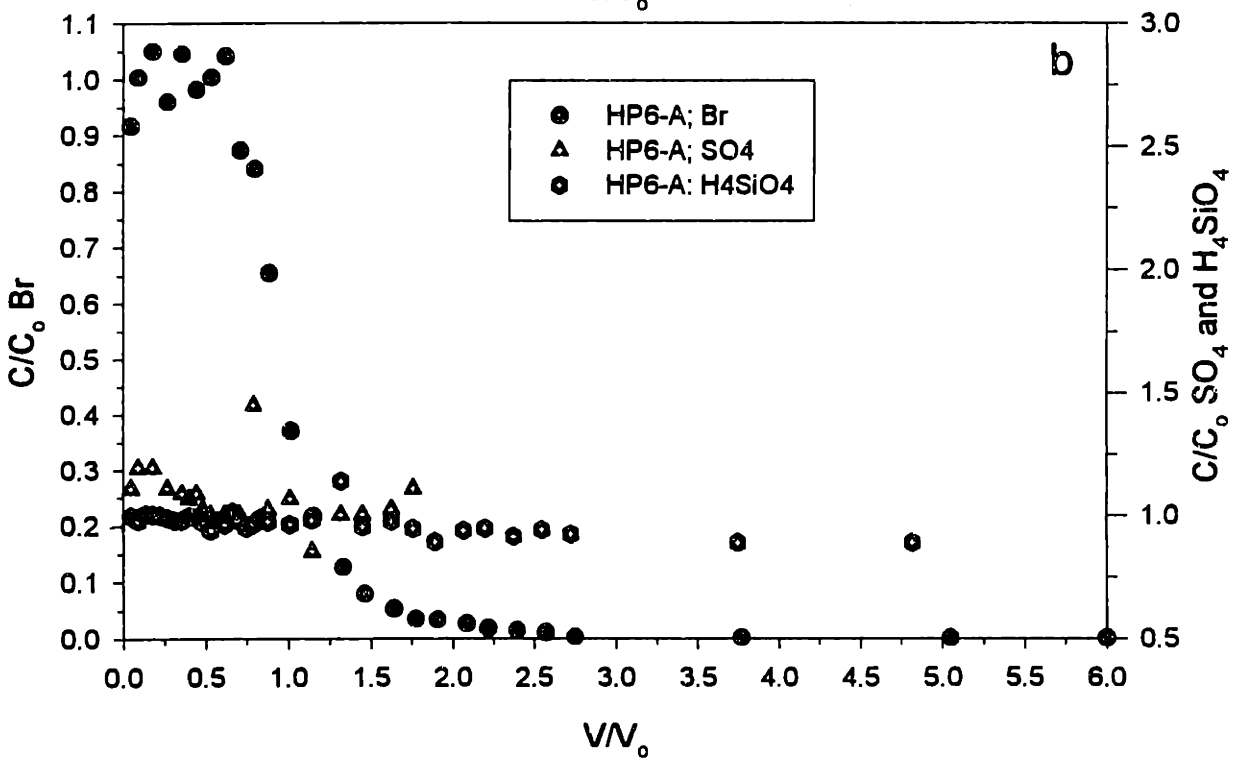
b
HP6-A; Br
HP6-A; SO4
HP6-A: H4SiO4
C/C$_o$ Br
C/C$_o$ SO$_4$ and H$_4$SiO$_4$
V/V$_o$

value of V/V_o, both with respect to the Br^- profile. However, mass balance calculations indicated that most of the injected SDS was retrieved (90%), in contrast to the retrieval of only 26% of the phosphate injected in HP9-B.

Note that no significant increase in the concentration of either sulfate or silicate was observed in retrieved samples of the injectate not affected by dispersive mixing with the ambient groundwater (V/V_o values less than approximately 0.5 in **Figure 5.6a**). Similar results were observed in the control experiment in which only Br^- amended groundwater was injected (HP6-A, **Figure 5.6b**). These results indicated that significant amounts of adsorbed sulfate and silicate were not displaced by the SDS anion. As no losses of SDS to the aquifer solids were observed for the retrieved samples unaffected by dispersive mixing (i.e., values of C/C_o for SDS equaled 1.0 in these samples), one would not expect displaced sulfate and silicate to appear in the samples (i.e., C/C_o values for sulfate and silicate should remain equal to 1.0). This behavior was similar to that exhibited by packed-columns containing the sediment, in which dissolved silicate levels in the effluent during flushing with even 10 mM SDS were not significantly different from levels in deionized water flushes (see Chapter 3). Sulfate was not measured in the packed-column systems.

Sulfate concentrations slightly elevated with respect to the injectate concentration (C/C_o values from 1.75 to 1.0) did appear in some retrieved samples of the 2 mM injectate (**Figure 5.6a**). The elevated sulfate levels occurred in samples which had been affected by dispersive mixing (i.e., beyond $V/V_o = 0.5$ in **Figure 5.6a**). However, no trend in the greatly scattered data was evident. These elevated levels of sulfate may reflect partial *in situ* biodegradation of the SDS molecule. Because the SDS molecule is actually a twelve carbon chain attached to a sulfate head group, biodegradation could have altered a portion of the SDS molecules to the point where they eluted chromatographically with SO_4^{2-} in the anion analysis. Such interference would create the appearance of elevated SO_4^{2-} in the samples. Note that SO_4^{2-} peaks chromatographically eluted from standard solutions containing SDS and prepared in deionized water were indistinguishable from peaks obtained for standards which contained

no SDS. Thus, the *pristine* SDS molecule did not appear to interfere with the chromatographic analysis for SO_4^{2-}. One would expect that greater residence times in the aquifer would result in greater concentrations of the biodegraded SDS molecule and larger artifactual increases in "sulfate" in the retrieved samples, as is exhibited in the data (**Figure 5.6a**). "Sulfate" would then decrease, as dispersive mixing lowered the concentration of SDS to levels where biodegradation would create minimal artifactual "sulfate" to confound the measurement of "real" SO_4^{2-} in the samples. "Sulfate" did begin to decrease toward initial injectate levels at larger discharge volumes (V/V_o equal to approximately 4.75, **Figure 5.6a**).

5.4 Relevance of Competitive Adsorption Effects to Colloid Mobilization

As mentioned previously, specifically adsorbing anionic adsorbates can only alter the surface charge and potential of the adsorbents if they can compete effectively for ligand exchange sites on surfaces. In aquifer systems, ligand exchange sites may be already filled with ambient adsorbates present in the groundwater. Adsorbates introduced into a system, perhaps as contaminants, must displace ambiently adsorbed ligands from these surface sites. Ligand exchange sites on the surfaces of the matrix constituents in the Georgetown aquifer appeared to be filled with a combination of sulfate, silicate, and carbonate species (in addition to the neutral OH ligand exchange groups), all of which have varying intrinsic affinities for these sites. These species, although specifically adsorbed, do not appear to be able to reverse the surface charge of goethite at the ambient groundwater pH (5.26) and their aqueous phase concentrations.

For example, Hansmann and Anderson, (1985), analyzed the electrophoretic mobility of goethite colloids suspended in solutions containing various concentrations of sulfate. They found that the goethite mobility remained virtually unchanged and positively charged (mobility equaled approximately 2.5 $\mu m\ cm\ V^{-1}\ sec^{-1}$) for sulfate concentrations of 5 μM to 20 μM at a solid to water ratio of 30 $mg\ L^{-1}$. As the sulfate concentration in the Georgetown groundwater is approximately 50 μM and the *in situ* solid-to-water ratio (with respect to goethite) is approximately 114 $mg\ L^{-1}$, one would not expect the sulfate present in the system

to impart negative charge to goethite and induce its repulsion from neighboring negatively charged kaolinite faces. The solid-to-water ratio cited above was calculated using a porosity of 0.30, a solids density (ρ_s) of 4.1, and a percent goethite by weight in the bulk sediment of 1.2 % (Swartz et al., 1997). On the other hand, a solution containing 5 μM phosphate reversed the mobility of goethite at pH 5.0 at the same solid to water ratio used for the sulfate analysis (Hansmann and Anderson, 1985), thus demonstrating the ability of adsorbed phosphate to impart greater negative charge to the goethite surface.

No electrophoretic mobility data could be found for carbonate-goethite systems at the elevated level of $H_2CO_3^*$ (320 μM) that occurs in the groundwater. Potentiometric titration studies of goethite in water containing atmospherically controlled levels of $H_2CO_3^*$ have shown that carbonate adsorption can shift the pH_{pzc} from values of 9.0-9.3 (systems purged in N_2) to 8.1-8.75 (Evans et al., 1979; Zeltner and Anderson, 1988). However, at the pH of the Georgetown groundwater (5.26) carbonate ($H_2CO_3^*$ and HCO_3^-) adsorption on goethite would be expected to produce neutral species based on triple layer modeling of adsorption edge data (Zachara et al., 1987), suggesting that adsorption of carbonate species on goethite would not impart significant negative charge to the goethite in the Georgetown sediment given the ambient pH.

No published electrophoretic mobility data for silicate-goethite systems could be found either. However, an analysis of alkalimetric titration data for goethite in a 0.8 mM silicate solution indicated that the pH_{pzc} of goethite was shifted downward from a value of 7.0 (in the absence of silicate) to 6.5 in the silicate solution (Hohl et al., 1980). In comparison, a 0.5 mM phosphate solution shifted the pH_{pzc} of goethite to approximately 5.2 in a system containing the same solid-to-water ratio as the silicate system (Hohl et al., 1980). This would indicate that 1 mM phosphate would be adequate to reverse the surface charge of goethite in the Georgetown sediment *if the phosphate molecule did not have to compete with other strongly adsorbing anions which produced weaker shifts in the pH_{pzc} of goethite.*

Given the comparatively higher intrinsic affinity constant of phosphate for surface sites

on goethite, one would expect that injection of 1 mM phosphate amended groundwater (HP9-B) into the Georgetown aquifer would result in displacement of the more weakly adsorbed sulfate, carbonate and silicate species. Obviously, these ambient adsorbates do not impart sufficient negative charge to the goethite present in the matrix, as ionic strength perturbations do not induce mobilization of colloids in this sediment (see Chapter 3). Such perturbations, by expanding and contracting the electric double layers of matrix constituents, would exacerbate any repulsive interactions being felt between negatively charged goethite and neighboring kaolinite faces. The inherent electrostatic stability of these goethite aggregates supports the existing electrophoretic mobility and titration data that indicate that adsorbed sulfate, bicarbonate and silicate do not impart sufficient negative charge to goethite at pH 5.2 to produce repulsive interactions among the goethite and kaolinite faces, although it is possible that these ligands may decrease the positive charge on the goethite.

One would also expect, then, that displacement of the more weakly bound adsorbates by phosphate would perhaps result in generation of negatively charged goethite surfaces that had not existed previously in the matrix. Indeed, the presence of somewhat elevated turbidity (in comparison to control levels) in retrieved samples of this injectate indicated that specific adsorption of the phosphate had altered matrix electrostatic interactions sufficiently to induce some mobilization of colloids (Chapter 4). Furthermore, the Al/Fe mole ratio (0.8±0.2) of the colloids suggested that the matrix constituents most able to respond to such an electrostatic perturbation, the goethite aggregates, had been mobilized predominantly by the phosphate treatment. It should be noted here that perhaps the response of the goethite aggregates to 1 mM phosphate was diminished from what it would be if no previously adsorbed sulfate or silicate were present. Competitive adsorption effects may have inhibited the ability of phosphate to impart the magnitude of negative charge that would be expected for model systems in equilibrium with 1 mM phosphate like those studied by Hohl et al. (1982).

Injection of groundwater amended with 2 mM SDS did not result in elevation of

ambient anion concentrations (**Figure 5.6a**). If one believes that SDS adsorbs on variably charged surfaces by counterion binding only, with no specific chemical coordination reaction with the surface functional groups involved, one would not expect to see elevation of ambient anion concentrations in the retrieved injectate. With a counterion binding model for SDS adsorption, the negatively charged head group of the SDS molecule would merely coordinate with positively charged functional groups on matrix surfaces (Schwarzenbach et al., 1993). When sufficient "head on" adsorption occurred, the carbon chains of the SDS molecules would then begin to associate in aggregates which would allow "head out" sorption, or admicelle formation, of the SDS molecules to occur (Lee and Koopal, 1996). Admicelle formation would cause surface charge reversal of the adsorbent (e.g., goethite), producing repulsive interactions between goethite and neighboring kaolinite faces in the Georgetown sediment. However, if positive charge on the goethite was diminished by ambiently adsorbed ligands like sulfate and silicate, counterion binding of the SDS molecule would be inhibited. The SDS molecule would then not have been able to generate repulsive interactions between goethite and kaolinite in the sediment and mobilize the goethite as phosphate was clearly able to do.

SDS and alkyl benzene sulfonates have been shown to adsorb above the pH_{pzc} of adsorbents like rutile and aluminum oxide, suggesting that specific adsorption of these ligands can occur (Böhmer and Koopal, 1992; Bitting and Harwell, 1987). If one believes that specific coordination reactions between the SDS molecule and adsorbent surface functional groups can occur, then the absence of elevation of ambiently adsorbed ligands during the 2 mM SDS injection (HP6-B, **Figure 5.6**) suggests that the SDS molecule could not displace these ligands from surface sites. Failure to displace these ligands would result in an inability to form admicelles on goethite surfaces in the Georgetown sediment and concomitantly, an inability to generate repulsive interactions among the goethite and neighboring kaolinite.

That turbidity in the retrieved injected during the 2 mM SDS injection experiment (HP6-B) was not significantly different from control levels (see **Figure 4.4**, Chapter 4)

indicates that SDS was not able to generate repulsive interactions among matrix constituents in the Georgetown aquifer, while phosphate appears to have been able to generate repulsive interactions. Whether one invokes specific adsorption or counterion binding models for adsorption of SDS to the matrix constituents, it appears clear that ambiently adsorbed ligands prevented SDS from imparting sufficient negative charge to the goethite to induce its mobilization from the matrix. Although SDS could impart greater negative charge to model goethite colloids than even 10 mM phosphate (see **Figure 3.4**, Chapter 3), SDS was hindered from doing so in a natural deposit (the Georgetown aquifer) because of the effect of competitive adsorption.

5.4 Conclusions

In situ competitive adsorption behavior observed in the Georgetown aquifer helps to explain why injection of phosphate amended groundwater resulted in mobilization of Fe-rich colloids (assumed to be predominantly goethite), while injection of an anionic surfactant (SDS) did not. While electrophoretic mobility studies using model goethite colloids indicated that 2 mM SDS would impart greater negative charge to the goethite than even 10 mM phosphate (Chapter 3), it appeared that only the injection of 1 mM phosphate into the aquifer was able to generate sufficient electrostatic repulsion among neighboring matrix constituents to mobilize the goethite aggregates.

Increases in the dissolved concentrations of sulfate and silicate, with respect to initial concentrations, upon retrieval of the 1 mM phosphate amended injectate suggested that phosphate effectively competed for surface sites on matrix constituents. The relative increases in the concentrations of these constituents were in order with the relative affinities of sulfate and silicate species for goethite surface sites, i.e., the increase observed for the dissolved concentration of the relatively weak adsorbate sulfate was greater than the increase observed for the more strongly bound silicate species. No such elevations in sulfate and silicate were observed upon retrieval of the 2 mM SDS amended injectate, indicating that SDS could not

displace these adsorbates from matrix surfaces.

Given that ambiently adsorbed sulfate and silicate were apparently ineffectual in generating sufficient repulsive interactions between goethite and neighboring constituents in the Georgetown sediment (e.g., kaolinite faces), these results demonstrate the importance of knowing what ambiently adsorbed species are present on surfaces in natural systems if one is to predict the effect of introduction of surface potential altering adsorbates into the system. Predictions of surface charge alterations made using electrophoretic mobility data generated with model systems may not apply for natural systems if competitive adsorption effects inhibit the adsorbate for specifically adsorbing. Knowledge of the ambiently adsorbed species, their intrinsic affinities for the surface, and their abilities to alter the surface charge properties of the solid surface are all important in predicting the effect of addition of a competing adsorbate in the natural system.

5.5 References

Ali M. and Dzombak D. A. (1996) Competitive sorption of simple organic acids and sulfate on goethite. *Environ. Sci. Technol.* **30**, 1061-1071.

Anderson M. A. and Malotky D. T. (1979) The adsorption of protolyzable anions on hydrous oxides at the isoelectric pH. *J. Colloid Int. Sci.* **72**, 413-427.

Balistrieri L. S. and Chao T. T. (1987) Selenium adsorption by goethite. *Soil Sci. Soc. Am. J.* **51**, 1145-1151.

Balistrieri L. S. and Chao T. T. (1990) Adsorption of selenium by amorphous iron oxyhydroxide and manganese dioxide. *Geochim. Cosmochim. Acta* **54**, 739-751.

Balistrieri L. S. and Murray J. W. (1987) The influence of the major ions of seawater on the adsorption of simple organic acids by goethite. *Geochim. Cosmochim. Acta* **51**, 1151-1160.

Bitting D. and Harwell J. H. (1987) Effects of counterions on surfactant surface aggregates at the alumina/aqueous solution interface. *Langmuir* **3**, 500-511.

Böhmer M. R. and Koopal L. K. (1992) Adsorption of ionic surfactants on variable-charge surfaces. 1. Charge effects and structure of the adsorbed layer. *Langmuir* **8**, 2649-2659.

CRC Handbook of Chemistry and Physics (1990) CRC Press, Inc.

Davis J. A. and Gloor R. (1981) Adsorption of dissolved organics in lake water by aluminum oxide. Effect of molecular weight. *Environ. Sci. Technol.* **15**, 1223-1229.

Davis J. A. and Leckie J. O. (1980) Surface Ionization and complexation at the oxide/water interface 3. Adsorption of anions. *J. Colloid Int. Sci.* **74**, 32-43.

Djafer M., Khandal R. K., and Terce M. (1991) Interactions between different anions and the goethite surface as seen by different methods. *Coll. Surf.* **54**, 209-218.

Dzombak D. A. and Morel F. M. M. (1990) *Surface Complexation Modeling Hydrous Ferric Oxide*. John Wiley and Sons.

Evans T. D., Leal J. R., and Arnold P. W. (1979) The interfacial electrochemistry of goethite (α-FeOOH) especially the effect of CO_2 contamination. *Journal of Electroanalytical Chemistry* **105**, 161-167.

Faure G. (1991) *Principles and Applications of Inorganic Geochemistry*. MacMillan.

Goldberg S. (1985) Chemical modeling of anion competition on goethite using the constant capacitance model. *Soil Sci. Soc. Am. J.* **49**, 851-856.

Hansmann D. D. and Anderson M. A. (1985) Using electrophoresis in modeling sulfate, selenite, and phosphate adsorption onto goethite. *Environ. Sci. Technol.* **19**, 544-551.

Hawke D., Carpenter P. D., and Hunter K. A. (1989) Competitive adsorption of phosphate on goethite in marine electrolytes. *Environ. Sci. Technol.* **23**, 187-191.

Hingston F. J., Posner A. M., and Quirk J. P. (1971) Competitive adsorption of negatively charged ligands on oxide surfaces. *Discussions Faraday Society* **52**, 334-342.

Hingston F. J., Posner A. M., and Quirk J. P. (1972) Anion adsorption by goethite and gibbsite. I. The role of the proton in determining adsorption envelopes. *J. Soil Sci.* **23**, 177-192.

Hohl H., Sigg L., and Stumm W. (1980) Characterization of surface chemical properties of oxides in natural waters. In *Particulates in water: Characterization, fate, effects, and removal* (ed. M. C. Kavanaugh and J. O. Leckie)1-31. American Chemical Society.

Holmén B. A. and Gschwend P. M. (1997) Estimating sorption rates of hydrophobic organic compounds in iron oxide- and aluminosilicate clay-coated aquifer sands. *Environ. Sci. Technol.* **31**, 105-113

Lee E. M. and Koopal L. K. (1996) Adsorption of cationic and anionic surfactants on metal oxide surfaces: surface charge adjustment and competition effects. *J. Colloid Int. Sci.* **177**, 478-489.

Liang L. and Morgan J. J. (1990a) Chemical aspects of iron oxide coagulation in water: Laboratory studies and implications for natural systems. *Aquatic Sci.* **52**, 32-55.

Liang L. and Morgan J. J. (1990b) Coagulation of iron oxide particles in the presence of organic materials. *American Chemical Society Symposium Series* **No. 146**, 293-308.

Mesuere K. and Fish W. (1992a) Chromate and oxalate adsorption on goethite. 1. Calibration of surface complexation models. *Environ. Sci. Technol.* **26**, 2357-2364.

Mesuere K. and Fish W. (1992b) Chromate and oxalte adsorption on goethite. 2. Surface complexation modeling of competitive adsorption. *Environ. Sci. Technol.* **26**, 2365-2370.

Morel F. M. M. and Hering J. G. (1993) *Principles and Applications of Aquatic Chemistry.* John Wiley and Sons, Inc.

Pyman M. A., Bowden J. W., and Posner A. M. (1979) The movement of titration curves in the presence of specific adsorption. *Aust. J. Soil Res.* **17**, 191-195.

Russell J. D., Paterson E., Faser A. R., and Farmer V. C. (1975) Adsorption of carbon dioxide on Goethite (α-FeOOH) surfaces, and its implication for anion adsorption. *J. Chem. Soc. Faraday Trans.* **71**, 1623-1630.

Ryan J. N. and Gschwend P. M. (1994) Effect of solution chemistry on clay colloid release from an iron oxide-coated aquifer sand. *Environ. Sci. Technol.* **28**, 1717-1726.

Schwarzenbach R. P., Gschwend P. M., and Imboden D. M. (1993) *Environmental Organic Chemistry.* John Wiley and Sons, Inc.

Sigg L. and Stumm W. (1980) The interaction of anions and weak acids with the hydrous goethite (α-FeOOH) surface. *Coll. Surf.* **2**, 101-117.

Swartz C. H., Ulery A. L., and Gschwend P. M. (1997) An AEM-TEM study of nanometer-scale mineral associations in an aquifer sand: Implications for colloid mobilization. *Geochim. Cosmochim. Acta* **61**, 707-718.

Standard Methods for the Examination of Water and Wastewater (1992) American Public Health Association, American Water Works Association, Water Environment Federation.

Tejedor-Tejedor M. I. and Anderson M. A. (1990) Protonation of phosphate on the surface of goethite as studied by CIR-FTIR and electrophoretic mobility. *Langmuir* **6**, 602-611.

Tipping E. (1981) Adsorption by goethite (α-FeOOH) of humic substances from three different lakes. *Chem. Geol.* **33**, 81-89.

Tipping E. and Cooke D. (1982) The effects of adsorbed humic substances on the surface charge of goethite (α-FeOOH) in freshwaters. *Geochim. Cosmochim. Acta* **46**, 75-80.

Torrent J., Schwertmann U., and Barron V. (1992) Fast and slow phosphate sorption by goethite-rich natural materials. *Clays Clay Min.* **40**, 14-21.

Williams T. M. and McCarthy J. F. (1991) Field-scale tests of colloid:facilitated transport. *National Research and Development Conference on the Control of Hazardous Materials*, 179-184.

Zachara J. M., Girvin D. C., Schmidt R. L., and Resch C. T. (1987) Chromate adsorption on amorphous iron oxyhydroxide in the presence of major groundwater ions. *Environ. Sci. Technol.* **21**, 589-594.

Zeltner W. A. and Anderson M. A. (1988) Surface charge development at the goethite/aqueous solution interface: Effects of CO_2 adsorption. *Langmuir* **4**, 469-474.

Chapter 6:

Summary and Future Work

6.1 Summary of Results

The primary objective of the research efforts detailed in this thesis was to understand the mechanisms binding clay-size solids in the iron oxyhydroxide- and kaolinite-rich interstitial matrix of a shallow, Southeastern Coastal Plain aquifer located in Georgetown, South Carolina. To that end, we believed that a knowledge of the nanometer-scale structure and the phase associations existing in the interstitial matrix of the sediment would aid us in interpreting studies of the chemical perturbations which induced release of the clay-size fines to pore fluids.

An analytical and transmission electron microscopic (AEM-TEM) investigation of the interstitial matrix of the Georgetown sediment, coupled with results from selective extraction techniques, implicated either, or both, an amorphous iron oxyhydroxide phase or an amorphous, Si-rich phase in binding the iron oxyhydroxide- and kaolinite-rich matrix. The amorphous, Si-rich phase was ubiquitous in AEM-TEM images of the matrix, and appeared to coat kaolinite aggregates released from the sediment as colloids. Selective extraction of this Si-rich phase indicated that it made up approximately 10% by weight of the <63 μm size fraction. It was hypothesized that such a phase might bind the matrix in a cementitious web that would require partial dissolution before mobilization of abundant kaolinite booklets would occur.

The presence of an amorphous iron oxyhydroxide phase was indicated by ammonium oxalate extraction of the <63 μm size fraction. The Fe associated with the amorphous phase was found to be only approximately 5% of the total Fe associated with oxyhydroxides in the <63 μm size fraction, quantified by selective extraction using the Ti (III)-citrate-EDTA method (Ryan and Gschwend, 1991). The other 95% of the Ti (III)-extractable Fe was thought to be incorporated in a crystalline phase, i.e., goethite. Goethite had been identified by analysis of x-ray diffraction patterns of the < 2 μm size fraction and lattice fringe imaging of high resolution TEM images of the matrix. Based on the selective extraction results,

goethite was calculated to constitute approximately 10% by weight of the <63 μm size fraction.

Although goethite represented a much larger portion of the iron oxyhydroxides in the sediment, it was found to be organized in discrete aggregates in the interstitial matrix upon AEM-TEM observation. In contrast, the amorphous iron oxyhydroxide phase was found to be distributed among, and intimately associated with, the abundant kaolinite booklets in the matrix. Differentiation of the amorphous iron oxyhydroxide phase in the AEM-TEM observations was made possible based on its Al/Fe mole ratio, which had been derived from the selective extractions.

Based on the distribution pattern of the amorphous iron oxyhydroxide phase, we thought that this phase must serve as the effective electrostatic or bonding intermediary among the kaolinite booklets. If acting as an electrostatic intermediary among negatively charged kaolinite basal plane surfaces, the amorphous iron oxyhydroxide would probably possess an ambient positive charge. Goethite would not play a role in mitigating any electrostatic repulsion among kaolinite booklet surfaces due to its discrete organization in the matrix.

The possible binding mechanism hypotheses developed from the AEM-TEM analysis were tested in packed-columns containing the Georgetown sediment. The experiments were organized so as to differentiate colloid mobilization induced by electrostatic perturbations from mobilization mechanisms requiring dissolution of cementitious phases or bond-breaking among matrix constituents.

The sediment did not release colloids in response to treatment with sequential high/low ionic strength solution flushes meant to cause the electric double layers of matrix constituents to expand. **Table 6.3** provides a summary of the major results for the column experiments and a comparison to the in situ results for comparable treatments. Lack of colloid release in response to this perturbation indicated that (1) similarly charged constituent surfaces were not juxtaposed in the matrix (e.g., the amorphous iron oxyhydroxide intermediaries among

Table 6.1: Summary and comparison among the laboratory packed-column and *in situ* mobilization experimental results

Perturbation	Treatment	Al/Fe mole ratio of colloids mobilized	
		Lab Column	Field
Expansion of Electric Double Layers	0.1 N $CaCl_2$ or 0.1 N NaCl followed by DI water, pH 5.5	NR[1]	NT[2]
Surface Charge Reversal	10 mM phosphate, pH 5.2 1 mM phosphate, pH 5.2 2 mM SDS, pH 5.3-5.4	0.5±0.3[3] NR NR	NT 0.8±0.2 NR
Reductive Dissolution	1 mM ascorbic acid, pH 5.2-5.3	NR	1.9±0.2
Reductive Dissolution and Surface Charge Reversal	0.5 mM ascorbic acid + 0.5 mM phosphate, pH 5.2 (pH 5.8 for field exp.)	2.3±0.9	2.5±0.6
Hydrolysis and Surface Charge Reversal (elevated pH)	pH 8.8 (pH_{imt}=9.6 for field exp.)	1.5±0.5	1.8±0.7
Proton-promoted Dissolution (acidic pH)	pH 2.6, 1 mM $CaCl_2$ (pH 2.5 , no added $CaCl_2$ for field exp)	NR	NR

[1]NR= no release observed. For the field experiments, this indicates that the turbidity of the amended injectates was indistiguishable from the control experiments

[2]NT= specified treatment was not tested *in situ*

[3]Release event occurred during the deionized water flush following the 10 mM phosphate treatment

kaolinite books were not negatively charged), or (2) the individual phases were not able to respond to these double layer perturbations due to physical binding by a cementitious phase (the amorphous silica) or the presence of bonds among the amorphous iron oxyhydroxides and the kaolinite books which hindered response to enhanced electrostatic repulsive forces.

We also tested the sediment response to ligands which would reverse the surface charge of the amorphous iron oxyhydroxides and enhance electrostatic repulsion among them and kaolinite books. An anionic surfactant, SDS, was unable to chemically induce mobilization of any colloids when flushed through the sediment at 2 mM levels (**Table 6.1**). A deionized water flush following treatment of the sediment with 10 mM phosphate did induce mobilization. However, the colloid phase appeared to comprise predominantly goethite based on analysis of the Al/Fe mole ratio of the released colloids and comparison of this Al/Fe mole ratio to that assumed to best represent the bulk matrix, i.e., the <63 μm size fraction. The discrete nature of the goethite aggregates within the matrix, as observed by AEM-TEM, would suggest that their mobilization could be induced by imparting them with a negative surface charge to enhance repulsive interactions with surrounding kaolinite surfaces. That the kaolinite-amorphous iron oxyhydroxide aggregates were not mobilized as well, even though phosphate adsorption would create repulsive interactions among the kaolinite books and amorphous iron oxyhydroxides surfaces, suggested that the kaolinite-amorphous iron oxyhydroxide associations were not free to respond to the purely electrostatic perturbations imparted by the phosphate treatment.

When the sediment was treated with ascorbic acid or oxalic acid, which dissolved iron oxyhydroxides in the sediment either reductively or through ligand-promoted dissolution mechanisms, colloids representative of the entire bulk matrix were mobilized. Dissolution of the amorphous silica phase was not apparent in the ascorbic acid and oxalic acid treatments, thus implying that this phase did not play a key role in binding the matrix and hindering the release of the kaolinite books. We surmised that the mobilization of the bulk matrix in response to oxalic and ascorbic acid was due to the fact that these ligands broke bonds among

the amorphous iron oxyhydroxides and kaolinite books as a result of dissolution processes, freeing these phases to respond to electrostatic perturbations. In addition, these ligands promoted repulsive interactions among the amorphous iron oxyhydroxides and kaolinite, when the pH of the pore fluids was high enough, due to specific adsorption on the iron oxyhydroxide surfaces. Therefore, it was the combination of these two effects, the breaking of bonds and the imparting of sufficient repulsive interactions among the matrix constituents, which allowed the ascorbic acid and oxalic acid to induce mobilization of the kaolinite-amorphous iron oxyhydroxide aggregates *along with* goethite from the sediment matrix.

Sustained contact with solutions with elevated pH (8.8) also eventually began mobilizing colloids more representative of the bulk matrix than occurred when the sediment was treated with phosphate (**Table 6.1**). Elevated pH was not as effective as ascorbic acid and oxalic acid in this regard, though. Elevated pH would be expected to break of bonds among the amorphous iron oxyhydroxides and kaolinite books through hydrolysis. The elevated pH would also result in surface charge reversal of the iron oxyhydroxides in the sediment, resulting in generation of repulsive interactions among the amorphous iron oxyhydroxides and kaolinite books and among the goethite and kaolinite books. Thus, the resulting mobilization of colloids more representative of the bulk matrix upon subjecting the sediment to elevated pH also supported the hypothesis that (1) the severing of bonds controlling the amorphous iron oxyhydroxide-kaolinite interactions, and (2) the imparting of sufficient repulsive interactions among the matrix constituents were both required to mobilize colloids representative of the entire bulk matrix in the Georgetown sediment.

We felt that it was important to verify these laboratory findings with "ground truth" data. To this end, we utilized a novel, single well injection-withdrawal method to study colloid mobilization in the Georgetown aquifer *in situ*. We subjected the aquifer to groundwater amended with chemically-perturbing solutes similar to those used in the column experiments. We found that the aquifer yielded colloids in response to the chemical perturbations in a similar manner as observed for the sediment in the packed-column studies.

Specifically, amendments to the groundwater which both broke bonds among the amorphous iron oxyhydroxides and kaolinite books through dissolution of the iron oxyhydroxides in the sediment *and* imparted sufficient repulsive interactions among the matrix constituents (e.g., groundwater amendment with 0.5 mM phosphate and 0.5 mM ascorbic acid and groundwater amendment with base, **Table 6.1**) induced mobilization of colloids more representative of the entire bulk matrix.

It is interesting that phosphate did not appear to be able to lyse bonds between the amorphous iron oxyhydroxides and kaolinite, while hydroxyl ions (i.e., the elevated pH experiments) were apparently able to lyse these bonds and mobilize colloids with a Al/Fe mole ratio closer to that of the bulk matrix. Perhaps steric hinderances prohibited phosphate from reaching these bonds. Also, the effect on the surface chemistry, and bonds between the amorphous iron oxyhydroxides and kaolinite, due to addition of OH^- anions to the system would be more quickly and easily propagated to the bonds of interest due to aqueous phase hydrolysis reactions.

As in the column studies, 2 mM SDS amended groundwater did not induce any colloid mobilization in the aquifer. 1 mM phosphate amended groundwater was able to induce somewhat elevated levels of turbidity in comparison to the control experiment. The Al/Fe mole ratio of these colloids indicated that phosphate induced the release of goethite preferentially in this experiment, just as occurred in the column experiments when the sediment was treated with 10 mM phosphate (**Table 6.1**). However, studies of the electrophoretic mobility of model goethite colloids suspended in 2 mM SDS and 10 mM phosphate had indicated that 2 mM SDS would impart greater negative charge to the iron oxyhydroxides in the Georgetown sediment than would 10 mM phosphate. An explanation for the discrepancy between the release behavior observed in the column and field experiments and that which would be predicted based on the mobilities of model goethite colloid systems was facilitated by analyzing the behavior of the major groundwater anions during the injection-withdrawal experiments. Phosphate was found to be capable of

displacing ambiently adsorbed sulfate, silicate, and other unidentified ligands, when injected into the aquifer. No such displacement was observed when 2 mM SDS was injected. Sulfate and silicate have been shown to be relatively ineffective at reversing the surface charge of iron oxyhydroxides at the ambient pH and concentrations of these two anions in the Georgetown aquifer (Hohl et al., 1980; Hansmann and Anderson, 1985). The ability of phosphate to displace these ligands from the surfaces of goethite in the sediment would allow it to impart greater negative charge to the goethite and concomitantly, greater repulsive interactions with neighboring kaolinite surfaces as well. The resulting mobilization of the goethite aggregates in response to treatment with phosphate, and the lack of mobilization in response to treatment with SDS, appears to be explained by this competitive adsorption behavior.

6.2 Implications of Results

Developing an understanding of the mechanisms which control release of colloids to groundwater in the Georgetown aquifer is relevant, as near-surface Coastal plain deposits characterized by iron oxyhydroxide- and kaolinite-coated quartz framework grains are numerously distributed along the Eastern coast of the United States and serve as initial repositories for groundwater recharge. These near-surface deposits are also prime candidates for exposure to contaminants producing geochemical alterations which induce mobilization of aquifer fines as colloids to groundwater. Concomitant colloid-facilitated transport of contaminants like heavy metals and organic chemicals may then occur. Indeed, leachates from seepage basins which received radionuclide and metal waste from the Savannah River nuclear materials processing facility have been implicated in the generation of inorganic colloids and the enhanced transport of metals such as Cr, Ni, Co, Cd, Pb, and U in the Barnwell aquifer, a Southeastern Coastal Plain deposit (Kaplan et al., 1995; Seaman et al., 1995).

In the few studies which have investigated colloid mobilization in natural deposits,

many have focused on the effects of electrostatic perturbations such as fluctuations in ionic strength, the sodium adsorption ratio (SAR) of the sediment, and the adsorption of dissolved organic matter on colloid mobilization (Kaplan et al., 1993; Kaplan et al., 1996; Roy and Dzombak, 1996). Many sediments do yield significant colloids in response to such electrostatic perturbations. For these sediments, it appears that electrostatic interactions acting among the clay-size constituents govern the colloid release behavior which is observed. These electrostatic interactions are thought to comprise van der Waals electrostatic forces, electric double layer forces (which can be attractive or repulsive), and possibly near-surface repulsive forces as well (Israelachvili, 1992). The net effect of these forces is described by the Derjaguin-Landau-Verwey-Overbeek (DLVO) theory of colloid stability (Derjaguin and Landau, 1941; Verwey and Overbeek, 1948). In these systems, the similarity or dissimilarity in surface charge, and corresponding double layer charge, of juxtaposed, *discrete phases* dictates whether repulsive surface interactions will be manifest as colloid release to pore fluids. A few attempts have been made to extend the use of DLVO theory beyond synthetic systems (Cerda, 1987; McDowell-Boyer, 1992; Ryan and Gschwend, 1994b; Roy and Dzombak, 1996) to explain colloid mobilization in natural porous media (Khilar and Fogler, 1984; Kia et al., 1987; Ryan and Gschwend, 1994; Roy and Dzombak, 1996).

However, diagenetic processes acting on natural sediments can create more complex interactions among matrix constituents. In such cases, juxtaposed phases may not be able to respond as discrete units to electrostatic perturbations. For example, cyclical oxidation and reduction of iron and manganese oxyhydroxides can produce oxyhydroxide phases which may be "linked" or cross-bonded to neighboring phases like kaolinite or other clay minerals. Such systems may not respond to electrostatic perturbations as readily as do mixtures of discrete, crystalline phases, making prediction of colloid release that much more difficult.

Golden and Dixon (1985) attempted to mimic such a system when they oxidized Fe^{2+} in the presence of kaolinite. They compared the behavior of these mixtures to those in which goethite and ferric-oxide gels were synthesized beforehand and then mechanically mixed with

kaolinite. They found that the iron oxides formed by the oxidation *remained attached to kaolinite basal plane surfaces even after treatment with silicate to enhance repulsion among the two phases.* In contrast, mechanical mixtures of goethite and ferric oxide gels separated upon treatment with silicate. They hypothesized that the iron oxides oxidized in the presence of kaolinite were perhaps grown under steps or ledges in the kaolinite surfaces, thus "keying" the two phases together, or that the two phases shared Al or Fe octahedra structural groups (Golden and Dixon, 1985).

The colloid mobilization behavior that the Georgetown sediment exhibited in laboratory- and *in situ*-based experiments indicated that such associations exist between the amorphous iron oxyhydroxides and the kaolinite books in this sediment matrix. Such associations appeared to inhibit electrostatic perturbations from inducing mobilization of these kaolinite-amorphous iron oxyhydroxide aggregates. Instead, only predominantly goethite aggregates were mobilized when sufficient electrostatic perturbations (e.g., phosphate) were introduced. Interestingly, this behavior does not appear to be confined to the Georgetown sediment. Recently, others have observed the preferential mobilization of goethite aggregates upon treatment of a Southeastern Coastal Plain sediment to electrostatic perturbations caused by cation exchange processes (Seaman et al., 1997).

The resistance of a large subset of the bulk matrix to mobilization by electrostatic perturbations would have significant implications for the prediction of the effects of contaminant plumes moving through aquifer systems on the aquifer structure itself. For example, a sewage plume composed mainly of a mixture of phosphate and ionic surfactants might only mobilize discrete goethite aggregates and leave the matrix pore structure predominantly unchanged. On the other hand, a plume containing an organic acid which dissolved iron oxyhydroxides, e.g., oxalate, would be expect to cause significant mobilization of the entire bulk matrix in an aquifer like that at Georgetown. Such reorganization of the matrix constituents might change the hydraulic properties of the aquifer significantly. Note that oxalate is a ubiquitous industrial contaminant and is a major cocontaminant with heavy

metal leachates in waste sites like that at the Hanford Nuclear Reservation (Osterhout, 1980). Oxalate is also present naturally in waters, being the product of microbial activity (Thurman, 1985; Djafer et al., 1991). Thus, major mobilization events involving the entire bulk matrix in aquifers like that at Georgetown are not confined to inducement by anthropogenic sources alone.

The potential for preferential mobilization of a subset of the bulk matrix has important ramifications for facilitated transport of contaminants in the subsurface. Heavy metals in particular readily sorb to sesquioxides like iron oxides (Kinniburgh et al., 1976; Dzombak and Morel, 1990; Fuller et al., 1996; Tessier et al., 1996). If such phases were preferential mobilized from aquifer sediments, colloid facilitate transport of these metals would occur, possibly producing a much larger zone of contamination in the aquifer than would exist if the sorbent phase remained stationary. On the other hand, such preferential mobilization could expedite remediation efforts. Perhaps preferential mobilization and recovery of the discrete goethite aggregates, laden with heavy metals, could be performed in a controlled manner, such as with a single well injection-withdrawal system. As only a subfraction of the matrix would be mobilized, one would avoid reductions in hydraulic conductivity caused by clogging of pores that have been observed as a result of significant dispersion of the matrix constituents in sediments and sandstones (Goldenberg and Margaritz, 1983; Lin, 1985).

Finally, the competitive adsorption effects observed during the phosphate and SDS treatments in our study demonstrated the necessity of knowing which ambiently adsorbed species exist on sediment surfaces if one is to predict the effect of introduced adsorbates on the electrostatic interactions among matrix constituents. Studies of electrophoretic mobility of model colloid systems, although prevalent in the literature (Hohl et al., 1980; Hansmann and Anderson, 1985; Liang and Morgan, 1990a; Liang and Morgan, 1990b), have dealt only with single solute systems, and do not take into account the role of preadsorbed species in determining the net surface potential, and resulting colloid stability, in mixed systems

containing more than one adsorbent. Such complex systems probably prevail in nature. Indeed, no literature could be found where comparisons or predictions were made of colloid mobilities between single sorbate systems and those containing preadsorbed or competing adsorbates. If adequate predictions of colloid stability in natural systems are to be made, such studies appear to be warranted.

6.3 Future Work

Use of Analytical electron microscopy

Analytical electron microscopy is a powerful tool for studying the elemental composition of natural deposits at the nanometer scale. This tool can be of great utility in helping to understand the distribution of phases at such small scales, as demonstrated in Chapter 2. For example, it may be possible to map the distribution of organic matter in sediment matrices like those of the Georgetown sediment. By mapping the distribution of carbon/nitrogen intensity ratios, one may be able to locate the organic matter in the matrix. For the case of the Georgetown sediment, the carbon/nitrogen ratio of the organic matter in the <63 μm size fraction (determined using a Perkin Elmer CHN analyzer; Holmén, 1994) is approximately 10 times higher than the carbon/nitrogen mole ratio of the nanoplast embedding resin. Thus, it may be possible to locate the organic matter in the sediment matrix, especially if it clusters in "pockets". Such a study might aid in elucidating whether organic matter is routinely associated with certain phases like amorphous iron oxyhydroxides or other amorphous phases. With a knowledge of the spatial distribution of organic matter in a sediment, one might be able to calculate tangible diffusion length scales to be used to model the sorption kinetics and transport behavior of hydrophobic organic contaminants in sediment. Such length scales are currently only estimated, or lumped into a fitting parameter, in such studies.

AEM can also be used to study metals speciation *in situ* using electron energy loss spectroscopy (EELS). This technique involves analysis of the energy loss spectrum of the

electron beam after it passes through the thin sectioned specimen (Egerton, 1986). The beam loses energy upon interaction with the specimen and specific regions of the energy loss spectrum can be ascribed to interaction with particular elements. Indeed, even the coordination environment and oxidation state of environmentally relevant metals like Fe, Mn, Cr, Cu, and As can be determined from differences in the fine structure of the energy loss spectrum in the regions ascribed to these elements (Otten et al., 1985; Rask et al., 1987). This ability makes EELS a powerful tool to study environmental issues like Cr and As speciation in aquifer solids, in colloidal phases in natural waters, and on atmospheric particles. Examples of EELS use for such studies is currently significantly underrepresented in the environmental literature, as only a few examples could be found (Maynard and Brown, 1992; Berghmans et al., 1994; Mavrocordatos et al., 1994).

Surface Speciation of Weak Acids

The ability to predict the effect of adsorption of weak acids on the surface potential of adsorbent surfaces is an important facet of understanding colloid mobilization in natural deposits. Contaminant plumes can be composed of a variety of organic (e.g., oxalate, phthalate) and inorganic ligands (e.g., phosphate, chromate, arsenate) which may alter electrostatic interactions among sediment matrix constituents through specific adsorption on constituent surfaces. Currently, surface complexation models are used predominantly to predict only magnitudes of sorption. Different surface species are used merely as fitting parameters to obtain model results which best match adsorption edge data. A limited number of attempts have been made to test whether such surface species are congruent with data representing surface charge/potential alteration of the adsorbent (i.e., zeta potential and titration measurements) by the adsorbate (Davis and Leckie, 1979; Davis and Leckie, 1980; Kummert and Stumm, 1980; Sigg and Stumm, 1980; Kallay and Matijevic, 1985; Crawford et al., 1996). The basis for such studies would be to use a surface complexation model in concert with surface potential measurements, and possibly even spectroscopic evidence (Tejedor-Tejedor and Anderson, 1990), to develop an model of the most realistic surface

species for a given system and to aid in developing a consistent means to predict the corresponding values of the pK_a's of *surface species* (Anderson and Malotky, 1979; Davis and Leckie, 1980). Such determinations would greatly aid the effort to predict the effect of specific adsorption of weak acids on the surface potential of adsorbates and resulting the electrostatic interactions in colloid systems.

For example, the finding that ascorbic acid shifted the pH_{pzc} of model goethite colloids to a significantly lower value (Chapter 3) was somewhat surprising given the relatively high aqueous pK_a's of this weak diprotic acid. In comparison, salicylic acid, which is also a weak, diprotic acid with pK_a values similar to that of ascorbic acid, did not shift the pH_{pzc} of the model goethite colloids significantly (data not presented in thesis). An explanation for the ability of ascorbic acid to cause a shift in the pH_{pzc} of goethite while salicylic acid lacks such an ability probably lies in the difference in the respective surface structures of these two ligands on goethite. Fourier transform infra-red spectroscopic studies of the adsorption of salicylic acid on goethite have indicated that the ligand forms bidentate mononuclear complexes with goethite surface functional groups (Yost et al., 1990; Biber and Stumm, 1994). This structure leaves neither the carboxylate nor phenolic ligand arm available for deprotonation, resulting in no added negative charge to the goethite surface upon specific adsorption of the salicylate. In contrast, the ascorbic acid must bind so that it leaves at least one of the protonizable hydroxyl groups free to deprotonate and effect the surface charge and potential of the goethite. The pK_a's of the ascorbate surface species are the key parameters which determine the magnitude of the shift in the pH_{pzc} of the goethite caused by specific adsorption of the ascorbate. *A priori* knowledge of the pK_a values for *surface species* would make prediction of electrostatic interactions in colloid systems where such specific adsorption occurs much easier.

Field Studies of Colloid Mobilization and Related Phenomena

Much more work could be done in studying *in situ* colloid mobilization and transport. The analysis of the kinetic behavior of the transport of the colloids mobilized in the single

well injection-withdrawal experiments (Chapter 4) would benefit from additional experiments designed to study the transport behavior of well-characterized colloids in such a flow system. Specifically, single well injection-withdrawal experiments could be conducted by injecting labeled, homogeneous synthetic colloids that possess a uniform surface charge. In this manner, one could study a range of systems in which the interactions between the colloids and the aquifer collector surfaces varied from uniformly attractive to repulsive. One could then analyze the kinetics of the transport behavior of these well-characterized colloids to see if this type of analysis is robust for the flow system involved in the single well method. The benefit of such a study would be in verifying the applicability of the kinetic analysis conducted with the colloids mobilized *in situ* in Chapter 4.

In addition, experimentation on the effects of colloid mobilization on the diffusive transport properties of aquifers is warranted. An initial study on this issue was conducted in a few of the colloid mobilization experiments conducted (Sanford, et al., unpublished data). Although no significant changes in diffusive transport in the aquifer material surrounding the well were found for the one set of valid data collected (Sanford, et al., unpublished data), such changes may be produced by a more prolonged mobilization event. Changes in the diffusive transport properties of aquifers as the result of colloid mobilization may also be more pronounced in other types of deposits. For example, mobilization of phases constituting the fracture fillings (Degueldre et al., 1989) or "skins" (Moench, 1995) in fractured rock systems may significantly alter the dual porosity behavior in these systems. The single well method utilizing tracers gases may be an efficient and controlled means to test this behavior in such hydrodynamically complex systems (Lessoff and Konikow, 1997).

Competitive Adsorption Issues in Colloid Mobilization and Stability

Further interpretation of the interesting competitive adsorption phenomena observed in the *in situ* experiments (Chapter 5) would require additional efforts involving a surface complexation model incorporating the solids present in the Georgetown aquifer. It would be worthwhile to see if such a model could qualitatively and quantitatively predict the

"equilibrium" plateau levels observed for sulfate and silicate in the samples from experiments in which displacement by phosphate occurred. Such a model, though, would require characterization of the more weakly bound ligands whose identities were not obtained. Additionally, intrinsic affinity constants for all involved adsorbates would have to be obtained. One would also want to test the robustness of the model by performing competitive adsorption experiments with a representative solid like goethite in aqueous systems containing all of the adsorbates of concern to see if the model could predict the net adsorption and final aqueous phase composition. Few studies have sought to test the robustness of surface complexation models where competitive adsorption phenomena may dominate (Balistrieri and Murray, 1987; Mesuere and Fish, 1992; Ali and Dzombak, 1996).

Finally, study of the electrophoretic mobilities of model goethite colloids in equilibrium with aqueous solutions mirroring the chemistry attained in the injectate might provide clues as to the ability of ligands such as phosphate and SDS to reverse surface charge in colloid systems where they must compete for surface sites. Obviously, the net change in surface charge and potential of these colloids at a given aqueous phase concentration of phosphate or SDS would differ from systems in which these ligands did not have to compete with other adsorbing anions which did not impart as great a shift in the pH_{pzc} of the goethite surfaces (e.g., silicate and sulfate). An understanding of such phenomena is critical if one is to begin to predict colloid stability in *natural systems*. Such studies have not been documented in the colloid literature at present.

6.4 References

Ali M. and Dzombak D. A. (1996) Competitive sorption of simple organic acids and sulfate on goethite. *Environ. Sci. Technol.* **30**, 1061-1071.

Anderson M. A. and Malotky D. T. (1979) The adsorption of protolyzable anions on hydrous oxides at the isoelectric pH. *J. Colloid Int. Sci.* **72**, 413-427.

Balistrieri L. S. and Murray J. W. (1987) The influence of the major ions of seawater on the adsorption of simple organic acids by goethite. *Geochim. Cosmochim. Acta* **51**, 1151-1160.

Berghmans P., Injuk J., vanGrieken R., and Adams F. (1994) Microanalysis of atmospheric particles and fibres by electron energy loss spectroscopy, electron spectroscopic imaging and scanning proton microscopy. *Anal. Chim. Acta* **297**, 27-42.

Biber M. and Stumm W. (1994) An in situ ATR-FTIR study: The surface coordination of salicylic acid on aluminum and iron (III) oxides. *Environ. Sci. Technol.* **28**, 763-768.

Cerda C. M. (1987) Mobilization of kaolinite fines in porous media. *Coll. Surf.* **27**, 219-241.

Crawford R. J., Harding I. H., and Mainwaring D. E. (1996) The zeta potential of iron and chromium hydrous oxides during adsorption and coprecipitation of aqueous heavy metals. *J. Colloid Int. Sci.* **181**, 561-570.

Davis J. A. and Leckie J. O. (1979) Speciation of adsorbed ions at the oxide/water interface. In *Chemical Modeling in Aqueous Systems* (ed. E. A. Jenne)299-317. American Chemical Society.

Davis J. A. and Leckie J. O. (1980) Surface Ionization and complexation at the oxide/water interface 3. Adsorption of anions. *J. Colloid Int. Sci.* **74**, 32-43.

Degueldre C., Baeyans B., Goerlich W., Riga J., Verbist J., and Stadelmann P. (1989) Colloids in water from a subsurface fracture in granitic rock, Grimsel test site, Switzerland. *Geochim. Cosmochim. Acta* **53**, 603-610.

Derjaguin B. V. and Landau L. (1941) *Acta Physicochim. URSS* **14**, 633-662.

Djafer M., Khandal R. K., and Terce M. (1991) Interactions between different anions and the goethite surface as seen by different methods. *Coll. Surf.* **54**, 209-218.

Dzombak D. A. and Morel F. M. M. (1990) *Surface Complexation Modeling Hydrous Ferric Oxide*. John Wiley and Sons.

Egerton R. F. (1986) *Electron Energy Loss Spectroscopy*. Plenum Press.

Fuller C. C., Davis J. A., Coston J. A., and Dixon E. (1996) Characterization of metal adsorption variability in a sand and gravel aquifer, Cape Cod, Massachusetts, U.S.A. *J. Contam. Hydrol.* **22**, 165-187.

Golden D. C. and Dixon J. B. (1985) Silicate and phosphate influence on Kaolin-iron oxide interactions. *Soil Sci. Soc. Am. J.* **49**, 1568-1576.

Goldenberg L. C. and Margaritz M. (1983) Experimental investigation on irreversible changes of hydraulic conductivity on the seawater-freshwater interface in coastal aquifers. *Water Resourc. Res.* **19**, 77-85.

Hansmann D. D. and Anderson M. A. (1985) Using electrophoresis in modeling sulfate, selenite, and phosphate adsorption onto goethite. *Environ. Sci. Technol.* **19**, 544-551.

Hohl H., Sigg L., and Stumm W. (1980) Characterization of surface chemical properties of oxides in natural waters. In *Particulates in water: Characterization, fate, effects, and removal* (ed. M. C. Kavanaugh and J. O. Leckie)1-31. American Chemical Society.

Holmén B. A. (1994) Polycyclic Aromatic Hydrocarbon Sorption Kinetics in Three Aquifer Sands. PhD. dissertation, Massachusetts Institute of Technology.

Israelachvili J. (1992) *Intermolecular and Surface Forces*. Academic Press.

Kallay N. and Matijevic E. (1985) Adsorption at solid/solution interfaces. 1. Interpretation of surface complexation of oxalic and citric acids with hematite. *Langmuir* **1**, 195-201.

Kaplan D. I., Bertsch P. M., and Adriano D. C. (1995) Facilitated transport of contaminant metals through an acidified aquifer. *Groundwater* **33**, 708-717.

Kaplan D. I., Bertsch P. M., Adriano D. C., and Miller W. P. (1993) Soil-borne mobile colloids as influenced by water flow and organic carbon. *Environ. Sci. Technol.* **27**, 1193-1200.

Kaplan D. I., Sumner M. E., Bertsch P. M., and Adriano D. C. (1996) Chemical conditions conducive to the release of mobile colloids from Ultisol profiles. *Soil Sci. Soc. Am. J.* **60**, 269-274.

Khilar K. C. and Fogler H. S. (1984) The existence of a critical salt concentration for particle release. *J. Colloid Int. Sci.* **101**, 214-224.

Kia S. F., Fogler H. S., and Reed M. G. (1987) Effect of pH on colloidally induced fines migration. *J. Colloid Int. Sci.* **118**, 158-168.

Kinniburgh D. G., Jackson M. L., and Syers J. K. (1976) Adsorption of alkaline earth, transition, and heavy metal cations by hydrous oxide gels of iron and aluminum. *Soil Sci. Soc. Am. J.* **40**, 796-799.

Kummert R. and Stumm W. (1980) The surface complexation of organic acids on hydrous gamma-Al2O3. *J. Colloid Int. Sci.* **75**, 373-385.

Lessoff S. C. and Konikow L. F. (1997) Ambiquity in measuring matrix diffusion with single-well injection/recovery tracer tests. *Groundwater* **35**, 166-176.

Liang L. and Morgan J. J. (1990a) Chemical aspects of iron oxide coagulation in water: Laboratory studies and implications for natural systems. *Aquatic Sci.* **52**, 32-55.

Liang L. and Morgan J. J. (1990b) Coagulation of iron oxide particles in the presence of organic materials. *American Chemical Society Symposium Series* **No. 146**, 293-308.

Lin F.-C. (1985) Clay-coating reduction of permeability during oil-sand testing. *Clays Clay Min.* **33**, 76-78.

Mavrocordatos D., Lienemann C.-P., and Perret D. (1994) Energy filtered transmission electron microscopy for the physico-chemical characterization of aquatic submicron colloids. *Mikrochim. Acta* **117**, 39-47.

Maynard A. D. and Brown L. M. (1992) Electron energy loss spectroscopy of ultrafine aerosol particles in the scanning transmission electron microscope. *J. Aerosol Sci.* **23, Supp 1**, S433-S436.

McDowell-Boyer L. M. (1992) Chemical mobilization of micron sized particles in saturated porous media under steady flow conditions. *Environ. Sci. Technol.* **26**, 586-593.

Mesuere K. and Fish W. (1992) Chromate and oxalte adsorption on goethite. 2. Surface complexation modeling of competitive adsorption. *Environ. Sci. Technol.* **26**, 2365-2370.

Moench A. F. (1995) Convergent radial dispersion in a double-porosity aquifer with fracture skin: Analytical solution and application to a field experiment in fractured chalk. *Water Resourc. Res.* **31**, 1823-1836.

Osterhout M. M. (1980) *Decontamination and Decommissioning of Nuclear Facilities.* Plenum Press.

Otten M. T., Miner B., Rask J. H., and Buseck P. R. (1985) The determination of Ti, Mn and Fe oxidation states in minerals by electron energy-loss spectroscopy. *Ultramicroscopy* **18**, 285-290.

Rask J. H., Miner B. A., and Buseck P. R. (1987) Determination of manganese oxidation states in solids by electron energy-loss spectroscopy. *Ultramicroscopy* **21**, 321-326.

Roy S. B. and Dzombak D. (1996) Colloid release and transport processes in natural and model porous media. *Coll. Surf.* **107**, 245-.

Ryan J. N. and Gschwend P. M. (1991) Extraction of iron oxides from sediments using reductive dissolution by titanium(III). *Clays Clay Min.* **39**, 509-518.

Ryan J. N. and Gschwend P. M. (1994) Effect of solution chemistry on clay colloid release from an iron oxide-coated aquifer sand. *Environ. Sci. Technol.* **28**, 1717-1726.

Ryan J. N. and Gschwend P. M. (1994b) Effects of ionic strength and flow rate on colloid release: Relating kinetics to intersurface potential energy. *J. Colloid Int. Sci.* **164**, 21-34.

Seaman J. C., Bertsch P. M., and Miller W. P. (1995) Chemical controls on colloid generation and transport in a sandy aquifer. *Environ. Sci. Technol.* **29**, 1808-1815.

Seaman J. C., Bertsch P. M., and Strom R. N. (1997) Characterization of colloids mobilized from Southeastern Coastal Plain sediments. *Environ. Sci. Technol.* **31**, 2782-2790.

Sigg L. and Stumm W. (1980) The interaction of anions and weak acids with the hydrous goethite (α-FeOOH) surface. *Coll. Surf.* **2**, 101-117.

Tejedor-Tejedor M. I. and Anderson M. A. (1990) Protonation of phosphate on the surface of goethite as studied by CIR-FTIR and electrophoretic mobility. *Langmuir* **6**, 602-611.

Tessier A., Fortin D., Belzile N., DeVitre R. R., and Leppard G. G. (1996) Metal sorption to diagenetic iron and manganese oxyhydroxides and associated organic matter: Narrowing the gap between field and laboratory measurements. *Geochim. Cosmochim. Acta* **60**, 387-404.

Thurman E. M. (1985) *Organic Geochemistry of Natural Waters*. Martinus Nijhoff.

Verwey E. J. W. and Overbeek J. T. G. (1948) *Theory of the Stability of Lyophobic Colloids*. Elsevier.

Yost E. C., Tejedor-Tejedor M. I., and Anderson M. A. (1990) In situ CIR-FTIR characterization of salicylate complexes at the goethite/aqueous solution interface. *Environ. Sci. Technol.* **24**, 822-828.

Appendix A:
Example Estimation of the Fraction Goethite in the Mobilized Colloids from the Column and Field Experiments

A.1 Motivation

In both the packed-column (Chapter 3) and *in situ* (Chapter 4) methods used to study the colloid release behavior in the Georgetown sediment, colloids representing only subfractions of the sediment bulk matrix appeared to be mobilized when the sediment was treated with certain chemical perturbations. This partial mobilization of the bulk matrix was indicated by comparing the chemical composition of the mobilized colloids to the chemical composition of the bulk matrix. Specifically, we measured the Al/Fe mole ratio of the colloids mobilized by a particular treatment and compared it to the Al/Fe mole ratio of the <63 μm size (silt- and clay-size) fraction of the sediment. We believed that this size fraction represented the material constituting the interstitial matrix that fills the voids between primary grains (quartz) in the Georgetown sediment. In this manner, we were able to determine whether colloids representative of the entire bulk matrix, or a subfraction of the bulk matrix, were generated with a specific chemical treatment.

For example, when sediment-packed columns were treated with 10 mM phosphate and subsequently flushed with deionized water (Chapter 3), colloids with an average Al/Fe mole ratio of 0.5±0.3 were generated (**Table 3.1**, Chapter 3). In contrast, the bulk matrix was found to possess an Al/Fe mole ratio of 3.2±0.2. Similarly, when groundwater amended with 1 mM phosphate was injected and withdrawn from the aquifer (Chapter 4), colloids with an average Al/Fe mole ratio of 0.8±0.2 were present in the retrieved injectate. However, when the sediment was treated with ligands with the ability to dissolve iron oxyhydroxides (oxalic acid, ascorbic acid), colloids more chemically representative of the bulk matrix were released. These colloids possessed Al/Fe mole ratios from 2.3 to 3.1 (Chapters 3 and 4). We interpreted the large differences between the colloidal Al/Fe mole ratios for colloids generated by the phosphate amended water and the Al/Fe mole ratio of the bulk matrix as an indication that possibly, preferential mobilization of goethite aggregates had occurred as a result of treating the sediment with the phosphate amended water. Because the Al/Fe mole ratio of

the goethite aggregates was found to be approximately 0.24, and these aggregates appeared to be discretely organized within the sediment matrix (Chapter 2; Swartz et al., 1997), it seemed reasonable to infer that preferential mobilization of the goethite had occurred in response to the assumedly purely electrostatic perturbation imparted by phosphate adsorption on the goethite.

Others have recently observed preferential mobilization of goethite in sediments similar in composition to the Georgetown sediment. Seaman et al. (1997) used transmission electron microscopy to analyze colloids mobilized from a Southeastern Coastal Plain aquifer in response to variations in the cation chemistry of the pore fluids. They found that goethite represented as much as 77% of the colloids mobilized from the sediment upon counting colloids trapped on filters and assigning mineralogy on the basis of chemical (energy dispersive x-ray, EDX) and structural (lattice fringe imaging) analysis of these colloids.

An analysis such as that performed by Seaman et al. (1997) is labor intensive and instrument-time intensive as well. We sought a relatively simple means to provide a "back-of-the envelope" estimation of the percent goethite in the colloids generated in our experiments. By relying on a few simplifying assumptions, we performed such a calculation, which is described below.

A.2 Determination of Colloidal Al/Fe Mole Ratios

The methods used to determine the Al/Fe mole ratios of the colloids released from the sediment in both the column and *in situ* field experiments is provided in detail elsewhere (see section 3.2.3, Chapter 3; and section 4.2.4, Chapter 4). Briefly, hydrofluoric acid (HF) was added to 1 mL subsamples of the aqueous samples collected from the column and field experiments to obtain a final concentration of 0.3 to 0.15 M HF. The samples were digested for 72 hrs and the resulting digestates were analyzed for Fe and Al by graphite furnace atomic absorption (A.A.) spectrometry. Standards prepared in similar concentrations of an HF solution were used to determine the concentrations of Fe and Al in the samples. The Al/Fe

mole ratio of the "bulk matrix" was determined by digestion of 0.1 g samples of the <63 μm size fraction of the sediment in concentrated HF and aqua regia (see section 2.2.1, Chapter 2). Fe and Al in these digestates were measured by graphite furnace A.A.

A.3 Sample Calculation

The basis for the calculation is a simple mole balance for the Al and Fe contained in the mobilized colloids. In the calculation, the Al/Fe mole ratio of the goethite aggregates was used along with a "composite" Al/Fe mole ratio for all other phases contributing Al and Fe to the <63 μm size fraction. These other phases would include predominantly kaolinite, as this mineral was found to be present in amounts greater than 40% by weight of the <2 μm size fraction (Chapter 2, Swartz et al., 1997). Minor amounts of vermiculite and gibbsite would also be included in this composite group. In addition, the amorphous iron oxhydroxide phases would be included in the composite group. These amorphous iron phases were found to be intimately associated with the clay minerals in the sediment matrix (Chapter 2, Swartz et al., 1997). Thus, they probably would be mobilized with the clay minerals given the appropriate chemical perturbation (i.e., treatments containing adsorbates which break bonds among the amorphous iron intermediaries and the kaolinite platelets, as hypothesized in Chapters 3 and 4). Note that, although quartz is probably the predominant mineral in the <63 μm size fraction, it does not enter into these calculations because it is assumed to containing little, if any Fe or Al.

The Al/Fe mole balance equation for the mobilized colloids can be expressed in the following manner:

$$(Al/Fe_G)(x) + (Al/Fe_o)(1-x) = (Al/Fe_C) \qquad (1)$$

where Al/Fe_G is the Al/Fe mole ratio of the goethite aggregates, x is the fraction of goethite in the colloids per g of total colloids containing Al and/or Fe, Al/Fe_o is the composite Al/Fe mole ratio of all other colloidal phases contributing Al and Fe, and Al/Fe_C is the Al/Fe mole ratio of the mobilized colloids.

To solve for x, the fraction of colloids which can be attributed to goethite, one must have values for Al/Fe_G , Al/Fe_o, and Al/Fe_C. For the Georgetown sediment, the value of Al/Fe_G was determined previously by selective extraction (i.e., use of the Ti (III)-citrate-EDTA method) for the iron oxyhydroxides in the <63 μm size fraction (0.23, Chapter 2, Swartz et al., 1997). This value was calculated using only Fe and Al assumed to be incorporated in the crystalline iron oxyhydroxides present in the <63 μm size fraction, as the Fe and Al present in amorphous iron oxyhydroxide phases (64 and 46 μmoles g^{-1} <63 μm size fraction, respectively, determined by ammonium oxalate extraction) were subtracted out of the Fe and Al numbers determined from the Ti (III)-citrate-EDTA extraction (1250 and 320 μmoles g^{-1} <63 μm size fraction, respectively, **Table 2.1**, Chapter 2, Swartz et al., 1997).

For the sample calculation presented below we used the value of Al/Fe_C (0.8±0.2) determined for the colloids mobilized by 1 mM phosphate amended groundwater in the *in situ* experiment HP9-B (Chapter 4). It was in this *in situ* experiment that the greatest amount of preferential mobilization of goethite was thought to have occurred based on the large difference between the Al/Fe mole ratio of the mobilized colloids and that of the <63 μm size fraction.

What remains to be determined is the value of Al/Fe_o. Its value was calculated using the total Al measured by digestion of the <63 μm size fraction (4300 μmoles g^{-1} <63 μm size fraction; Chapter 2) and subtracting from it the Al assumed to be incorporated in the crystalline iron oxyhydroxides (i.e., goethite). The Al incorporated in goethite (274 μmoles g^{-1} <63 μm size fraction) was determined by the difference between the Al in the Ti (III)-citrate-EDTA extracts of the <63 μm size fraction (320 μmoles g^{-1} <63 μm size fraction; **Table 2.1**, Chapter 2) and the Al in the ammonium oxalate extracts of the <63 μm size fraction (46 μmoles g^{-1} <63 μm size fraction; Chapter 2). Likewise, the total Fe measured by digestion of the <63 μm size fraction (1350 μmoles g^{-1} <63 μm size fraction; **Table 2.1**, Chapter 2) was corrected for the Fe incorporated in goethite (1190 μmoles g^{-1} <63 μm size fraction, Chapter 2). The resulting value for Al/Fe_o was found to be approximately 25 (4046

μmoles Al g^{-1} <63 μm size fraction divided by 160 μmoles Fe g^{-1} <63 μm size fraction).

With all the required terms obtained for the mole balance equation (1) above, the value of x was solved for when Al/Fe_C equals 0.8. The resulting value of x was approximately 0.97, indicating that 97% by weight of the colloids *containing Fe and Al* mobilized in experiment HP9-B could be attributed to goethite. Note that other colloids such as quartz, amorphous silica, titanium oxides could also have been mobilized. However, these phases probably would not contribute Fe and Al to the colloidal population in the digested samples. The relatively large fraction goethite of the mobilized colloids obtained from this "back of the envelope" estimation does indeed suggest that preferential mobilization of goethite occurred in experiment HP9-B (Chapter 4).

A.4 References

Seaman J. C., Bertsch P. M., and Strom R. N. (1997) Characterization of colloids mobilized from Southeastern Coastal Plain sediments *Environ. Sci. Technol.* **31**, 2782-2790.

Swartz C. H., Ulery A. L., and Gschwend P. M. (1997) An AEM-TEM study of nanometer-scale mineral associations in an aquifer sand: Implications for colloid mobilization. *Geochim. Cosmochim. Acta* **61**, 707-718.

Appendix B:

Estimating Aquifer Heterogeneity Using Br^- Concentration Profiles Obtained During the *in situ* Colloid Mobilization Experiments

B.1 Introduction

For the single well injection-withdrawal experiments described in Chapter 4, a conservative tracer (Br^-) was added to the amended groundwater injected. The presence of the tracer in the injectate allowed us to monitor and quantify the retrieval of the injected slug. The presence of the tracer also allowed us to identify the portion of the retrieved slug which had not been dispersively mixed with unamended groundwater. The ability to discriminate samples unaffected by dispersive mixing provided valuable information on both colloid mobilization and transport behavior (see Chapter 4) and competitive adsorption phenomena observed in the injection-withdrawal experiments (see Chapter 5). In addition, the normalized concentration profile of the Br^- tracer as a function of retrieved volume provided information on the aquifer heterogeneity encountered by the injectates in each of the emplaced wells.

Using an analytical solution developed to estimate the effects of flow nonuniformity on longitudinal dispersion in porous media (Gelhar and Collins, 1971), we were able to compare fits of the Br^- normalized concentration profiles to the analytical solutions for radial and spherical flow from a well for a recharge-discharge cycle. The analytical solution developed by Gelhar and Collins (1971) involves transformation of the advective-dispersive equation into one of simple heat conduction. The solution to this equation provides generality with respect to flow-field geometry of the system studied because the flow-field characteristics are implicitly included in the solution (Gelhar and Collins, 1971). Thus, the Br^- profiles could be compared with the analytical solution for a particular flow-field geometry using dispersivity as a fitting parameter. The analytical model did not allow us to discriminate whether or not a spherical or radial flow-field geometry actually characterized our injection-withdrawal experiments, but it did allow us to obtain an idea of the relative flow-field heterogeneity encountered by the injectates among wells. Comparison of fitted dispersivity values allowed us to obtain this estimate of the relative heterogeneity among wells. Note, however, that these dispersivity values should not be taken as truly

representative of the aquifer properties, as the injection-withdrawal procedure inherently confounds the analysis of dispersion due to flow reversal (Gelhar, personal communication, 1994). One may think of the dispersivity values as lower limits on the true dispersivities.

B.2 Analytical solution derivation

Gelhar and Collins (1971) describe the detailed derivation of the analytical solution. Briefly, the advective-dispersive equation in the absence of sources and sinks

$$\frac{\partial C}{\partial t} = \frac{\partial}{\partial x_i}\left(D_{ik}\frac{\partial C}{\partial x_k} - u_i C\right) + D_m \frac{\partial}{\partial x_i}\left(\frac{\partial C}{\partial x_i}\right) \qquad (1)$$

is first converted to a curvilinear coordinate system where transverse dispersion is neglected:

$$\partial\frac{C}{\partial t} + u\frac{\partial C}{\partial s} = \alpha u\frac{\partial^2 C}{\partial s^2} + D_m\left(\frac{\partial^2 C}{\partial s^2} - \frac{1}{u}\frac{\partial u}{\partial s}\frac{\partial C}{\partial s}\right) \qquad (2)$$

In this equation, α is the longitudinal dispersivity and s is an arc length along the direction of flow. A boundary layer approximation to the solution to this equation is accomplished by first transforming (2) with dimensionless variables to:

$$\frac{\partial C}{\partial T} + U\frac{\partial C}{\partial S} = \epsilon U\frac{\partial^2 C}{\partial S^2} + \epsilon D\left(\frac{\partial C^2}{\partial S^2} - \frac{1}{U}\frac{\partial C}{\partial S}\frac{\partial U}{\partial S}\right) \qquad (3)$$

where $T = t/T_o$ (i.e., dimensionless time), $S = s/L_o$ (dimensionless distance), and $U = u/U_o$ (dimensionless velocity), $\epsilon = \alpha/L_o$, and $D = D_m T_o/\alpha L_o$. A variable, X(S),

$$X(S) = \int_{So}^{S} U^{-1} dS \qquad (4)$$

which represents a transformed spatial coordinate equal to the dimensionless time required ($T-T_o$) to move some distance ($S-S_o$), allows removal of the nonconstant coefficient (U) in (3).

Upon substitution, the following equation is produced:

$$\frac{\partial C}{\partial T} + \frac{\partial C}{\partial X} = \left(\frac{\epsilon}{U}\right)\left(\frac{\partial^2 C}{\partial X^2} - \frac{\partial U}{\partial S}\frac{\partial C}{\partial X}\right) + \left(\frac{\epsilon D}{U^2}\right)\left(\frac{\partial^2 C}{\partial X^2} - \frac{\partial U}{\partial S}\frac{\partial C}{\partial X} - \frac{\partial U}{\partial S}\frac{\partial C}{\partial X}\right) \qquad (5)$$

This equation is further transformed with a space-time combined variable, H = X-T, which is a measure of the distance from the convected front (Gelhar and Collins, 1971) and which is identical to:

$$\int_S^S \frac{dS}{U(S)} \qquad (6)$$

The substitution results in the following equation:

$$\frac{\partial C}{\partial T} = \left(\frac{\epsilon}{U}\right)\left(\frac{\partial^2 C}{\partial H^2} - \frac{\partial U}{\partial S}\frac{\partial C}{\partial H}\right) + \left(\frac{\epsilon D}{U^2}\right)\left(\frac{\partial^2 C}{\partial H^2} - 2\frac{\partial U}{\partial S}\frac{\partial C}{\partial H}\right) \qquad (7)$$

Introduction of a magnified boundary layer coordinate ξ in the expression $H = \xi\epsilon^{1/2}$ allows the dispersive nature of the resulting equation to be maintained (Gelhar and Collins, 1971). After the U^{-1} and U^{-2} are expanded in a Taylor series, a first order approximation is carried out, and (7) reduces to:

$$\frac{\partial C}{\partial T} = \frac{U(S') + D}{U^2(S')}\frac{\partial^2 C}{\partial \xi^2} \qquad (8)$$

Defining $\Omega = \Omega(T)$ as:

$$\Omega = \int_{So}^{S'} \frac{U(S')+D}{U^3(S')}\, dS' \qquad (9)$$

allows (8) to be reduced to the equivalent dimensional form:

$$\frac{\partial C}{\partial \omega} = \alpha \frac{\partial^2 C}{\partial \eta^2} \tag{10}$$

where $\eta = x - t$, and x, t, and ω are defined as follows:

$$x = \int_{so}^{s} u(s)^{-1}\, ds \tag{11}$$

$$t = \int_{so}^{s'} u(s)\, ds \tag{12}$$

and

$$\omega = \int_{so}^{s'} \frac{u(s') + D_m/\alpha}{u^3(s')}\, ds' \tag{13}$$

The solution for (13) when a step change in concentration occurs at the origin (i.e., at the well screen) has the form:

$$C(x,t) = \frac{1}{2} C_o erfc\{(x-t)/[4\alpha\omega(t)]^{1/2}\} \tag{14}$$

This equation (14) can be solved for a variety of diverging flow geometries, which take the general form:

$$u(s) = A/s^k \tag{15}$$

where A and k are constants particular to the flow geometry. It is here that the solution to the heat equation can be tailored to the particular flow-field geometry. By plugging in the constants A and k for a particular geometry into (15), one can evaluate the integrals for x (11), t (12), and ω (13), substitute these values into (14) and solve for the concentration profile of the step input of a tracer as a function of distance from the origin (well screen).

Gelhar and Collins (1971) solved (14) for the case of a step input of tracer from a

fully penetrating well into a confined aquifer under radial flow conditions. In this case, A= $q_1/2\pi nb$ and k=1, where q_1 is the recharge rate, n is porosity, and b is the thickness of the aquifer. Upon evaluating the integrals for x , t, and ω when s = r - r_w, (14) takes the form:

$$\frac{C}{C_o} = \frac{1}{2}\,erfc\left\{\frac{r^2 - r^{*2}}{\left[16\alpha\left(\frac{r^{*3} - r_w^3}{3} + \frac{D_m}{\alpha A_1}\,\frac{r^{*4} - r_w^4}{4}\right)\right]^{1/2}}\right\} \qquad (16)$$

where r is any distance from the well screen, r* is the plume front, and r_w is the well radius. The equation for the concentration profile of the tracer in the recovery phase (i.e., $q_2 = -q_1$, and $r = R_1$, the maximum extent of the plume) is obtained by now integrating the equations for x, t, and ω at $s = R_1 - r$, and takes the following form:

$$\frac{C}{C_o} = erfc\left\{\frac{r^2 - r^{*2}}{\left\{16\alpha\left[\frac{2R_1^3 - r^{*3} - r_w^3}{3} + \frac{D_m}{4\alpha A_2}\left(R_1^4 + \frac{A_2}{A_1}(R_1^4 - r_w^4) - r^{*4}\right)\right]\right\}^{1/2}}\right\} \qquad (17)$$

By setting $r = r_w$, the concentration profile at the well can be obtained. By assuming that diffusion is negligible with respect to advection and that r_w is negligible as well, the solution for the concentration profile at the well can be rearranged into the form:

$$\frac{C}{C_o} = \frac{1}{2}\,erfc\left\{\frac{\frac{\forall_2}{\forall_1} - 1}{\left[\frac{16}{3}\,\frac{\alpha}{R_1}\left(2 - \left|1 - \frac{\forall_2}{\forall_1}\right|^{1/2}\left(1 - \frac{\forall_2}{\forall_1}\right)\right)\right]^{1/2}}\right\} \qquad (18)$$

where $\forall_1$ is the volume recharged into the aquifer, and $\forall_2$ is the volume discharged at any time.

In a similar fashion, the equation for the concentration profile of a tracer can be solved for with a spherical geometry using $A=q/(4\pi n)$ and k = 2. The solution for this system takes

the form:

$$\frac{C}{C_o} = erfc\left\{\frac{r^3 - r^{*3}}{\left\{36\alpha\left[\frac{2R_1^5 - r^{*5} - r_w^5}{5} + \frac{D_m}{7\alpha A_2}\left(R_1^7 + \frac{A_2}{A_1}(R_1^7 - r_w^7) - r^{*7}\right)\right]\right\}^{1/2}}\right\} \quad (19)$$

and the concentration at the well is given by:

$$\frac{C}{C_o} = \frac{1}{2}erfc\left\{\frac{\frac{\forall_2}{\forall_1} - 1}{\left[\frac{36}{5}\frac{\alpha}{R_1}\left(2 - \left|1 - \frac{\forall_2}{\forall_1}\right|^{2/3}\left(1 - \frac{\forall_2}{\forall_1}\right)\right)\right]^{1/2}}\right\} \quad (20)$$

The solutions for tracer concentration at the well with respect to radial and spherical flow were used to calculate a predicted Br^- concentration profile. The value of R_1 was calculated for each case based on the volume of water injected (approximately 11500 mL) in each of the *in situ* colloid mobilization experiments (Chapter 4). This volume was divided by an assumed porosity (0.3) of the aquifer to calculate R_1 for the sphere and the disk which would be created by injection of 11,500 mL into the aquifer. These radii were calculated to be 20.9 cm and 40.0 cm for the spherical and radial flow cases, respectively. No attempt was made to correct for r_w, the radius of the well (10.2 cm) in calculating these radii. The values of V/V_o calculated for the actual Br^- data points were used as V/V_o values for the predicted Br^- concentrations. The value of the longitudinal dispersivity (α) was used as the fitting parameter, as the value of R_1 calculated for each case from the injection volume was assumed to be known reasonably well. Fits to the predicted values of Br^- concentration were made visually.

A sensitivity analysis of the solution for the radial flow case was performed with respect to the two variables α (dispersivity) and R_1 (maximum radius of the plume) (**Figure B.1**). Dispersitivities were varied by ± 43% about the value 0.35 cm (**Figure B.1a**).

Similarly, the variable R_1 (radius of the disk, or maximum extent of the plume) was varied by ± 43% (**Figure B.1b**). Note that the magnitude of the change in the Br^- profile is similar regardless of whether the dispersivity or the radius is varied by 43%. However, the changes produced in the profile due to variation of either variable oppose each other. For example, decreasing the plume radius produces increasingly elevated tailing of the Br^- profile, whereas decreasing the dispersity (α) sharpens the front and decreases tailing. We chose to use the dispersivity as the sole fitting parameter and assumed the calculation of R_1 using the known injection volume and well screen height was appropriate for the radial and spherical flow cases.

B.3 Results and Discussion

For most of the wells, the Br^- concentration profiles were fit with a relatively narrow range of dispersivities (**Figures B.2** through **B.7**). For each case, the Br^- concentration profile for either the "before" or "after" control conducted in the well was used to make the comparison. Predicted Br^- values were fit to measured Br^- concentration profiles with dispersivity values ranging from 0.35 cm (**Figure B.2**) to 1.5 cm (**Figure B.6**) for the radial flow case. For the spherical flow case, dispersivities in the range 0.15 cm (**Figure B.2**) to 0.5 cm (**Figure B.6**) were obtained. Br^- profiles for wells HP3, HP4, HP6 and HP7 were fit most closely with the analytical solution, whereas the Br^- profiles for HP9 deviated somewhat from the best visual fit profile (α = 1.0 cm for radial flow, α = 0.35 for spherical flow) in the steepest portion of the profile (**Figure B.7**). For HP8 (**Figure B.6**), the deviation from the best fit (α = 1.5 cm for radial flow, α = 0.5 for spherical flow) was even greater in the steepest portion of the profile.

Studying the curve for HP8-A more closely (**Figure B.6**), one notes that the measured value of C/C_o equal to 0.5 did not correspond to a value of V/V_o equal to 1.0, as predicted by simple advective-dispersive transport. Rather, the value of C/C_o appeared earlier (V/V_o = 0.8) in the recovery of the injectate pore volume. In addition, the tail of the Br^- profile for HP8-A

was elevated with respect to the tracer profiles in other wells at comparable values of V/V_o (see **Figure 4.13**, Chap. 4). The measured Br^- profile for HP8-B was nearly identical to that of HP8-A (data not shown). Early elution of the first "pore volume" and elevated concentrations in the tail of the discharge profile may indicate that diffusion-limited transport operated in this well. It is possible that when the inner well apparatus was emplaced in HP8, surging of running sands upward around the screen and packers caused the packers to not inflate tightly around the casing. This effect may have caused a "pocket" of sand to form in the well annulus. Perhaps transport of the Br^- tracer was limited by diffusion into and out of this pocket of sand, causing distortion of shape of the Br^- profile upon discharge. It would appear that such a sand pocket would have to be rather large to have such a significant effect on the measured profile. Although retardation of the Br^- would also cause such features in the recovery profile, it is unlikely that the Br^- would be retarded to such an extent only in the aquifer material surrounding well HP8.

Note that the Br^- mass recoveries for the experiments conducted in HP8 were somewhat lower in comparison to the other wells (**Table 4.1**, Chapter 4). If irretrievable loss of injectate volume to the annulus had occurred, such as loss would shift the curve to the left, as V/V_o would be underestimated based on calculation using the known volume sent down the well. Leftward shifting of the profile was simulated with the radial flow model. First, normalized Br^- concentrations were *calculated* using the radial solution, the same value of dispersivity (1.5 cm), and the *actual values of* V/V_o used for plotting the measured data and the initial predictions, which were calculated assuming the entire volume injected contacted the aquifer and was retrieved. Once calculated, however, the values of C/C_o Br^- were *plotted* with V/V_o values calculated assuming an injected volume *overestimated by 10%* (which results in a 10% underestimation of V/V_o). Expectedly, this manipulation shifts the predicted curve leftward, so that the C/C_0 value corresponding to $V/V_0 = 1.0$ is now < 0.50, more similar in behavior to that exhibited by the measured profile (**Figure B.6**). However, even with 10% underestimation of V/V_o, almost twice the discrepancy in percent mass Br^-

recovered from the HP8 experiments, the predicted profile did not capture the shape of the observed profile. Note also that the elevated tail of the measured Br^- profile was not captured by shifting the predicted profile leftward. Thus, irretrievable loss of tracer mass alone can not explain the shape of the measured Br^- profile. It is possible, though, that diffusion-limited transport and some irretrievable loss of injected volume occurred concomitantly in the HP8 experiments, producing the observed profile shape.

Figure B.1 appears on the next page

Figure B.1: Comparison of the effect of varying (a) R_1 (radius of maximum extent of plume) and (b) α (dispersivity) on the shape of the predicted normalized Br^- concentration profile using the radial flow case. The x axis represents the ratio of volume discharged to volume rechared. In (a), R_1 was varied by ±43% of the best fit value (40 cm) for the measured Br^- for experiment HP3-A. The α value is 0.35 cm for all profiles. In (b), α was varied by ±43% of the best fit value (0.35 cm) for HP3-A. R_1 is equal to 40 cm for all profiles.

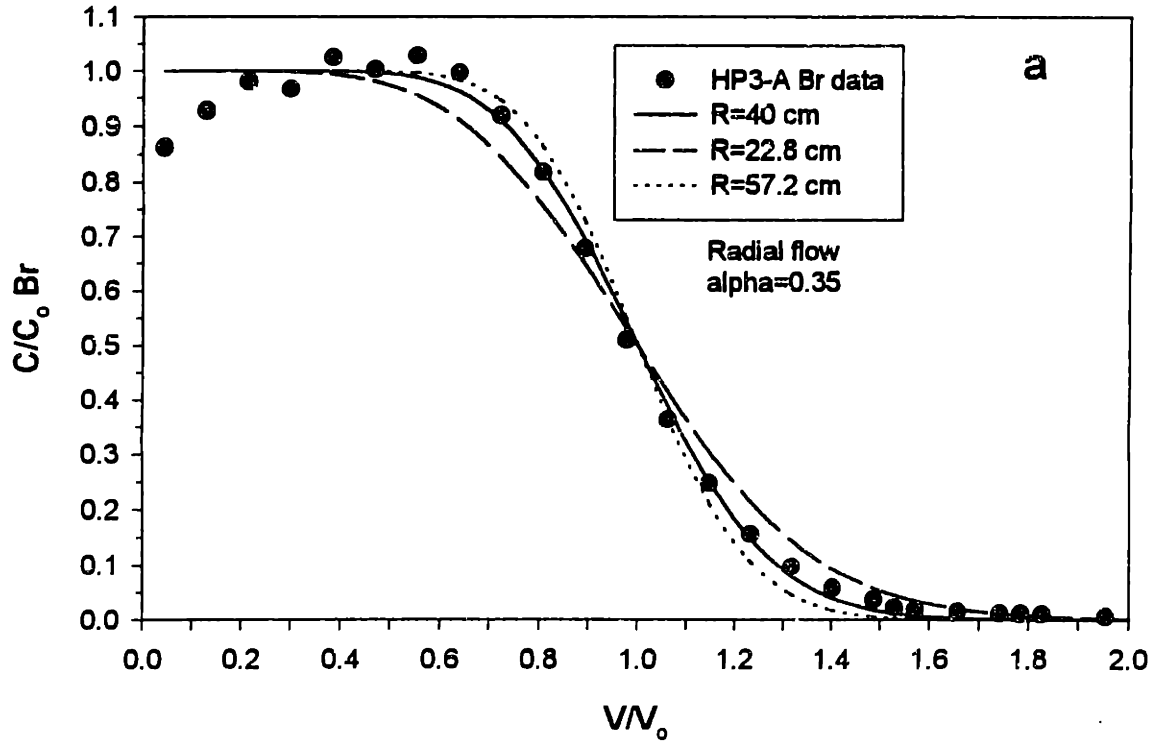
a
HP3-A Br data
R=40 cm
R=22.8 cm
R=57.2 cm
Radial flow
alpha=0.35
C/C$_o$ Br
V/V$_o$

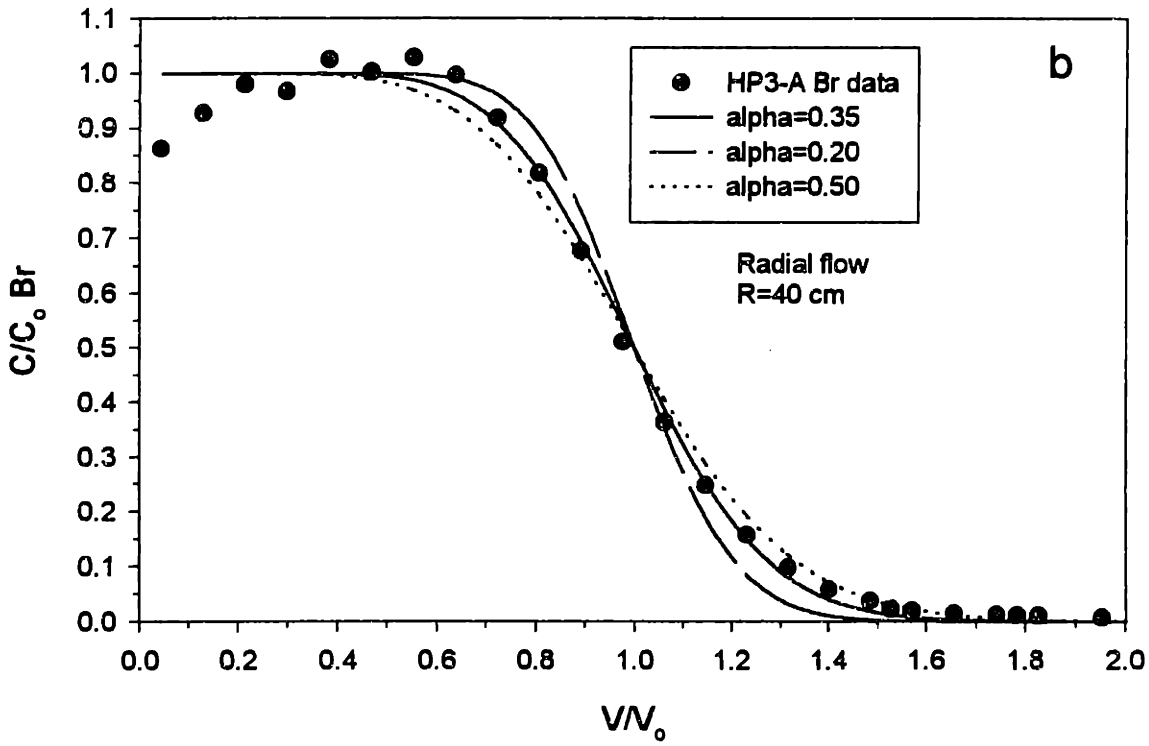
b
HP3-A Br data
alpha=0.35
alpha=0.20
alpha=0.50
Radial flow
R=40 cm
C/C$_o$ Br
V/V$_o$

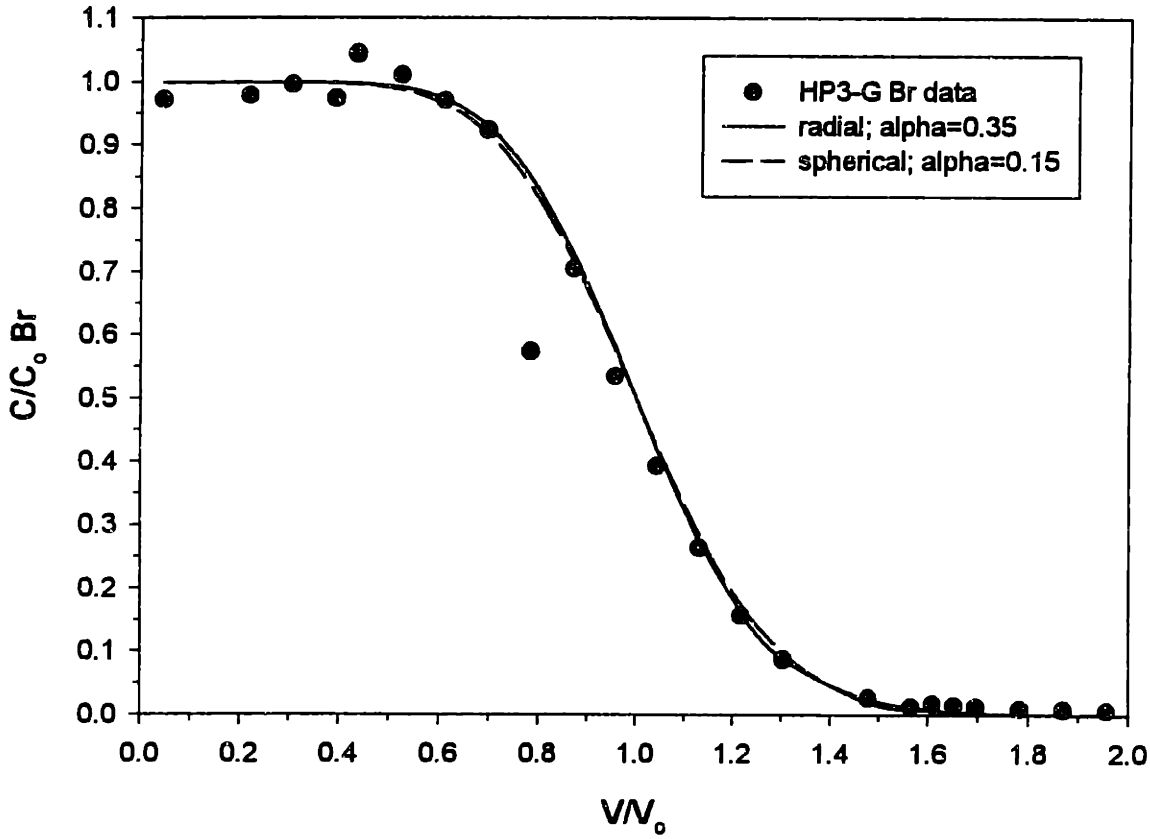

Figure B.2: Measured normalized Br^- concentration profile versus the ratio of volume discharged to volume recharged for HP3-G and the best fit model prediction for the radial flow (solid line) and spherical flow (dashed line) cases. $\alpha = 0.35$, $R_1 = 40$ cm for the radial flow case. The spherical flow prediction is based on $R_1 = 20.9$ cm, and $\alpha = 0.15$.

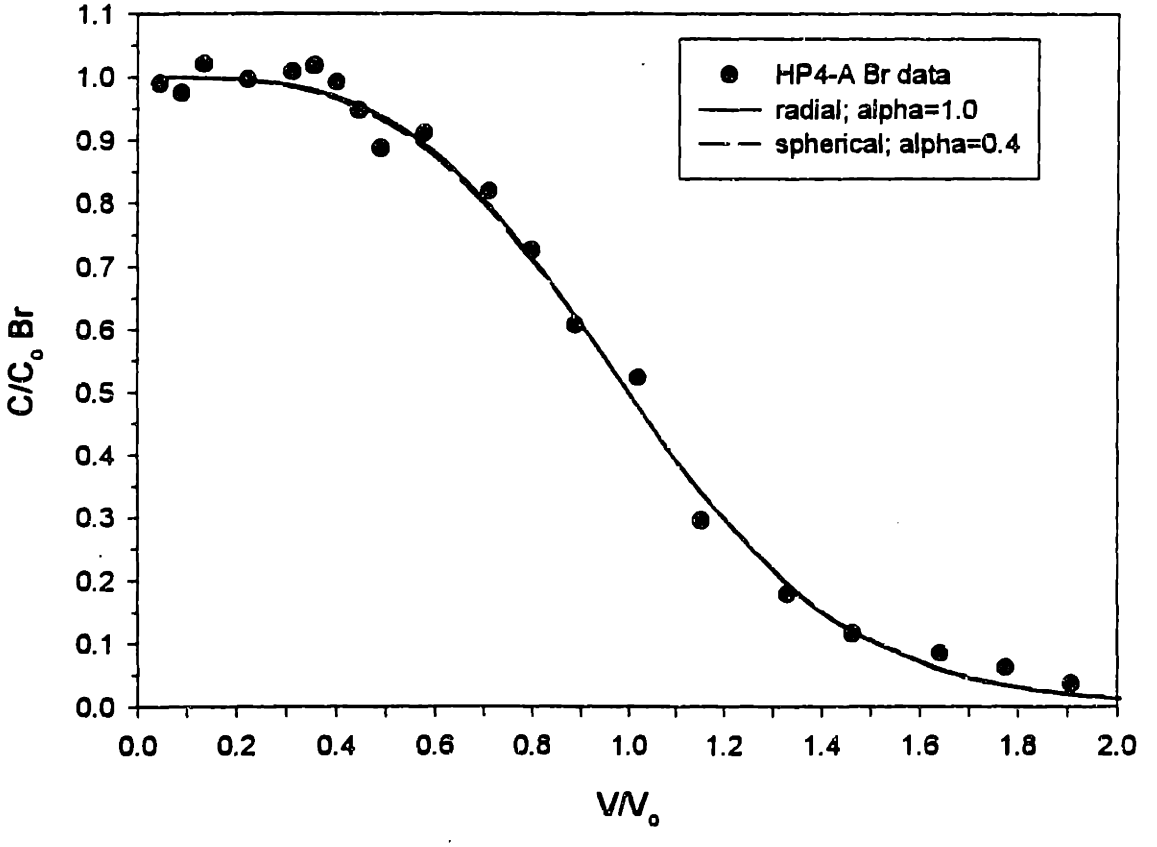

Figure B.3: Measured normalized Br^- concentration profile versus the ratio of volume discharged to volume recharged for HP4-A and the best fit model prediction for the radial flow (solid line) and spherical flow (dashed line) cases. α = 1.0, R_1 = 40 cm for the radial flow case. The spherical flow prediction is based on R_1 = 20.9 cm, and α = 0.4.

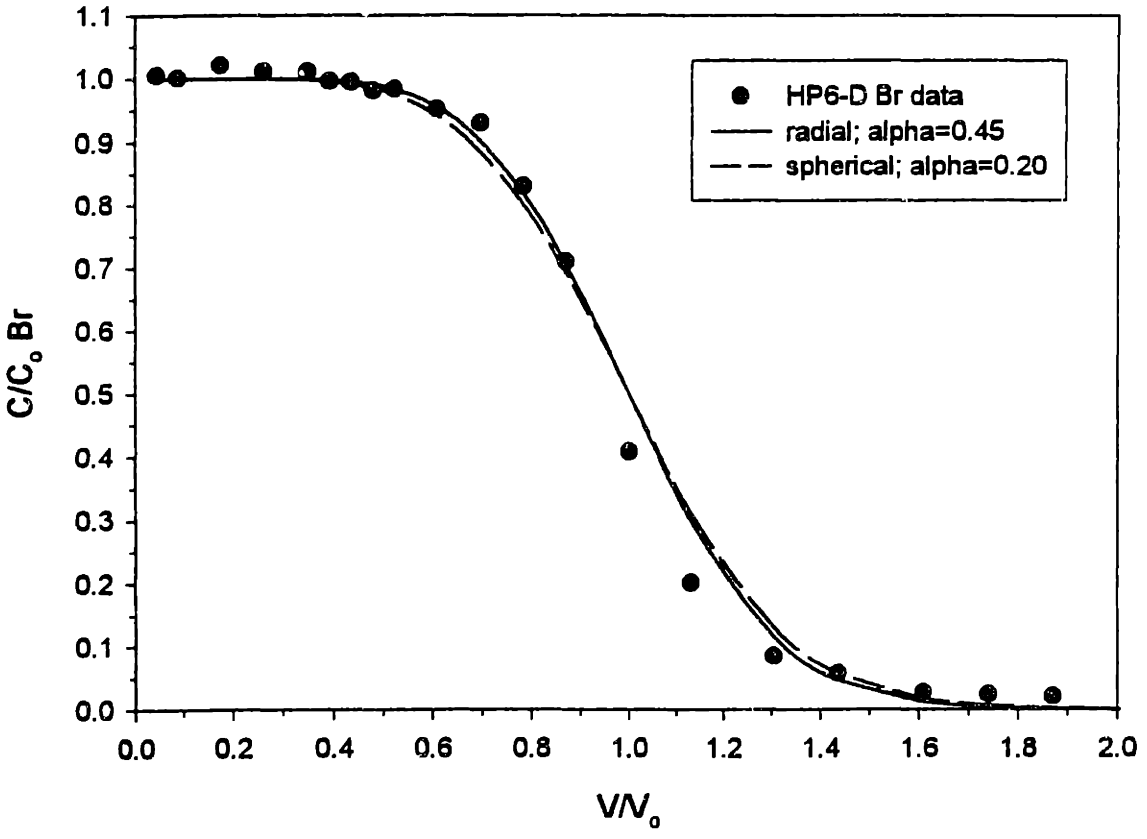

Figure B.4: Measured normalized Br^- concentration profile versus the ratio of volume discharged to volume recharged for HP6-D and the best fit model prediction for the radial flow (solid line) and spherical flow (dashed line) cases. $\alpha = 0.45$, $R_1 = 40$ cm for the radial flow case. The spherical flow prediction is based on $R_1 = 20.9$ cm, and $\alpha = 0.2$.

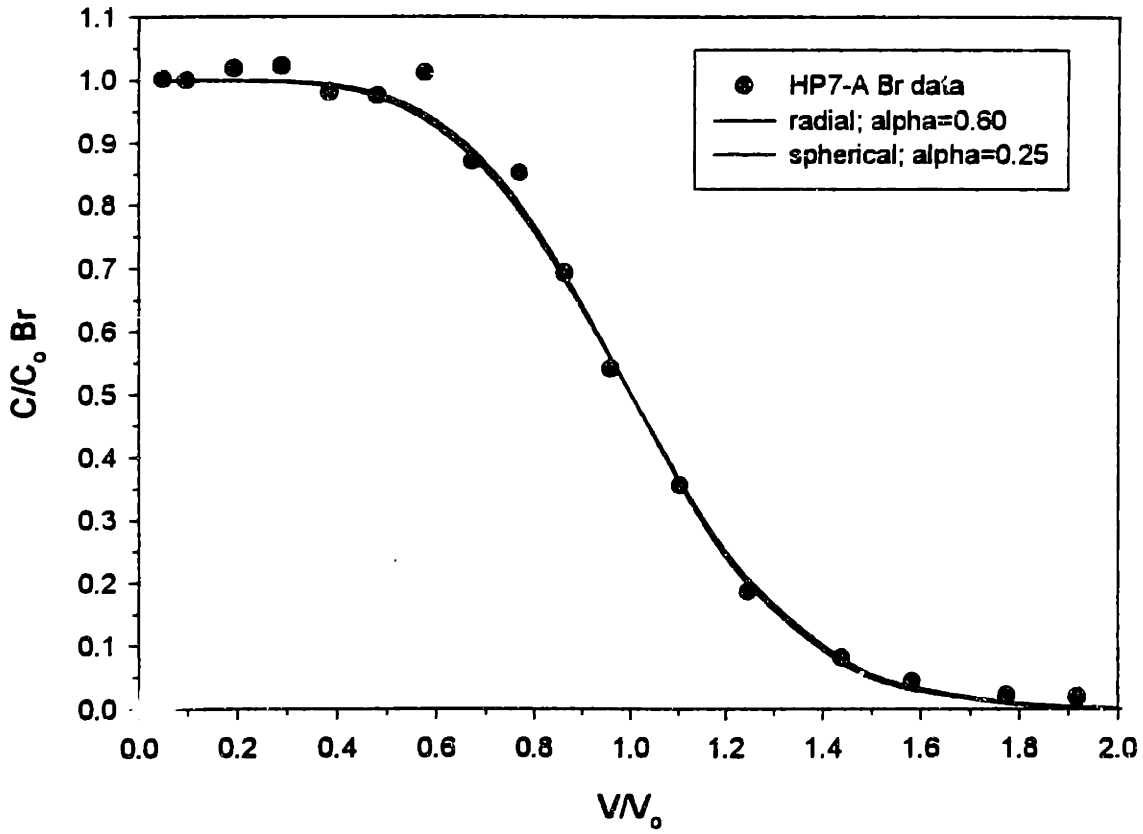

Figure B.5: Measured normalized Br^- concentration profile versus the ratio of volume discharged to volume recharged for HP7-A and the best fit model prediction for the radial flow (solid line) and spherical flow (dashed line) cases. $\alpha = 0.60$, $R_1 = 40$ cm for the radial flow case. The spherical flow prediction is based on $R_1 = 20.9$ cm, and $\alpha = 0.25$.

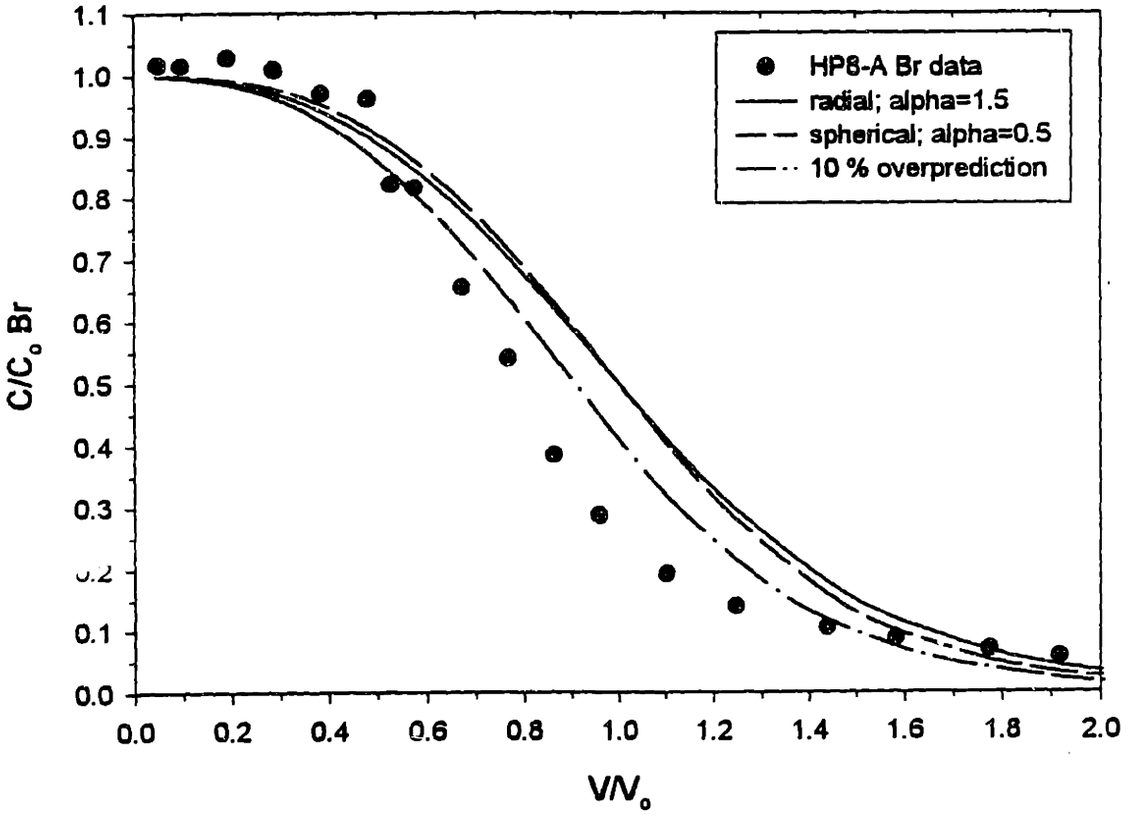

Figure B.6: Measured normalized Br^- concentration profile versus the ratio of volume discharged to volume recharged for HP8-A and the best fit model prediction for the radial flow (solid line) and spherical flow (dashed line) cases. α = 1.5, R_1 = 40 cm for the radial flow case. The spherical flow prediction is based on R_1 = 20.9 cm, and α = 0.5. In addition, a line (dot-dashed) is shown which represents predicted normalized Br^- concentration values for the radial flow case *calculated* with the same values for V/V_o as used for the first two predicted profiles, but *plotted* with values of V/V_o overpredicted by 10%. This profile simulates the effect of irretrievable loss of 10% of the injectate volume and hence, underprediction of V/V_o values for a given data point.

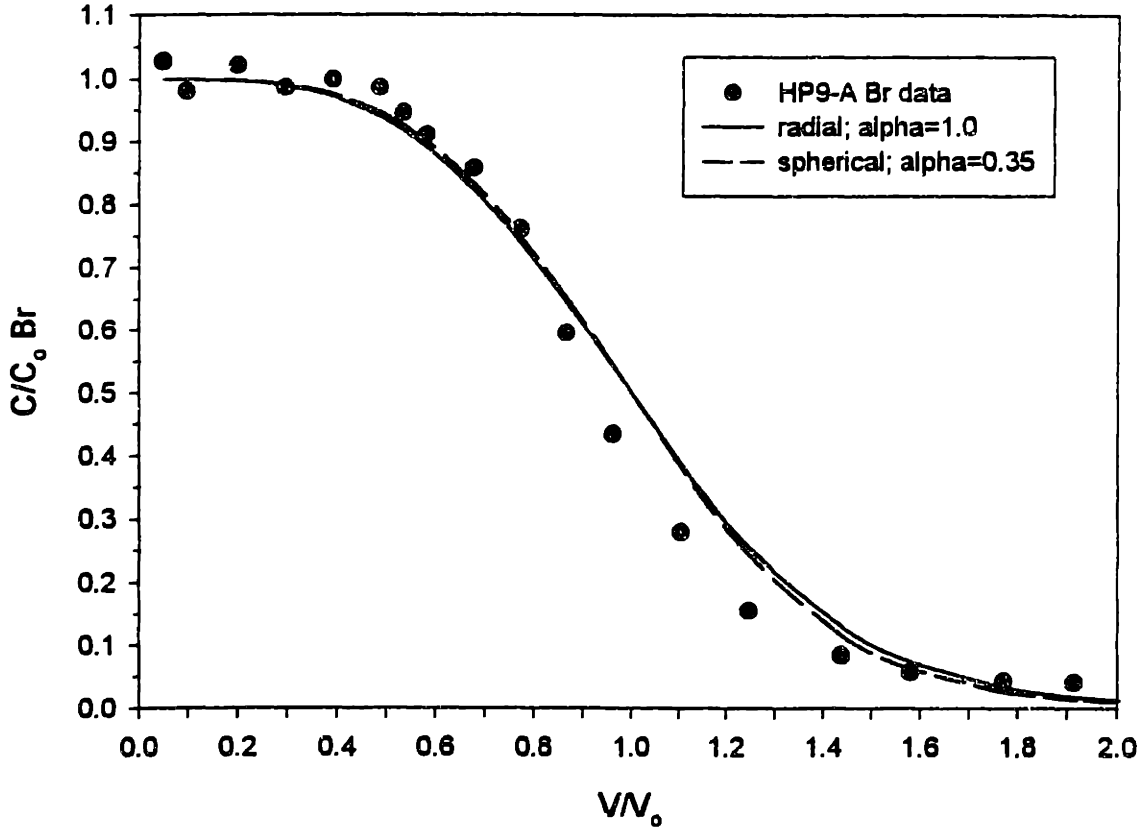

Figure B.7: Measured normalized Br^- concentration profile versus the ratio of volume discharged to volume recharged for HP9-A and the best fit model prediction for the radial flow (solid line) and spherical flow (dashed line) cases. α = 1.0, R_1 = 40 cm for the radial flow case. The spherical flow prediction is based on R_1 = 20.9 cm, and α = 0.35.

B.4 References

Gelhar L. W. (1994) personal communication. Ralph M. Parsons Lab, Massachusetts Institute of Technology, Cambridge, MA.

Gelhar L. W. and Collins M. A. (1971) General analysis of longitudinal dispersion in nonuniform flow. *Water Resourc. Res.* 7, 1511-1521.